Volume 25, Number 2, 2025 ISSN 1562-8353

NONLINEAR DYNAMICS AND SYSTEMS THEORY
An International Journal of Research and Surveys

Volume 25 Number 2 2025

CONTENTS

 ISSN 1562-8353 Printed in Ukraine
To receive contents and abstracts by e-mail, visit our Website at: **http://www.e-ndst.kiev.ua**

NONLINEAR DYNAMICS & SYSTEMS THEORY

Volume 25, No. 2, 2025

Nonlinear Dynamics and Systems Theory

An International Journal of Research and Surveys

InforMath Publishing Group
http://www.e-ndst.kiev.ua

Nonlinear Dynamics and Systems Theory

An International Journal of Research and Surveys

INSTRUCTIONS FOR CONTRIBUTORS

(1) General. Nonlinear Dynamics and Systems Theory (ND&ST) is an international journal devoted to publishing peer-refereed, high quality, original papers, brief notes and review articles focusing on nonlinear dynamics and systems theory and their practical applications in engineering, physical and life sciences. Submission of a manuscript is a representation that the submission has been approved by all of the authors and by the institution where the work was carried out. It also represents that the manuscript has not been previously published, has not been copyrighted, is not being submitted for publication elsewhere, and that the authors have agreed that the copyright in the article shall be assigned exclusively to InforMath Publishing Group by signing a transfer of copyright form. Before submission, the authors should visit the website:

http://www.e-ndst.kiev.ua

for information on the preparation of accepted manuscripts. Please download the archive Sample_NDST.zip containing example of article file (you can edit only the file Samplefilename.tex).

(2) Manuscript and Correspondence. Manuscripts should be in English and must meet common standards of usage and grammar. To submit a paper, send by e-mail a file in PDF format directly to

Professor A.A. Martynyuk, Institute of Mechanics,
Nesterov str.3, 03057, Kiev-57, Ukraine
e-mail: journalndst@gmail.com

or to one of the Regional Editors or to a member of the Editorial Board. Final version of the manuscript must typeset using LaTex program which is prepared in accordance with the style file of the Journal. Manuscript texts should contain the title of the article, name(s) of the author(s) and complete affiliations. Each article requires an abstract not exceeding 150 words. Formulas and citations should not be included in the abstract. AMS subject classifications and key words must be included in all accepted papers. Each article requires a running head (abbreviated form of the title) of no more than 30 characters. The sizes for regular papers, survey articles, brief notes, letters to editors and book reviews are: (i) 10-14 pages for regular papers, (ii) up to 24 pages for survey articles, and (iii) 2-3 pages for brief notes, letters to the editor and book reviews.

(3) Tables, Graphs and Illustrations. Each figure must be of a quality suitable for direct reproduction and must include a caption. Drawings should include all relevant details and should be drawn professionally in black ink on plain white drawing paper. In addition to a hard copy of the artwork, it is necessary to attach the electronic file of the artwork (preferably in PCX format).

(4) References. Each entry must be cited in the text by author(s) and number or by number alone. All references should be listed in their alphabetic order. Use please the following style:

Journal: [1] H. Poincare, Title of the article. *Title of the Journal* **volume** (issue) (year) pages. [Language]

Book: [2] A.M. Lyapunov, *Title of the Book.* Name of the Publishers, Town, year.

Proceeding: [3] R. Bellman, Title of the article. In: *Title of the Book.* (Eds.). Name of the Publishers, Town, year, pages. [Language]

(5) Proofs and Sample Copy. Proofs sent to authors should be returned to the Editorial Office with corrections within three days after receipt. The corresponding author will receive a sample copy of the issue of the Journal for which his/her paper is published.

(6) Editorial Policy. Every submission will undergo a stringent peer review process. An editor will be assigned to handle the review process of the paper. He/she will secure at least two reviewers' reports. The decision on acceptance, rejection or acceptance subject to revision will be made based on these reviewers' reports and the editor's own reading of the paper.

NONLINEAR DYNAMICS AND SYSTEMS THEORY
An International Journal of Research and Surveys
Published by InforMath Publishing Group since 2001

Volume 25 Number 2 2025

CONTENTS

Founded by A.A. Martynyuk in 2001.
Registered in Ukraine Number: KB No 5267 / 04.07.2001.

NONLINEAR DYNAMICS AND SYSTEMS THEORY

An International Journal of Research and Surveys

Impact Factor from SCOPUS for 2023: SJR – 0.298, SNIP – 1.032 and CiteScore – 1.6

Nonlinear Dynamics and Systems Theory (ISSN 1562–8353 (Print), ISSN 1813–7385 (Online)) is an international journal published under the auspices of the S.P. Timoshenko Institute of Mechanics of National Academy of Sciences of Ukraine and Curtin University of Technology (Perth, Australia). It aims to publish high quality original scientific papers and surveys in areas of nonlinear dynamics and systems theory and their real world applications.

AIMS AND SCOPE

Nonlinear Dynamics and Systems Theory is a multidisciplinary journal. It publishes papers focusing on proofs of important theorems as well as papers presenting new ideas and new theory, conjectures, numerical algorithms and physical experiments in areas related to nonlinear dynamics and systems theory. Papers that deal with theoretical aspects of nonlinear dynamics and/or systems theory should contain significant mathematical results with an indication of their possible applications. Papers that emphasize applications should contain new mathematical models of real world phenomena and/or description of engineering problems. They should include rigorous analysis of data used and results obtained. Papers that integrate and interrelate ideas and methods of nonlinear dynamics and systems theory will be particularly welcomed. This journal and the individual contributions published therein are protected under the copyright by International InforMath Publishing Group.

PUBLICATION AND SUBSCRIPTION INFORMATION

Nonlinear Dynamics and Systems Theory will have 6 issues in 2025, printed in hard copy (ISSN 1562–8353) and available online (ISSN 1813–7385), by InforMath Publishing Group, Nesterov str., 3, Institute of Mechanics, Kiev, MSP 680, Ukraine, 03057. Subscription prices are available upon request from the Publisher, EBSCO Information Services (mailto:journals@ebsco.com), or website of the Journal: http://e-ndst.kiev.ua. Subscriptions are accepted on a calendar year basis. Issues are sent by airmail to all countries of the world. Claims for missing issues should be made within six months of the date of dispatch.

ABSTRACTING AND INDEXING SERVICES

Papers published in this journal are indexed or abstracted in: Mathematical Reviews / MathSciNet, Zentralblatt MATH / Mathematics Abstracts, PASCAL database (INIST–CNRS) and SCOPUS.

Nonlinear Dynamics and Systems Theory, **25** (2) (2025) 113–127

Domination of Hyperbolic Systems with Respect to the Gradient Observation

H. Aichaoui* and S. Benhadid

Department of Mathematics, Faculty of Exact Sciences, University of Constantine 1 Mentouri Brothers, Constantine, Algeria

Received: June 8, 2024; Revised: February 28, 2025

Abstract: In this paper, we introduce the notions of domination for a class of controlled and observed hyperbolic systems. We study, with respect to the gradient observation, the possibility to make a comparison of input operators of a controlled system. We give various characterizations and main properties in the general case and then by means of the choice of actuators and sensors. As an application, we examine the case of a one dimension wave equation.

Keywords: *hyperbolic systems; domination; gradient; control; actuators; sensors.*

Mathematics Subject Classification (2020): 35L20, 93B05, 93B07, 93C20.

1 Introduction

Modeling a system consists in representing its dynamic behavior by a mathematical model. The mathematical model obtained is generally in the form of linear or nonlinear differential equations. The methods used in the analysis of linear systems are very powerful because of the existence of available tools. However, these linear analysis methods have several limitations because most systems are not linear, so linear methods are only applicable in a limited domain. These limitations explain the complexity and diversity of nonlinear systems and the analysis methods that apply to them. Therefore, there are no general theories for nonlinear systems, but there are several methods adapted to certain classes of nonlinear systems to overcome these difficulties, a linearization of the system and the output which consists in transforming the dynamics of the nonlinear system into a completely (or partially) linear system, so that the techniques of linear systems can be applied. Therefore, we can extend the concepts presented for linear systems to nonlinear

* Corresponding author: mailto:houda.aichaoui@umc.edu.dz

systems, and among these concepts, there is the concept of domination, which has been discussed in this paper.

This work is an extension of the previous works which concern the analysis of a class of linear systems within certain concepts. These concepts consist of a set of notions such as controllability [13], detectability, observability [10], remediability [3] and domination [5,6] which enable a better knowledge and understanding of the system to be obtained. For some related studies in nonlinear cases, see [8, 12].

The extensions of these concepts that are very important in practical applications are those of gradient controllability [9, 11], gradient detectability [7], gradient observability [15], gradient remediability [14].

This work concerns the notion of domination for a general class of controlled and observed hyperbolic systems used to study the possibility of comparing the input operators with respect to the gradient observation. It is an extension of the previous works on parabolic distributed systems [1, 5]. A more general approach is given in [2–4] for controlled and observed systems in the global, regional and asymptotic cases.

This paper is organized as follows. In Section 2, we present the systems. We define and characterize the concepts of exact and weak domination for controlled hyperbolic systems with respect to the gradient observation in Section 3. In Section 4, we give the main properties and characterization results and the case of sensors and actuators is also examined. Finally, we examine the case of a one dimension wave equation.

2 Considered System

Let Ω be an open and bounded subset of $\mathbb{R}^n$ with a sufficiently regular boundary and $]0, T[$ be the finite time interval. We consider the following system:

$$\begin{cases} \dfrac{\partial^2 y}{\partial t^2}(x,t) = Ay(x,t) + B_1 u_1(t) + B_2 u_2(t), & \Omega\times]0,T[, \\ y(x,0) = y^0(x),\, \frac{\partial y_1}{\partial t}(x,0) = y^1(x), & \Omega, \\ y(\xi,t) = 0, & \partial\Omega\times]0,T[, \end{cases} \tag{1}$$

where A is a second order elliptic linear operator given by

$$A = \sum_{i,j=1}^{n} \frac{\partial}{\partial x_i}\left(a_{ij}\frac{\partial}{\partial x_j}\right),$$

with the domain $D(A) = H_0^1(\Omega) \cap H^2(\Omega)$ and verified elliptic conditions

$$\begin{cases} a_{ij} = a_{ji} \in L^\infty(\Omega),\ 1 \le i,j \le n, \\ \exists \alpha > 0, \forall \xi = (\xi_1, \xi_2, \ldots, \xi_n) \in \mathbb{R}^n,\ \sum_{i,j=1}^n a_{ij}(x)\xi_i\xi_j \ge \alpha \sum_{i=1}^n |\xi_i|^2, \quad \text{pp. in } \Omega, \end{cases}$$

$B_1 \in \mathcal{L}(U_1, X)$, $B_2 \in \mathcal{L}(U_2, X)$, $u_1 \in L^2(0,T;U_1)$ and $u_2 \in L^2(0,T;U_2)$, where U_1 and U_2 are two Hilbert spaces (control spaces) and $X = H_0^1(\Omega)$ is the state space.

For $\left(y^0, y^1\right)$ in $H_0^1(\Omega) \times L^2(\Omega)$, the system (1) admits a unique solution y in $C\left(0,T; H_0^1(\Omega)\right) \cap C^1\left(0,T; L^2(\Omega)\right)$. The system (1) is augmented with the output equation

$$z(t) = C\nabla y(t), \tag{2}$$

where $C \in \mathcal{L}\left(\left(L^2(\Omega)\right)^n, \mathcal{O}\right), \mathcal{O}$ is the observation space (Hilbert space). In the case of an observation with q sensors, we take generally $\mathcal{O} = \mathbb{R}^q$.

The gradient operator ∇ is given by the formula

$$\begin{aligned} \nabla : H_0^1(\Omega) &\to \left(L^2(\Omega)\right)^n, \\ y &\mapsto \nabla y = \left(\frac{\partial y}{\partial x_1}, \frac{\partial y}{\partial x_2}, \cdots, \frac{\partial y}{\partial x_n}\right). \end{aligned}$$

We consider the operator $\bar{A}$ defined by

$$\bar{A}\left(y_1, y_2\right) = \left(y_2, A y_1\right), \forall \left(y_1, y_2\right) \in D(\bar{A}),$$

with $D(\bar{A}) = D(A) \times H_0^1(\Omega)$. The operator $\bar{A}$ is linear, closed with a dense domain in the state space $\bar{X} = H_0^1(\Omega) \times H_0^1(\Omega)$, which is a Hilbert space for the inner product

$$\left\langle \left(y_1, y_2\right), \left(z_1, z_2\right)\right\rangle_{H_0^1(\Omega) \times L^2(\Omega)} = \left\langle \sqrt{-A} y_1, \sqrt{-A} z_1 \right\rangle_{L^2(\Omega)} + \left\langle y_2, z_2 \right\rangle_{L^2(\Omega)}.$$

The adjoint operator of $\bar{A}$ is given by $\bar{A}^* = -\bar{A}$.

The operator $\bar{A}$ generates on $\bar{X}$ a strongly continuous semi-group $(S(t))_{t \geq 0}$ defined by

$$S(t)\begin{pmatrix} y_1 \\ y_2 \end{pmatrix} = \begin{pmatrix} W_1(t)\begin{pmatrix} y_1 \\ y_2 \end{pmatrix} \\ W_2(t)\begin{pmatrix} y_1 \\ y_2 \end{pmatrix} \end{pmatrix},$$

with

$$W_1(t)\begin{pmatrix} y_1 \\ y_2 \end{pmatrix} = \sum_{m \geq 1} \sum_{j=1}^{r_m} \left(\left\langle y_1, w_{mj} \right\rangle_{L^2(\Omega)} \cos \sqrt{-\lambda_m} t + \frac{1}{\sqrt{-\lambda_m}} \left\langle y_2, w_{mj} \right\rangle_{L^2(\Omega)} \sin \sqrt{-\lambda_m} t \right) w_{mj}$$

and

$$W_2(t)\begin{pmatrix} y_1 \\ y_2 \end{pmatrix} = \sum_{m \geq 1} \sum_{j=1}^{r_m} \left(-\sqrt{-\lambda_m} \left\langle y_1, w_{mj} \right\rangle_{L^2(\Omega)} \sin \sqrt{-\lambda_m} t + \left\langle y_2, w_{mj} \right\rangle_{L^2(\Omega)} \cos \sqrt{-\lambda_m} t \right) w_{mj}.$$

Its adjoint is $S^*(t) = S(-t), \ \forall t \geq 0$. On the other hand, we consider the operators

$$\begin{aligned} \bar{B}_1 &: U_1 \to \bar{X} & \text{and} \quad \bar{B}_2 &: U_2 \to \bar{X} \\ u_1 &\mapsto \bar{B}_1 u_1 = (0, B_1 u_1)^{tr} & u_2 &\mapsto \bar{B}_2 u_2 = (0, B_2 u_2)^{tr}. \end{aligned}$$

If we put $\bar{y}(t) = \left(y(t), \dfrac{\partial y(t)}{\partial t}\right)^{tr}$, $\bar{y}^0 = \left(y^0, y^1\right)^{tr}$ and $\dfrac{\partial \bar{y}}{\partial t}(t) = \left(\dfrac{\partial y(t)}{\partial t}, \dfrac{\partial^2 y(t)}{\partial t^2}\right)^{tr}$, then the system (1) is equivalent to the following system:

$$\left\{ \begin{array}{l} \dfrac{\partial \bar{y}}{\partial t}(t) = \bar{A}\bar{y}(t) + \bar{B}_1 u_1(t) + \bar{B}_2 u_2(t), \quad 0 < t < T, \\ \bar{y}(0) = \bar{y}^0. \end{array} \right. \tag{3}$$

The unique solution of system (3) is

$$\bar{y}(t) = S(t)\bar{y}^0 + \int_0^t S(t-s)\bar{B}_1 u_1(s) ds + \int_0^t S(t-s)\bar{B}_2 u_2(s) ds.$$

The system (3) is augmented by the output equation

$$\bar{z}(t) = \bar{C}\bar{\nabla}\bar{y}(t), \tag{4}$$

where $\bar{C}$ is defined by

$$\bar{C}\,(y_1, y_2) = Cy_1, \quad \forall (y_1, y_2) \in \left(L^2(\Omega)\right)^n \times \left(L^2(\Omega)\right)^n,$$

and

$$\begin{aligned} \bar{\nabla}: \quad & H_0^1(\Omega) \times H_0^1(\Omega) \to \left(L^2(\Omega)\right)^n \times \left(L^2(\Omega)\right)^n \\ & (y_1, y_2) \mapsto \bar{\nabla}\,(y_1, y_2) = (\nabla y_1, \nabla y_2)\,. \end{aligned}$$

We consider the following operators:

$$\begin{aligned} H_1: \quad & L^2(0,T;U_1) \to \bar{X} \\ & u_1 \mapsto H_1 u_1 = \int_0^T S(T-s)\bar{B}_1 u_1(s) ds \end{aligned}$$

and

$$\begin{aligned} H_2: \quad & L^2(0,T;U_2) \to \bar{X} \\ & u_2 \mapsto H_2 u_2 = \int_0^T S(T-s)\bar{B}_2 u_2(s) ds, \end{aligned}$$

while their adjoints, denoted by H_1^* and H_2^*, are given by $H_1^* = \bar{B_1}^* S(\cdot - T)$ and $H_2^* = \bar{B_2}^* S(\cdot - T)$, respectively. The state of system (3) at time T is given by

$$\bar{y}(T) = S(T)\bar{y}^0 + H_1 u_1 + H_2 u_2.$$

3 Domination with respect to C

Definition 3.1 We say that

1. B_1 dominates B_2 exactly on $[0,T]$ with respect to C if for any $u_2 \in L^2\,(0,T;U_2)$, there exists a control $u_1 \in L^2\,(0,T;U_1)$ such that

$$\bar{C}\bar{\nabla}H_1 u_1 + \bar{C}\bar{\nabla}H_2 u_2 = 0.$$

2. B_1 dominates B_2 weakly on $[0,T]$ with respect to C if for any $\epsilon > 0$ and for any $u_2 \in L^2\,(0,T;U_2)$, there exists a control $u_1 \in L^2\,(0,T;U_1)$ such that

$$\|\bar{C}\bar{\nabla}H_1 u_1 + \bar{C}\bar{\nabla}H_2 u_2\|_{\mathcal{O}} < \epsilon.$$

Lemma 3.1 *Let V, W and Z be reflexive Banach spaces, $P \in \mathcal{L}(V,Z)$ and $Q \in \mathcal{L}(W,Z)$. Then the following properties are equivalent:*

1. $\operatorname{Im} P \subset \operatorname{Im} Q$.

2. $\exists \gamma > 0$ *such that* $\|P^* z^*\|_{V^*} \leq \gamma \|Q^* z^*\|_{W^*}, \quad \forall z^* \in Z^*$.

Proposition 3.1 *The following properties are equivalent:*

1. B_1 dominates B_2 exactly on $[0,T]$ with respect to C.

2. $\operatorname{Im}\left(\bar{C}\bar{\nabla}H_2\right) \subset \operatorname{Im}\left(\bar{C}\bar{\nabla}H_1\right)$.

3. *There exists* $\gamma > 0$ *such that for every* $\theta \in \mathcal{O}^*$, *we have*

$$\left\|\bar{B}_2^* S(\cdot - T)\bar{\nabla}^*\bar{C}^*\theta\right\|_{L^2\left(0,T;U_2^*\right)} \leq \gamma \left\|\bar{B}_1^* S(\cdot - T)\bar{\nabla}^*\bar{C}^*\theta\right\|_{L^2\left(0,T;U_1^*\right)}.$$

Proof.
- $1 \Leftrightarrow 2:$ B_1 dominates B_2 exactly on $[0,T]$ with respect to C if and only if

$$\forall u_2 \in L^2(0,T;U_2),\ \exists u_1 \in L^2(0,T;U_1),\ \ \text{such that}\ \ \bar{C}\bar{\nabla}H_1u_1 + \bar{C}\bar{\nabla}H_2u_2 = 0,$$

i.e., if and only if

$$\forall u_2 \in L^2(0,T;U_2),\ \exists u \in L^2(0,T;U_1),\ \ \text{such that}\ \ \bar{C}\bar{\nabla}H_1u_2 = \bar{C}\bar{\nabla}H_2u,$$

where $u = -u_1 \in L^2(0,T;U_1)$, this is equivalent to saying that $\operatorname{Im}\left(\bar{C}\bar{\nabla}H_2\right) \subset \operatorname{Im}\left(\bar{C}\bar{\nabla}H_1\right)$.
- $2 \Leftrightarrow 3:$ In Lemma 3.1, we put

$$P = \bar{C}\bar{\nabla}H_2 \quad \text{and} \quad Q = \bar{C}\bar{\nabla}H_1,$$

where

$$H_1^* = \bar{B_1}^* S(\cdot - T) \quad \text{and} \quad H_2^* = \bar{B_2}^* S(\cdot - T).$$

Hence the result. □

Proposition 3.2 *The following properties are equivalent:*

1. B_1 *dominates* B_2 *weakly on* $[0,T]$ *with respect to* C.
2. $\operatorname{Im}\left(\bar{C}\bar{\nabla}H_2\right) \subset \overline{\operatorname{Im}\left(\bar{C}\bar{\nabla}H_1\right)}$.
3. $\ker\left(\bar{B_1}^* S(\cdot - T)\bar{\nabla}^*\bar{C}^*\right) \subset \ker\left(\bar{B_2}^* S(\cdot - T)\bar{\nabla}^*\bar{C}^*\right)$.

Proof.
- $1 \Leftrightarrow 2:$ B_1 dominates B_2 weakly on $[0,T]$ with respect to C if and only if

$$\forall \varepsilon > 0,\ \forall u_2 \in L^2(0,T;U_2),\ \exists u_1 \in L^2(0,T;U_1) \text{ such that } \|\bar{C}\bar{\nabla}H_1u_1 + \bar{C}\bar{\nabla}H_2u_2\|_{\mathcal{O}} < \varepsilon,$$

i.e., if and only if

$$\forall \varepsilon > 0,\ \forall u_2 \in L^2(0,T;U_2),\ \exists u \in L^2(0,T;U_1) \text{ such that } \|\bar{C}\bar{\nabla}H_2u_2 - \bar{C}\bar{\nabla}H_1u\|_{\mathcal{O}} < \varepsilon,$$

where $u = -u_1 \in L^2(0,T;U_1)$, this is equivalent to saying that

$$\operatorname{Im}(\bar{C}\bar{\nabla}H_2u_2) \subset \overline{\operatorname{Im}(\bar{C}\bar{\nabla}H_1)}.$$

- $2 \Rightarrow 3:$ Let $\sigma \in \ker\left(\bar{B_1}^* S(\cdot - T)\bar{\nabla}^*\bar{C}^*\right)$, we have

$$\operatorname{Im}(\bar{C}\bar{\nabla}H_2) \subset \overline{\operatorname{Im}(\bar{C}\bar{\nabla}H_1)},$$

then

$$\operatorname{Im}(\bar{C}\bar{\nabla}H_2) \subset \left[\ker\left(\bar{B_1}^* S(\cdot - T)\bar{\nabla}^*\bar{C}^*\right)\right]^{\perp},$$

hence

$$\langle \bar{C}\bar{\nabla}H_2u_2, \sigma\rangle_{\mathcal{O}\times\mathcal{O}^*} = 0, \quad \forall u_2 \in L^2(0,T;U_2),$$

then $\sigma \in [\mathrm{Im}(\bar{C}\bar{\nabla}H_2)]^{\perp}$, this gives $\sigma \in \ker\left(\bar{B_2}^* S(\cdot - T)\bar{\nabla}^*\bar{C}^*\right)$.
- $3 \Rightarrow 2$: We assume that

$$\ker\left(\bar{B_1}^* S(\cdot - T)\bar{\nabla}^*\bar{C}^*\right) \subset \ker\left(\bar{B_2}^* S(\cdot - T)\bar{\nabla}^*\bar{C}^*\right),$$

let $\sigma \in \ker(\bar{B_1}^* S(\cdot - T)\bar{\nabla}^*\bar{C}^*)$, then $\bar{B_2}^* S(\cdot - T)\bar{\nabla}^*\bar{C}^*\sigma = 0$, and

$$\langle \bar{C}\bar{\nabla}H_2u_2, \sigma\rangle_{\mathcal{O}\times\mathcal{O}^*} = 0,\ \forall u_2 \in L^2(0,T;U_2),$$

hence

$$\bar{C}\bar{\nabla}H_2u_2 \in \left[\ker\left(\bar{B_1}^* S(\cdot - T)\bar{\nabla}^*\bar{C}^*\right)\right]^{\perp} = \overline{\mathrm{Im}(\bar{C}\bar{\nabla}H_1)},\ \forall u_2 \in L^2(0,T;\bar{X}). \quad \square$$

Remark 3.1 Let us give the following properties and remarks:

1. In the case where C is the identity operator, we say that B_1 dominates B_2 exactly on $[0,T]$ (respectively weakly).
2. The exact domination with respect to C implies the weak domination with respect to C but the converse is not true.
3. If the system

$$\begin{cases} \dfrac{\partial^2 y}{\partial t^2}(x,t) = Ay(x,t) + B_1u_1(t), & \Omega\times]0,T[, \\ y(x,0) = y^0(x),\, \frac{\partial y_1}{\partial t}(x,0) = y^1(x) & \Omega, \\ y(\xi,t) = 0, & \partial\Omega\times]0,T[, \end{cases}$$

is gradient controllable exactly (respectively weakly), or equivalently to $\mathrm{Im}\left(\bar{\nabla}H_1\right) = \bar{X}$ [9] (respectively $\overline{\mathrm{Im}\left(\bar{C}\bar{\nabla}H_1\right)} = \bar{X}$), then B_1 dominates exactly (respectively weakly) any operator B_2 with respect to any output operator C.

4 Domination with respect to C and Actuators

This section focuses on the notions of actuators and sensors.
In the case where $U_1 = \mathbb{R}^{p_1}$ and $U_2 = \mathbb{R}^{p_2}$, i.e., the system (1) is excited by p_1 zone actuators $(\Omega_i, \mathsf{a}_i)_{1\le i\le p_1}$, where $\mathsf{a}_i \in L^2(\Omega_i), \Omega_i = \mathrm{supp}(\mathsf{a}_i) \subset \Omega$, for $i = 1,2,\ldots,p_1$, and by other p_2 zone actuators $\left(\tilde{\Omega}_i, \tilde{\mathsf{a}}_i\right)_{1\le i\le p_2}$, where $\tilde{\mathsf{a}}_i \in L^2\left(\tilde{\Omega}_i\right), \tilde{\Omega}_i = \mathrm{supp}(\tilde{\mathsf{a}}_i) \subset \Omega$, for $i = 1,2,\ldots,p_2$, the operators $\bar{B_1}$ and $\bar{B_2}$ are given by

$$\begin{aligned} \bar{B_1} \ :\ & \mathbb{R}^{p_1} \to \bar{X} \\ & u_1(t) = \left(u_1^1(t), u_1^2(t), \ldots, u_1^{p_1}(t)\right) \mapsto \bar{B_1}u_1(t) = \begin{pmatrix} 0 & \sum\limits_{i=1}^{p_1} \chi_{\Omega_i}(x)\mathsf{a}_i(x)u_1^i(t) \end{pmatrix}^{tr} \end{aligned}$$

and

$$\begin{aligned} \bar{B_2} \ :\ & \mathbb{R}^{p_2} \to \bar{X} \\ & u_2(t) = \left(u_2^1(t), u_2^2(t), \ldots, u_2^{p_2}(t)\right) \mapsto \bar{B_2}u_2(t) = \begin{pmatrix} 0 & \sum\limits_{i=1}^{p_2} \chi_{\tilde{\Omega}_i}(x)\tilde{\mathsf{a}}_i(x)u_2^i(t) \end{pmatrix}^{tr}, \end{aligned}$$

and their adjoints are, respectively,

$$\bar{B_1}^*(y_1, y_2) = \begin{pmatrix} \langle \mathtt{a}_1, y_2 \rangle_{\Omega_1} & \langle \mathtt{a}_2, y_2 \rangle_{\Omega_2} & \dots & \langle \mathtt{a}_{p_1}, y_2 \rangle_{\Omega_{p_1}} \end{pmatrix}^{tr} \in \mathbb{R}^{p_1},$$

$$\bar{B_2}^*(y_1, y_2) = \begin{pmatrix} \langle \tilde{\mathtt{a}}_1, y_2 \rangle_{\tilde{\Omega}_1} & \langle \tilde{\mathtt{a}}_2, y_2 \rangle_{\tilde{\Omega}_2} & \dots & \langle \tilde{\mathtt{a}}_{p_2}, y_2 \rangle_{\tilde{\Omega}_{p_2}} \end{pmatrix}^{tr} \in \mathbb{R}^{p_2}.$$

Corollary 4.1 *$(\Omega_i, \mathtt{a}_i)_{1 \le i \le p_1}$ dominates $\left(\tilde{\Omega}_i, \tilde{\mathtt{a}}_i\right)_{1 \le i \le p_2}$ exactly on $[0, T]$ with respect to C if and only if there exists $\gamma > 0$ such that for all σ in $\mathcal{O}^*$, we have*

$$\sum_{i=1}^{p_2} \int_0^T \left\langle \tilde{\mathtt{a}}_i, W_2(s-T)\bar{\nabla}^* \bar{C}^* \sigma \right\rangle_{\tilde{\Omega}_i}^2 \, \mathrm{d}s \le \gamma \sum_{i=1}^{p_1} \int_0^T \left\langle \mathtt{a}_i, W_2(s-T)\bar{\nabla}^* \bar{C}^* \sigma \right\rangle_{\Omega_i}^2 \, \mathrm{d}s.$$

Proof. According to Proposition 3.1, B_1 dominates B_2 exactly on $[0, T]$ if and only if there exists $\gamma > 0$ such that for all σ in $\mathcal{O}^*$, we have

$$\left\| \bar{B_2}^* S(\cdot - T)\bar{\nabla}^* \bar{C}^* \sigma \right\|_{L^2(0,T;\mathbb{R}^{p_2})}^2 \le \gamma \left\| \bar{B_1}^* S(\cdot - T)\bar{\nabla}^* \bar{C}^* \sigma \right\|_{L^2(0,T;\mathbb{R}^{p_1})}^2.$$

Firstly, we have

$$S(\cdot - T)\bar{\nabla}^* \bar{C}^* \sigma = \begin{pmatrix} W_1(\cdot - T)\bar{\nabla}^* \bar{C}^* \sigma \\ W_2(\cdot - T)\bar{\nabla}^* \bar{C}^* \sigma \end{pmatrix},$$

and we have then

$$\left\| \bar{B_2}^* S(\cdot - T)\bar{\nabla}^* \bar{C}^* \sigma \right\|_{L^2(0,T;\mathbb{R}^{p_2})}^2 = \sum_{i=1}^{p_2} \int_0^T \left\langle \tilde{\mathtt{a}}_i, W_2(s-T)\bar{\nabla}^* \bar{C}^* \sigma \right\rangle_{\tilde{\Omega}_i}^2 \, \mathrm{d}s$$

and

$$\left\| \bar{B_1}^* S(\cdot - T)\bar{\nabla}^* \bar{C}^* \sigma \right\|_{L^2(0,T;\mathbb{R}^{p_1})}^2 = \sum_{i=1}^{p_1} \int_0^T \left\langle \mathtt{a}_i, W_2(s-T)\bar{\nabla}^* \bar{C}^* \sigma \right\rangle_{\Omega_i}^2 \, \mathrm{d}s.$$

Hence the result. $\square$

Corollary 4.2 *$(\Omega_i, \mathtt{a}_i)_{1 \le i \le p_1}$ dominates $\left(\tilde{\Omega}_i, \tilde{\mathtt{a}}_i\right)_{1 \le i \le p_2}$ exactly on $[0, T]$ with respect to C if and only if there exists $\gamma > 0$ such that for all σ in $\mathcal{O}^*$, we have*

$$\sum_{i=1}^{p_2} \int_0^T \left[\sum_{m \ge 1} \sqrt{-\lambda_m} \sin\left(\sqrt{-\lambda_m}(T-s)\right) \sum_{j=1}^{r_m} \left\langle C^* \sigma, \nabla w_{m_j} \right\rangle_{(L^2(\Omega))^n} \left\langle \tilde{\mathtt{a}}_i, w_{m_j} \right\rangle_{\tilde{\Omega}_i} \right]^2 \mathrm{d}s \le$$

$$\gamma \sum_{i=1}^{p_1} \int_0^T \left[\sum_{m \ge 1} \sqrt{-\lambda_m} \sin\left(\sqrt{-\lambda_m}(T-s)\right) \sum_{j=1}^{r_m} \left\langle C^* \sigma, \nabla w_{m_j} \right\rangle_{(L^2(\Omega))^n} \left\langle \mathtt{a}_i, w_{m_j} \right\rangle_{\Omega_i} \right]^2 \mathrm{d}s.$$

Proof. We have

$$\begin{aligned}
&\sum_{i=1}^{p_1}\int_0^T \left\langle \mathsf{a}_i, W_2(s-T)\bar{\nabla}^*\bar{C}^*\sigma\right\rangle_{\Omega_i}^2 \, \mathrm{d}s \\
=&\sum_{i=1}^{p_1}\int_0^T \left\langle \chi_{\Omega_i}\mathsf{a}_i, \sum_{m\geq 1}\sum_{j=1}^{r_m} -\sqrt{-\lambda_m}\left\langle \nabla^* C^*\sigma, w_{m_j}\right\rangle_\Omega \sin\left(\sqrt{-\lambda_m}(s-T)\right) w_{m_j}\right\rangle_\Omega^2 \mathrm{d}s \\
=&\sum_{i=1}^{p_1}\int_0^T \left[\sum_{m\geq 1}\sqrt{-\lambda_m}\sin\left(\sqrt{-\lambda_m}(T-s)\right)\sum_{j=1}^{r_m}\left\langle C^*\sigma, \nabla w_{m_j}\right\rangle_{(L^2(\Omega))^n}\left\langle \mathsf{a}_i, w_{m_j}\right\rangle_{\Omega_i}\right]^2 \mathrm{d}s
\end{aligned}$$

and

$$\begin{aligned}
&\sum_{i=1}^{p_2}\int_0^T \left\langle \tilde{\mathsf{a}}_i, W_2(s-T)\bar{\nabla}^*\bar{C}^*\sigma\right\rangle_{\tilde{\Omega}_i}^2 \, \mathrm{d}s \\
=&\sum_{i=1}^{p_2}\int_0^T \left\langle \chi_{\tilde{\Omega}_i}\tilde{\mathsf{a}}_i, \sum_{m\geq 1}\sum_{j=1}^{r_m} -\sqrt{-\lambda_m}\left\langle \nabla^* C^*\sigma, w_{m_j}\right\rangle_\Omega \sin\left(\sqrt{-\lambda_m}(s-T)\right) w_{m_j}\right\rangle_\Omega^2 \mathrm{d}s \\
=&\sum_{i=1}^{p_2}\int_0^T \left[\sum_{m\geq 1}\sqrt{-\lambda_m}\sin\left(\sqrt{-\lambda_m}(T-s)\right)\sum_{j=1}^{r_m}\left\langle C^*\sigma, \nabla w_{m_j}\right\rangle_{(L^2(\Omega))^n}\left\langle \tilde{\mathsf{a}}_i, w_{m_j}\right\rangle_{\tilde{\Omega}_i}\right]^2 \mathrm{d}s.
\end{aligned}$$

Hence, the result follows immediately from Corollary 4.1. □

Corollary 4.3 *$(\Omega_i, \mathsf{a}_i)_{1\leq i\leq p_1}$ dominates $\left(\tilde{\Omega}_i, \tilde{\mathsf{a}}_i\right)_{1\leq i\leq p_2}$ weakly on $[0,T]$ with respect to C if and only if*

$$\begin{aligned}
&\sum_{j=1}^{r_m}\langle C^*\sigma, \nabla w_{m_j}\rangle_{(L^2(\Omega))^n}\langle \mathsf{a}_i, w_{m_j}\rangle_{\Omega_i} = 0,\ \forall i\in\{1,2,\cdots,p_1\},\ \forall m\geq 1 \\
\Rightarrow &\sum_{j=1}^{r_m}\langle C^*\sigma, \nabla w_{m_j}\rangle_{(L^2(\Omega))^n}\langle \tilde{\mathsf{a}}_i, w_{m_j}\rangle_{\tilde{\Omega}_i} = 0,\ \forall i\in\{1,2,\cdots,p_2\},\ \forall m\geq 1.
\end{aligned}$$

Proof. We assume that $(\Omega_i, \mathsf{a}_i)_{1\leq i\leq p_1}$ dominates $\left(\tilde{\Omega}_i, \tilde{\mathsf{a}}_i\right)_{1\leq i\leq p_2}$ weakly on $[0,T]$ with respect to C and

$$\sum_{j=1}^{r_m}\langle C^*\sigma, \nabla w_{m_j}\rangle_{(L^2(\Omega))^n}\langle \mathsf{a}_i, w_{m_j}\rangle_{\Omega_i} = 0,\ \forall i\in\{1,2,\cdots,p_1\},\ \forall m\geq 1.$$

Since $\bar{B_1}^*S(\cdot-T)\bar{\nabla}^*\bar{C}^*\sigma$ is equal to

$$\left(\sum_{m\geq 1}\sqrt{-\lambda_m}\sin\left(\sqrt{-\lambda_m}(T-\cdot)\right)\sum_{j=1}^{r_m}\left\langle C^*\sigma, \nabla w_{m_j}\right\rangle_{(L^2(\Omega))^n}\left\langle \mathsf{a}_i, w_{m_j}\right\rangle_{\Omega_i}\right)_{1\leq i\leq p_1},$$

one has

$$\sigma\in\ker\left(\bar{B_1}^*S(\cdot-T)\bar{\nabla}^*\bar{C}^*\right),$$

hence

$$\sigma \in \ker\left(\bar{B_2}^* S(\cdot - T)\bar{\nabla}^* \bar{C}^*\right),$$

i.e., for all $i \in \{1, \ldots, p_2\}$, we have

$$\sum_{m\geq 1} \sqrt{-\lambda_m} \sin\left(\sqrt{-\lambda_m}(T - \cdot)\right) \sum_{j=1}^{r_m} \left\langle C^*\sigma, \nabla w_{m_j} \right\rangle_{(L^2(\Omega))^n} \left\langle \tilde{\mathtt{a}}_i, w_{m_j} \right\rangle_{\tilde{\Omega}_i} = 0.$$

The set $\left(\sin(\sqrt{-\lambda_m}(T - .))\right)_{m\geq 1}$ forms a complete orthogonal set of $L^2(0, T)$, then

$$\sum_{j=1}^{r_m} \left\langle C^*\sigma, \nabla w_{m_j} \right\rangle_{(L^2(\Omega))^n} \left\langle \tilde{\mathtt{a}}_i, w_{m_j} \right\rangle_{\tilde{\Omega}_i} = 0, \ \forall i \in \{1, \ldots, p_2\}, \ \forall m \geq 1.$$

Conversely, we assume that

$$\begin{aligned} &\sum_{j=1}^{r_m} \langle C^*\sigma, \nabla w_{m_j} \rangle_{(L^2(\Omega))^n} \langle \mathtt{a}_i, w_{m_j} \rangle_{\Omega_i} = 0, \ \forall i \in \{1, 2, \cdots, p_1\}, \ \forall m \geq 1 \\ &\Rightarrow \sum_{j=1}^{r_m} \langle C^*\sigma, \nabla w_{m_j} \rangle_{(L^2(\Omega))^n} \langle \tilde{\mathtt{a}}_i, w_{m_j} \rangle = 0, \ \forall i \in \{1, 2, \cdots, p_2\}, \ \forall m \geq 1, \end{aligned}$$

we have

$$\begin{aligned} &\sigma \in \ker\left(\bar{B_1}^* S(\cdot - T)\bar{\nabla}^* \bar{C}^*\right) \\ \Rightarrow &\sum_{j=1}^{r_m} \langle C^*\sigma, \nabla w_{m_j} \rangle_{(L^2(\Omega))^n} \langle \mathtt{a}_i, w_{m_j} \rangle_{\Omega_i} = 0, \ \forall i \in \{1, 2, \cdots, p_1\}, \ \forall m \geq 1 \\ \Rightarrow &\sum_{j=1}^{r_m} \langle C^*\sigma, \nabla w_{m_j} \rangle_{(L^2(\Omega))^n} \langle \tilde{\mathtt{a}}_i, w_{m_j} \rangle_{\tilde{\Omega}_i} = 0, \ \forall i \in \{1, 2, \cdots, p_2\}, \ \forall m \geq 1 \\ \Rightarrow &\ \sigma \in \ker\left(\bar{B_2}^* S(\cdot - T)\bar{\nabla}^* \bar{C}^*\right), \end{aligned}$$

then $(\Omega_i, \mathtt{a}_i)_{1\leq i\leq p_1}$ dominates $\left(\tilde{\Omega}_i, \tilde{\mathtt{a}}_i\right)_{1\leq i\leq p_2}$ weakly on $[0, T]$ with respect to C. $\square$

In order to give it a characterization, we use the following definitions: for $m \geq 1$,
- The matrix A_m of order $(p_1 \times r_m)$ is defined by

$$A_m = \left(\langle \mathtt{a}_i, w_{m_j} \rangle_{\Omega_i}\right)_{ij}, \quad 1 \leq i \leq p_1 \quad \text{and} \quad 1 \leq j \leq r_m.$$

- The matrix $\tilde{A}_m$ of order $(p_2 \times r_m)$ is defined by

$$\tilde{A}_m = \left(\langle \tilde{\mathtt{a}}_i, w_{m_j} \rangle_{\tilde{\Omega}_i}\right)_{ij}, \quad 1 \leq i \leq p_2 \quad \text{and} \quad 1 \leq j \leq r_m.$$

Corollary 4.4 *$(\Omega_i, \mathtt{a}_i)_{1\leq i\leq p_1}$ dominates $\left(\tilde{\Omega}_i, \tilde{\mathtt{a}}_i\right)_{1\leq i\leq p_2}$ weakly on $[0, T]$ with respect to C if and only if*

$$\bigcap_{m\geq 1} \ker\left(A_m g_m\right) \subset \bigcap_{m\geq 1} \ker\left(\tilde{A}_m g_m\right).$$

Here, for $\sigma \in \mathbb{R}^q$ and $m \geq 1$,

$$g_m(\sigma) = \left(\ \langle C^*\sigma, \nabla w_{m_i} \rangle_{(L^2(\Omega))^n} \ \right)_{1\leq i\leq r_m}.$$

Proof. We assume that $(\Omega_i, \mathtt{a}_i)_{1\leq i\leq p_1}$ dominates $\left(\tilde{\Omega}_i, \tilde{\mathtt{a}}_i\right)_{1\leq i\leq p_2}$ weakly on $[0,T]$ with respect to C and $\sigma \in \bigcap\limits_{m\geq 1} \ker(A_m g_m)$, then $A_m g_m(\sigma) = 0$, $\forall m \geq 1$. Since

$$A_m g_m(\sigma) = \begin{pmatrix} \sum\limits_{j=1}^{r_m} \left\langle C^*\sigma, \nabla w_{m_j}\right\rangle_{(L^2(\Omega))^n} \left\langle \mathtt{a}_1, w_{m_j}\right\rangle_{\Omega_1} \\ \sum\limits_{j=1}^{r_m} \left\langle C^*\sigma, \nabla w_{m_j}\right\rangle_{(L^2(\Omega))^n} \left\langle \mathtt{a}_2, w_{m_j}\right\rangle_{\Omega_2} \\ \vdots \\ \sum\limits_{j=1}^{r_m} \left\langle C^*\sigma, \nabla w_{m_j}\right\rangle_{(L^2(\Omega))^n} \left\langle \mathtt{a}_{p_1}, w_{m_j}\right\rangle_{\Omega_{p_1}} \end{pmatrix}, \quad \forall m \geq 1,$$

one has

$$\sum_{j=1}^{r_m} \left\langle C^*\sigma, \nabla w_{m_j}\right\rangle_{(L^2(\Omega))^n} \left\langle \mathtt{a}_i, w_{m_j}\right\rangle_{\Omega_i} = 0,\ \forall i \in \{1,\ldots,p_1\},\ \forall m \geq 1,$$

hence

$$\sum_{j=1}^{r_m} \left\langle C^*\sigma, \nabla w_{m_j}\right\rangle_{(L^2(\Omega))^n} \left\langle \tilde{\mathtt{a}}_i, w_{m_j}\right\rangle_{\tilde{\Omega}_i} = 0,\ \forall i \in \{1,\ldots,p_2\},\ \forall m \geq 1,$$

i.e.,

$$\tilde{A}_m g_m(\sigma) = 0,\ \forall m \geq 1,$$

and therefore $\sigma \in \bigcap\limits_{m\geq 1} \ker\left(\tilde{A}_m g_m\right)$. $\square$

Now, in the case where $\mathcal{O} = \mathbb{R}^q$, i.e., the output of the system (4) is given by q sensors $(D_i, \mathtt{s}_i)_{1\leq i\leq q}$, where $\mathtt{s}_i \in L^2(D_i)$, $D_i = \operatorname{supp}(\mathtt{s}_i) \subset \Omega$ for $i = 1, 2, \ldots, q$, and $D_i \cap D_j = \emptyset$ for $i \neq j$, the operator $\overline{C} = \begin{pmatrix} C & 0 \end{pmatrix}$ is given by

$$\begin{aligned} C \quad : \quad & \left(L^2(\Omega)\right)^n \to \mathbb{R}^q \\ & y \mapsto Cy = \Big(\sum_{i=1}^{n} \langle \mathtt{s}_1, y_i\rangle_{D_1} \quad \sum_{i=1}^{n} \langle \mathtt{s}_2, y_i\rangle_{D_2} \quad \cdots \quad \sum_{i=1}^{n} \langle \mathtt{s}_q, y_i\rangle_{D_q}\Big)^{tr}, \end{aligned}$$

and its adjoint is $\overline{C}^* = \begin{pmatrix} C^* & 0 \end{pmatrix}^{tr}$, and for $\sigma = (\sigma_1, \sigma_2, \ldots, \sigma_q) \in \mathbb{R}^q$,

$$C^*\sigma = \Big(\sum_{i=1}^{q} \chi_{D_i}(x)\sigma_i \mathtt{s}_i(x) \quad \sum_{i=1}^{q} \chi_{D_i}(x)\sigma_i \mathtt{s}_i(x) \quad \ldots \quad \sum_{i=1}^{q} \chi_{D_i}(x)\sigma_i \mathtt{s}_i(x)\Big)^{tr}. \tag{5}$$

In this case, the exact and weak dominations with respect to the gradient observation are equivalent. The following result gives a necessary and sufficient condition for domination with respect to the sensors.

Corollary 4.5 *$(\Omega_i, \mathtt{a}_i)_{1\leq i\leq p_1}$ dominates $\left(\tilde{\Omega}_i, \tilde{\mathtt{a}}_i\right)_{1\leq i\leq p_2}$ on $[0,T]$ with respect to the sensors $(D_i, \mathtt{s}_i)_{1\leq i\leq q}$ if and only if there exists $\gamma > 0$ such that for all σ in $\mathbb{R}^q$, we have*

$$\begin{aligned} &\sum_{i=1}^{p_2} \int_0^T \Big[\sum_{m\geq 1} \sqrt{-\lambda_m} \sin(\sqrt{-\lambda_m}(T-s)) \sum_{j=1}^{r_m}\sum_{l=1}^{q}\sum_{k=1}^{n} \sigma_l \langle \mathtt{s}_l, \frac{\partial w_{m_j}}{\partial x_k}\rangle_{D_l} \langle \tilde{\mathtt{a}}_i, w_{m_j}\rangle_{\tilde{\Omega}_i}\Big]^2 \mathrm{d}s \\ \leq \gamma &\sum_{i=1}^{p_1} \int_0^T \Big[\sum_{m\geq 1} \sqrt{-\lambda_m} \sin(\sqrt{-\lambda_m}(T-s)) \sum_{j=1}^{r_m}\sum_{l=1}^{q}\sum_{k=1}^{n} \sigma_l \langle \mathtt{s}_l, \frac{\partial w_{m_j}}{\partial x_k}\rangle_{D_l} \langle \mathtt{a}_i, w_{m_j}\rangle_{\Omega_i}\Big]^2 \mathrm{d}s. \end{aligned}$$

Proof. It suffices to use Corollary 4.2 and the relation (5). □

In order to give it another characterization, we pose the following definition: for $m \geq 1$, -The matrix S_m of order $(q \times r_m)$ is defined by

$$S_m = \left(\sum_{k=1}^{n} \left\langle \mathtt{s}_i, \frac{\partial w_{m_j}}{\partial x_k} \right\rangle_{D_i} \right)_{ij}, \quad 1 \leq i \leq q \quad \text{and} \quad 1 \leq j \leq r_m.$$

Corollary 4.6 $(\Omega_i, \mathtt{a}_i)_{1 \leq i \leq p_1}$ *dominates* $\left(\tilde{\Omega}_i, \tilde{\mathtt{a}}_i\right)_{1 \leq i \leq p_2}$ *on* $[0,T]$ *with respect to the sensors* $(D_i, \mathtt{s}_i)_{1 \leq i \leq q}$ *if and only if*

$$\bigcap_{m \geq 1} \ker\left(A_m S_m^{tr}\right) \subset \bigcap_{m \geq 1} \ker\left(\tilde{A}_m S_m^{tr}\right).$$

Proof. Let $\sigma \in \mathbb{R}^q$, we have

$$\sigma \in \bigcap_{m \geq 1} \ker\left(A_m S_m^{tr}\right) \Leftrightarrow \sigma \in \ker\left(A_m S_m^{tr}\right),\ \forall m \geq 1 \Leftrightarrow A_m S_m^{tr} \sigma = 0,\ \forall m \geq 1$$
$$\Leftrightarrow \sum_{l=1}^{q} \sum_{j=1}^{r_m} \sum_{k=1}^{n} \sigma_l \langle \mathtt{s}_l, \frac{\partial w_{m_j}}{\partial x_k} \rangle_{D_l} \left\langle \mathtt{a}_i, w_{m_j} \right\rangle_{\Omega_i} = 0,\ \forall i \in \{1,2,\ldots,p_1\},\ \forall m \geq 1$$
$$\Leftrightarrow \sum_{j=1}^{r_m} \left\langle C^* \sigma, \nabla w_{m_j} \right\rangle_{(L^2(\Omega))^n} \left\langle \mathtt{a}_i, w_{m_j} \right\rangle_{\Omega_i} = 0,\ \forall i \in \{1,2,\ldots,p_1\},\ \forall m \geq 1$$
$$\Leftrightarrow (A_m g_m)(\sigma) = 0, \forall m \geq 1 \Leftrightarrow \sigma \in \ker(A_m g_m), \forall m \geq 1 \Leftrightarrow \sigma \in \bigcap_{m \geq 1} \ker(A_m g_m),$$

this gives

$$\bigcap_{m \geq 1} \ker\left(A_m S_m^{tr}\right) = \bigcap_{m \geq 1} \ker(A_m g_m).$$

By the same method, we obtain

$$\bigcap_{m \geq 1} \ker\left(\tilde{A}_m S_m^{tr}\right) = \bigcap_{m \geq 1} \ker\left(\tilde{A}_m g_m\right).$$

From Corollary 4.4, we get the result. □

Corollary 4.7 $(\Omega_i, \mathtt{a}_i)_{1 \leq i \leq p_1}$ *dominates* $\left(\tilde{\Omega}_i, \tilde{\mathtt{a}}_i\right)_{1 \leq i \leq p_2}$ *on* $[0,T]$ *with respect to the sensors* $(D_i, \mathtt{s}_i)_{1 \leq i \leq q}$ *if and only if*

$$\sum_{j=1}^{r_m} \sum_{k=1}^{n} \langle \mathtt{s}_l, \frac{\partial w_{m_j}}{\partial x_k} \rangle_{D_l} \left\langle \mathtt{a}_i, w_{m_j} \right\rangle_{\Omega_i} = 0,\ \forall l \in \{1,2,\ldots,q\},\ \forall i \in \{1,2,\ldots,p_1\},\ \forall m \geq 1$$
$$\Rightarrow \sum_{j=1}^{r_m} \sum_{k=1}^{n} \langle \mathtt{s}_l, \frac{\partial w_{m_j}}{\partial x_k} \rangle_{D_l} \left\langle \tilde{\mathtt{a}}_i, w_{m_j} \right\rangle_{\tilde{\Omega}_i} = 0,\ \forall l \in \{1,2,\ldots,q\},\ \forall i \in \{1,2,\ldots,p_2\},\ \forall m \geq 1.$$

Proof. It suffices to use Corollary 4.3. □

Corollary 4.8 *If there exists* $m_0 \geq 1$ *such that* $\operatorname{rank}\left(A_{m_0} S_{m_0}^{tr}\right) = q$, *then* $(\Omega_i, \mathsf{a}_i)_{1\leq i\leq p_1}$ *dominates any zone actuators* $\left(\tilde{\Omega}_i, \tilde{\mathsf{a}}_i\right)_{1\leq i\leq p_2}$ *on* $[0,T]$ *with respect to the sensors* $(D_i, \mathsf{s}_i)_{1\leq i\leq q}$.

Proof. If there exists $m_0 \geq 1$ such that $\operatorname{rank}\left(A_{m_0} S_{m_0}^{tr}\right) = q$, and the matrix $\left(A_{m_0} S_{m_0}^{tr}\right)$ is of order $(p \times q)$, then from the rank-nullity theorem, we have

$$\operatorname{rank}\left(A_{m_0} S_{m_0}^{tr}\right) + \dim\left(\ker\left(A_{m_0}^1 S_{m_0}^{tr}\right)\right) = q,$$

then $\dim\left(\ker\left(A_{m_0} S_{m_0}^{tr}\right)\right) = 0$, which is equivalent to $\ker\left(A_{m_0} S_{m_0}^{tr}\right) = \{0\}$, then

$$\bigcap_{m\geq 1} \ker\left(A_m S_m^{tr}\right) = \{0\}.$$

From Corollary 4.6, the operator $(\Omega_i, \mathsf{a}_i)_{1\leq i\leq p_1}$ dominates any zone actuators $\left(\tilde{\Omega}_i, \tilde{\mathsf{a}}_i\right)_{1\leq i\leq p_2}$ with respect to the sensors $(D_i, \mathsf{s}_i)_{1\leq i\leq q}$. □

Corollary 4.9 *If there exists* $m_0 \geq 1$ *such that*

$$\operatorname{rank}\left(A_{m_0}\right) = r_{m_0} \quad \text{and} \quad \operatorname{rank}\left(S_{m_0}^{tr}\right) = q,$$

then $(\Omega_i, \mathsf{a}_i)_{1\leq i\leq p_1}$ *dominates any zone actuators* $\left(\tilde{\Omega}_i, \tilde{\mathsf{a}}_i\right)_{1\leq i\leq p_2}$ *on* $[0,T]$ *with respect to the sensors* $(D_i, \mathsf{s}_i)_{1\leq i\leq q}$.

Proof. We suppose that

$$\operatorname{rank}\left(S_{m_0}^{tr}\right) = q \text{ and } \operatorname{rank}\left(A_{m_0}\right) = r_{m_0}.$$

The matrix $\left(S_{m_0}^{tr}\right)$ is of order $(r_{m_0} \times q)$, then from the rank-nullity theorem, we have

$$\operatorname{rank}\left(S_{m_0}^{tr}\right) + \dim\left(\ker\left(S_{m_0}^{tr}\right)\right) = q,$$

then

$$\dim\left(\ker\left(S_{m_0}^{tr}\right)\right) = 0,$$

which is equivalent to

$$\ker\left(S_{m_0}^{tr}\right) = \{0\}. \tag{6}$$

Similarly, the matrix (A_{m_0}) is of order $(p \times r_{m_0})$, then from the rank-nullity theorem, we have

$$\operatorname{rank}\left(A_{m_0}\right) + \dim\left(\ker\left(A_{m_0}\right)\right) = r_{m_0},$$

then

$$\dim\left(\ker\left(A_{m_0}\right)\right) = 0,$$

which is equivalent to

$$\ker\left(A_{m_0}\right) = \{0\}. \tag{7}$$

On the other hand, if $\sigma \in \ker\left(A_{m_0} S_{m_0}^{tr}\right)$, then $\left(A_{m_0} S_{m_0}^{tr}\right)\sigma = 0$, which gives

$$A_{m_0}\left(S_{m_0}^{tr}\sigma\right) = 0.$$

From (6), we obtain $S^{tr}_{m_0}\sigma = 0$, and from (7), we obtain $\sigma = 0$. Then

$$\ker\left(A_{m_0} S^{tr}_{m_0}\right) = \{0\}.$$

From Corollary 4.6, $(\Omega_i, \mathtt{a}_i)_{1\leq i\leq p_1}$ dominates any zone actuators $\left(\tilde{\Omega}_i, \tilde{\mathtt{a}}_i\right)_{1\leq i\leq p_2}$ with respect to the sensors $(D_i, \mathtt{s}_i)_{1\leq i\leq q}$. $\square$

5 Application to the Wave Equation

We consider a hyperbolic system described by the following wave equation:

$$\begin{cases} \dfrac{\partial^2 y}{\partial t^2}(x,t) = \Delta y(x,t) + \sum\limits_{i=1}^{p_1} \chi_{\Omega_i} \mathtt{a}_i(x) u_1^i(t) + \sum\limits_{i=1}^{p_2} \chi_{\tilde{\Omega}_i} \tilde{\mathtt{a}}_i(x) u_2^i(t), & \Omega\times]0,T[, \\ y(x,0) = y^0(x),\ \dfrac{\partial y}{\partial t}(x,0) = y^1(x), & \Omega, \\ y(\xi,t) = 0, & \partial\Omega\times]0,T[, \end{cases} \tag{8}$$

where $\Omega \subset \mathbb{R}^n$ is an open and bounded domain with a sufficiently regular boundary, and we consider the system (8) augmented by the output equation

$$z(t) = \left(\sum_{i=1}^{n} \langle \mathtt{s}_1, \frac{\partial y}{\partial x_i}(\cdot,t)\rangle_{D_1} \quad \sum_{i=1}^{n} \langle \mathtt{s}_2, \frac{\partial y}{\partial x_i}(\cdot,t)\rangle_{D_2} \quad \dots \quad \sum_{i=1}^{n} \langle \mathtt{s}_q, \frac{\partial y}{\partial x_i}(\cdot,t)\rangle_{D_q} \right)^{tr}.$$

There exists an orthonormal basis of eigenfunctions $\left(w_{m_j}\right)_{\substack{m\geq 1\\ 1\leq j\leq r_m}}$ of Δ associated to eigenvalues $(\lambda_m)_{m\geq 1}$ with multiplicity r_m and given by $\Delta w_{m_j} = \lambda_m w_{m_j}$, $\forall m \geq 1$ and $j = 1, 2, \dots, r_m$.
For $\Omega =]0,1[$, the eigenfunctions of Δ are

$$w_m(x) = \sqrt{2}\sin(m\pi x),\ \forall m \geq 1,$$

and the simple associated eigenvalues are

$$\lambda_m = -m^2\pi^2,\ \forall m \geq 1.$$

The semigroup generated by Δ is

$$S(t)\begin{pmatrix} y_1 \\ y_2 \end{pmatrix} = \begin{pmatrix} \sum\limits_{m\geq 1} (\langle y_1, w_m\rangle_\Omega \cos(m\pi t) + \dfrac{1}{m\pi}\langle y_2, w_m\rangle_\Omega \sin(m\pi t)) w_m \\ \sum\limits_{m\geq 1} (-m\pi\langle y_1, w_m\rangle_\Omega \sin(m\pi t) + \langle y_2, w_m\rangle_\Omega \cos(m\pi t)) w_m \end{pmatrix}.$$

If $D = \operatorname{supp}(\mathtt{s}) \subset]0,1[$, ($q = 1$ and $\mathcal{O} = \mathbb{R}$), the system is augmented with the following output equation:

$$z(t) = \langle \mathtt{s}, \frac{\partial y}{\partial x}(\cdot,t)\rangle_D,$$

and the system (8) is excited by the zone actuators $(\Omega_1, \mathtt{a}_1)$ and $(\tilde{\Omega}_1, \tilde{\mathtt{a}}_1)$ such that $\Omega_1 = \operatorname{supp}(\mathtt{a}_1) \subset]0,1[$ and $\tilde{\Omega}_1 = \operatorname{supp}(\tilde{\mathtt{a}}_1) \subset]0,1[$.

Using Corollary 4.7, we deduce the following characterization.

Proposition 5.1 (Ω_1, a) *dominates* $\left(\tilde{\Omega}_1, \tilde{a}\right)$ *on* $[0, T]$ *with respect to the sensors* $(D, \mathtt{s})$ *if and only if*

$$\left(\langle \mathtt{s}, w'_m \rangle_D \langle a, w_m \rangle_{\Omega_1} = 0, \ \forall m \geq 1 \right) \Rightarrow \left(\langle \mathtt{s}, w'_m \rangle_D \langle \tilde{a}, w_m \rangle_{\tilde{\Omega}_1} = 0, \ \forall m \geq 1 \right).$$

If there exists m_0 such that $\left\langle \mathtt{s}, w'_{m_0} \right\rangle_D \neq 0$, then, from Corollary 4.9, an actuator (Ω_1, a_1) dominates $\left(\tilde{\Omega}_1, \tilde{a}_1\right)$ if

$$\langle a_1, w_{m_0} \rangle_{\Omega_1} = \int_{\Omega_1} a_1 \left(x\right) \sin\left(m_0 \pi x\right) \mathrm{d}x \neq 0.$$

Thus, for example, if $\mathtt{a}_1 = w_{m_0}$, then the actuator $(\Omega_1, \mathtt{a}_1)$ dominates any zone actuator $\left(\tilde{\Omega}_1, \tilde{\mathtt{a}}_1\right)$ weakly on $[0, T]$ with respect to the considered sensor $(D, \mathtt{s})$.

6 Conclusion

In this paper, important results and general properties related to the notion of domination of a general class of controlled and observed hyperbolic systems with respect to gradient observation are obtained. The role of actuators and sensors is also examined. The obtained results are related to the choice of convenient efficient actuators. An application to the case of a one dimension wave equation was conducted, it illustrates the notion proposed and confirms the results obtained. Many questions remain open, namely some cases of linear and nonlinear systems. These questions are still under consideration and the results will appear in separate papers.

References

[1] L. Afifi, E. M. Magri and A. El Jai. Weak and Exact Domination in Distributed Systems. *International Journal of Applied Mathematics and Computer Science* **20** (3) (2010) 419–426.

[2] L. Afifi, N. Amimi, A. El Jai and E. M. Magri. Regional Domination in Distributed Systems. *Applied Mathematical Sciences* **6** (19) (2012) 913–924.

[3] L. Afifi, M. Joundi, N. Amimi and M. Bahadi. Asymptotic Classification of Distributed Linear Systems. *Applied Mathematical Sciences* **7** (51) (2013) 2537–2554.

[4] L. Afifi, M. Joundi, E. M. Magri and A. El Jai. An Extended Regional Classification of Distributed Systems. *International Journal of Mathematical Analysis* **7** (28) (2013) 1363–1377.

[5] L. Afifi, M. Joundi, E. M. Magri and A. El Jai. Domination in Controlled and Observed Distributed Parameter Systems. *Intelligent Control and Automation* **4** (2) (2013) 217–226.

[6] L. Afifi, M. Joundi and E. M. Magri. Domination in Hyperbolic Distributed Systems. *International Journal of Mathematical Analysis* **7** (56) (2013) 2765–2780.

[7] R. Al-Saphory, N. J. Al-Jawari and I. Al-Qaisi. Regional Gradient Detectability for Infinite Dimensional Systems. *Tikrit Journal of Pure Science* **15** (2) (2010) 100–104.

[8] M. Bohner, C. Duque and H. Leiva. Controllability of Dynamic Equations with Memory. *Nonlinear Dynamics and Systems Theory* **22** (5) (2022) 489–502.

[9] H. Bourray, A. Boutoulout and I. El Harraki. Gradient Controllability for Hyperbolic Systems. *Information Sciences Letters* **3** (1) (2014) 11–19.

[10] A. El Jai, M. C. Simon and E. Zerrik. Regional Observability and Sensor Structures. *Sensors and Actuators A: Physical* **39** (2) (1993) 95–102.

[11] I. El Harraki, A. Khazarib and A. Boutoulout. Exact Gradient Controllability with Strategic Actuators. *Automatic Control and Computer Sciences* **51** (6) (2017) 377–390.

[12] M. Jidou Khayar, A. Brouri and M. Ouzahra. Exact Controllability of the Reaction-Diffusion Equation under Bilinear Control. *Nonlinear Dynamics and Systems Theory* **22** (5) (2022) 538–549.

[13] J. L. Lions. *Contrôlabilité Exacte. Perturbation et Stabilisation des Systems Distribués, Tome1.* Masson, Paris, 1988.

[14] S. Rekkab, S. Benhadid and R. Al-Saphory. An Asymptotic Analysis of the Gradient Remediability Problem for Disturbed Distributed Linear Systems. *Baghdad Science Journal* **19** (6) (2022) 1623–1635.

[15] E. Zerrik and H. Bourray. Gradient Observability for Diffusion Systems. *International Journal of Applied Mathematics and Computer Science* **13** (2) (2003) 139–150.

Nonlinear Dynamics and Systems Theory, **25** (2) (2025) 128–143

Spectral Density Estimation in Time Series Analysis for Dynamical Systems

A. Chahad[1], M. Bassoudi[2*] and Z. Chikr Elmezouar[3]

[1] *Department of Agricultural Sciences and Biotechnology, Faculty of Natural and Life Sciences, Ahmed Draia University, Adrar 01000, Algeria.*
[2] *Department of Science and Technology, Faculty of Technology, Amar Teledji University, Laghouat 03000, Algeria.*
[3] *Department of Mathematics, College of Science, King Khalid University, Abha 61413, Saudi Arabia.*

Received: March 20, 2024; Revised: March 9, 2025

Abstract: The study proposed in this paper introduces an innovative approach for estimating spectral density in time series analysis within the framework of dynamical systems, which is considered to be the most powerful tool in the statistical treatment of stochastic processes. Spectral density estimation is a crucial tool for understanding the frequency domain characteristics of time series data, particularly in complex dynamical systems. Our analytical results are validated by numerical simulation of the stochastic model. The Yule-Walker technique is used to show the attainment level of the model parameter estimation and the comparison is also made for this estimation. Our approach improves accuracy in capturing spectral characteristics, addressing the challenges posed by nonlinearities inherent in the data. Through empirical and theoretical validation, we demonstrate its efficacy in unraveling time series complexities.

Keywords: *asymptotic properties; ARMA models; Fourier analysis; dynamical periodogram; spectral density.*

Mathematics Subject Classification (2020): 93E10, 62G07, 62M15, 37M05, 37M10.

* Corresponding author: mailto:m.bassoudi@lagh-univ.dz

1 Introduction

In various scenarios, information about a particular medium is often depicted as a series of measurements taken over consecutive time intervals, commonly known as a time series. The key disparity between the analysis of time series and situations typically examined in classical statistics lies in the fact that measurements within a time series tend to exhibit stochastic dependence, whereas classical statistics assumes independence among observations. One potential contributor to the intricate nature of time series is the presence of random elements such as measurement errors, system noise, and so forth. At the highest level of randomness, we may encounter a time series representing a sequence of outcomes from independent random variables without any discernible structure. Conversely, the theory of dynamical systems explores the opposite of pure randomness, where future evolution is uniquely determined by the initial state and governing laws. However, the behavior of a deterministic system is not necessarily straightforward. Indeed, advancements in nonlinear dynamical systems reveal the existence of deterministic time series exhibiting highly erratic behavior, resembling realizations of random processes. Such instances are often referred to as chaotic dynamics.

The primary objective of time series analysis revolves around capturing the relationship between future observations and their preceding ones. Dating back to Yule's introduction of linear autoregression in 1927 to analyze sunspot data, linear models have held sway in time series analysis for roughly fifty years. To accommodate complex behaviors within such a simplistic framework, the presence of external random perturbations is necessary. In conventional models propelled by noise, for example, the AR and ARMA models, a future observation is construed as a combination of a specific number of preceding observations and random disturbances, often Gaussian in nature, referred to as innovations (see [1]). However, there are straightforward examples of time series such as those related to chaotic dynamical systems. This poses new challenges: how to recognize such time series and which methods to employ for their modeling and prediction.

In general, when discussing stationary time series, we have a concept of representing the model X_t, where $t \in \mathbb{Z}$, representing the observations of the dynamical system, from which we can define a set of autocovariance as

$$\gamma(t;s) = E\left[(X_t - \mu)(X_s - \mu)\right].$$

This autocovariance depends only on the distance between t and s, $\gamma(t;s) = \gamma(t+h;s+h)$ for all $h \in \mathbb{Z}$. The idea here is to approximate an analytical function by a weighted sum of sine or cosine functions [12], [13]. The idea is as follows: we seek a model of the form

$$X_t = \sum_i a_i \cos(\omega_i t) + b_i \sin(\omega_i t) + \varepsilon_i = \sum_i \sqrt{a_i^2 + b_i^2}\sin(\omega_i - \theta_i) + \varepsilon_i, \tag{1}$$

where (ε_i) is a sequence of independently and identically distributed random variables. If we define $\rho_i = \sqrt{a_i^2 + b_i^2}$, then ρ_i represents the amplitude of the i^{th} periodic component, indicating the weight of that component within the sum.

When considering a sample $X_0, X_2, ...X_{N-1}$ and using frequencies $\omega_j = \frac{2\pi j}{N}$, the dynamical periodogram is defined as

$$I(\omega_j) = \frac{1}{2\pi N} \left| \sum_{k=0}^{k=N-1} X_k e^{ik\omega_j} \right|^2 .$$

It is then possible to demonstrate that $\frac{I(\omega_j)}{N}$ is a consistent estimator of ρ_j in the sense that this estimator converges in probability as the number of observations increases.

Spectral density estimation is an important problem and there is a rich literature. However, restrictive structural conditions have been imposed in many earlier results. For example, Brillinger [5] assumed that all moments existed and cumulants of all orders were summable. Reuman et al. [8] revealed a spectral analysis of stochasticity on nonlinear population dynamics. Recently, Grytsay and Musatenko [4] gave invariant measurements in studying the dynamics of a metabolic process for spectral analysis. Spectral analysis is commonly used in signal processing with the aim of enhancing our understanding of a signal by exploring its frequency domain. Spectral analysis seeks to extract the energy spectrum of a signal. When assuming stationarity, the spectrum becomes a one-dimensional representation of frequency and fully describes the signal's energy content up to the second order. Since most signals originate from random processes, spectral analysis often relies on the domains of probability and statistics [15], [16]. A spectrum can be estimated through a diverse range of methods that utilize information from the observed signal and possibly a priori signal models, whether they are physical or mathematical models. This leads to algorithmic complexity generated by a set of parameters whose choice influences performance. The choices made, the a priori assumptions, and the statistical performance are crucial elements for interpreting the spectrum [10].

Our work involves the analysis of time series for the system with estimation of the spectral density. We employ a technique to construct a spectral density estimator, this is carried out as an asymptotic study. The paper is organized as follows. Section 2 presents the formulation of the baseline model, including some essential concepts and our problem definition. Section 3 lists the asymptotic properties, and exhibits our results. In Section 4, we present a numerical example with simulations.

2 Baseline Model Formulation

Consider any set of observations $x_1, \ldots, x_n$ that can take complex values. If $u = (u_1, \ldots, u_n)'$ and $v = (v_1, \ldots, v_n)'$ are two vectors in $\mathbb{C}^n$, we can define the inner product of u and v as follows:

$$\langle u, v \rangle = \sum_{i=1}^{i=n} u_i \overline{v_i}. \tag{2}$$

Let F_n be a dynamical system of Fourier frequencies defined as

$$F_n = j \in \mathbb{Z}, -\pi < \omega_j = \frac{2\pi j}{n} \leq \pi = -[\frac{n-1}{2}], \ldots, [\frac{n}{2}],$$

where $[x]$ denotes the floor function of x.

We define the vectors e_j for j in F_n as

$$e_j = n^{-1/2}(e^{i\omega j}, e^{2i\omega j}, \ldots, e^{ni\omega j})'. \tag{3}$$

Proposition 2.1 *The vectors e_j, for $j \in F_n$, defined above form an orthonormal basis for $\mathbb{C}^n$.*

Proof. We have

$$\begin{aligned}\langle e_j, e_k\rangle &= n^{-1}\sum_{r=1}^{r=n} e^{ir(\omega_j-\omega_k)} \\ &= \begin{cases} n^{-1}\sum_{r=1}^{r=n} e^0 = \frac{n}{n} = 1, \text{if } j = k; \\ n^{-1}e^{i(\omega_j-\omega_k)}(\frac{1-e^{in(\omega_j-\omega_k)}}{1-e^{i(\omega_j-\omega_k)}}) = 0, \text{if} j \neq k. \end{cases}\end{aligned}$$

Let us further justify the case when $j \neq k$. The first equality arises because we have a geometric series with a common ratio of $e^{i(\omega_j-\omega_k)}$.

Furthermore, the numerator of the fraction becomes zero because, by the definition of ω_j and ω_k,

$$e^{in(\omega_j-\omega_k)} = e^{i2\pi(j-k)} = 1$$

since $j - k$ is a non-zero integer. □

The value $I(\omega j)$ of the dynamical periodogram of the vector $x = (x1, \dots, x_n)$ at frequency $\omega_j = \frac{2\pi j}{n}$ is given by

$$\begin{aligned} I(\omega_j) &= \frac{1}{n}\left|\sum_{t=1}^{t=n} x_t e^{-it\omega j}\right|^2 \\ &= \frac{1}{n}\left[\left(\sum t = 1^{t=n} x_t \cos\omega j t\right)^2 + \left(\sum t = 1^{t=n} x_t \sin\omega_j t\right)^2\right]. \end{aligned} \tag{4}$$

The dynamical periodogram is a powerful tool for detecting a signal because if X contains a sinusoidal component with frequency ω_0, then, when we are close to this frequency, the factors $X(t)$ and $e^{-i\omega_0 t}$ are in phase and make a significant contribution to the sum in equation (4). For other values of ω, some terms in the sum are positive, while others are negative, thus canceling each other out in the sum, which becomes small. In summary, we can detect the presence of a sinusoidal signal when a large value of $I(.)$ appears for a certain value of ω.

Proposition 2.2 *If ω_j is a non-zero Fourier frequency, then*

$$I(\omega_j) = \sum_{|K|<n} \widehat{\gamma}(k)e^{-ik\omega_j},$$

where

$$\widehat{\gamma}(k) = n^{-1}\sum_{t=1}^{t=n-k}(x_{t+k} - m)(\overline{x_t} - \overline{m})$$

with m being the empirical mean of x_i, $m = n^{-1}\sum_{t=1}^{t=n} x_t$, and $\overline{(.)}$ denoting complex conjugation. Also, $\widehat{\gamma}(-k) = \overline{\widehat{\gamma}(k)}$ when $k < 0$.

We show a strong resemblance between the obtained expression for $I(\omega_j)$ and the expression of the spectral density of a stationary dynamical system given by

$$f(\omega) = \frac{1}{2\pi} \sum_{k=-\infty}^{+\infty} \gamma(k) e^{-ik\omega} \quad \text{when} \quad \sum_{k=-\infty}^{+\infty} |\gamma(k)| < \infty.$$

So, we can take $\frac{I(\omega_j)}{2\pi}$ as an estimator of $f(\omega_j)$.

3 Asymptotic Properties and Main Results

In this section, we will focus on the asymptotic properties of the periodogram of a stationary dynamical system with a mean μ and a covariance function that is absolutely summable, i.e., $\sum_{k=-\infty}^{+\infty} |\gamma(k)| < \infty$. Based on the previous remark, we take the estimator of $f(\omega_j)$ as $I(\omega_j)/(2\pi)$.

We begin by extending the dynamical periodogram to all $\omega \in [-\pi, \pi]$ so that it is no longer limited to the Fourier frequencies.
For any $\omega \in [-\pi, \pi]$, the dynamical periodogram is defined as follows:

$$I_n(\omega) = \begin{cases} I_n(\omega_j) & = n^{-1} |\sum_{t=1}^{t=n} X_t e^{-it\omega_j}|^2 \\ & \text{if } \frac{-\pi}{n} < \omega \leq \frac{\pi}{n} \text{and} \quad \omega \in [0, \pi]; \\ I_n(-\omega) & \text{if } \omega \in [-\pi, 0]. \end{cases}$$

For every $\omega \in [0, \pi]$, let us denote $g(n, \omega)$ as the multiple of $\frac{2\pi}{n}$ closest to ω. For every $\omega \in [-\pi, 0]$, we define $g(n, \omega) = g(n, -\omega)$. Thus

$$I_n(\omega) = I_n(g(n, \omega)).$$

Proposition 3.1 *Let $(X_t)t \in \mathbb{Z}$ be a second-order stationary dynamical system with a mean μ and an absolutely summable autocovariance function $\gamma(.)$ $\left(\sum_{k=-\infty}^{\infty} |\gamma(k)| < \infty \right)$, then*

$$\textit{when} \quad n \to \infty : \begin{cases} (E(I_n(0)) - n\mu^2) \longrightarrow 2\pi f(0), \\ E(I_n(\omega)) \longrightarrow 2\pi f(\omega) \quad \textit{if} \quad \omega \neq 0 \end{cases}$$

with

$$I_n(0) = n|\overline{X}|^2 \quad \textit{and} \quad I(\omega_j) = \sum_{|K|<n} \widehat{\gamma}(k) e^{-ik\omega_j} \quad \textit{if} \quad \omega_j \neq 0.$$

Remark 3.1 If $\mu = 0$, then $E(I_n(\omega))$ converges uniformly to $2\pi f(\omega)$ for all $\omega \in [-\pi, \pi]$.

Proof.

$$E(I_n(0)) = nE(|\overline{X}|^2) = n[Var(\overline{X}) + (E(\overline{X}))^2] = nVar(\overline{X}) + n\mu^2.$$

So

$$E(I_n(0)) - n\mu^2 \quad = \quad nVar(\overline{X}).$$

On the other hand,

$$nVar(\overline{X}) = \frac{1}{n}\sum_{i=1}^{i=n}\sum_{j=1}^{j=n} cov(X_i, X_j) = \sum_{|h|<n}(1 - \frac{|h|}{n})\gamma(h)$$

if $\sum_{k=-\infty}^{\infty}|\gamma(k)| < \infty$. According to the dominated convergence theorem (Theorem 3.3.1) from [6], we have

$$\lim_{n\to\infty} nVar(\overline{X}) = \lim_{n\to\infty}\sum_{|h|<n}(1 - \frac{|h|}{n})\gamma(h) = \sum_{h=-\infty}^{\infty}\gamma(h) = 2\pi f(0),$$

$$E(I_n(\omega)) = \sum_{|k|<n}\frac{1}{n}\sum_{t=1}^{n-|k|} E\left[(X_t-\mu)(X_{t+|k|}-\mu)\right]e^{-ikg(n,\omega)} = \sum_{|k|<n}\big(1-\frac{|k|}{n})\gamma(k)e^{-ikg(n,\omega)}.$$

Since $\sum_{k\in\mathbb{Z}}|\gamma(k)| < \infty$ and according to the dominated convergence theorem (Theorem 3.3.1) from [6],

$$\sum_{|k|<n}\big(1 - \frac{|k|}{n})\gamma(k)e^{-ikg(n,\lambda)} \quad \to \quad 2\pi f(\lambda).$$

On the other hand, we have $g(n,\omega) \to \omega$. So

$$E(I_n(\omega)) \quad \to \quad 2\pi f(\omega).$$

□

Theorem 3.1 *Let $\{X_t\}$ be a time series process defined by*

$$X_t = \sum_{k=-\infty}^{+\infty}\psi_k\varepsilon_{t-k},$$

where ε_t is a strong white noise $IID(0,\sigma^2)$ with $\mathbb{E}(\varepsilon_t^2) < \infty$. We assume that $\sum_{j=-\infty}^{+\infty}|\psi_j||j|^{\frac{1}{2}}$ and $\psi(e^{-i\lambda}) = \sum_{k=-\infty}^{+\infty}\psi_k e^{-ik\lambda} \neq 0$. We know that

$$f_X(\omega) = \frac{\sigma^2}{2\pi}|\psi(e^{-i\omega})|^2.$$

1. *For fixed frequencies $0 < \lambda_1 < \ldots\lambda_m < \pi$ as $n \to +\infty$, the random vector $(I_{n,X}(\lambda_1)/f_X(\lambda_1), ..., I_{n,X}(\lambda_m)/f_X(\lambda_m))'$ converges by law to a vector of independent random variables with the same exponential distribution with a mean of 1.*

2. *We have*

$$Var(I_{n,X}(\omega_j)) = \begin{cases} 2f_X^2(\omega_j) & +O(n^{-\frac{1}{2}}) \\ & \text{if } \omega_j = 0 \text{ or } \pi; \\ f_X^2(\omega_j) & +O(n^{-\frac{1}{2}}) \\ & \text{if } 0 < \omega_j < \pi \end{cases}$$

and $\quad Cov(I_{n,X}(\omega_j), I_{n,X}(\omega_k)) = O(n^{-1}) \quad$ *if* $\quad \omega_j \neq \omega_k.$

Thus, we show the previous Theorem 3.1 by using the following intermediate lemmas.

Lemma 3.1 *Let* $\{\varepsilon_t\}_{\{t\in\mathbb{Z}\}}$ *be an i.i.d. white noise process with a zero mean and finite variance* $\sigma^2 < \infty$. *Its spectral distribution has a density function of* $f_\varepsilon(\omega) = \frac{\sigma^2}{2\pi}$ *and let* I_n *be the dynamical periodogram of* $\{\varepsilon_t\}$.

1. *Suppose* $0 < \lambda_1 < \lambda_2 < \dots \lambda_m < \pi$ *are fixed frequencies. Then, as* $n \to +\infty$, *the random vector* $(I_n(\lambda_1), I_n(\lambda_2), \dots, I_n(\lambda_m))'$ *converges by law to a vector of independent random variables same as a mean of* $\frac{\sigma^2}{2\pi}$*;*

2. *If* $E(\varepsilon_t^4) = \eta\sigma^4 < \infty$ *and* $0 \leq \omega_j = \frac{2\pi j}{n} \leq \pi$ *are the Fourier frequencies, then*

$$Var(I_n(\omega_j)) = \begin{cases} 2f_\varepsilon^2(\omega_j) \quad +\frac{\kappa_4}{4\pi^2 n} \\ \quad \textit{if } \omega_j = 0 \textit{ or } \pi; \\ f\varepsilon^2(\omega_j) \quad +\frac{\kappa_4}{4\pi^2 n} \\ \quad \textit{if} \quad 0 < \omega_j < \pi \end{cases} = \begin{cases} \frac{\sigma^4}{2\pi^2} \quad +\frac{\kappa_4}{4\pi^2 n} \\ \quad \textit{if } \omega_j = 0 \textit{ or } \pi; \\ \frac{\sigma^4}{4\pi^2} \quad +\frac{\kappa_4}{4\pi^2 n} \\ \quad \textit{if} \quad 0 < \omega_j < \pi \end{cases}$$

and $\quad Cov(I_n(\omega_j), I_n(\omega_k)) = \frac{\kappa_4}{4\pi^2 n} \quad$ *if* $\quad \omega_j \neq \omega_k$, *where* κ_4 *is the fourth-order cumulant of the variable* ε_t *defined as* $\kappa_4 = \mathbb{E}\{\varepsilon_t^4\} - 3(\mathbb{E}\{\varepsilon_t^2\})^2$*;*

3. *Let us assume that the random variables* ε_t *are Gaussian. In this case,* $\kappa_4 = 0$ *and for all* n, *the random variables* $I_n(\omega_k)/f_\varepsilon(\omega)$, $k \in \{1, \dots \lfloor\frac{(n-1)}{2}\rfloor\}$ *are independent and identically distributed according to an exponential distribution with a mean of 1.*

Proof.

1. Let us note

$$\begin{cases} \alpha_n(\omega_j) = \sqrt{2\pi n}\sum_{t=1}^n \varepsilon_t cos(\omega_j t), \\ \beta_n(\omega_j) = \sqrt{2\pi n}\sum_{t=1}^n \varepsilon_t sin(\omega_j t) \end{cases} \tag{5}$$

are the real and imaginary parts of the discrete Fourier transform of ε_t at the frequency points $\omega_j = \frac{2\pi j}{n}$. For an arbitrary frequency ω, we have

$$I_n(\omega_j) = \frac{1}{2}(\alpha_n^Z(g(n,\omega_j))^2 + \beta_n^Z(g(n,\omega_j))^2)^2.$$

Recall that if a sequence of random vectors Y_n converges by law to a random variable Y and ϕ is a continuous function, then $\phi(Y_n)$ converges by law to $\phi(Y)$. It is sufficient to show that the random vector

$$(\alpha_n(\omega_1), \beta_n(\omega_1), \dots, \alpha_n(\omega_m), \beta_n(\omega_m)) \tag{6}$$

converges by law to a normal distribution with a zero mean and an asymptotic covariance matrix $(\frac{\sigma^2}{4\pi})I_{2m}$, where I_2m is the identity matrix $(2m \times 2m)$. We will first focus on the case $m = 1$. The proof follows from the following corollary.

Corollary 3.1 *Let $U_{n,t}$, where $t = 1, \dots, n$ and $n = 1, 2, \dots,$ be a triangular sequence of centered random variables with finite variances. For all n, the dynamics variables $\{U_{n,1}, \dots, U_{n,n}\}$ are independent. We define $Y_n = \sum_{t=1}^n U_{n,t}$ and $\vartheta_n^2 = \sum_{t=1}^n var(U_{n,t})$. Then, if for every $\epsilon > 0$,*

$$\lim_{n\to+\infty} \sum_{t=1}^{n} \frac{1}{\vartheta_n^2} \mathbb{E}\left[U_{n,t}^2 \mathbf{I}(|U_{n,t}| > \epsilon\vartheta_n)\right] = 0,$$

we have

$$Y_n/\vartheta_n \longrightarrow_d \mathcal{N}(0,1).$$

Let u and v be arbitrary fixed real numbers, and $\omega_j \in (0, \pi)$. Consider the variable $Y_n = u\alpha_n(g(n, \omega_j)) + v\beta_n(g(n, \omega_j))$, which can also be written as

$$Y_n = \sum_{t=1}^{n} U_{n,t}, \text{where} \quad U_{n,t} = \frac{1}{\sqrt{2\pi n}}(u\cos(g(n,\omega_j)t) + v\sin(g(n,\omega_j)t))\varepsilon_t.$$

Note that, for a fixed n, the random variables $\{U_{n,t}\}$ are independent. Furthermore, for all $\omega_j \neq 0$, it is easy to verify that

$$\sum_{t=1}^{n} \cos^2(g(n,\omega_j)t) = \sum_{t=1}^{n} \sin^2(g(n,\omega_j)t) = \frac{n}{2}$$

and

$$\sum_{t=1}^{n} \cos(g(n,\omega_j)t)\sin(g(n,\omega_j)t) = 0.$$

As a result, we can write

$$\begin{aligned}
\vartheta_n^2 &= \sum_{t=1}^{n} \mathrm{var}(U_{n,t}) \\
&= \frac{1}{2\pi n} \sum_{t=1}^{n} \Big[u^2\cos^2(g(n,\omega_j)t) + v^2\sin^2(g(n,\omega_j)t) \\
&\quad + 2uv\cos(g(n,\omega_j)t)\sin(g(n,\omega_j)t)\Big] \\
&= \frac{(u^2+v^2)}{4\pi} = \vartheta_1^2.
\end{aligned}$$

Hence, by setting $c_0 = (|u| + |v|)/2\pi\vartheta_1$ and $\epsilon' = \epsilon\sqrt{2\pi}\vartheta_1/(|u| + |v|)$, we have

$$\sum_{t=1}^{n} \frac{1}{\vartheta_n^2} \mathbb{E}\left[U_{n,t}^2 \mathbf{I}(|U_{n,t}| \geqslant \epsilon\vartheta_n)\right] \leq \frac{c_0}{n} \sum_{t=1}^{n} \mathbb{E}\left[\varepsilon_t^2 \mathbf{I}(|\varepsilon_t| \geqslant \epsilon'\sqrt{n})\right] = c_0 \mathbb{E}\left[\varepsilon_t^2 \mathbf{I}(|\varepsilon_t| \geqslant \epsilon'\sqrt{n})\right].$$

The last term tends to 0 as we have $\mathbb{E}\left[\varepsilon_1^2 \mathbf{I}(|\varepsilon_1| \geqslant \epsilon'\sqrt{n})\right] \leq \mathbb{E}\left[|\varepsilon_1|^3\right]/\epsilon'\sqrt{n})$ and $\mathbb{E}\left[|\varepsilon_1|^3\right] < \infty$ since $\mathbb{E}\left[|\varepsilon_1|^4\right] < \infty$.

The proof can be easily extended to a set of frequencies $\omega_1 \dots \omega_m$ using the Cramer-Wold method as we recall the following. Let $\{V_n\}_{n\geqslant 0}$ be a sequence of real random vectors of dimension m. $V_n \longrightarrow_d W$ if and only if, for any sequence $\{\omega_1 \dots \omega_m\} \in \mathbb{R}^m$, the random variable $Y_n = \omega_1 V_{n,1} + \cdots + \omega_m V_{n,m} \longrightarrow_d \omega_1 W_1 + \cdots + \omega_m W_m$.

2. By definition of $I_n(\omega_j)$, we have, at the first order,

$$\mathbb{E}\left[I_n(\omega_j)\right] = \frac{1}{2\pi n}\sum_{s,t=1}^{n}\mathbb{E}\left[\varepsilon_s\varepsilon_t\right]e^{i\omega_j(t-s)} = \frac{\sigma^2}{2\pi}. \tag{7}$$

At the second order, we have

$$\mathbb{E}\left[I_n(\omega_j)I_n^Z(\omega_k)\right] = \frac{1}{(2\pi n)^2}\times\sum_{s,t,u,v=1}^{n}\mathbb{E}\left[\varepsilon_s\varepsilon_t\varepsilon_u\varepsilon_v\right]e^{i(\omega_j(t-s)+\omega_k(v-u))}. \tag{8}$$

Using the fact that the random variables ε_t are independent, centered, have the same variance σ^2 and finite fourth moments, and setting $\mathbb{E}[\varepsilon_1^4] = \kappa_4 + 3\sigma^4$, we obtain

$$\mathbb{E}\left[\varepsilon_s\varepsilon_t\varepsilon_u\varepsilon_v\right] = \kappa_4\delta_{s,t,u,v} + \sigma^4(\delta_{s,t}\delta_{u,v} + \delta_{s,u}\delta_{t,v} + \delta_{s,v}\delta_{t,u}). \tag{9}$$

Plugging this expression into 8, we get

$$\mathbb{E}\left[I_n(\omega_j)I_n(\omega_k)\right] = \frac{\kappa_4}{(4\pi^2 n)} + \frac{\sigma^4}{(4\pi^2 n^2)}\times\left[n^2 + \left|\sum_{t=1}^{n}e^{i(\omega_j+\omega_k)t}\right|^2 + \left|\sum_{t=1}^{n}e^{i(\omega_k-\omega_j)t}\right|^2\right]$$

and therefore

$$\begin{aligned} cov\left[I_n(\omega_j), I_n(\omega_k)\right] &= \mathbb{E}\left[I_n(\omega_j)I_n(\omega_k)\right] - \mathbb{E}\left[I_n(\omega_j)\right]\mathbb{E}\left[I_n(\omega_k)\right] \\ &= \frac{\kappa_4}{(4\pi^2 n)} + \frac{\sigma^4}{(4\pi^2 n^2)}\times\left[\left|\sum_{t=1}^{n}e^{i(\omega_j+\omega_k)t}\right|^2 + \left|\sum_{t=1}^{n}e^{i(\omega_k-\omega_j)t}\right|^2\right]. \end{aligned}$$

This allows us to conclude.

3. When $\{\varepsilon_t\}$ is a centered Gaussian variable, the vector

$$Q_n = \left[\alpha_n(\omega_1)\ \beta_n(\omega_1)\ \ldots\ \alpha_n(\omega_{\tilde{n}})\beta_n(\omega_{\tilde{n}})\right].$$

It is sufficient to calculate the mean vector and its covariance matrix. It is easy to verify that the mean vector is zero, and that for $0 < \omega_k \neq \omega_j < \pi$, we have

$$\begin{aligned} &\mathbb{E}\left[(\alpha_n(\omega_k))^2\right] = \mathbb{E}\left[(\beta_n(\omega_k))^2\right] = \frac{1}{4\pi}, && \mathbb{E}\left[\alpha_n(\omega_k)\beta_n(\omega_k)\right] = 0, \\ &\mathbb{E}\left[\alpha_n(\omega_k)\alpha_n(\omega_j)\right] = \mathbb{E}\left[\beta_n(\omega_k)\beta_n^Z(\omega_j)\right] = 0, && \mathbb{E}\left[\alpha_n(\omega_k)\beta_n(\omega_j)\right] = 0. \end{aligned}$$

The covariance matrix is thus $\frac{\sigma^2 I_{\tilde{n}}}{4\pi}$, where $I_{\tilde{n}}$ is the identity matrix of size $\tilde{n}$. Consequently, the components of Q_n are independent. Recall that

$$I_n(\omega_j) = (\alpha_n(\omega_j))^2 + (\beta_n(\omega_j))^2.$$

From the independence of the components of Q_n, we deduce that the random variables $I_n(\omega_j)$ are themselves independent, and that $\frac{4\pi I_n(\omega_j)}{\sigma^2}$ is the sum of the squares of two independent, centered, identically distributed Gaussian variables, each with a variance of 1, whose probability distribution is the law of χ^2 distribution with two degrees of freedom. This concludes the proof. □

The following lemma shows that there is a similar relationship to the previous one that relates the dynamical periodogram $I_{n,X}(\omega)$ of the time series process $\{X_t\}$ and the dynamical periodogram $I_{n,\varepsilon}(\omega)$ of the strong white noise $\{\varepsilon_t\}$.

Lemma 3.2 *Let $\{X_t\}$ be a strong time series process, $X_t = \sum_{k=-\infty}^{+\infty} \psi_k \varepsilon_{t-k}$. Suppose $\sum_{j=-\infty}^{+\infty} |\psi_j||j|^{\frac{1}{2}} < \infty$ and $\mathbb{E}\{\varepsilon_t^4\} < \infty$. Then we have*

$$I_{n,X}(\omega_k) = |\psi(e^{-i\omega_k})|^2 I_{n,\varepsilon}(\omega_k) + R_n(\omega_k),$$

where $R_n(\omega_k)$ satisfies

$$\max_{k\in\{1,...\lfloor\frac{(n-1)}{2}\rfloor\}} \mathbb{E}\{|R_n(\omega_k)|^2\} = O(\frac{1}{n}) \tag{10}$$

and $\omega_k = \frac{2\pi k}{n}$, where $k \in \{1, ...\lfloor\frac{(n-1)}{2}\rfloor\}$ are the Fourier frequencies.

Proof. Let us denote $d_n^X(\omega_k)$ and $d_n^Z(\omega_k)$ as the dynamical system of the discrete Fourier transforms of the sequences $\{X_1, ..., X_n\}$ and $\{Z_1, ..., Z_n\}$ at the frequency point $\frac{2\pi k}{n}$ with $k \in \{1, ..., [\frac{(n-1)}{2}]\}$. We can write successively:

$$\begin{aligned}
d_n^X(\omega_k) &= \frac{1}{2\pi n}\sum_{t=1}^{n} X_t e^{-i\omega_k t} \\
&= \frac{1}{2\pi n}\sum_{j=-\infty}^{+\infty} \psi_j e^{-i\omega_k j}\left(\sum_{t=1}^{n} Z_{t-j} e^{-i\omega_k (t-j)}\right) \\
&= \frac{1}{2\pi n}\sum_{j=-\infty}^{+\infty} \psi_j e^{-i\omega_k j}\left(\sum_{t=1-j}^{n-j} Z_t e^{-i\omega_k t}\right) \\
&= \frac{1}{2\pi n}\sum_{j=-\infty}^{+\infty} \psi_j e^{-i\omega_k j}\left(\sum_{t=1}^{n} Z_t e^{-i\omega_k t} + U_{n,j}(\omega_k)\right) \\
&= \psi(e^{-i\omega_k}) d_n^Z(\omega_k) + Y_n(\omega_k).
\end{aligned}$$

Here, we have defined

$$U_{n,j}(\omega_k) = \sum_{t=1-j}^{n-j} Z_t e^{-i\omega_k t} - \sum_{t=1}^{n} Z_t e^{-i\omega_k t} \tag{11}$$

and

$$Y_n(\omega_k) = \frac{1}{\sqrt{2\pi n}}\sum_{j=-\infty}^{+\infty} \psi_j e^{-i\omega_k j} U_{n,j}(\omega_k). \tag{12}$$

We observe that, for $|j| < n$, $U_{n,j}(\omega_k)$ is a sum of $2|j|$ independent centered variables with variance σ^2, while for $|j| \geq n$, $U_{n,j}(\omega_k)$ is a sum of $2n$ independent centered variables with variance σ^2. Therefore, using (11), we have

$$\mathbb{E}\left[|U_{n,j}(\omega_k)|^2\right] \leq 2\sigma^2 \min(|j|, n) \tag{13}$$

and

$$\mathbb{E}\left[|U_{n,j}(\omega_k)|^4\right] \leq C_R\sigma^4(\min(|j|,n))^2, \tag{14}$$

where $C_R < \infty$ is a constant. To establish (14), we only need to set $\mathbb{E}\left[Z_t^4\right] = \eta\sigma^4$ and use the inequality (15) for $p = 4$:

$$\mathbb{E}\left[|\sum_{k=1}^{n} X_k|^p\right] \leq C(p)\left(\left(\sum_{k=1}^{n}\mathbb{E}[X_k^2]\right)^{\frac{p}{2}} + \sum_{k=1}^{n}\mathbb{E}[|X_k|^p]\right). \tag{15}$$

Now, use (14) to bound $\mathbb{E}\left[|Y_n(\omega_k)|^4\right]$. By adapting the notation $\|X\|_p = (\mathbb{E}[|X|^p])^{\frac{1}{p}}$ (for $p > 0$), we get, following the triangular inequality (Minkovski inequality) $\|X+Y\|_p \leq \|X\|_p + \|Y\|_p$,

$$\sup_{k\in\{1,\ldots,[\frac{(n-1)}{2}]\}} \|Y_n(\omega_k)\|_4 \leq \sup_{k\in\{1,\ldots,[\frac{(n-1)}{2}]\}} \frac{1}{\sqrt{2\pi n}}\sum_{j=-\infty}^{+\infty}|\psi_j|\|U_{(n,j)}(\omega_k)\|_4.$$

From (14), $\|U_{(n,j)}(\omega_k)\|_4 \leq C\sigma\min(|j|,n)^{\frac{1}{2}}$. Therefore

$$\sup_{k\in\{1,\ldots,[\frac{(n-1)}{2}]\}} \|Y_n(\omega_k)\|_4 \leq C\sigma(\frac{1}{\sqrt{2\pi n}})\sum_{j=-\infty}^{+\infty}|\psi_j|\min(|j|,n)^{\frac{1}{2}}.$$

Now we can write

$$\sum_{j=-\infty}^{+\infty}|\psi_j|\min(|j|,n)^{\frac{1}{2}} \leq \sum_{j=-\infty}^{+\infty}|\psi_j||j|^{\frac{1}{2}}.$$

Therefore, $\|Y_n(\omega_k)\|_4$ is of the same order as $O(n^{\frac{-1}{2}})$.
We can now express $R_n(\omega_k) = I_n^X(\omega_k) - |\psi(e^{-i\omega_k})|^2 I_n^Z(\omega_k)$ in terms of $Y_n(\omega_k) = d_n^X(\omega_k) - \psi(e^{-i\omega_k})d_n^Z(\omega_k)$. It follows that

$$\begin{aligned}R_n(\omega_k) &= |\psi(e^{-i\omega_k})d_n^Z(\omega_k) + Y_n(\omega_k)|^2 - |\psi(e^{-i\omega_k})|^2 I_n^Z(\omega_k)\\ &= \psi(e^{-i\omega_k})d_n^Z(\omega_k)Y_n(-\omega_k) + \psi(e^{-i\omega_k})d_n^Z(-\omega_k)Y_n(\omega_k) + |Y_n(\omega_k)|^2.\end{aligned}$$

According to Holder's inequality, $\|XY\|_r \leq \|X\|_p\|Y\|_q$ if $\frac{1}{p} + \frac{1}{q} = \frac{1}{r}$. Taking $p = q = 4$ and $r = 2$, we get

$$(\mathbb{E}\left[|R_n(\omega_k)|^2\right])^{\frac{1}{2}} = \|R_n(\omega_k)\|_2 \leq 2\sum_j|\psi_j|\|d_n^Z(\omega_k)\|_4\|Y_n(\omega_k)\|_4 + \|Y_n(\omega_k)\|_4.$$

According to Lemma 3.1, $\|d_n^Z(\omega_k)\|_4$ is of the order of $\frac{\sigma}{\sqrt{2\pi}}$. Therefore, $\|R_n(\omega_k)\|_2$ is of the order of $\frac{1}{\sqrt{n}}$ and $\mathbb{E}[|R_n(\omega_k)|^2] = \|R_n(\omega_k)\|_2^2$ is of the order of $\frac{1}{n}$.

This completes the proof of Theorem 3.1. □

4 Applications

4.1 Numerical example

Let X_t be an AR(p) process defined by the equation

$$X_t + \phi_1 X_{t-1} + \phi_2 X_{t-2} + \cdots + \phi_p X_{t-p} = \varepsilon_t. \tag{16}$$

This equation can be written in the following form. Let X_t be an AR(p) process defined by the equation

$$\sum_{k=0}^{p} \phi_k X_{t-k} = \varepsilon_t \quad \text{with} \quad \phi_0 = 1. \tag{17}$$

By multiplying equation (17) by X_{t-1}, we get

$$\sum_{k=0}^{p} \phi_k E\left\{X_{t-k} X_{t-l}\right\} = E\left\{\varepsilon_t X_{t-l}\right\} \quad , a_0 = 1. \tag{18}$$

We can easily identify the terms of autocorrelation and cross-correlation in the Yule-Walker equation:

$$\sum_{k=0}^{N} \phi_k \rho_{xx}[l-k] = \rho_{\varepsilon x}[l] \quad \text{with} \quad \phi_0 = 1. \tag{19}$$

The next step is to calculate the identified cross-correlation term $\rho_{\varepsilon x}(l)$ and relate it to the autocorrelation term $\rho_{xx}(l-k)$.
The term X_{t-l} can also be obtained from equation (16):

$$X_{t-l} = -\sum_{k=1}^{p} \phi_k X_{t-k-l} + \varepsilon_{t-l}. \tag{20}$$

Note that the data and the noise are uncorrelated, so $(X_{t-l} w_t = 0)$. Also, the autocorrelation of the noise is zero at all lags, except for lag 0, where its value is equal to σ^2 (recall the flat power spectral density of white noise and its autocorrelation). These two properties are used in the following steps. We restrict the lags only to non-negative values and zero,

$$\begin{aligned} \rho_{\varepsilon X}(l) &= E\left\{\varepsilon_t X_{t-l}\right\} \\ &= E\left\{\varepsilon_t \left(-\sum_{k=1}^{N} \phi_k X_{t-k-l} + \varepsilon_{t-l}\right)\right\} \\ &= E\left\{-\sum_{k=1}^{N} \phi_k X_{t-k-l}\varepsilon_t + \varepsilon_{t-l}\varepsilon_t\right\} \\ &= E\left\{0 + \varepsilon_{t-l}\varepsilon_t\right\} \\ &= E\left\{\varepsilon_{t-l}\varepsilon_t\right\} \\ &= \begin{cases} 0 & , l > 0 \\ \sigma^2 & , l = 0. \end{cases} \end{aligned} \tag{21}$$

By substituting equation (21) into equation (19), we obtain

$$\sum_{k=0}^{N} \phi_k \rho_{xx}[l-k] = \begin{cases} 0, \ l > 0, \\ \sigma^2, \ l = 0, \end{cases} \qquad a_0 = 1. \tag{22}$$

Here, there are two cases to solve, when $(l > 0)$ and when $(l = 0)$. For the case when $l > 0$, equation (22) becomes

$$\sum_{k=1}^{N} \phi_k \rho_{xx}[l-k] = -\rho_{xx}[l]. \tag{23}$$

Equation (23) can be written in the matrix form

$$\begin{pmatrix} \rho_{xx}(0) & \dots & \rho_{xx}(2-P) & \rho_{xx}(1-P) \\ \rho_{xx}(1) & \dots & \rho_{xx}(3-P) & \rho_{xx}(2-P) \\ \vdots & \ddots & \vdots & \vdots \\ \rho_{xx}(P-1) & \dots & \rho_{xx}(1) & \rho_{xx}(0) \end{pmatrix} \begin{pmatrix} \phi_1 \\ \phi_2 \\ \vdots \\ \phi_P \end{pmatrix} = - \begin{pmatrix} \rho_{xx}(1) \\ \rho_{xx}(2) \\ \vdots \\ \rho_{xx}(P) \end{pmatrix}. \quad (24)$$

This is the Yule-Walker system, which consists of a set of P equations and P unknown parameters. Represent equation (24) in a compact format

$$\bar{\varrho}\bar{\phi} = -\bar{\rho}. \quad (25)$$

The solutions $\bar{a}$ can be obtained by

$$\bar{\phi} = -\bar{\varrho}^{-1}\bar{\rho}. \quad (26)$$

Once we solve for $\bar{\phi}$, which corresponds to the model parameters ϕ_k, the noise variance σ^2 is obtained by applying the estimated ϕ_k in equation (22) with $l = 0$. Matlab's "aryule" efficiently solves the Yule-Walker system using the Levinson Algorithm.

4.2 Simulation

We will generate an AR(3) process and assume that we know nothing about the model parameters (see Figure 1).

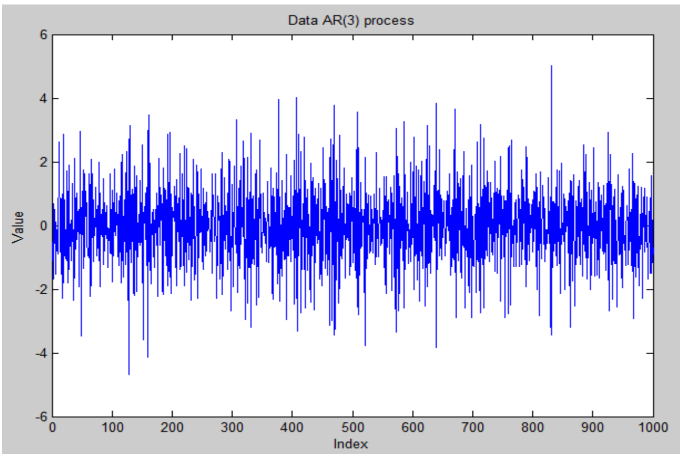

Figure 1: Simulated data for an AR(3) process.

We will take this as an input to the Yule-Walker system and check if it can correctly estimate the model parameters.

$$X_t = -X_{t-1} - 0.8X_{t-2} - 0.4X_{t-3} + \varepsilon_t.$$

Generation of data from the AR(3) process is given above.

To execute the simulation and determine which model order fits best, one should follow the steps below.

Step 1. Plot the dynamical periodogram (Power Spectral Density - PSD) of the simulated data for reference (see Figure 2).

Step 2. Estimate the PSD for three different model orders (e.g., AR(2), AR(3), AR(4)).

Step 3. Compare the estimated PSD for each model order to the reference dynamical periodogram to see which model order best fits the data.

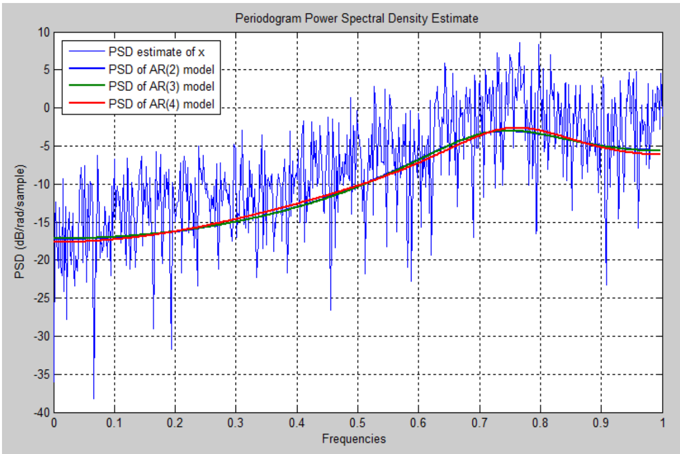

Figure 2: Dynamical periodogram (estimator of the Power Spectral Density "PSD").

The order (P)	The estimated parameters (ϕ_k)	The prediction error
2	[1 0.83 0.43]	1.010
3	[1 0.81 0.39 -0.037]	1.009
4	[1 0.81 0.39 -0.045 -0.009]	1.009

Table 1: The estimated model parameters and the prediction errors.

The estimated model parameters and the noise variances calculated by the Yule-Walker system are provided in Table 1.

It can be established that the estimated parameters are nearly identical to what is expected. See how the error decreases as the model order 'p' increases. The optimal model order in this case is $P = 3$ since the error did not change significantly when increasing the order, and also, the model parameter $\phi 4$ of the AR(4) process is not significantly different from zero.

5 Conclusion

In this paper, the estimation of spectral density provides useful insights into the analysis of time series data. The study emphasizes the importance of understanding the frequency domain of time series by applying techniques of spectral analysis, providing a unique point of view that complements traditional descriptive methods. Incorporating weighted windows, and addressing bias and variance, highlights the possibility for improvements in estimation accuracy. Additionally, one of the most notable achievements of spectral analysis for time series data is its ability to reveal hidden frequencies, allowing for the detection of underlying patterns and behaviors that may not be readily identifiable in the time domain.

It is important to add spectral analysis to the tools for studying time series data, the spectral analysis provides a "frequency" perspective on time series data, the dynamical periodogram is a more sophisticated estimator of the spectrum compared to the autocorrelation function, and the dynamical periodogram is a simple method for estimating the spectral density. This estimator has drawbacks (bias, variance) that can be problematic depending on its use. It is possible to improve this estimator by multiplying it by a weighting window to reduce bias and variance. One of the successes of spectral analysis for time series data is the detection of hidden frequencies.

Our research of spectral density estimation expands our toolbox for analyzing time series data and opens the door to fresh perspectives and potential applications in a variety of disciplines, including signal processing, finance, and economics. The study highlights the usefulness of spectrum analysis in revealing hidden dynamics in time series, making it a potent tool for researchers and analysts in the field.

References

[1] S. A. Borovkova. Estimation and prediction for nonlinear time series. *University of Groningen Library.* Netherlands, 1998.

[2] M. C. Edwards, R. Mayer and N. Christensen. Bayesian nonparametric spectral density estimation using B-spline-priors. *Statistics and Computing* **29** (426) (2019) 67–78.

[3] M. M. Gabr and L. M. Fatehy. Time Series Classification. *Journal of Statistics Applications & Probability* **2** (2) (2013) 123–133.

[4] V. I. Grytsay and I. V. Musatenko. Spectral Analysis and Invariant Measure in Studying the Dynamics of a Metabolic Process in the Glycolysis-Gluconeogenesis System. *Nonlinear Dynamics and Systems Theory* **24** (1) (2024) 54–64.

[5] D. R. Brillinger. Asymptotic properties of spectral estimates of second order. *Biometrika.* **56** (1969) 375–390.

[6] D. Hong, J. Wang and R. B. Gardner. Real analysis with an Introduction to Wavelets and Applications. *Elsevier.* Amsterdam, Netherlands, 2005.

[7] Y. M. Kim, S. N. Lahiri and D. J. Nordman. Non-Parametric Spectral Density Estimation Under Long-Range Dependence. *Journal of Time Series Analysis* **39** (3) (2018) 380–401.

[8] D. C. Reuman, R. A. Desharnais, R. F. Costantino, O. S. Ahmad and J. E. Cohen. Power spectra reveal the influence of stochasticity on nonlinear population dynamics. *Proceedings of the National Academy of Sciences of the USA* **103** (3) (2006) 18860–18865.

[9] T. Mcelroy, and D. Politis. Estimation the Spectral Density at Frequencies Near Zero. *A Preprint* **1** (2019) 1–19.

[10] A. Muhith, I. H. Susanto, D. Rahmalia, D. Adzkiya and T. Herlambang. The Analysis of Demand and Supply of Blood in Hospital in Surabaya City Using Panel Data. *Nonlinear Dynamics and Systems Theory* **22** (5) (2022) 550–560.

[11] E. Paparoditis and D. N. Politis. Nonlinear spectral density estimation: thresholding the correlogram. *Journal of Time Series Analysis* **33** (3) (2012) 386–397.

[12] E. Parzen. On consistent estimates of the spectrum of a stationary time series. *Annals of Mathematical Statistics* **28** (2) (1957) 329–348.

[13] E. Parzen. On asymptotically efficient consistent estimates of the spectral density function of a stationary time series. *Journal of the Royal Statistical Society. Series B (Methodological)* **20** (2) (1958) 303–322.

[14] Y. Pawitan and F. O'Sullivan. Nonparametric Spectral Density Estimation Using Penalized Whittle Likelihood. *Journal of American Statistical Association* **89** (426) (1994) 600–610.

[15] M. B. Priestley. Spectral analysis and time series. *Academic Press New York.* New York, 1981.

[16] H. Rust. Spectral Analysis of Stochastic Processes. *Lecture Notes for: GIACS Summer School.* Comorova, Romania, 2007.

[17] X. Shao and W. B. Wu. Asymptotic spectral theory for nonlinear time series. *Annals Statist.* **35** (4) (2007) 1773–1801.

[18] W. A. Woodward, H. L. Gray and A. C. Elliott. Applied Time Series Analysis. *Taylor and francis group.* Boca Raton-Florida, U. S. A, 2011.

[19] S. Zhang. Nonparametric Bayesian inference for the spectral density based on irregularly spaced data. *Computational Statistics & Data Analysis* **151** (2020) 1–14.

[20] Z. Zhou. Inference of weighted V-statistics for nonstationary time series and its applications. *The Annals of Statistics* **42** (1) (2014) 87–114.

Nonlinear Dynamics and Systems Theory, **25** (2) (2025) 144–152

Hybrid GW-PSO Algorithm for Enhanced Maximum Power Point Tracking under Various Conditions

N. Douifi [1*], A. Abbadi [2,3], F. Hamidia [2,3], N. Rai [1] and A. Tlemçani [2,3]

[1] *Laboratory of Advanced Electronic Systems -LAES, Electrical Engineering Department, Faculty of Technology, University of Medea, Medea, Algeria.*
[2] *Research Laboratory of Electrical Engineering and Automation-RLEA, Electrical Engineering Department, Faculty of Technology. University of Medea, Medea, Algeria.*
[3] *Renewable Energy and Materials Laboratory-LERM, Electrical Engineering Department, Faculty of Technology. University of Medea, Medea, Algeria.*

Received: May 29, 2024; Revised: February 27, 2025

Abstract: Photovoltaic (PV) systems face challenges in maximizing their output potential due to non-uniform sunlight distribution and unpredictable weather conditions, known as partial shading. To address these challenges, hybrid control algorithms have emerged as a promising solution. This paper presents a novel hybrid algorithm called HGW-PSO, which combines the strengths of Particle Swarm Optimization (PSO) and Grey Wolf Optimization (GWO). The hybrid approach utilizes the exploration capabilities of GWO and the convergence capabilities of PSO to achieve faster convergence, reduced oscillations, and improved implementation efficiency. The performance of the proposed HGW-PSO algorithm was evaluated under various scenarios of uniform and non-uniform shading. The results showed that HGW-PSO outperformed PSO, GWO, and Peafowl Optimization Algorithm (POA) in terms of tracking accuracy and convergence speed. Specifically, HGW-PSO achieved an average efficiency of 99.96% and a convergence time of less than 40 milliseconds, compared to 99.51% for GWO, 99.28% for POA, and 99.11% for PSO. These results demonstrate the effectiveness of the HGW-PSO algorithm in maximizing power tracking outcomes under challenging shading conditions.

Keywords: *global maximum power point; Grey Wolf Optimization; maximum power point tracker; partial shading conditions; Particle Swarm Optimization; Peafowl Optimization algorithm; photovoltaic.*

Mathematics Subject Classification (2020): 93C95, 93C10, 49M37, 68T20, 65K10, 37M05, 03D15.

* Corresponding author: mailto:douifi.nadia@univ-medea.dz

1 Introduction

In the last decade, the world has seen an increase in demand for energy due to the rapid growth of industrial technology and urbanization, which in turn increases the use of fossil fuels and traditional sources of energy [1], [2]. Therefore, it became essential to search for new clean energy sources to replace traditional ones and reduce their serious negative effects on the environment. Photovoltaic (PV) energy, in particular, has become the most attractive among all renewable energy sources.

The performance of PV panels is mainly impacted by several factors such as solar irradiation, temperature, and load values [3]. Moreover, in large-scale PV systems installed in urban areas, the PV system commonly faces a major problem known as partial shading (PS), which occurs when the PV array receives non-uniform irradiance levels [4]. Solar radiation is distributed unequally on the PV array because of obstacles in the surrounding installation sector such as clouds, trees, and buildings. The power-voltage characteristics of a photovoltaic array under partially shaded conditions (PSCs) are highly nonlinear, exhibiting multiple local peaks and a global peak denoted as GMPP [5], [6].

The maximum power is harvested from the photovoltaic panel only when the global peak is tracked. Therefore, a maximum power point tracking (MPPT) controller with proper technique becomes an essential component in any PV system to locate and track the specific maximum power point (MPP) regardless of the operating conditions of the PV system [7]. MPPT's main function is to control the duty cycle of the boost converter with the help of meta-heuristic algorithms to match the output power of the PV array to the load, guaranteeing power optimization and improving system efficiency.

Among all the MPPT techniques existing in the literature, Artificial Intelligence techniques (AI) including Artificial Fuzzy Logic (FL) [8], Ant Colony Optimization (ACO) [9], and Whale Optimization Algorithm (WOA) [10] are the most popular and widely used because of their accuracy and capabilities in dealing with MPP tracking, especially under PSC. Despite the merits of these MPPT techniques, they still have some demerits in relation to each other. Furthermore, no technique can assure the best result in all terms and under all circumstances [11]. Hence, hybrid algorithms have been presented in research papers to overcome the drawbacks of the original algorithms and merge their strength features.

In this paper, a new intelligent hybrid algorithm is proposed as an MPPT technique. The exploration potential of the GWO algorithm is combined with the exploitation potential of the PSO algorithm to develop the suggested Hybrid Grey Wolf-Particle Swarm Optimization (HGW-PSO) algorithm. The performance of the proposed HGW-PSO was evaluated under various weather conditions, including the Standard Test Conditions (STC), uniform fast-varying irradiance conditions as well as three different non-uniform (partial shading) scenarios.

A comprehensive comparison was conducted between HGW-PSO and three of the most commonly used MPPT techniques including GWO [12], Peafowl Optimization Algorithm (POA) [13], and PSO [14]. By testing the system under different scenarios, the study aimed to assess its ability to effectively track the maximum power output in dynamic and challenging conditions and to achieve a balance between response time, energy efficiency, and stability.

2 Proposed MPPT Algorithm

2.1 PSO

Particle Swarm Optimization algorithm is one of the most used and well-known population-based optimization techniques. It was first developed in 1995 by Kennedy [15], inspired by the intelligent swarm behaviour of birds. Initially, in the PSO technique, particles are distributed randomly in the search area with a unique position x_i and velocity v_i.

During the search process for the optimum solution, a particle's position is updated based on the best solution found by the particle in the neighbourhood P_{best_i} and the global best solution suggested by the whole population G_{best}. Accordingly, the position of the particle x_i is modified by using the relations [16]

$$x_i^{k+1} = x_i^k + v_i^{k+1}, \tag{1}$$

$$v_i^{k+1} = \omega v_i^k + c_1 r_1 (P_{best_i} - x_i^k) + c_2 r_2 (G_{best} - x_i^k), \tag{2}$$

where ω is the inertia weight, c_1, c_2 are the acceleration coefficients, r_1, r_2 denote the random values within the interval [0, 1] and k is the current iteration number.

2.2 GWO

Grey Wolf Optimizion (GWO) is a bio-inspired meta-heuristic algorithm introduced by Mirjalili et al. [17] in 2014, based on the hunting behavior and hierarchical structure of grey wolves. Wolves are categorized into alpha (α), beta (β), delta (δ), and omega (ω). In GWO, α represents the best solution, followed by β and δ. The hunting process updates wolves' positions through encircling, hunting, and attacking prey [18].

The encircling behaviour of grey wolves is mathematically modelled as follows [19]:

$$\vec{D} = |\vec{C}.\vec{X}_P^k - \vec{X}^k|, \tag{3}$$

$$\vec{X}^{k+1} = \vec{X}_P^k - \vec{A}.\vec{D}, \tag{4}$$

$\vec{D}$, $\vec{A}$ and $\vec{C}$ are the coefficient vectors, while k is the current iteration. $\vec{X}$ and $\vec{X}_P$ denote the position vector of the search agent and the optimum solution (prey position), respectively. The vectors $\vec{A}$ and $\vec{C}$ are calculated as

$$\vec{A} = 2.\vec{a}.\vec{r}_1 - \vec{a}, \tag{5}$$

$$\vec{C} = 2.\vec{r}_2, \tag{6}$$

r_1, and r_2 are the random vectors in the range [0,1]. The value a linearly decreases from 2 to 0 over the iterations.

In Grey Wolf Optimization, Alpha leads the hunt, assuming the best solution (prey location), with Beta and Delta as the next best. Other wolves, including Omega, update their positions to follow the best candidate. The search agent's position is updated using the formulas [20]

$$\vec{D}_\alpha = |\vec{C}_1.\vec{X}_\alpha^k - \vec{X}^k|, \quad \vec{D}_\beta = |\vec{C}_2.\vec{X}_\beta^k - \vec{X}^k|, \quad \vec{D}_\delta = |\vec{C}_3.\vec{X}_\delta^k - \vec{X}^k|, \tag{7}$$

$$\vec{X}_1 = \vec{X}_\alpha - \vec{A}_1.\vec{D}_\alpha, \quad \vec{X}_2 = \vec{X}_\beta - \vec{A}_2.\vec{D}_\beta, \quad \vec{X}_3 = \vec{X}_\delta - \vec{A}_3.\vec{D}_\delta, \tag{8}$$

$$\vec{X}^{k+1} = (\frac{\vec{X}_1 + \vec{X}_2 + \vec{X}_3}{3}). \tag{9}$$

2.3 HGW-PSO

This algorithm was developed by Narinder Singh et al. [21] in 2017. The main hybridization principle of the HGW-PSO algorithm is to merge the exploration ability of GWO with the exploitation ability of the PSO algorithm. In other words, the PSO algorithm mechanism is used to replace the updating function of GWO represented in (9). This hybridization is done to obtain the advantages and strengths of the individual algorithms and reduce their limitations. In the suggested HGW-PSO algorithm, the effect of delta wolves δ is eliminated to enhance its convergence time and efficiency. P_{best_i} and G_{best} in the velocity equation of the PSO algorithm are replaced with the Alpha solution X_1 and the agent's updated position is calculated using (9). In the HGW-PSO algorithm, the position of search agents is then updated using the mathematical expressions

$$v_i^{k+1} = \omega v_i^k + c_1 r_1 (X_1 - x_i^k) + c_2 r_2 (X - x_i^k), \tag{10}$$

$$x_i^{k+1} = x_i^k + v_i^{k+1}. \tag{11}$$

To apply the proposed HGW-PSO algorithm for MPPT in a PV system, each grey wolf position is set as the duty cycle (D_c) of the boost converter and (11) is modified as presented in the equations

$$\vec{D}_\alpha = |\vec{C}_1.\vec{D}^k_{c_\alpha} - \vec{D}^k_c|, \quad \vec{D}_\beta = |\vec{C}_2.\vec{D}^k_{c_\beta} - \vec{D}^k_c|, \tag{12}$$

$$\vec{D}_{c_1} = \vec{D}_{c_\alpha} - \vec{A}_1.\vec{D}_\alpha, \quad \vec{D}_{c_2} = \vec{D}_{c_\beta} - \vec{A}_2.\vec{D}_\beta, \tag{13}$$

$$D_c^{k+1} = \frac{D_{c_1} + D_{c_2}}{2}, \tag{14}$$

$$\Delta D_{c_i}^{k+1} = \omega.\Delta D_{c_i}^k + c_1 r_1 (D_{c_1} - D_{c_i}^k) + c_2 r_2 (D_c - D_{c_i}^k), \tag{15}$$

$$D_{c_i}^{k+1} = D_{c_i}^k + \Delta D_{c_i}^{k+1}. \tag{16}$$

3 Simulation Results and Analysis

To verify the abilities of the proposed MPPT HGW-PSO algorithm, a PV system illustrated in the block diagram shown in Figure 1a is modelled and simulated with MATLAB-Simulink. The PV array used as a PV source in the aforementioned system consists of three series-connected sub-arrays with a total power of 100.37 kW in standard test conditions (STC). The first and second-row sub-arrays contain 2*66 sub-modules, and the third-row sub-array consists of 1*66 sub-modules.

The suggested MPPT algorithm is tested for various scenarios of uniform (fast varying irradiance) and non-uniform shading (PSC) to validate its capabilities in tracking GMPP. The simulated operating conditions are summarized in Table 1, and their corresponding PV characteristic curves are shown in Figure 1b. The performance of the HGW-PSO is also compared to the performance of the GWO, PSO, and POA algorithms to prove its efficacy.

Figures 2 and 3 show the output power performance of the tested MPPT algorithms under the studied scenarios of shading and fast varying irradiance. For a fair comparison, all the obtained results are summarized in Table 2.

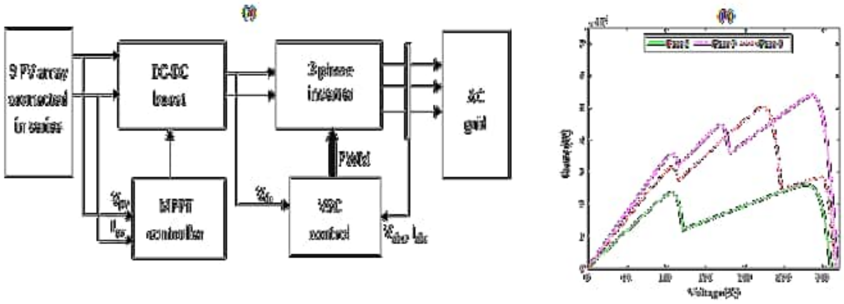

Figure 1: a. Block diagram of the simulated PV system.-b. PV characteristic curves of the studied PSC scenarios.

Case	PV1 (KW/m^2)	PV2 (KW/m^2)	PV3 (KW/m^2)	P_{MPP} (kW)
1	1, 0.3, 0.8, 0.5, 1	1, 0.3, 0.8, 0.5, 1	1, 0.3, 0.8, 0.5, 1	100.37, 29.418, 80.16, 49.704
2	0.6	0.25	0.6	26.016
3	0.5	0.9	0.7	53.85
4	0.8	0.6	0.25	50.29

Table 1: Irradiance levels for Cases 1 to 4.

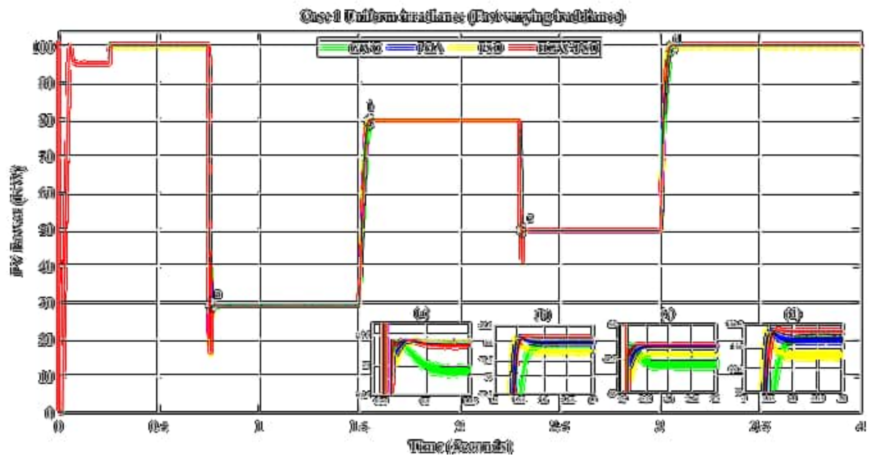

Figure 2: Output power performance of MPPT GWO, POA, PSO and HGW-PSO for uniform fast varying irradiance (Case 1).

3.1 Uniform irradiance

3.1.1 Case 1

This case study involves uniform irradiance levels that undergo an abrupt change from 1 KW/m^2 to 0.3 KW/m^2, as detailed in Table 1. In response to the rapid changes in irradiance, all techniques exhibit rapid changes in output power. This can be observed from Figure 2 and Table 2. While all techniques achieve stable output, the suggested technique stands out by attaining a steady output power with minimal oscillation and the highest efficiency of 99.96%. The POA technique follows closely with an efficiency of 99.88%, followed by PSO with 99.65% and GWO with 99.40%. Furthermore, the proposed HGW-PS technique exhibits desirable tracking speeds of around 30 ms in the fast-varying irradiance condition.

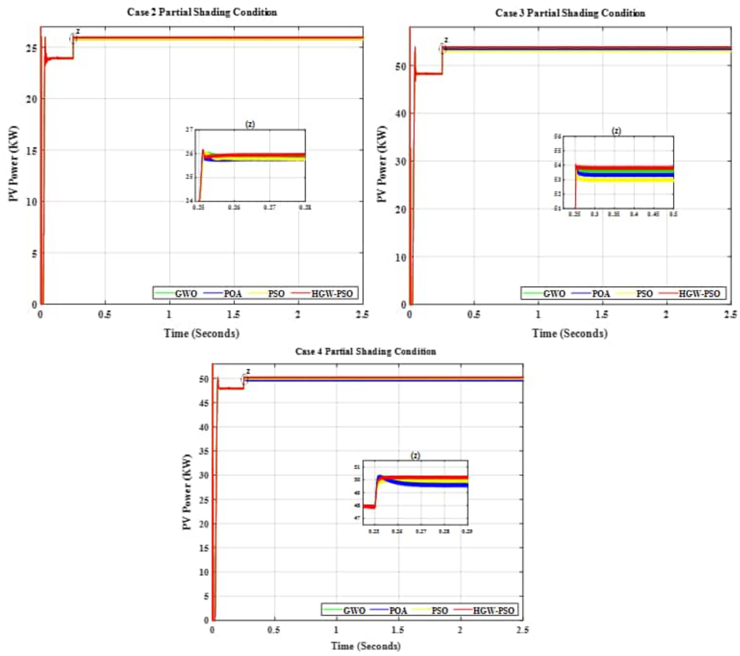

Figure 3: Output power performance of MPPT GWO, POA, PSO and HGW-PSO for partial shading Cases 2,3 and 4.

3.2 Non uniform irradiance

3.2.1 Case 2

In this scenario, as illustrated in Figure 1b, the PV curve depicts the response of the photovoltaic system under partial shading conditions. The shading induces two closely spaced operating points on the curve: LMPP at 23.542 kW and GMPP at 26.016 kW. The proposed technique effectively avoids the local peak and stabilises at the GMPP in under 35 ms, outperforming other techniques. The HGW-PSO algorithm achieves the highest efficiency of 99.98%, followed by GWO with 99.55%, POA with 99.36%, and PSO with 99.13%.

3.2.2 Case 3

Under this scenario of partial shading conditions, the three PV sub-arrays receive different irradiance levels, resulting in a characteristic curve with three multiple peaks, including two closely spaced LMPPs and one global peak at 50.87 kW. The proposed HGW-PSO algorithm demonstrates robustness against local peaks and efficiently reaches the GMPP with minimal power loss. HGW-PSO achieves the highest efficiency of 99.96%, outperforming GWO, POA, and PSO, which achieve efficiencies of 99.61%, 99.02%, and 98.40%, respectively. These results highlight the superior power output, faster convergence, and superior tracking capabilities of the suggested algorithm under partial shading conditions.

3.2.3 Case 4

To enhance the comprehensiveness of the comparative study, an additional partial shading case is included in Figure 1b, along with its corresponding PV curve. The maximum output power achieved by HGW-PSO, GWO, POA, and PSO is 50.26 kW, 50.02 kW, 49.72 kW, and 49.92 kW, respectively. Particularly, HGW-PSO achieves the highest efficiency of 99.94% among the considered techniques. In contrast, GWO, POA, and PSO achieve lower efficiencies of less than 99.46%. Moreover, HGW-PSO reaches the GMPP faster, within 25 ms.

Technique	Case	MPP tracked (kW)	Tc (s)	Efficiency(%)
GWO	1	100.15,28.90,79.97,49.40,100.15	0.284	99.40 (avg)
	2	25.90	0.275	99.55
	3	53.66	0.30	99.61
	4	50.02	0.272	99.46
POA	1	100.19,29.415,80.03,49.68,100.19	0.28	99.88 (avg)
	2	25.85	0.285	99.36
	3	53.34	0.29	99.02
	4	49.72	0.276	98.87
PSO	1	99.87,29.405,79.78,49.57,99.87	0.285	99.65 (avg)
	2	25.79	0.285	99.13
	3	53.01	0.282	98.40
	4	49.92	0.275	99.26
HGW-PSO	1	100.36,29.37,80.16,49.70,100.36	0.285	99.96 (avg)
	2	26.01	0.262	99.98
	3	53.85	0.286	99.96
	4	50.26	0.265	99.94

Table 2: Comparative analysis of MPPT GWO, POA, PSO and HGW-PSO.

When analyzing the results presented in Table 2, it becomes apparent that the proposed MPPT HGW-PSO algorithm exhibits a remarkable performance compared to the other tested algorithms, particularly in terms of MPP tracking efficiency and convergence time. Across all examined cases, HGW-PSO consistently achieves the highest efficiency, boasting an average efficiency of 99.96%. This surpasses the performance of GWO, POA, and PSO, which achieve average efficiencies of 99.40%, 99.88%, and 99.65%, respectively. Moreover, HGW-PSO demonstrates quicker convergence times across most cases, further underlining its effectiveness in optimizing power generation within photovoltaic systems across a spectrum of operating conditions.

4 Conclusion

In conclusion, this paper introduces and investigates a novel HGW-PSO MPPT-based algorithm designed to optimize power harvesting within the proposed PV system across various operating conditions. A 100 kW PV system was meticulously modeled and simulated using MATLAB-Simulink software to assess the performance of the HGW-PSO algorithm under various shading scenarios, including uniform and partial shading conditions (PSC). Through comparative analysis with existing MPPT techniques, namely GWO, POA, and PSO algorithms, the capabilities of the proposed MPPT method were rigorously validated. The results obtained across the four operating scenarios demonstrate the superior performance of the HGW-PSO algorithm in terms of GMPP tracking efficiency and convergence time.

Importantly, the nonlinear dynamics underlying the PV system behavior plays a crucial role in the performance of the proposed HGW-PSO MPPT algorithm. The existence of multiple local maxima and the complex interactions between environmental factors such as shading patterns, result in highly nonlinear power-voltage characteristics in the PV array. The HGW-PSO method's ability to rapidly converge to the global maximum power point, even under partial shading, indicates its strong capacity to navigate these nonlinear landscapes. By incorporating both global and local search strategies, the HGW-PSO algorithm effectively overcomes the challenges posed by the inherent nonlinearities in the PV system. This highlights the significance of the obtained results for advancing nonlinear optimization techniques applied to renewable energy systems.The insights gained from this work have important implications for enhancing the power generation efficiency of photovoltaic installations in real-world, dynamically changing operating conditions.

References

[1] A. K. Bilhan. Integrated solar-based PEMWEs for green electricity production. *International Journal of Hydrogen Energy* **75** (2024) 415–427.

[2] A. Medjber, A. Moualdia and A. Morsli. PI-Fuzzy Control Applied to the Hybrid PV / Wind Pumping System with Energy Storage. *Nonlinear Dynamics and Systems Theory* **22** (3) (2022) 319–329.

[3] A. Morsli, A. Tlemcani and H. Nouri. Control of a Shunt Active Power Filter by the Synchronous Referential Method Connected with a Photovoltaic Solar Energy. *Nonlinear Dynamics and Systems Theory* **22** (4) (2022) 424–431.

[4] M. Neethu and R. Senthilkumar. Soft Computing Based MPPT Controller for Solar Powered Battery Charger Under Partial Shading Conditions. In: *2019 Fifth International Conference on Electrical Energy Systems (ICEES)*. IEEE, Chennai, India, 2019, 1–6.

[5] F. Hamidia, A. Abbadi, M. R. Skender, A. Morsli, F. Bettache, A. Medjber and A. Tlemcani. Maximum Power Point Tracking Based on Remora Algorithm under PSC. *Nonlinear Dynamics and Systems Theory* **23** (4) (2023) 381–389.

[6] C. B. Oguz, E. Avci and S. B. Ozturk. Analysis of PV power plant performance considering combination of different MPPT algorithms, shading patterns and connection types. *Engineering Science and Technology, an International Journal* **48** (2023) 101559.

[7] M. A. Ebrahim, A. Osama, K. M. Kotb and F. Bendary. Whale inspired algorithm based MPPT controllers for grid-connected solar photovoltaic system. *Energy Procedia* **162** (2019) 77–86.

[8] T. Hai, J. Zhou and K. Muranaka. An efficient fuzzy-logic based MPPT controller for grid-connected PV systems by farmland fertility optimization algorithm. *Optik* **267** Elsevier, (2022) 169636.

[9] G. S. Krishnan, S. Kinattingal, S. P. Simon and P. S. R. Nayak. MPPT in PV systems using ant colony optimisation with dwindling population. *IET Renewable Power Generation* **14** (7) 1105–1112. Wiley Online Library, 2020.

[10] D. E. Zabia, H. Afghoul and O. Kraa. Maximum power point tracking of a photovoltaic system under partial shading condition using whale optimization algorithm. *Artificial Intelligence and Heuristics for Smart Energy Efficiency in Smart Cities: Case Study: Tipasa, Algeria.* Springer, 2022, 121–132.

[11] S. Sarwar, M. Y. Javed, M. H. Jaffery, J. Arshad, A. Ur Rehman, M. Shafiq and J.G. Choi. A novel hybrid MPPT technique to maximize power harvesting from pv system under partial and complex partial shading. *Applied Sciences.* **12** (2) (2022) 587.

[12] D. K Kishore, M. R. Mohamed, K. Sudhakar and K. Peddakapu. An improved grey wolf optimization based MPPT algorithm for photovoltaic systems under diverse partial shading conditions. *Journal of Physics: Conference Series* **2312** (1) (2022) 012063.

[13] D. Li, J. Li and N. Wang. A Novel Technique Based on Peafowl Optimization Algorithm for Maximum Power Point Tracking of PV Systems Under Partial Shading Condition. *Frontiers in Energy Research* **9** (2021) 801571.

[14] A. I. Nusaif and A. L. Mahmood. MPPT algorithms (PSO, FA, and MFA) for PV system under partial shading condition, case study: BTS in Algazalia, Baghdad. *International Journal of Smart Grid-ijSmartGrid* **4** (3) (2020) 100–110.

[15] A. Khernane. Numerical Approximation of the Exact Control for the Vibrating Rod with Improvement of the Final Error by Particle Swarm Optimization. *Nonlinear Dynamics and Systems Theory* **20** (2) (2020) 179–190.

[16] C. B. Regaya, H. Hamdi, F. Farhani, A. Marai, A. Zaafouri and A. Chaari. Real-time implementation of a novel MPPT control based on the improved PSO algorithm using an adaptive factor selection strategy for photovoltaic systems. *ISA transactions* **146** (2024) 496–510.

[17] S. Mirjalili, S. M. Mirjalili and A. Lewis. *Grey Wolf Optimizer. Advances in Engineering Software* **69** (2014) 46–61.

[18] J. A. Salim, B. M. Albaker, M. S. Alwan and M. Hasanuzzaman. Hybrid MPPT approach using Cuckoo Search and Grey Wolf Optimizer for PV systems under variant operating conditions. *Global Energy Interconnection* **5** (6) (2022) 627–644.

[19] K. Atici, I. Sefa and N. Altin Grey wolf optimization based MPPT algorithm for solar PV system with sepic converter. In: *2019 4th International Conference on Power Electronics and their Applications (ICPEA).* IEEE, Elazig, Turkey, 2019, 1–6.

[20] B. Laxman, A. Annamraju and N. V. A. Srikanth. A grey wolf optimized fuzzy logic based MPPT for shaded solar photovoltaic systems in microgrids. *International Journal of Hydrogen Energy* **46** (18) (2021) 10653–10665.

[21] N. Singh and S. B. Singh. Hybrid algorithm of particle swarm optimization and grey wolf optimizer for improving convergence performance. *Journal of Applied Mathematics* **2017** (2017) 15 pages.

Nonlinear Dynamics and Systems Theory, **25** (2) (2025) 153–160

Forecasting Air Pollution Levels Using Support Vector Regression and K-Nearest Neighbor Algorithm

I. Indasah [1*], A. Y. P. Asih [2], T. Herlambang [3], P. Triwinanto [4] and K. Oktafianto [5]

[1] *Master of Public Health Department, Universitas STRADA Indonesia, Kediri, Indonesia.*
[2] *Department of Public Health, Faculty of Health, Universitas Nahdlatul Ulama Surabaya, Surabaya, Indonesia.*
[3] *Department of Information System, Universitas Nahdlatul Ulama Surabaya, Indonesia.*
[4] *National Research and Innovation Agency, Indonesia.*
[5] *Department of Mathematics, University of PGRI Ronggolawe, Indonesia.*

Received: October 21, 2024; Revised: March 31, 2025

Abstract: Air pollution is one of the problems faced by big cities, including Surabaya. One of the factors that drives air pollution in big cities is high population mobility. As known, air is composed of oxygen (O2), carbon dioxide (CO2), tropospheric ozone (O3), nitrogen (N2), and particles (PM10 and PM 2.5). High concentration levels of O3 pollutants in an urban area can endanger human health and ecosystems. To monitor air quality in Surabaya city, the city government uses monitoring equipment and air control station facilities. The data obtained becomes a reference for predicting air conditions at that time and forecasting future conditions using certain methods. In this research, the methods used for forecasting are Support Vector Regression (SVR) and K-Nearest Neighbor (K-NN). The Support Vector Regression (SVR) method showed the best error value of 0.0583 and the K-Nearest Neighbor (K-NN) method had the best error value of 0.0486.

Keywords: *pollution; forecasting; Support Vector Regression; K-Nearest Neighbor.*

Mathematics Subject Classification (2020): 62J05, 70-10, 90Bxx.

* Corresponding author: `mailto:indasah.strada@gmail.com`

1 Introduction

Air pollution is a serious problem faced in big cities, including Surabaya. Some of the contributing factors include high mobility and motorized vehicles. According to the Air Visual's AQI (Air Quality Index) publication in 2019, Surabaya was ranked seventh among the most polluted cities in Indonesia and ranked 226th among the cities of the world [1]. Based on this fact, the Surabaya city government made efforts by issuing Local Regulation Number 3 of 2008 concerning Air Pollution Control of Surabaya City [2].

The air condition of Surabaya with high population mobility is directly proportional to the massive use of motorized vehicles. This is shown by two-wheeled vehicles increasing 7.03% per year from 1,944,802 vehicles in 2015 to 2,081,449 vehicles in 2016 and 2,159,069 in 2017. This resulted in the traffic in the city of Surabaya having a negative impact in the form of air pollution from emissions released by vehicles [3]. Based on these conditions, it is necessary to make a directed and scientific solution for handling such air pollution.

By the development of information technology, it is possible to make a machine learning-based prediction system. The advantages of machine learning are that it provides easier implementation with low computational costs, as well as fast training, validation, testing, and evaluation with high performance compared to physical models, and is relatively less complicated [4].

In this research, we use two methods, namely Support Vector Regression (SVR) and K-Nearest Neighbor (K-NN). Support Vector Regression (SVR) is a development method of the Support Vector Machine (SVM) which is applied for solving regression cases and provides output in the form of continuous data with real numbers so that it can be used for forecasting [5]. K-Nearest Neighbor (K-NN) is a machine learning algorithm used for classification and regression. This algorithm is based on the idea that similar data instances tend to be close to each other in feature space [6], [7].

In previous research, the SVR algorithm was successfully used to forecast the air quality index in Makassar City [8], while the K-NN algorithm was successfully used in predicting air quality in Jakarta City [9]. This research aims to develop and to compare the performance of each method in predicting air pollution levels in the city of Surabaya.

2 Research Methods

The dataset used in this study comes from the Surabaya City air condition data dated 01/01/2020 to 31/12/2020. An overview of the research can be seen in Figure 1 below.

1. **Problem Identification**: This study deals with a case study on the prediction of the air pollution level in the city of Surabaya.

2. **Data Acquisition**: The data used in this study is secondary data sourced from the Surabaya City air conditions as of 01/01/2020 to 31/12/2020.

3. **Data Preprocessing and Analytics**: Basically, data preprocessing and analytics are used to see the initial condition of the dataset obtained from the source. At this stage, the dataset is identified from the data type to missing values that may occur.

4. **Feature Selection**: This study uses the Pearson Product correlation analysis technique to find a linear relationship between two variables having a normal dis-

DATE	PM10	SO2	CO	O3	NO2	MAX	RESULT
01/01/2020	30	20	10	32	9	32	GOOD
02/01/2020	27	22	12	29	8	29	GOOD
03/01/2020	39	22	14	32	10	39	GOOD
04/01/2020	34	22	14	38	10	38	GOOD
05/01/2020	35	22	12	31	9	35	GOOD
06/01/2020	46	23	16	32	9	46	GOOD
07/01/2020	37	23	26	33	11	37	GOOD
08/01/2020	41	26	20	30	11	41	GOOD
09/01/2020	52	23	29	24	12	52	AVERAGE
10/01/2020	24	24	18	25	8	25	GOOD
11/01/2020	34	31	25	23	8	34	GOOD
12/01/2020	27	23	9	33	4	33	GOOD
13/01/2020	33	26	12	36	8	36	GOOD
14/01/2020	34	28	13	27	7	34	GOOD
15/01/2020	29	22	13	36	8	36	GOOD
01/01/2020	30	20	10	32	9	32	GOOD
16/01/2020	52	60	19	30	8	60	AVERAGE
...	...	...	...	...	...	...	...
31/12/2020	18	13	6	24	3	24	GOOD

Table 1: Dataset.

tribution [10]. Below is the function of the Pearson Product:

$$r_{xy} = \frac{N\Sigma XY - (X)(Y)}{\sqrt{N\Sigma X^2 - \Sigma X^2 N\Sigma Y^2 - \Sigma Y^2}}. \tag{1}$$

Notes: r_{xy} is the relationship coefficient; N is the number of samples used; X is the total score of questions; Y is the sum of total scores.

5. **Model Selection**: Support Vector Regression (SVR) is a development algorithm of the Support Vector Machine (SVM) algorithm introduced by Cortes and Vapnik [11]. Like SVM, SVR also uses the best hyperplane in the form of a regression function by making the error as small as possible. The function of the SVR can generally be written as follows:

$$f(x) = w\varphi(x) + b \tag{2}$$

with $f(x)$ being the regression function; w being the vector; b being the bias and the decision boundary equation

$$\begin{aligned} W_x + b &= +e \\ W_x + b &= -e \end{aligned}$$

so that the hyperplane fulfills the inequality

$$e < y - W_x + b < +e$$

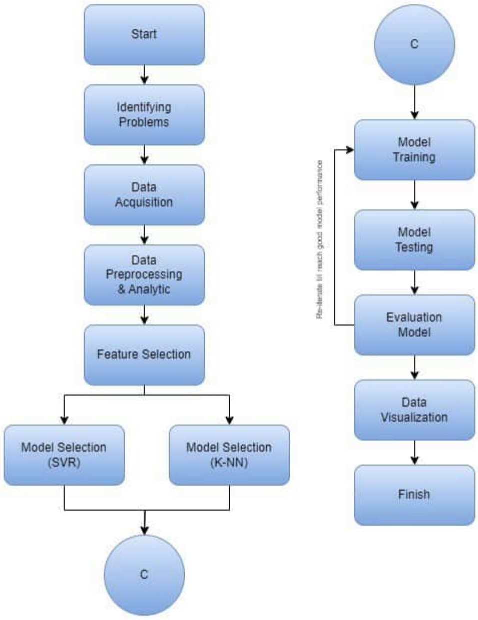

Figure 1: Research methods.

with the minimization function

$$MIN\ \frac{1}{2}\|w^2\| + C\sum_{i=1}^{n}|\xi_i|$$

and the constraint function

$$|y_i - w_i x_i| \leq \varepsilon + |\xi_i|.$$

Then, for the K-Nearest Neighbor (K-NN) algorithm calculated using the Euclidean rule, the mathematical function can be written as follows:

$$D = \sqrt{(x_2 - x_1) * 2 - (y_2 - y_1) * 2} \tag{3}$$

with D being the distance; x being the data sample; y being the testing data.

6. **Model Training**: At this stage, the predicted values of the Support Vector Regression (SVR) and K-Nearest Neighbor (K-NN) algorithms are trained based on the division of training data and testing data to obtain error values and accuracy values.

7. **Model Testing**: Model testing of the learning outcomes with the prepared test data.

8. **Evaluation Model**: At the evaluation stage, the model trained and tested is calculated for accuracy based on the resulting error value. This study uses the

Root Mean Square Error (RMSE) method to calculate the error value generated by the model. The function of the Root Mean Square Error (RMSE) is as follows:

$$RMSE = \sqrt{\frac{\Sigma(y_i - \hat{y}_i)^2}{n}} \tag{4}$$

with n being the quantity of data; y_i being the actual value at the i-th data; $\hat{y}_i$ being the predicted value at the i-th data.

3 Result and Discussion

This study tries to implement two machine learning algorithms, namely SVR and KNN, to forecast air pollution using the Python programming language. This study shows the comparison based on the methods and the difference in the quantity of training data and testing data shown in Figures 2-4. Figure 2 is the simulation result of the SVR and K-NN algorithms with 70% of training data and 30% of testing data.

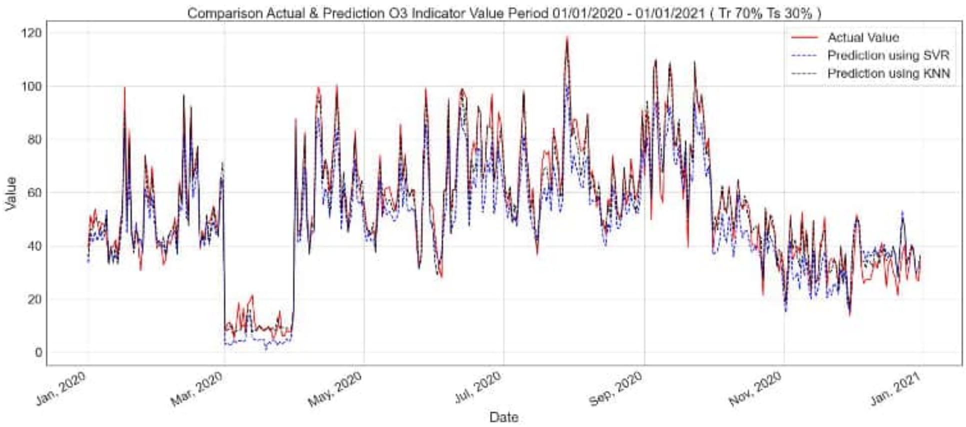

Figure 2: Results of forecasting air pollution by 70% of training data and 30% of testing data.

The simulation results in Figure 2 show the performance comparison of the SVR and K-NN methods in predicting O3 levels in Surabaya with a data split into 70% of training data and 30% of testing data. It appears in the simulation results in Figure 2, that the simulation results using the KNN have a smaller error than those of the SVR, with the RMSE of the KNN of around 0.0486 and the RMSE of the SVR of around 0.0583.

It can be seen that the prediction using the KNN (marked by the black line) is more accurate and consistently close to the actual value (marked by the red line) compared to the prediction using the SVR (marked by the blue line). The graph clearly illustrates that the KNN is more effective in following the fluctuations and dynamics of O3 historical data, thus providing predictions that are closer to reality.

The simulation results in Figure 3 show the performance comparison of the SVR and K-NN methods in predicting O3 levels in Surabaya with a data split into 80% of training data and 20% of testing data. It appears in the simulation results in Figure 3 that the simulation results using the KNN have a smaller error than those of the SVR, with the RMSE of the KNN of around 0.0504 and the RMSE of the SVR of around 0.0588.

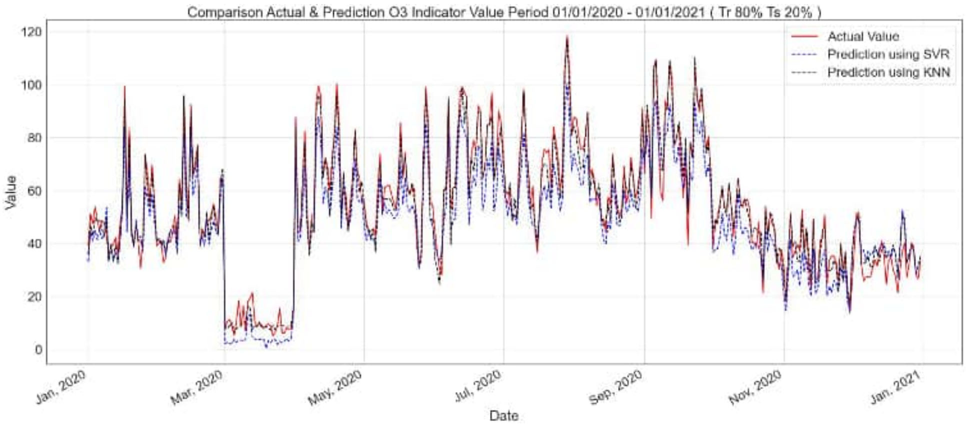

Figure 3: Results of forecasting air pollution by 80% of training data and 20% of testing data.

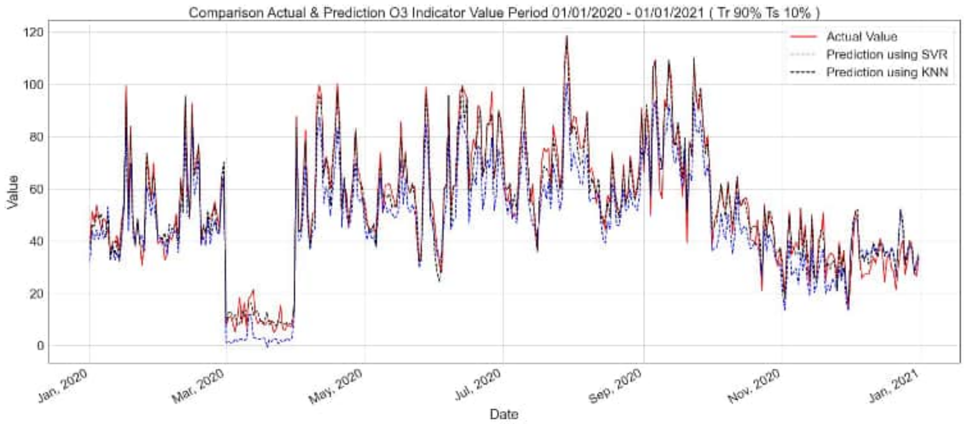

Figure 4: Results of forecasting air pollution by 90% of training data and 10% of testing data.

The simulation results in Figure 4 show the performance comparison of the SVR and K-NN methods in predicting O3 levels in Surabaya with a data split into 90% of training data and 10% of testing data. It appears in the simulation results in Figure 4 that the simulation results using the KNN have a smaller error than those of the SVR, with the RMS of the KNN method having a smaller error than that of the SVR method. A recapitulation of the results of each simulation can be seen in Tables 2-4.

In Table 2, it can be seen that the RMSE value produced by the SVR algorithm is the best in the first simulation with a ratio of 70% of training data and 30% of testing data. Then, in the second and third simulations, there is an increase in the RMSE value with a difference of 0.0005 to 0.0046 compared to the first simulation.

In Table 3, it can be seen that the RMSE value produced by the KNN algorithm is best in the first simulation with a ratio of 70% of training data and 30% of testing data. Then, in the second and third simulations, there is an increase in the RMSE value, which has a difference of 0.0014 to 0.0018 compared to the first simulation. A complete

	70% Training Data and 30% Testing Data	80% Training Data and 20% Testing Data	90% Training Data and 10% Testing Data
RMSE from Forecasting Results	0.0583	0.0588	0.0629

Table 2: Comparison of SVR RMSE Values

	70% Training Data and 30% Testing Data	80% Training Data and 20% Testing Data	90% Training Data and 10% Testing Data
RMSE from Forecasting Results	0.0486	0.0504	0.0500

Table 3: Comparison of SVR-KNN RMSE values.

comparison of the RMSE values of the two algorithms can be seen in Table 4.

	70% Training Data and 30% Testing Data		80% Training Data and 20% Testing Data		90% Training Data and 10% Testing Data	
	SVR	KNN	SVR	KNN	SVR	KNN
RMSE from Forecasting Results	0.0583	0.0486	0.0588	0.0504	0.0629	0.0500

Table 4: Comparison of KNN RMSE values.

In Table 4, it can be seen that the RMSE value produced by the SVR and KNN algorithms is the best in the first simulation with a ratio of 70% of training data and 30% of testing data. Then, in the second and third simulations, there is an increase in the RMSE value occurring in each algorithm. The table above shows that the RMSE value of the simulation results generated by the two algorithms does not touch 1%.

4 Conclusion

Based on the simulation results obtained, it can be concluded that the first simulation results of the SVR and KNN algorithms are the best simulation results with an SVR RMSE value of 0.0583 and a KNN RMSE value of 0.0486. These results prove that the SVR and KNN methods provide good prediction results.

References

[1] M. M. Syaifulloh. Prediction of Air Pollution Standard Index in Surabaya City Based on Carbon Monoxide Gas Concentration. *Jambura Journal of Probability and Statistics* **2** (2) (2021) 86–95.

[2] M. R. Fithori, M. N. Ubaidillah and M. Z. A. Mukminin. Air Pollution Control Through Regional Regulations. *Ma'mal: Journal of Sharia and Law Laboratory* **5** (1) (2024) 73–94.

[3] G. A. Setyo and R. E. Handriyono. Analysis of the Distribution of Carbon Monoxide (CO) Gas from Transportation Sources on Kertajaya Indah Highway, Surabaya. *Environmental Engineering Journal ITATS* **1** (1) (2021) 18–26.

[4] N. M. O. W. S. Sari, H. Elindra and A. H. Saputra. Carbon Monoxide Prediction Using Machine Learning Model Based on Comparison of Time Series Models Case Study of DKI Jakarta. *Collaborative Journal of Science* **7** (3) (2024) 1116–1128.

[5] M. E. S. Wicaksono, G. M. A. Sasmita and I. P. A. E. Pratama. Air Quality Forecasting in Central Jakarta City Using Long Short-Term Memory and Support-Vector Regression Methods. *JITTER - Scientific Journal of Technology and Computers* **4** (1) (2023).

[6] I. Irwansyah and A. D. Wiranata. Comparison of Decision Tree Algorithms, Naive Bayes and K-Nearest Neighbor to Determine Air Quality in DKI Jakarta Province. *Infotech: Journal of Technology Information* **9** (2) (2023) 193–198.

[7] T. Herlambang, V. Asy'ari, R. P. Rahayu, A. A. Firdaus and N. Juniarta. Comparison of Naive Bayes and K-Nearest Neighbor Models for Identifying the Highest Prevalence of Stunting Cases in East Java. *BAREKENG: Journal of Mathematics and Its Applications* **18** (4) (2024) 2153–2164.

[8] R. W. Rahmat, S. Annas and Z. Rais. Support Vector Regression (SVR) Analysis to Predict Air Quality Index in Makassar City. *VARIANSI: Journal of Statistics and Its application on Teaching and Research* **5** (3) (2023) 104–117.

[9] A. Amalia, A. Zaidiah and I. N. Isnainiyah. Air Quality Prediction Using K-Nearest Neighbor Algorithm. *JIPI (Scientific Journal of Informatics Research and Learning)* **7** (2) (2022) 496–507.

[10] R. M. Tedja, M. Arifin and E. S. Agustian. Correlation Analysis of Airbus A320-200 Aircraft Age Against the Amount of Corrosion Occurring Using the Pearson Product Moment Correlation Method. *JIPI (Journal of Aerospace Technology)* **8** (2) (2023).

[11] R. Puspita, H. Cipta and R. Aprilia. Application of the Support Vector Regression Method with the Grid Search Algorithm to Predict Movement Gold Price. *Science Incandescent Journal* **19** (2) (2024) 380–385.

[12] V. Asy'ari, M. Y. Anshori, T. Herlambang, I. W. Farid, D. F. Karya, and M. Adinugroho. Forecasting average room rate using k-nearest neighbor at Hotel S. In: *International Conference on Advanced Mechatronics, Intelligent Manufacture and Industrial Automation (ICAMIMIA)*, IEEE, Nov. 2023, 496-500.

[13] D. Novita, T. Herlambang, V. Asy'ari, A. Alimudin, and H. Arof. Comparison Of K-Nearest Neighbor And Neural Network For Prediction International Visitor In East Java. In: *BAREKENG: Journal of Mathematics and Applied Sciences* **18** (3) (2024) 2057–2070.

[14] M. Y. Anshori, V. Asy'ari, T. Herlambang, and I. W. Farid. Forecasting occupancy rate using neural network at Hotel R. In: *International Conference on Advanced Mechatronics, Intelligent Manufacture and Industrial Automation (ICAMIMIA)*, IEEE, Nov. 2023, 347-351.

[15] F. A. Susanto, M. Y. Anshori, D. Rahmalia, K. Oktafianto, D. Adzkiya, P. Katias and T. Herlambang. Estimation of Closed Hotels and Restaurants in Jakarta as Impact of Corona Virus Disease (Covid-19) Spread Using Backpropagation Neural Network. In: *Nonlinear Dynamics and Systems Theory: An International Journal of Research and Surveys* **22** (4) (2022) 457–467.

[16] M. Y. Anshori, T. Shawyun, D. V. Madrigal, D. Rahmalia, F. A. Susanto, T. Herlambang, and D. Adzkiya. Estimation of closed hotels and restaurants in Jakarta as impact of corona virus disease spread using adaptive neuro fuzzy inference system. In: *IAES International Journal of Artificial Intelligence (IJ-AI)* **11** (2) (2022) 462–472.

Nonlinear Dynamics and Systems Theory, **25** (2) (2025) 161–170

A Novel Chaotic Jerk System with Multistability and Its Circuit Implementation

K. Kalaichelvi, R. Rameshbabu*, V. Dharshini Priya,
P. Gokula Rithanya, G. K. Bhavadharani and K. S. Gayathiri

Department of Electronics and Communication Engineering,
V.S.B. Engineering College, Karur, Tamilnadu, India - 639111

Received: March 27, 2024; Revised: April 1, 2025

Abstract: In this research paper, a new chaotic jerk system is presented. The specialty of the new system is that it can produce coexisting multiple attractors for different initial conditions. This special behavior of the new system can be used to increase the security of the communication system. The bifurcation diagram, Lyapunov exponents, attractor diagrams, and basin of attraction are the important tools used to validate the multistability of the proposed system. The simulation results indicate that there are multiple coexisting attractors in the new system. Finally, an electronic circuit is designed for the proposed system to realize the coexisting attractors in practice.

Keywords: *jerk system; multistability; bifurcation analysis; circuit simulation.*

Mathematics Subject Classification (2020): 93A30, 70K99.

1 Introduction

In recent years, chaotic jerk systems have been introduced with hidden attractors [1], multi-scroll attractors [2], multi-stability [3], mega-stability [4], hypogenetic system [5], memristor [6], and coexisting attractors [7]. The invention of the chaotic jerk system with coexisting multiple attractors is very important in recent days because of its many engineering applications such as secure communication systems [8], image processing [9], random number generation [10], etc. The coexisting attractors, which means multiple attractors, can be observed in any nonlinear dynamical system for different initial conditions and system parameters. This special behavior of the system increases its complexity

* Corresponding author: mailto:rameshbaburamar@vsbec.org

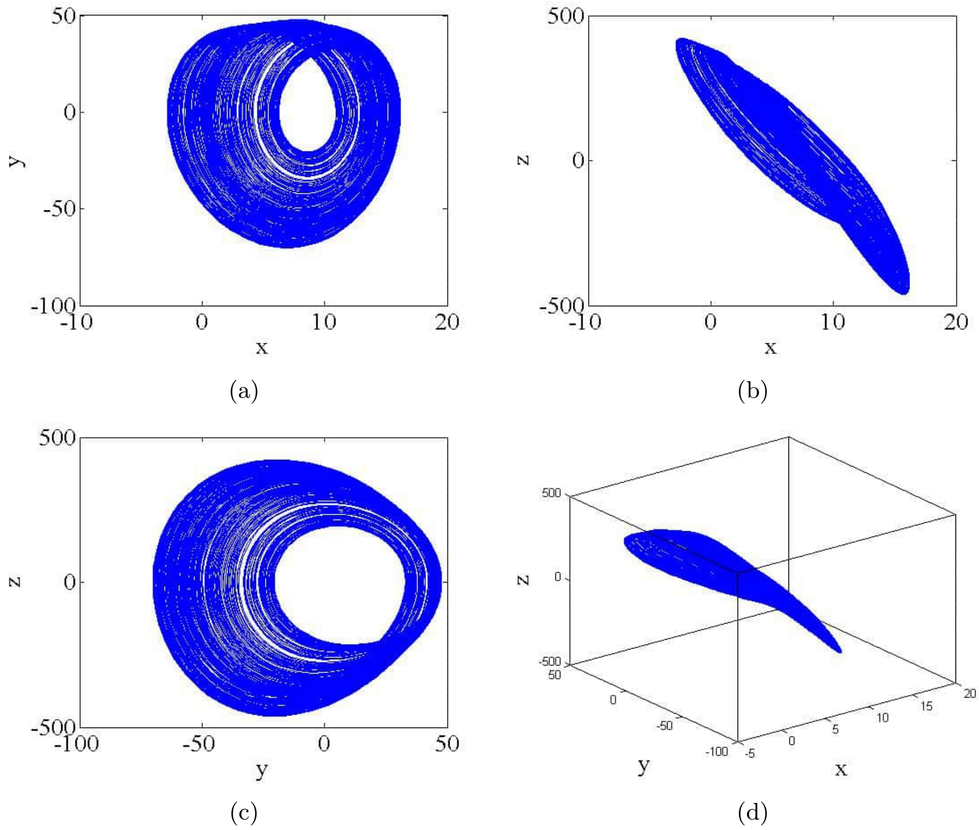

Figure 1: (a-d) The attractors of the new system in 2D and 3D planes.

and can be used to improve the security of the communication system. Recently, many researchers [11–14] introduced chaotic jerk systems with coexisting multiple attractors and analyzed their dynamical properties employing a bifurcation diagram and Lyapunov exponents. It was understood through dynamic analysis that the chaotic system can have coexisting chaotic attractors, stable node attractors, and limit cycle attractors for a certain range of system parameters. When the system produces an infinite number of coexisting attractors for the variation of initial conditions, the phenomenon is called extreme multistability.

The proposed chaotic jerk system has only one cubic nonlinearity and exhibits coexisting attractors in both periodic and chaotic states when initial conditions are changed. The chaotic and coexisting attractor behavior in the new system is verified through the bifurcation diagram, Lyapunov exponents spectrum, and attractor diagram. The dissipativity, equilibrium points, and stability analysis were also conducted to verify the chaotic nature of the proposed system. Furthermore, an electronic circuit is designed for the proposed system using basic electronic components such as resistors, capacitors, and OPAMP and simulated in Multisim software. As a result of the simulation, the chaotic attractors are obtained for the practical implementation of the proposed system.

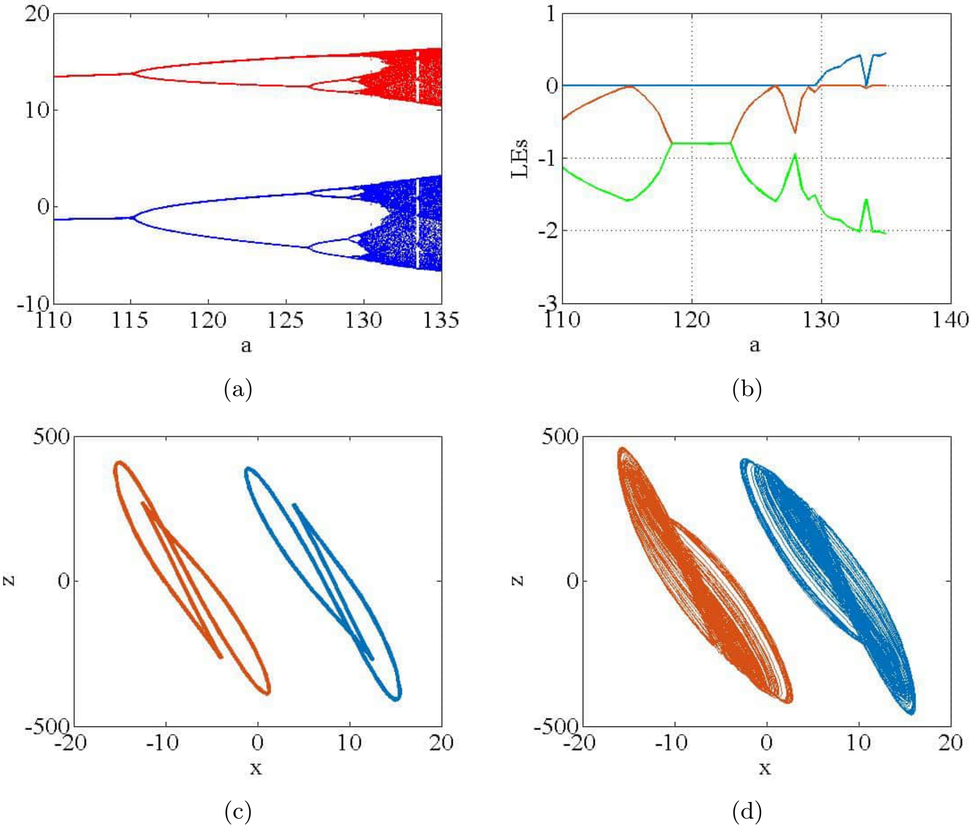

Figure 2: (a) Bifurcation diagram with $X_1(0)$ (Blue) and $X_2(0)$ (Red); (b) Lyapunov exponent plots of the system (1) under the parameter a; (c-d) Coexisting attractors in the xz-plane at $a = 125$ and $a = 133$, respectively.

2 Theoretical Model of Novel Chaotic Jerk System

In this section, a new jerk system is introduced and its dynamical behaviors, including dissipativity, equilibrium points, stability, Lyapunov exponents, and Lyapunov dimension, are analyzed in detail. The new system is of the form

$$\begin{aligned} \dot{x} &= y, \\ \dot{y} &= z, \\ \dot{z} &= ax - x^3 - by - cz. \end{aligned} \tag{1}$$

Here, x,y,z are the state variables and $a = 133$, $b = 51$, $c = 1.6$ are the parameters of the system (1).

2.1 Lyapunov exponents and Lyapunov dimension

The numerical values of Lyapunov exponents for the new system (1) can be calculated as $LE_1 = 0.404527, LE_2 = 0, LE_3 = -2.028421$. The Lyapunov dimension (D_L) can be

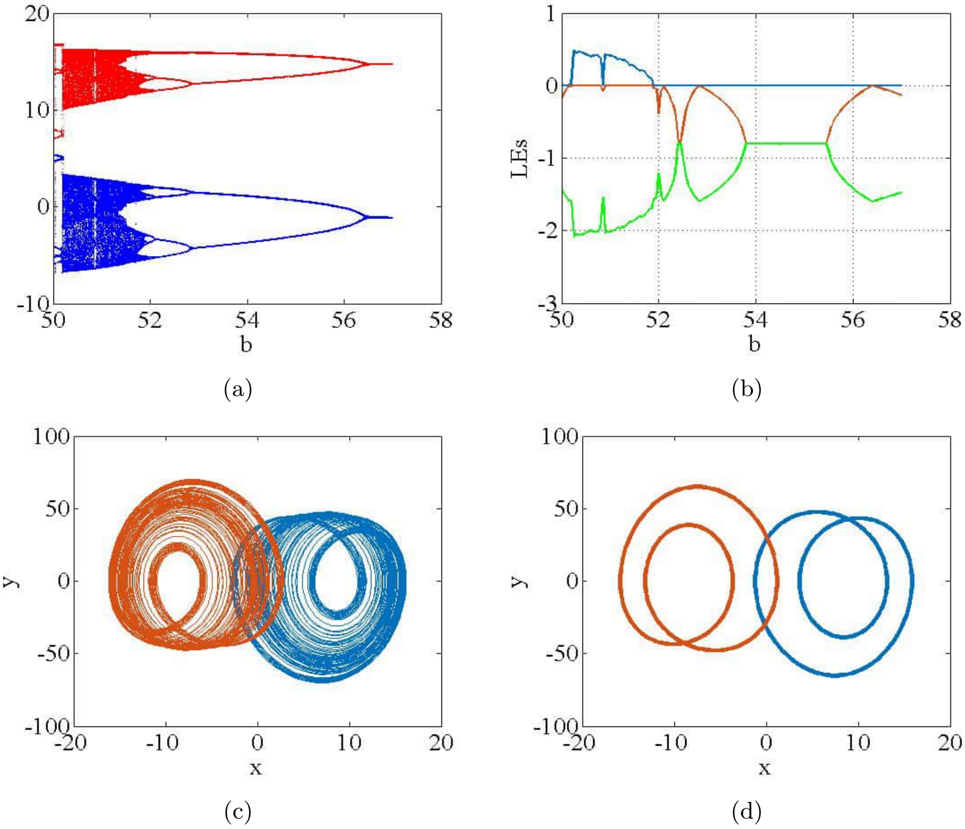

Figure 3: (a) Bifurcation diagram with $X_1(0)$ (Blue) and $X_2(0)$ (Red); (b) Lyapunov exponent plots of the system (1) under the parameter b; (c-d) Coexisting attractors in the xy-plane at $b = 51$ and $b = 54$, respectively.

obtained as $D_L = 2 + \frac{LE_1+LE_2}{|LE_3|} = 2.199$, which indicates the fractional dimension of the proposed system (1).

2.2 Equilibrium points and stability

The equilibrium points can be calculated by letting $\dot{x} = 0, \dot{y} = 0$ and $\dot{z} = 0$ in (1) as given by

$$\begin{aligned} &y = 0, \\ &z = 0, \\ &ax - x^3 - by - cz = 0. \end{aligned} \tag{2}$$

The solution of (2) can be obtained as $x = \pm\sqrt{a}$ and thus the equilibrium points are

$$E_1 = \begin{bmatrix} 0, & 0, & 0 \end{bmatrix}, \quad E_{2,3} = \begin{bmatrix} \pm\sqrt{a}, & 0, & 0 \end{bmatrix}.$$

Now, the Jacobian matrix (J) of the new system (1) can be written as

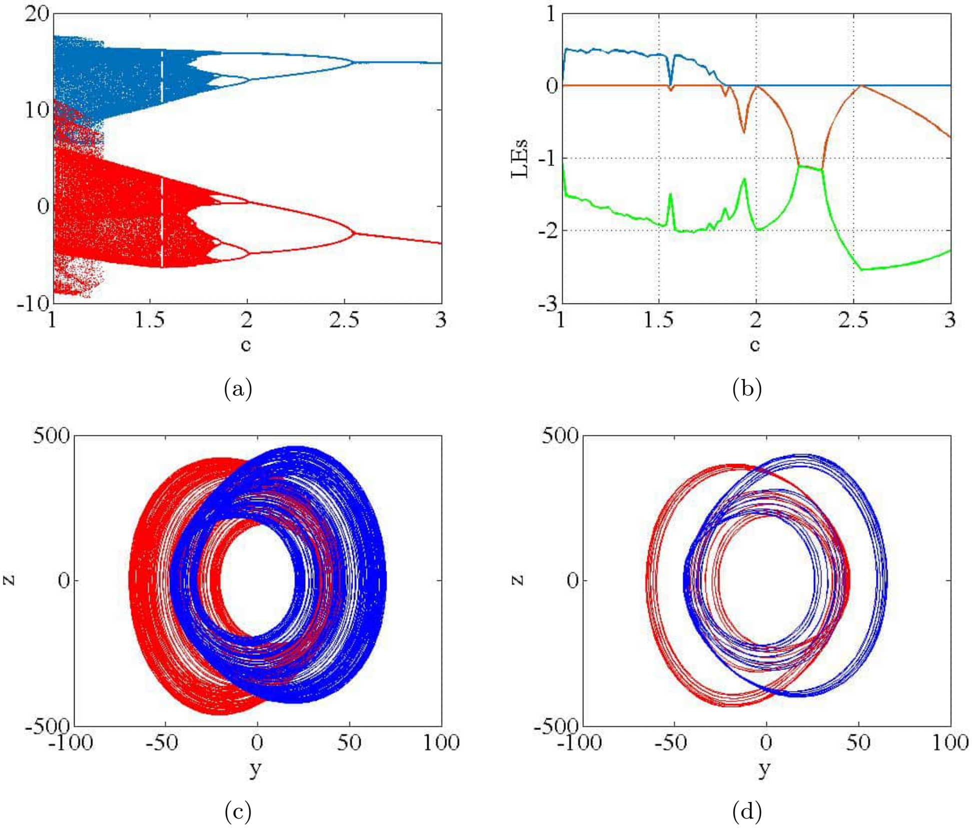

Figure 4: (a) Bifurcation diagram with $X_1(0)$ (Blue) and $X_2(0)$ (Red); (b) Lyapunov exponent plots of the system (1) under the parameter c; (c-d) Coexisting attractors in the yz-plane at $c = 16$ and $c = 18$, respectively.

$$J = \begin{pmatrix} 0 & 1 & 0 \\ 0 & 0 & 1 \\ a - 3x^2 & -b & -c \end{pmatrix}. \tag{3}$$

The Jacobian matrix at the equilibrium point E_1 can be written as

$$J(E_1) = \begin{pmatrix} 0 & 1 & 0 \\ 0 & 0 & 1 \\ a & -b & -c \end{pmatrix}. \tag{4}$$

The corresponding eigenvalues are

$$\lambda_1 = 2.233, \lambda_2 = -1.917 - j7.476, \lambda_3 = -1.917 + j7.476.$$

Since λ_1 is positive, the new system (1) is unstable at the equilibrium point E_1. The Jacobian matrix at the equilibrium points E_2 and E_3 can be written as

$$J(E_2) = J(E_3) = \begin{pmatrix} 0 & 1 & 0 \\ 0 & 0 & 1 \\ -2a & -b & -c \end{pmatrix} \tag{5}$$

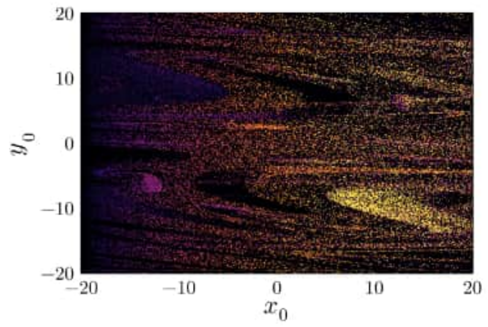

Figure 5: Basin of attraction in the $x_0 - y_0$ plane.

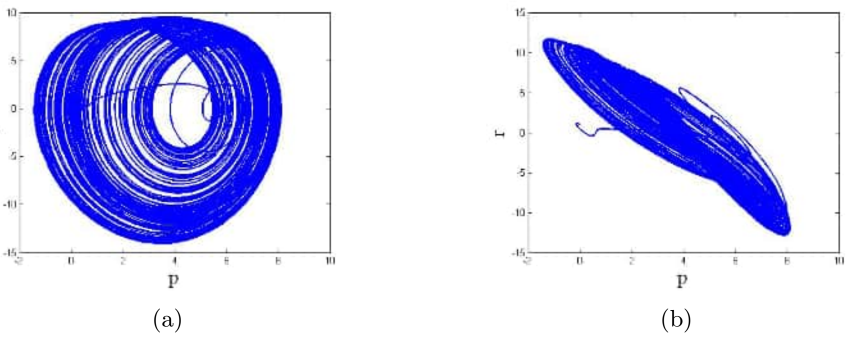

Figure 6: (a-b) Chaotic attractors of the scaled system (6).

The corresponding eigen values are

$$\lambda_1 = 1.333 + j7.784,\ \lambda_2 = 1.333 - j7.784,\ \lambda_3 = -4.265.$$

Since the real parts of eigenvalues λ_1 and λ_2 are positive, the new system (1) is unstable at the equilibrium points E_2 and E_3. Hence, we can conclude that the proposed system (1) is unstable at all the equilibrium points. The attractors of the system (1) are given in Figure 1 with the initial conditions $X_1(0) = (0, 1, -1)$.

3 Dynamic Analysis

In this section, the multistability in the proposed system (1) is shown with the help of bifurcation diagrams, Lyapunov exponents spectrum, and attractor diagrams. When the initial conditions are changed, the system (1) presents multistability with the same parameter values. The bifurcation diagram and Lyapunov exponents spectrum diagram can be obtained by varying the particular parameter by keeping other parameters constant. All the simulation results of the attractor diagram for the multistability are obtained with the initial conditions $X_1(0) = (0, 1, -1)$ (blue color) and $X_2(0) = (0, -1, 1)$ (red color). The new system (1) presents periodic and chaotic states when we vary the parameter values and coexisting attractors are evolved in both chaotic and periodic states in the new system (1). The simulation results indicate that there is a wealth of chaotic dynamics and the existence of coexisting attractors in the proposed system (1).

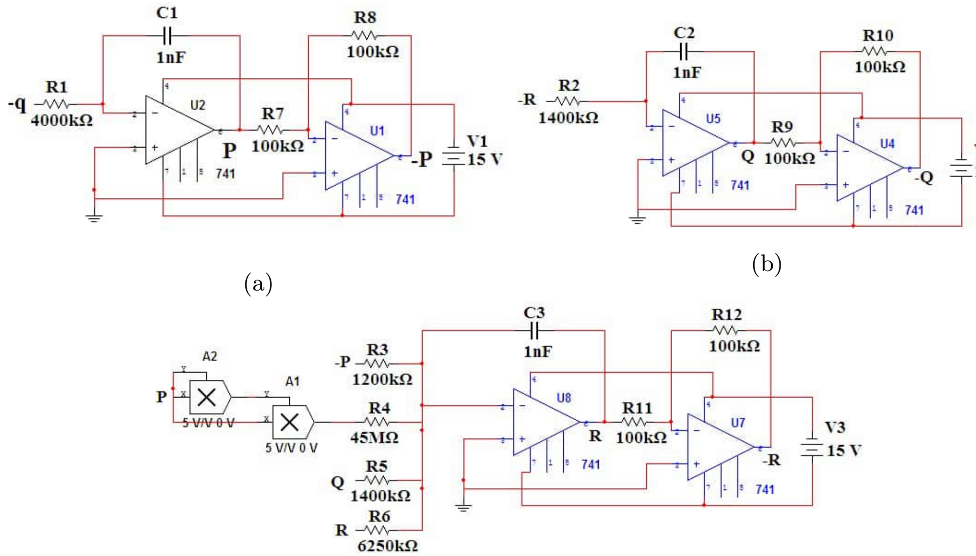

(a) (b) (c)

Figure 7: (a-c) Electronic system design for the scaled system (6).

The dynamical behavior of the system (1)) is analysed under the parameters $a\epsilon[110-135]$. Figure 2a shows the bifurcation diagram for the parameter a with the initial conditions $(0, 1, -1)$ (Blue) and $(0, -1, 1)$ (Red). It is found that the system (1) has a periodic state in $a\epsilon[110-130]$ and a chaotic state beyond $a = 130$. The non-overlapping regions in Figure 2a indicate that there is the presence of coexisting multiple attractors in the system (1). Figure 2b represents the variation of Lyapunov exponent values under the parameter a and has at least one positive value beyond $a = 130$. Figures 2c and 2d show the coexisting attractors of the system (1) under chaotic and periodic regions.

Next, the dynamic property of the system (1) is analyzed under the parameter $b\epsilon[49-57]$. The corresponding bifurcation diagram and Lyapunov exponents spectrum are shown in Figures 3a and 3b, which demonstrate that there is an inverse periodic doubling nature in the system, i.e., the system (1) is in the chaotic state within $b\epsilon[50.4-51.5]$ and then it enters into the periodic state.

It is also observed from Figure 3a that the states of the system are not modified by the different initial conditions but the bifurcation values are changed. Thus, we can conclude that the system (1) produces coexisting multiple attractors for the different values of initial conditions. The coexisting attractors of the system (1) under $b = 51$ and $b = 54$ are given in Figures 3c and 3d, respectively.

The dynamic property of the system (1) is analyzed under the parameter $c \in [1-2]$. The corresponding bifurcation diagram and Lyapunov exponents spectrum are shown in Figures 4a and 4b, which demonstrate that the system (1) is in the chaotic state within $c\epsilon[1-1.7]$ and then it produces period - 4, period - 2 and limit cycle attractors.

It is also observed from Figure 4a that the states of the system are not modified by the different initial conditions but the bifurcation values are changed. Thus, we can conclude that the system (1) produces coexisting multiple attractors for the different values of initial conditions. The coexisting attractors of the system (1) under $c = 16$ and

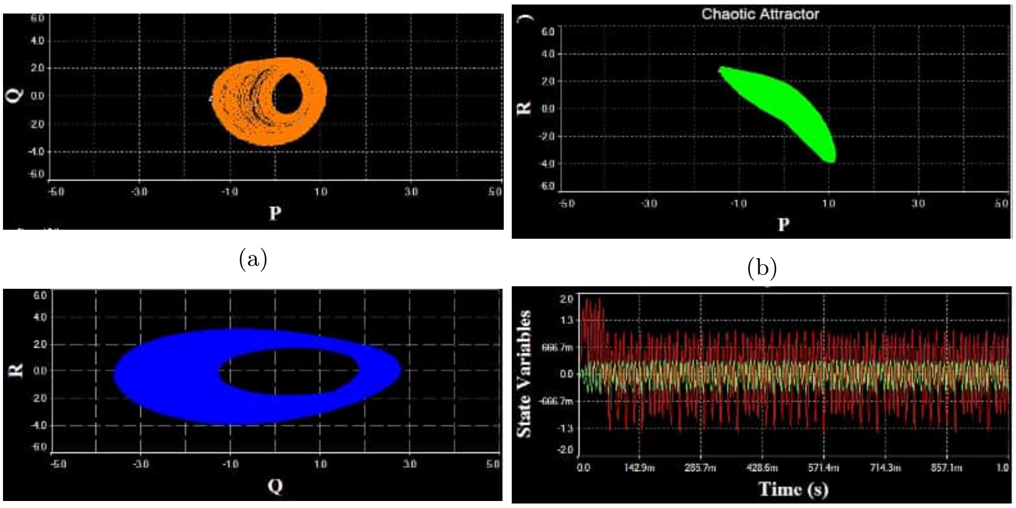

(a) (b) (c) (d)

Figure 8: (a-d) Electronic simulation results with $a = 133, b = 51, c = 1.6$.

$c = 18$ are given in Figures 4c and 4d, respectively.

Finally, the presence of coexisting attractors in the proposed system is verified by plotting the riddled basin of attraction relative to the x_0 - y_0 plane as shown in Figure 5, which indicates two types of attractors in the proposed system.

4 Electronic Circuit Implementation

In this section, an electronic circuit is designed for the proposed coexisting attractor jerk system (1) to obtain its attractors for practical applications [15–17]. It is observed from Figure(1) that the range of state signals x,y and z is $(-4, 17)$, $(-50, 70)$ and $(-500, 400)$, respectively. Since the practical circuit realization uses the voltage range $(-15, 15)Volt$, the range of state signals also must be $(-15, 15)Volt$. This can be achieved by scaling the proposed system (1). Now, assume that $p = \frac{x}{2}$, $q = \frac{y}{5}$ and $r = \frac{z}{36}$, where p, q and r are the scaled state variables of the system (1). Thus, the scaled system can be written as in (6), and its attractors are given in Figure 6 with $a = 133, b = 51, c = 1.6$. Note that the phase diagrams of the scaled system are identical to those in Figure 1 but the range of state variables is reduced within $(-15, +15)$.

$$\begin{aligned} \dot{p} &= 2.5q, \\ \dot{q} &= 7.2r, \\ \dot{r} &= \tfrac{2a}{36}p - \tfrac{8}{36}p^3 - \tfrac{5b}{36}q - cr. \end{aligned} \tag{6}$$

The equations for the proposed system in terms of electrical parameters are given by

$$\begin{aligned} \dot{p} &= \tfrac{-1}{R_1C_1}(-q), \\ \dot{q} &= \tfrac{-1}{R_2C_2}(-r), \\ \dot{r} &= \tfrac{-1}{R_3C_3}(-p) + \tfrac{-1}{R_4C_3}(p^3) + \tfrac{-1}{R_5C_3}(q) + \tfrac{-1}{R_6C_3}(r). \end{aligned} \tag{7}$$

By comparing (6) and (7), the electrical equations for the parameter values can be obtained as follows:

$$
\begin{aligned}
a &= \frac{18}{R_3 C_3}, \\
b &= \frac{36}{5R_5 C_3}, \\
c &= \frac{1}{R_6 C_3}.
\end{aligned}
\tag{8}
$$

The electronic circuit design for (7) is displayed in Figure 7, it uses basic components such as resistors, capacitors, and opamps. The resistance values can be obtained with the parameters $a = 133, b = 51, c = 1.6$ and the capacitance $C = C_1 = C_2 = C_3 = 1nF$ as

$$R_1 = 4000K\Omega, R_2 = 1400K\Omega, R_3 = 1200K\Omega, R_4 = 45M\Omega, R_5 = 1400K\Omega, R_6 = 6250K\Omega.$$

The Multisim simulation results for chaotic attractors are given in Figure 8, which is almost identical to Figure 6.

5 Conclusions

In this paper, a new 3-dimensional coexisting multiple attractors chaotic jerk system is presented and its dynamical properties are analyzed in detail. The parameters of the proposed system are analyzed under chaotic and periodic states using a bifurcation diagram with different initial conditions. The dynamic analysis shows that the proposed system can have multiple coexisting attractors under the variation of initial conditions. The riddle basin of attraction is plotted, which confirms the presence of different attractors in the proposed system. The proposed electronic system design for the new system is verified using Multisim software and can be used to solve many issues in practice. The attractors obtained by the Multisim simulation are identical to those obtained by numerical simulation. The complex dynamics and circuit implementation of the proposed nonlinear dynamical system can be used in many practical applications such as communication system. It can be concluded that the proposed system has chaotic and unpredictable behavior.

References

[1] B. Li, B. Sang, M. Liu, X. Hu, X. Zhang and N. Wang. Some jerk systems with hidden chaotic dynamics. *International Journal of Bifurcation and Chaos* **33** (06) (2023) 2350069.

[2] F. Li and J. Zeng. Multi-scroll attractor and multi-stable dynamics of a three-dimensional Jerk system. *Energies* **16** (5) (2023) 2494.

[3] S. Vaidyanathan, I.M. Moroz, A. A. A. El-Latif, B. Abd-El-Atty and A. Sambas. A new multistable jerk system with Hopf bifurcations, its electronic circuit simulation and an application to image encryption. *International Journal of Computer Applications in Technology* **67** (1) (2021) 29–46.

[4] M. Karami, R. Ramamoorthy, A. M. A. Ali and V. T. Pham. Jagged-shape chaotic attractors of a megastable oscillator with spatially square-wave damping. *The European Physical Journal Special Topics* **231** (11) (2022) 2445–2454.

[5] C. Li, J. C. Sprott and H. Xing. Hypogenetic chaotic jerk flows. *Physics Letters A* **380** (11-12) (2016) 1172–1177.

[6] X. Wu, S. He, W. Tan and H. Wang. From memristor-modeled jerk system to the nonlinear systems with memristor. *Symmetry* **14** (4) (2016) 659.

[7] Q. Wang, Z. Tian, X. Wu and W. Tan. Coexistence of multiple attractors in a novel simple jerk chaotic circuit with CFOAs implementation. *Frontiers in Physics* **10** (2022) 835188.

[8] A. Sambas, W. S. Sanjaya, M. Mamat and R. Putra Prastio. Mathematical modelling of chaotic jerk circuit and its application in secure communication system. *Advances in chaos theory and intelligent control* (2016) 133–153.

[9] R. Premkumar, M. Mahdal and M. Elangovan. An efficient chaos-based image encryption technique using bitplane decay and genetic operators. *Sensors* **22** (10) (2022) 8044.

[10] R. Ramar, S. Vaidyanathan, S. Akgul and B. Emin. A new chaotic jerk system with cubic and hyperbolic sine nonlinearities and its application to random number generation and biomedical image encryption. *Scientia Iranica* (2024), Accepted Manuscripts.

[11] H. Chen, S. He, A. D. Pano Azucena, A. Yousefpour, H. Jahanshahi, M. A. Lopez and R. Alcaraz. A multistable chaotic jerk system with coexisting and hidden attractors: Dynamical and complexity analysis, FPGA-based realization, and chaos stabilization using a robust controller. *Symmetry* **12** (4) (2020) 569.

[12] D. Veeman, M. Mehrabbeik, H. Natig, K. Rajagopal, S. Jafari and I. Hussain. A new chaotic system with coexisting attractors. *International Journal of Bifurcation and Chaos* **32** (03) (2022) 2230007.

[13] P. P. Singh and B. K. Roy. Pliers shaped coexisting bifurcation behaviors in a simple jerk chaotic system in comparison with 21 reported systems. *IFAC-PapersOnLine* **55** (1) (2022) 920–926.

[14] Q. Lai, P. D. Kamdem Kuate, H. Pei and H. Fotsin. Infinitely many coexisting attractors in no-equilibrium chaotic system. *Complexity* **2020** (2020) Article ID 8175639.

[15] T. Bonny, S. Vaidyanathan, A. Sambas, K. Benkovide, W. Al Nassan and O. Naqaweh. Multistability and bifurcation analysis of a novel 3d jerk system: Electronic circuit design, fpga implementation, and image cryptography scheme. *IEEE Access* **11** (2023) 78584–78600.

[16] A. Sambas, S. Vaidyanathan, S. F. Al-Azzawi, M. K. M. Nawawi, M. A. Mohamed, Z. A. Zakaria, S. S. Abas and M. Mamat. Modelling and MultiSim Simulation of a New Hyperchaos System with No Equilibrium Point. *Nonlinear Dynamics and Systems Theory* **23** (4) (2023) 422–433.

[17] S. Rouar and O. Zehrour. A new fractional-order three-dimensional chaotic flows with identical eigenvalues. *Nonlinear Dynamics and Systems Theory* **22** (4) (2022) 447–456.

Nonlinear Dynamics and Systems Theory, **25** (2) (2025) 171–186

Variational Analysis and Error Estimate of Contact Problem for Thermo-Viscoelastic Bodies with Long-Term Memory

Roufaida Ketfi [1*], Abdelmoumene Djabi [2] and Ilyas Boukaroura [3]

[1] *Laboratory of Applied Mathematics, Faculty of Sciences, University of Ferhat Abbas-Setif 1, Setif 19000, Algeria.*
[2] *Laboratory of Applied Mathematics, Faculty of Economics, Commerce and Management Sciences, University of Ferhat Abbas-Setif 1, Setif 19000, Algeria.*
[3] *Laboratory of Applied Mathematics, Faculty of Sciences, University of Ferhat Abbas-Setif 1, Setif 19000, Algeria.*

Received: August 25, 2024; Revised: March 23, 2025

Abstract: This paper investigates a contact problem involving the quasistatic interaction between two bodies characterized by thermo-viscoelasticity with long-term memory. The mechanical, thermal contact is captured through the sub-differential condition, which represents the frictional interaction. We establish a variational formulation for the model and we prove the existence of a unique weak solution. Subsequently, a numerical investigation is conducted, employing both finite element and finite difference methods. This computational approach allows for the derivation of a discrete approximation of the error associated with the analyzed model.

Keywords: *fixed point; frictional contact; finite element method; thermo-piezoelectric; weak solution.*

Mathematics Subject Classification (2020): Primary 35A15; Secondary 35Q40.

* Corresponding author: mailto:roufaida.ketfi@univ-setif.dz

1 Introduction

Mathematics has always been the beating heart of the science, and the interaction between them has been crucial for centuries. Mathematical theories and fundamental concepts have enabled the description of aspects of the natural world, including motion in mechanics, electricity, gravity, and general relativity.

The connection between mathematics and mechanics is profound as mechanics elucidates the motion of objects influenced by specific forces within the realm of physics. The mathematical exploration of mechanics commences with the definition of physical quantities and geometric representations, often leading to the formulation of graphs and diagrams. Contact mechanics, a subfield of mechanics, delves into the deformation of materials in contact with one another. Mathematical modeling and analysis play pivotal roles in comprehension [11], with nonlinear partial differential equations and variational inequalities being among the primary mathematical tools employed, along with hemivariational inequalities.

Thermal phenomena are closely linked to the mechanics of contact. For example, certain crystals such as quartz, tourmaline, and Rochelle salt exhibit mechanical stresses due to thermal expansion when exposed to heat [5]. Research has extensively explored the laws that govern these thermo-mechanical interactions. The models of thermo-elastic bodies are elaborated in [1]. Additionally, studies examining changes in piezoelectric materials in relation to thermal effects are presented in [4] and [12]. Frictional contact between bodies has taken a considerable place in research, see [7], dealing with a contact problem between materials and physical phenomena (friction, damage and wear), while for a dynamic problem of frictional contact in mechanics in other studies on mathematical numerical solutions of variational inequalities, one can refer to [9].

Furthermore, there are results and research focusing on abstract hemivariational inequalities and numerical simulation outcomes providing numerical evidence regarding the theoretically predicted optimal convergence order, as referenced in [6, 8, 10]. Additionally, in [1], the study delves into the hemivariational inequality and the frictional contact problem with damage, furthermore, there are other studies focusing on numerical aspects, which can be found in [2]. The paper is structured as follows. Notations and preliminaries are detailed in Section 2, while the model, a list of assumptions, and a variational formulation of the problem will be discussed in Section 3. Subsequently, in Section 4, we will cite the results concerning existence and uniqueness as presented in Theorem 4.1. The proof of this theorem relies on variational and hemivariational inequalities as well as results related to the existence and uniqueness of Banach fixed points. Finally, in Section 5, we will present the numerical study, employing the finite element method and finite differences to achieve a precise numerical approach to the solution.

2 Notations and Preliminaries

We present the notations and recall some preliminary concepts.

Let us consider $\Omega^l \subset \mathbb{R}^d$ as a bounded domain with an outer Lipschitz boundary denoted by Γ^l, and let ν represent the unit outer normal on $\partial\Omega^l = \Gamma^l$. We define the spaces

$$H^l = L^2(\Omega^l)^d = \left\{\mathbf{v^l} = \left(v_i^l\right) : v_i^l \in L^2(\Omega^l)\right\}, \quad \mathcal{H}^l = \left\{\boldsymbol{\tau^l} = \left(\tau_{ij}^l\right) \tau_{ij}^l = \tau_{ji}^l \in L^2(\Omega^l)\right\},$$

$$H_1^l(\Omega^l)^d = \{\mathbf{v}^l = \left(v_i^l\right) \in H^1 : \varepsilon(\mathbf{v}^l) \in \mathcal{H}^l\}, \quad \mathcal{H}_1^l = \{\boldsymbol{\tau^l} \in \mathcal{H}^l : Div\boldsymbol{\tau^l} \in H^1\},$$

H^l, $\mathcal{H}^l$, $H_1^l(\Omega^l)^d$ and $\mathcal{H}_1^l$ are real Hilbert spaces equiped with the usual inner products and the associated norms, we also introduce the closed subspaces of $H_1^l(\Omega^l)$ defined by

$$\begin{aligned} V^l &= \left\{\mathbf{v^l} \in H_1^l(\Omega^l)^d : \mathbf{v} = 0 \text{ on } \Gamma_1^l\right\}, \\ Q^l &= \left\{\theta^l \in H_1^l(\Omega^l) : \theta^l = 0 \text{ in } \Gamma_1^l\right\}. \end{aligned}$$

Given that $\mu(\Gamma_a^l) > 0$ and $\mu(\Gamma_1^l) > 0$, the Korn and Friedrichs-Poincaré inequalities are satisfied,

$$\exists C_0 > 0 \quad \|\varepsilon(\mathbf{v}^l)\|_{\mathcal{H}^l} \geq C_0 \|\mathbf{v}^l\|_{H_1^l(\Omega^l)^d}, \quad \forall \mathbf{v}^l \in V^l, \tag{1}$$

$$\exists C_2 > 0 \quad \|\nabla \mathbf{w}^l\|_{H^l} \geq C_2 \|\mathbf{w}^l\|_{H_1^l(\Omega^l)}, \forall \mathbf{w}^l \in Q^l. \tag{2}$$

Moreover, by the Sobolev trace theorem the positive constants C_0 and C_2 exist so that

$$\|\mathbf{v}^l\|_{L^2(\Gamma_3^l)^d} \leq C_0 \|\mathbf{v}^l\|_{V^l}, \forall \mathbf{v}^l \in V^l, \tag{3}$$

$$\|\mathbf{z}^l\|_{L^2(\Gamma_3^l)} \leq C_2 \|\mathbf{z}^l\|_{Q^l}, \forall z^l \in Q^l. \tag{4}$$

We denote v_ν and $\mathbf{v}_\tau^l$ as the normal and tangential components of $\mathbf{v}^l$ on Γ^l, where v_ν is the perpendicular component and $\mathbf{v}_\tau^l$ is the parallel component, as described in Green's formulas in [4].
For a simpler notation, we use the following spaces:

$$\mathbb{V} = V_1 \times V_2, \quad \mathbb{H} = H^1 \times H^2, \quad \mathbb{H}_1 = H_1^1 \times H_1^2, \quad \mathbb{Q} = Q^1 \times Q^2.$$

2.1 Subdifferential boundary conditions

In the mechanical problem $(\mathcal{P})$, we will use contact laws expressed in terms of the subdifferential $\kappa_\nu \in \partial j(u_\nu)$, in which κ_ν represents an interface force, u_ν signifies the normal displacement and $\partial j(u_\nu)$ represents the subdifferential in the sense of Clarke such that $j : \mathbb{R} \longrightarrow \mathbb{R}$ is a locally Lipschitz function. The generalized (Clarke) directional derivative of j at $x \in \mathbb{R}$ in the direction $v \in \mathbb{R}$ is defined by

$$j^0(x; v) = \limsup_{y \to x, \lambda \downarrow 0} \frac{j(y + \lambda v) - j(y)}{\lambda}.$$

The generalized subdifferential of j at x is a subset of $\mathbb{R}$ expressed as

$$\partial j(x) = \{\zeta \in \mathbb{R} \quad | \quad j^0(x; v) \geq \zeta v \quad \forall v \in \mathbb{R}\}.$$

Some properties of the subdifferential for locally Lipschitz functions can be found in [11].

3 The Model and Assumptions on the Data

Let $\Omega^l, l = 1, 2$, be a bounded domain in $\mathbb{R}^d$ $(d = 2, 3)$ with the outer Lipschitz surface Γ^l, we define two thermo-viscoelastic bodies occupying Ω^l, their boundary is divided into three open disjoint parts Γ_1^l, Γ_2^l and Γ_3^l on one hand, and a partition of $\Gamma_1^l \cup \Gamma_2^l$ into two open parts $\Gamma_a^l$and Γ_b^l on the other hand. We assume that $\mu(\Gamma_1^l) > 0$. Let $T > 0$ and $[0, T]$ be the time interval of interest. The two bodies are subjected to the effect of body forces with specific density $\mathbf{f}_0$, a heat source of constant strength q_{th}^l.

The two bodies are clamped on $\Gamma_1^l \times (0,T)$, so the displacement field vanishes there. A surface traction of density $\mathbf{f}_2^l$ acts on $\Gamma_2^l \times (0,T)$. Also, we suppose that the temperature vanishes on $\left(\Gamma_1^l \cup \Gamma_2^l\right) \times (0,T)$. Moreover, we suppose that the body forces and tractions vary slowly in time, and therefore, the accelerations in the system may be neglected. Neglecting the inertial terms in the equation of motion leads to a quasistatic approach to the process. In the reference configuration, the two bodies can enter in contact along the common part $\Gamma_3^1 = \Gamma_3^2 = \Gamma_3$. The contact model is characterized by the sub-differential of locally Lipschitz functions and the non linear boundary condition of thermal conductivity modeling electric potential exchange between the bodies.

Problem 3.1 For $l = 1, 2$, find the displacement field $u^l : \Omega^l \times [0,T] \to \mathbb{R}^d$ and the temperature $\theta^l : \Omega^l \times [0,T] \to \mathbb{R}$ such that

$$\boldsymbol{\sigma}^{\boldsymbol{l}}(t) = \mathcal{A}^l(\varepsilon(\dot{u}^l(t))) + \mathcal{B}^l\varepsilon(\mathbf{u}^l(t)) + \int_0^T \mathcal{G}^l(t-s)u^l(s)\mathrm{d}s - \mathcal{C}^l\theta^l(t) \quad \text{in } \Omega^l \times (0,T) \tag{5}$$

$$\dot{\theta}^l(t) - div\mathcal{K}^l\left(\nabla\theta^l(t)\right) = \mathcal{M}^l(\varepsilon(\dot{u}^l(t))) + h_0^l \quad \text{in } \Omega^l \times (0,T) \tag{6}$$

$$Div\boldsymbol{\sigma}^l(t) + f_0^l(t) = 0 \quad \text{in } \Omega^l \times (0,T), \tag{7}$$

$$u^l(t) = 0 \quad \text{on } \Gamma_1^l \times (0,T), \tag{8}$$

$$\sigma^l\nu^l = f_2^l \quad \text{on } \Gamma_2^l \times (0,T), \tag{9}$$

$$\begin{cases} \sigma_\upsilon^1(t) = \sigma_\upsilon^2(t) = \sigma_\upsilon(t) \quad -\sigma_\upsilon(t) \in \partial j_\upsilon(\dot{u}_\upsilon(t)) \quad \text{on } \Gamma_3 \times (0,T), \\ \sigma_\tau^1(t) = \sigma_\tau^2(t) = \sigma_\tau(t) \quad -\sigma_\tau(t) \in \partial j_\tau(\dot{u}_\tau(t)) \quad \text{on } \Gamma_3 \times (0,T), \end{cases} \tag{10}$$

$$u_\upsilon^1(t) + u_\tau^2(t) = 0 \quad \text{on } \Gamma_3 \times (0,T) \tag{11}$$

$$-\mathcal{K}\left(\nabla\theta(t)\right)\upsilon \in \partial j_\theta(\theta(t)) \quad \text{on } \Gamma_3 \times (0,T), \tag{12}$$

$$\theta^l = 0 \quad \text{on } (\Gamma_1 \cup \Gamma_2) \times (0,T), \tag{13}$$

$$q(t)^l \cdot \nu^l = h_n \quad \text{on } \Gamma_2^l \times (0,T), \tag{14}$$

$$u^l(0) = u_0^l, \quad \theta^l(0) = \theta_0^l \quad \text{in } \Omega^l. \tag{15}$$

Now, progress to the mechanical presentation of (5)-(15) and provide explanation of the equations and the boundary conditions.

Equations (5) and (6) represent the thermo-viscoelastic with long-term memory constitutive laws between two bodies, where $\mathcal{A}^l$ is a given nonlinear operator, $\mathcal{G}^l$ is the relaxation operator, $\mathcal{B}^l$ represents the elasticity operator and $\mathcal{C}^l$ is the thermal operator, the thermo-viscoelastic constitutive law includes temperature effects described by the parabolic equation given by (6), where $\mathcal{M}^l$ is the thermal expansion tensor and $\mathcal{K}^l$ is the thermal conductivity tensor, equation (7) is the equilibrium equation for the stress, where Div denotes the divergence operator for tensors, then (8), (9), (13) and (14) are the mechanical and thermal boundary conditions and (11) indicates that there is no space between the two bodies, the equations (10) represent the normal stres and normal velocity satisfying the non-monotone damped response condition and the friction law, in which j_ν, j_τ are locally Lipschitz functions and $\partial j_\nu, \partial j_\tau$ denotes the generilized Clarke gradient of the functions j_ν and j_τ, the relation (12) represents the heat exchange between two body, finally, (15) denotes the initial displacement and the temperature conditions.

3.1 Assumptions on the data

We will now enumerate the assumptions regarding the problem's data.
The *viscosity operator* $\mathcal{A}^l : \Omega^l \times \mathbb{S}^d \to \mathbb{S}^d$ satisfies

$$\begin{cases} (a) \quad \mathcal{A}^l(.,\varepsilon) \text{ is Lebesgue measurable on } \Omega^l \text{ for any } \varepsilon \in \mathbb{S}^d, \\ (b) \quad \text{There exists } L_{\mathcal{A}^l} > 0 \text{ such that} \\ \|\mathcal{A}^l(\mathbf{x},\varepsilon_1) - \mathcal{A}^l(\mathbf{x},\varepsilon_2)\| \le L_{\mathcal{A}^l}\|\varepsilon_1 - \varepsilon_2\| \text{ for all } \varepsilon_1, \varepsilon_2 \in \mathbb{S}^d, \\ (c) \quad \text{There exists } m_{\mathcal{A}^l} > 0 \text{ such that for all } \varepsilon_1, \varepsilon_2 \in \mathbb{S}^d, \\ (\mathcal{A}^l(\mathbf{x},\varepsilon_1) - \mathcal{A}^l(\mathbf{x},\varepsilon_2)) \cdot (\varepsilon_1 - \varepsilon_2) \ge m_{\mathcal{A}^l}\|\varepsilon_1 - \varepsilon_2\|^2 \quad \text{(a.e)}\mathbf{x} \in \Omega^l, \\ (d) \quad \mathcal{A}^l(x,0) = 0 \text{ for all } x \in \Omega^l. \end{cases} \tag{16}$$

The elasticity operator $\mathcal{B}^l : \Omega^l \times \mathbb{S}^d \to \mathbb{S}^d$ satisfies

$$\begin{cases} (a) \quad \mathcal{B}^l(x,\varepsilon) \text{ is Lebesgue measurable on } \omega \text{ for all } \varepsilon \in \mathbb{S}^d, \\ (b) \quad \text{There exists } L_{\mathcal{B}^l} > 0 \text{ such that for all } \varepsilon_1, \varepsilon_2 \in \mathbb{S}^d, \\ \|\mathcal{B}^l(\mathbf{x},\varepsilon_1) - \mathcal{B}^l(\mathbf{x},\varepsilon_2)\| \le L_{\mathcal{B}^l}\|\varepsilon_1 - \varepsilon_2\| \quad \text{(a.e)}\mathbf{x} \in \Omega^l, \\ (c) \quad \mathcal{B}^l(x,0) = 0 \text{ for all } x \in \Omega^l. \end{cases} \tag{17}$$

The *relaxation function* $\mathcal{G}^l : \Omega^l \to \mathbb{R}^d$ satisfies

$$\begin{cases} (a) \quad \mathcal{G}^l(\mathbf{x}) \text{ is Lebesgue measurable on } \Omega^l \text{ for any } \mathbf{x} \in \mathbb{R}^d, \\ (b) \quad \text{There exists } L_{\mathcal{G}^l} > 0 \text{ such that} \\ \qquad \|\mathcal{G}^l(\mathbf{x}_1) - \mathcal{G}^l(\mathbf{x}_2)\| \le L_{\mathcal{G}^l}\|\mathbf{x}_1 - \mathbf{x}_2\| \text{ for all } \mathbf{x}_1, \mathbf{x}_2 \in \mathbb{R}^d. \end{cases} \tag{18}$$

The *function* $j_\nu : \Gamma_3^l \times \mathbb{R} \to \mathbb{R}$ satisfies

$$\begin{cases} (a) \quad j_{\nu(.,r)} \text{ is Lebesgue measurable on } \Gamma_3^l \text{ for all } x \in \mathbb{R}, \\ (b) \quad j_{\nu(x,.)} \text{ is locally Lipschitz on } \mathbb{R} \text{ for all } x \in \Gamma_3^l, \\ (c) \quad \text{there exist } c_{0\nu}, c_{1\nu} \geqslant 0 \text{ such that for all } r \in \mathbb{R} \text{ and } x \in \Gamma_3^l \text{ we have} \\ \qquad |\partial j_\nu(x,r)| \le c_{0\nu} + c_{1\nu}|r|, \\ (d) \quad \text{there exists } \alpha_{j\nu} \ge 0 \text{ such that for all } r_1, r_2 \in \mathbb{R} \text{ and } x \in \Gamma_3^l, \text{ we have} \\ \qquad j_\nu^0(x,r_1;r_2 - r_1) + j_\nu^0(x,r_2;r_1 - r_2) \le \alpha_{j\nu}|r_1 - r_2|^2. \end{cases} \tag{19}$$

The *function* $j_\tau : \Gamma_3^l \times \mathbb{R}^d \to \mathbb{R}$ satisfies

$$\begin{cases} (a) \quad j_\tau(.,\xi) \text{ is measurable on } \Gamma_3^l \text{ for all } x \in \mathbb{R}, \\ (b) \quad j_\tau(x,.) \text{ is locally Lipschitz on } \mathbb{R}^d \text{ for all } x \in \Gamma_3^l, \\ (c) \quad \text{there exist } c_{0\tau}, c_{1\tau} \ge 0 \text{ such that for all } r \in \mathbb{R}\text{and } x \in \Gamma_3^l, \text{ we have} \\ \qquad \| \partial j_\tau(x,r) \| \le c_{0\tau} + c_{1\tau} \| \xi \|_{\mathbb{R}}, \\ (d) \quad \text{there exists } \alpha_{j\tau} \ge 0 \text{ such that for all } \xi_1, \xi_2 \in \mathbb{R} \text{ and } x \in \Gamma_3^l, \text{ we have} \\ \qquad j_\tau^0(x,\xi_1;\xi_2 - \xi_1) + j_\tau^0(x,\xi_2;\xi_1 - \xi_2) \le \alpha_{j\tau} \| \xi_1 - \xi_2 \|^2 . \end{cases} \tag{20}$$

The *function* $j_\theta : \Gamma_3 \times \mathbb{R} \to \mathbb{R}$ satisfies

$$\begin{cases} (a) \quad j_\theta(.,r) \text{ is Lebesgue measurable on } \Gamma_3^l \text{ for all } x \in \mathbb{R}, \\ (b) \quad j_\theta(x,.) \text{ is locally Lipschitz on } \mathbb{R}^d \text{ for all } x \in \Gamma_3^l, \\ (c) \quad \text{there exist } c_{0\theta}, c_{1\theta} \ge 0 \text{ such that for all } r \in \mathbb{R} \text{ and } x \in \Gamma_3^l, \text{ we have} \\ \qquad |\partial j_\theta(x,r)| \le c_{0\theta} + c_{1\theta}|r|, \\ (d) \quad \text{there exists } \alpha_{j\theta} \ge 0 \text{ such that for all } r_1, r_2 \in \mathbb{R} \text{ and } x \in \Gamma_3, \text{ we have} \\ \qquad j_\theta^0(x,r_1;r_2 - r_1) + j_\theta^0(x,r_2;r_1 - r_2) \le \alpha_{j\theta}|r_1 - r_2|^2. \end{cases} \tag{21}$$

On the other hand, we need conditions for the thermal operator $\mathcal{C}^l$, the function $\mathcal{M}^l$ and the thermal conductivity operator$\mathcal{K}^l$, see [6].

Now, we define the forces, tractions, volume and surface charges, as well as the initial functions as follows:

$$f_0^l \in L^2(\Omega^l)^d \quad f_2^l \in L^2(\Gamma_2^l)^d \quad h_0^l \in L^2(\Omega^l)^d.$$

$$h_n^l \in L^2(\Gamma_b^l)^d \quad k \geq 0 \quad u_0 \in V \quad \theta_0 \in Q.$$

By utilizing Riesz's representation theorem, we examine the elements $f^l \in V^l$ and $h \in Q^l$ defined by

$$\langle F, v\rangle_V = \sum_{l=1}^{2} \int_{\Omega^l} f_0^l(t) v^l \mathrm{d}x + \sum_{l=1}^{2} \int_{\Gamma_2^l} f_2^l(t) v^l \mathrm{d}x \quad \text{for all } v \in V$$

$$\langle h, \xi\rangle_Q = \sum_{l=1}^{2} \int_{\Omega^l} h_0^l(t) \xi^l \mathrm{d}x + \sum_{l=1}^{2} \int_{\Gamma_b^l} h_n^l(t) \xi^l \mathrm{d}x \quad \text{for all } \xi \in Q.$$

With the notations mentioned earlier and Green's formulas, we can derive the variational formulation of the mechanical problem $(\mathcal{P})$ for all functions $v^l \in V^l$, $w^l \in Q^l$ and a.e $t \in (0, T)$ given as follows.

3.2 Problem $\mathcal{P}_V$

Find the displacement field $\mathbf{u} = (\mathbf{u}^1, \mathbf{u}^2) : [0, T] \to \mathbb{V}$ and the temperature $\theta = (\theta^1, \theta^2) : [0, T] \to \mathbb{Q}$ such that

$$\begin{aligned} &\sum_{l=1}^{2} \left(\sigma^l(t), \varepsilon(v^l - \dot{u}^l(t))\right)_{\mathcal{H}^l} + \int_{\Gamma_3} \left(j_\nu^0(\dot{u}_\nu(t); v_\nu - \dot{u}_\nu(t)) + j_\tau^0(\dot{u}_\tau(t); v_\tau - \dot{u}_\tau(t))\right) \mathrm{d}a, \\ &\qquad \geq \langle F(t), v - \dot{u}(t)\rangle_{\mathbb{V}}. \end{aligned} \tag{22}$$

$$\begin{aligned} &\sum_{l=1}^{2} \left(\dot{\theta}^l(t), \lambda^l - \theta^l(t)\right)_{\mathcal{H}^l} + \left(\mathcal{K}^l \nabla\theta^l(t), \nabla(\lambda^l - \theta^l(t))\right)_{\mathcal{H}^l} - \left(\mathcal{M}^l \varepsilon(u^l(t)), \lambda^l - \theta^l(t)\right)_{\mathcal{H}^l}, \\ &\qquad + \int_{\Gamma_3} j_\theta^0(\theta(t); \lambda^l - \theta^l(t))\, \mathrm{d}a \geq \langle h(t), \lambda - \theta(t)\rangle_{\mathbb{Q}}, \\ &\qquad \mathbf{u}(0) = \mathbf{u}_0, \qquad \theta(0) = \theta_0. \end{aligned} \tag{23}$$

4 Existence and Uniqueness of a Solution

Let us consider that the following smallness conditions are satisfied:

$$\begin{array}{rcl} \alpha_{\mathcal{A}}^l & \geq & c_0^2(\alpha_{j_\nu} + \alpha_{j_\tau})\sqrt{\mu(\Gamma_3)}, \\ \alpha_{\mathcal{K}}^l & \geq & c_0^2 \alpha_{j_\theta} \sqrt{\mu(\Gamma_3)}, \\ \alpha_{\mathcal{K}}^l - c_0^2 \alpha_{j_\theta} \sqrt{\mu(\Gamma_3)} & \geq & L_{\mathcal{M}}^l T/2. \end{array} \tag{24}$$

Now, we present our result on existence and uniqueness.

Theorem 4.1 *Assume hypotheses (3.16)-(3.29) and (24) are satisfied, then Problem* $(\mathcal{P}_V)$ *has a unique solution* $(\mathbf{u}, \theta)$ *such that*

$$\mathbf{u} \in L^2(0, T, \mathbb{V}), \quad \theta \in L^2(0, T, \mathbb{Q}).$$

In the proof of Theorem (4.1), we follow several steps, based on the results of hemi-variational inequalities and fixed point arguments.

To prove the theorem, we consider the following the auxiliary problems for given $\eta \in L^2(0, T, \mathcal{H}), z \in L^2(0, T, Q)$.

4.1 Problem $\mathcal{PV}_\eta$

Find a displacement field $u_\eta = (u^1_\eta, u^2_\eta) : [0, T] \to \mathbb{V}$ such that for all $t \in [0, T]$, we have

$$\begin{aligned} &\sum_{l=1}^{2} (\mathcal{A}^l \varepsilon(\dot{u}^l_\eta(t)), \varepsilon(v^l - \dot{u}^l_\eta(t)))_{\mathcal{H}^l} + \int_{\Gamma_3} (j^0_\nu(\dot{u}_{\eta\nu}(t); v_\nu - \dot{u}_{\eta\nu}(t)) \\ &+ (j^0_\tau(\dot{u}_{\eta\tau}(t); v_\tau - \dot{u}_{\eta\tau}(t))\mathrm{d}a + (\eta(t), \varepsilon(v - \dot{u}(t)))_{\mathbb{V}} \geq \langle F(t), v - \dot{u}_\eta(t)\rangle_{\mathbb{V}} \qquad (25) \\ &\qquad u_\eta\,(0) = u_0. \end{aligned}$$

4.2 Problem $\mathcal{PV}_\theta$

Find the temperature $\theta_{\eta z} = (\theta^1_{\eta z}, \theta^2_{\eta z}) : [0, T] \to \mathbb{Q}$ such that for all $t \in [0, T]$ and all $\lambda \in \mathbb{Q}$, we have

$$\begin{aligned} &\sum_{l=1}^{2} (\dot{\theta}^l_{\eta z}(t), \lambda^l - \theta^l_{\eta z}(t))_{\mathcal{H}} + (\mathcal{K}^l \nabla \theta^l_{\eta z}(t), \nabla(\lambda^l - \theta^l_{\eta z}(t)))_{\mathcal{H}} - (\mathcal{M}^l \varepsilon(u^l_\eta(t)), \lambda - \theta^l_{\eta z}(t)) \\ &+ \int_{\Gamma_3} j^0_\theta(\theta_{\eta z}(t); \lambda^l - \theta_{\eta z}(t))\mathrm{d}a \geq \langle h(t), \lambda - \theta_{\eta z}(t)\rangle_{\mathbb{Q}} \qquad (26) \\ &\qquad \theta_{\eta z}\,(0) = \theta_0. \end{aligned}$$

Lemma 4.1 *Problem* (25) *has a unique solution. Moreover, there exists a constant* $c > 0$ *such that*

$$\| u_{\eta_1} - u_{\eta_2} \|^2_{\mathbb{V}} \leq c \int_0^T \| \eta_1(s) - \eta_2(s) \|^2_{\mathbb{V}^*} \,\mathrm{d}s. \qquad (27)$$

In this context, (u_{η_i}) refers to the solution of problem (25) associated with η_i,$i = 1 : 2$.

Proof. [Proof (of Lemma 4.1)] To start the demonstration, let us begin with the aspect of existence of solution of problem (25) corresponding to η_i with $i = 1, 2$ for the estimate (27). Let $u_{\eta i}$ be the solution of problem (25) corresponding to $\eta_i \in L^2(0, T; \mathcal{H})$ with $i = 1, 2$, then, $\forall t \in (0, T)$ and $\forall v \in \mathbb{V}$, we write

$$\begin{aligned} &\sum_{l=1}^{2} (\mathcal{A}^l \varepsilon(\dot{u}^l_{\eta_1}(t)), \varepsilon(v^l - \dot{u}^l_{\eta_1}(t)))_{\mathcal{H}^l} + \int_{\Gamma_3} (j^0_\nu(\dot{u}_{\eta_1\nu}(t)); v_\nu - \dot{u}_{\eta_1\nu}(t))\mathrm{d}a \qquad (28) \\ &\quad + \int_{\Gamma_3} (j^0_\tau(\dot{u}_{\eta_1\tau}(t)); v_\tau - \dot{u}_{\eta_1\tau}(t))\mathrm{d}a + (\eta_1(t), \varepsilon(v - \dot{u}_{\eta_1}(t)))_{\mathbb{V}} \\ &\qquad \geq (F(t), v - \dot{u}_{\eta_1}(t))_{\mathbb{V}} \end{aligned}$$

$$\sum_{l=1}^{2}(\mathcal{A}^l\varepsilon(\dot{u}^l_{\eta_2}(t)),\varepsilon(v^l-\dot{u}^l_{\eta_2}(t)))_{\mathcal{H}^l}+\int_{\Gamma_3}(j^0_\nu(\dot{u}_{\eta_2\nu}(t));v_\nu-\dot{u}_{\eta_2\nu}(t))\mathrm{d}a \tag{29}$$
$$+\int_{\Gamma_3}(j^0_\tau(\dot{u}_{\eta_2\tau}(t));v_\tau-\dot{u}_{\eta_2\tau}(t))\mathrm{d}a+(\eta_2(t),\varepsilon(v-\dot{u}_{\eta_2}(t))\rangle_{\mathbb{V}}$$
$$\geq (F(t),v-\dot{u}_{\eta_2}(t)\rangle_{\mathbb{V}}.$$

Taking $v=\dot{u}_{\eta_2}$ in (28) and $v=\dot{u}_{\eta_1}$ in (29), we sum up the obtained inequalities to derive

$$\sum_{l=1}^{2}(\mathcal{A}^l\varepsilon(\dot{u}^l_{\eta_1}(t))-\mathcal{A}^l\varepsilon(\dot{u}^l_{\eta_2}(t)),\varepsilon(u^l_{\eta_1}(t)-\dot{u}^l_{\eta_2}(t)))_{\mathcal{H}^l} \tag{30}$$
$$\leq(\eta_1(t)-\eta_2(t),\varepsilon(\dot{u}_{\eta_2}(t)-\dot{u}_{\eta_1}(t)))_{\mathbb{V}}+\int_{\Gamma_3}j^0_\nu(\dot{u}_{\eta_1\nu}(t),\dot{u}_{\eta_2\nu}(t)-\dot{u}_{\eta_1\nu}(t))\mathrm{d}a$$
$$+\int_{\Gamma_3}j^0_\nu(\dot{u}_{\eta_2\nu}(t),\dot{u}_{\eta_1\nu}(t)-\dot{u}_{\eta_2\nu}(t))\mathrm{d}a+\int_{\Gamma_3}j^0_\tau(\dot{u}_{\eta_1\tau}(t),\dot{u}_{\eta_2\tau}(t)-\dot{u}_{\eta_1\tau}(t))\mathrm{d}a$$
$$+\int_{\Gamma_3}j^0_\tau(\dot{u}_{\eta_2\tau}(t),\dot{u}_{\eta_1\tau}(t)-\dot{u}_{\eta_2\tau}(t))\mathrm{d}a.$$

Then we combine the inequalities (16)-c, (19)-d and (20)-d to deduce

$$(\alpha_{\mathcal{A}^l}-c_0^2(\alpha_{j_\nu}+\alpha_{j_\tau})\sqrt{\mu(\Gamma^l_3)})\parallel\dot{u}^l_{\eta_1}(t)-\dot{u}_{\eta_2}(t)\parallel^2_{\mathbb{V}}\leq(\eta_1(t)-\eta_2(t),\varepsilon(\dot{u}_{\eta_1})-\varepsilon(\dot{u}_{\eta_2}))_{\mathcal{H}}.$$

Remembering $u_{\eta_1}(0)=u_{\eta_2}(0)=u_0$, we perform integration by parts on the preceding inequality over (0, T) to discover

$$(\alpha_{\mathcal{A}^l}-c_0^2(\alpha_{j_\nu}+\alpha_{j_\tau}))\sqrt{\mu(\Gamma^l_3)}\int_0^T\parallel\dot{u}^l_{\eta_1}(s)-\dot{u}^l_{\eta_2}(s)\parallel^2_{\mathbb{V}}\mathrm{d}s$$
$$\leq c\int_0^T\parallel\dot{u}^l_{\nu_1}(s)-\dot{u}_{\nu_2}(s)\parallel^2_{\mathbb{V}}\mathrm{d}s+\frac{1}{4c}\int_0^T\parallel\eta_1(s)-\eta_2(s)\parallel\mathrm{d}s. \tag{31}$$

Thus, from the previous inequality, we conclude

$$(\alpha_{\mathcal{A}^l}-c^2(\alpha_{j_\nu}+\alpha_{j_\tau})\sqrt{\mu(\Gamma^l_3)}-c)\int_0^T\parallel\dot{u}^l_{\eta_1}(s)-\dot{u}^l_{\eta_2}(s)\parallel^2_{\mathbb{V}}\mathrm{d}s\leq\frac{1}{4c}\int_0^T\parallel\eta_1(s)-\eta_2(s)\parallel_{\mathbb{V}^*}\mathrm{d}s.$$

Finally, we use the condition (24) and the Cauchy inequality to get the desired estimation (27).

Lemma 4.2 *Problem (26) has a unique solution. Moreover, there exists a constant $c>0$ such that*

$$\parallel\theta_{\eta_1,z_1}(t)-\theta_{\eta_2,z_2}(t)\parallel^2_{\mathbb{Q}}\leq c\int_0^T\parallel\eta_1(s)-\eta_2(s)\parallel^2_{\mathbb{V}^*}+\parallel z_1(s)-z_2(s)\parallel^2_{\mathbb{Q}^*}\mathrm{d}s. \tag{32}$$

Here, θ_{η_1,z_1} and θ_{η_2,z_2} are the solutions of problem (26) for (η_i,z_i), $i=1,2$.

Proof. [Proof (of Lemma 4.2)] For the estimation (32), let $\theta_{\eta_i,z_i}(t)$ represent the solution to problem (26) associated with $\eta_i,z_i\in L^2(0,T;\mathcal{H}\times Q)$ with $i=1,2$, hence, for all $t \in (0,t)$ and all $\lambda \in \mathbb{Q}$, we find that

$$\sum_{l=1}^{2}(\dot{\theta}^l_{\eta_1 z_1}(t), \lambda^l - \theta^l_{\eta_1 z_1}(t))_{\mathcal{H}} + \langle \mathcal{K}^l \nabla \theta^l_{\eta_1 z_1}(t), \nabla(\lambda^l - \theta^l_{\eta_1 z_1}(t))\rangle_{\mathcal{H}},$$
$$+\langle \mathcal{M}^l \varepsilon(u^l_{\eta_1}(t)), \lambda - \theta^l_{\eta_1 z_1}(t)\rangle + \int_{\Gamma_3} j^0_\theta(\theta^l_{\eta_1 z_1}(t); \lambda^l - \theta^l_{\eta_1 z_1}(t))\mathrm{d}a, \tag{33}$$
$$\geq (h(t), \lambda - \theta_{\eta_1 z_1}(t))_{\mathbb{Q}}.$$

$$\sum_{l=1}^{2}(\dot{\theta}^l_{\eta_2 z_2}(t), \lambda^l - \theta^l_{\eta_2 z_2}(t))_{\mathcal{H}} + \langle \mathcal{K}^l \nabla \theta^l_{\eta_2 z_2}(t), \nabla(\lambda^l - \theta^l_{\eta_2 z_2}(t))\rangle_{\mathcal{H}},$$
$$-\langle \mathcal{M}^l \varepsilon(u^l_{\eta_2}(t)), \lambda^l - \theta^l_{\eta_2 z_2}(t)\rangle - \int_{\Gamma_3} j^0_\theta(\theta^l_{\eta_2 z_2}(t); \lambda^l - \theta^l_{\eta_2 z_2}(t))\mathrm{d}a, \tag{34}$$
$$\geq \langle h(t), \lambda - \theta_{\eta_2 z_2}(t)\rangle_{\mathbb{Q}}.$$

By setting $\lambda = \theta_{\eta_2 z_2}(t)$ in (33) and $\lambda = \theta_{\eta_1 z_1}(t)$ in (34), we combine the two derived inequalities

$$\frac{1}{2} \parallel \theta_{\eta_1, z_1} - \theta_{\eta_2, z_2} \parallel^2_{\mathbb{Q}} + \left(\alpha_{\mathcal{K}^l} - c_0^2 \alpha_{j_\theta}\sqrt{\mu(\Gamma_3)} - \frac{L_{\mathcal{M}}+1}{4c}\right)\int_0^T \parallel \theta_{\eta_1 z_1}(s) - \theta_{\eta_2 z_2}(s) \parallel^2_{\mathbb{Q}} \mathrm{d}s,$$
$$\leq c\int_0^T \left(\parallel u_{\eta_1}(s) - u_{\eta_2}(s) \parallel^2_{\mathbb{V}^*}\right)\mathrm{d}s.$$

Finally, we conclude that the estimation (32) is verified.

To complete the proof of Theorem (4.1), we consider the following operator:

$$\Lambda : L^2(0,T;\mathcal{H}\times Q^*) \to L^2(0,T;\mathcal{H}\times Q^*)$$
$$\Lambda(\eta, z) = (\Lambda_1(\eta, z), \tag{35}$$

where Λ_1 are given for all $\eta, z \in L^2(0,T;\mathcal{H}\times Q^*)$ and $t \in (0,T)$ by

$$\langle \Lambda_1(\eta, z), \varepsilon^l(v)\rangle = \langle \mathcal{B}^l \varepsilon(\mathbf{u}^l_\eta(t)) + \int_0^T \mathcal{G}^l(t-s)u^l_\eta(s)\mathrm{d}s - \mathcal{C}^l\theta^l_{\eta,z}(t), \varepsilon^l(v)\rangle, \tag{36}$$

where $\mathbf{u}_\eta$ and $\theta_{\eta,z}$ are, respectively, the solutions of problems (25) and (26).
We have the following result.

Lemma 4.3 *(1) The operator Λ defined by (36) has a unique fixed point.*
(2) If $\mathbf{u}_1$ and $\mathbf{u}_2$ are two solutions of (25) and (26) corresponding to (η_1, z_1) and (η_2, z_2), then there exists $c > 0$ such that, for $t \in (0,T)$,

$$\|\dot{\mathbf{u}}_1(t) - \dot{\mathbf{u}}_2(t)\|_{\mathbb{V}} \leq c(\|\eta_1(t) - \eta_2(t)\|_{\mathbb{V}} + \|\mathbf{u}_1(t) - \mathbf{u}_2(t)\|). \tag{37}$$

Proof. [Proof [of Lemma 4.3]] Consider (η_1, z_1) and $(\eta_2, z_2) \in L^2(0,T;\mathcal{H}\times\mathbb{Q}^*)$, from the definition of Λ, we get

$$\|\Lambda(\eta_1, z_1)(t) - \Lambda(\eta_2, z_2)(t)\|^2_{\mathcal{H}\times\mathbb{Q}^*}$$
$$= \|\Lambda_1(\eta_1, z_1)(t) - \Lambda_1(\eta_2, z_2)(t)\|^2_{\mathcal{H}\times\mathbb{Q}^*} + \|\Lambda_2(\eta_1, z_1)(t) - \Lambda_2(\eta_2, z_2)(t)\|^2_{\mathcal{H}\times\mathbb{Q}^*}.$$

Using the relations (17)-b and the condition in [6], also $\mathbf{u}_i(t) = \int_0^T \dot{\mathbf{u}}_i(s)\mathrm{d}s + \mathbf{u}_0(t), \forall t \in (0,T)$, we have

$$\|\mathbf{u}_1(t) - \mathbf{u}_2(t)\|_{\mathbb{V}} \leq \int_0^T \|\dot{\mathbf{u}}_1(s) - \dot{\mathbf{u}}_2(s)\|_{\mathbb{V}}$$

and using this inequality in (37), Gronwall's inequality, and applying the previous lemmas, we deduce that there exists a constant $C > 0$ such that

$$\|\Lambda(\eta_1, z_1)(t) - \Lambda(\eta_2, z_2)(t)\|^2_{\mathcal{H}\times\mathbb{Q}^*} \leq c\int_0^T \|(\eta_1, \eta_2) - (z_1, z_2)\|^2_{\mathbb{V}^*\times\mathbb{Q}^*}\mathrm{d}s.$$

Finally, the operator Λ has a unique fixed point.

Now, let $(\eta^*, z^*) \in L^2((0,T), \mathcal{H}^l \times Q^*)$ be the unique solution of the operator Λ (fixed point for the operator), to demonstrate the solution of theorem (4.1), we considered $\mathbf{u} = \mathbf{u}_{\eta^*}$ and $\theta = \theta_{\eta^*,z^*}$ as the solutions to problems (25) and (26), respectively. Furthermore, the uniqueness of the fixed-point operator defined in (35) and (36) implies the uniqueness aspect of the theorem.

5 Numerical Analysis of Problem ($\mathcal{P}$)

Numerical approaches are essential for approximating solutions in practical applications due to the complexity of the challenges at hand. In this work, we primarily examine fully discrete approximation systems, in which the temporal and spatial variables are discretized. The spatial domain is discretized using the finite element method, and the time derivatives are discretized using finite differences. We establish the existence and uniqueness of each numerical scheme's solution and derive optimal order error estimates for the continuous problem's solution under specific regularity assumptions.

In this section, we present a fully discrete approach for Problem ($\mathcal{P}_V$), we use the finite-difference method to approximate the derivative of function. We consider the uniform partition :$0 < t_0 < t_1 < \cdots < t_N = T$ of $(0,T)$ with a time step-size $k = T/N+1$ and for each continuous function v, we denote

$$v(t_n) = v_n \qquad \delta v_n = \frac{v_n - v_{n-1}}{k}.$$

Moreover, we apply the finite element method for the spatial discretization. Let Ω be the polygonal domain, then we consider a regular family of partitions $(\mathcal{T}^h)$ of $\bar{\Omega}$ into triangles that are compatible with the partition of the boundary $\partial\Omega$ into $\Gamma = \Gamma_1 \cup \Gamma_2 \cup \Gamma_3$ and $\Gamma_1 \cup \Gamma_2{=}\Gamma_a \cup \Gamma_b$. Here, $h > 0$ denotes the discretization parameter, and c denotes a generic positive constant which does not depend on the discretization parameters h and k. To approximate the spaces V, W and Q, respectively, we introduce the following linear finite element spaces corresponding to $\mathcal{T}^h$:

$$V^h = \{v^h \in C(\bar{\Omega}) | v^h_{|T} \text{ for } T \in \mathbb{P}_1(T), v^h = 0 \text{ on } \Gamma_1\}$$

$$Q^h = \{\theta^h \in C(\bar{\Omega}) | \theta^h_{|T} \text{ for } T \in \mathbb{P}_1(T), \theta^h = 0 \text{ on } \Gamma_1\}.$$

We introduce the following piecewise constant finite element space for the stress field:

$$\mathcal{H}^h = \{\tau^h \in \mathcal{H} | \tau^h_{|T} \text{ for } T \in \mathbb{R}^{d\times d}, \text{ for } T \in \mathcal{T}^h\}.$$

Let $u_0^{hk} = u_0^h \in V^h$ and $\theta_0^{hk} = \theta_0^h \in Q^h$ be appropriate approximations of the initial conditions u_0, θ_0, respectively, such that $\|u_0 - u_0^h\| < ch$ and $\|\theta_0 - \theta_0^h\| < ch$. Hence, the discrete scheme for Problem ($\mathcal{P}_V$) is given as follows.

5.1 Problem $\mathcal{P}_V^{hk}$

Find a displacement $\{u_n^{hk}\}_{n=0}^N \subset V^h$, a temperature $\{\theta_n^{hk}\}_{n=0}^N \subset Q^h$ such that for $n = 0, 1, \cdots, N$, we have

$$\sum_{l=1}^{2} \langle \mathcal{A}^l \varepsilon(w_n^{hk}), \varepsilon(v_n^h - w_n^{hk})\rangle_{\mathcal{H}} + \left\langle \mathcal{B}^l \varepsilon(u_n^{hk}) - \mathcal{C}^l \theta_n^{hk}, \varepsilon(v_n^h - w_n^{hk})\right\rangle +$$
$$\left\langle \int_0^T \mathcal{G}^l(t-s) u_n^{hk}\, \mathrm{d}s, \varepsilon(v_n^h - w_n^{hk}) \right\rangle + \int_{\Gamma_1} \left(j_\nu^0(w_{\nu n}^{hk}; v_{\nu n}^h - w_{\nu n}^{hk}) + j_\tau^0(w_{\tau n}^{hk}; v_{\tau n}^h - w_{\tau n}^{hk}) \right) \mathrm{d}s$$
$$+ \int_{\Gamma_1} \left(j_\nu^0(w_{\nu n}^{hk}; v_{\nu n}^{hk} - w_{\nu n}^{hk}) + j_\tau^0(w_{\tau n}^{hk}; v_{\tau n}^{hk} - w_{\tau n}^{hk}) \right) \mathrm{d}s \geq \left\langle F_n, v_n^h - w_n^{hk} \right\rangle \quad \forall v_n^h \in V^h \tag{38}$$

$$\sum_{l=1}^{2} \left\langle \delta\theta_n^{hk}, \lambda_n^h - \theta_n^{hk}) \right\rangle_{\mathcal{H}} + \left\langle \mathcal{K}\nabla\theta_n^{hk}, \nabla(\lambda_n^h - \theta_n^{hk}) \right\rangle_{\mathcal{H}} - (\mathcal{M}^l \varepsilon((u_n^{hk})^l(t)), (\lambda_n^h)^l - (\theta_n^{hk})^l(t))_{\mathcal{H}}$$
$$+ \int_{\Gamma_3} j_\theta^0(\theta_n^{hk}(t); (\lambda_n^h)^l - (\theta_n^{hk})^l(t)) \mathrm{d}a \quad \geq \left\langle h_n, \lambda_n^h - \theta_n^{hk}(t) \right\rangle \quad \forall w_n^h \in W^h. \tag{39}$$

Here, the sequences $\{u_n^{hk}\}_{n=0}^N$ and $\{w_n^{hk}\}_{n=0}^N$ are related by the following equalities:

$$w_n^{hk} = \delta u_n^{hk} \text{ and } \quad u_0^h + k \sum_{j=0}^{n} w_j^{hk} n = 1, ...N.$$

From assumptions (16)−(21), using the same arguments as for Problem (Pv), we conclude that Problem $\mathcal{P}_V^{hk}$ has a unique solution $(u_n^{hk}, \theta_n^{hk}) \subset V^h. \times Q^h$. It will be derived using the Céa inequalities for error estimations.

Theorem 5.1 *Assume that the conditions in Theorem* 4.1 *still hold. Consider* (u^l, θ^l) *as the approximate solution to Problem* $\mathcal{P}_V$ *and* $(u_n^{hk}, \theta_n^{hk})$ *as the solution to Problem* $\mathcal{P}_V^{hk}$*. Then for* $n = 1, \ldots, N$*, the following error estimate holds:*

$$\max_{1 \leq n \leq N} \left(\|w_n^l - w_n^{hk}\|_V^2 + \|u_n^l - u_n^{hk}\|_V^2 \right)$$
$$\leq C \max_{1 \leq n \leq N} \left(\|w_n^l - v_n^h\|_V^2 + \|w_n^l - v_n^h\|_{L^2(\Gamma_3)}^2 \right) + C \sum_{n=1}^{N} \|\theta_n^l - \lambda_n^h\|_Q^2 + \|\theta_n^l - \lambda_n^h\|_{L^2(\Gamma_3)}$$
$$+ C \sum_{n=1}^{N-1} \|(\theta_n^l - \lambda_n^h) + (\theta_{n+1}^l - \lambda_{n+1}^h\| + C \left(\|\theta_0 - \theta_0^h\|_Q^2 + \|\theta_1 - \lambda_1^h\|_Q^2 + c(h^2 + k^2) \right).$$

Proof. [Proof (of Theorem 5.1)] First, the following equality holds:

$$\sum_{l=1}^{2} \langle \mathcal{A}^l \varepsilon(w_n) - \mathcal{A}^l \varepsilon(w_n^{hk}), \varepsilon(w_n - w_n^{hk})\rangle_{\mathcal{H}}$$
$$= \sum_{l=1}^{2} \langle \mathcal{A}^l \varepsilon(w_n) - \mathcal{A}^l \varepsilon(w_n^{hk}), \varepsilon(w_n - v_n^h)\rangle_{\mathcal{H}} + \langle \mathcal{A}^l \varepsilon(w_n), \varepsilon(v_n^h - w_n)\rangle_{\mathcal{H}}$$
$$\langle \mathcal{A}^l \varepsilon(w_n), \varepsilon(w_n - w_n^{hk})\rangle_{\mathcal{H}} + \langle \mathcal{A}^l \varepsilon(w_n^{hk}), \varepsilon(w_n^{hk}) - \varepsilon(v_n^h)\rangle_{\mathcal{H}}. \tag{40}$$

Furthermore, by taking $t = t_n$ and $v = w_n^{hk}$ in the inequality (22), we combine the equality (40) with hypothesis (16) to derive

$$\begin{aligned}
\alpha_{\mathcal{A}^l}\|w_n - w_n^{hk}\|_{\mathbb{V}}^2 \le \sum_{l=1}^{2}&\langle \mathcal{A}\varepsilon(w_n) - \mathcal{A}^l\varepsilon(w_n^{hk}), \varepsilon(w_n - v_n^h)\rangle_{\mathcal{H}} + \langle \mathcal{A}^l\varepsilon(w_n), \varepsilon(v_n^h - w_n)\rangle_{\mathcal{H}}\\
&+\langle F_n, w_n - v_n^h\rangle_{\mathbb{V}} + \langle \mathcal{B}^l(\varepsilon(u_n)), \varepsilon(w_n^{hk} - w_n)\rangle_{\mathcal{H}} + \langle \mathcal{B}^l(\varepsilon(u_n^{hk})), \varepsilon(v_n^h - w_n^{hk})\rangle_{\mathcal{H}}\\
&+\langle \int_0^T \mathcal{G}^l(t-s)u_n \mathrm{d}s, \varepsilon(w_n^{hk} - w_n)\rangle_{\mathcal{H}} + \langle \int_0^T \mathcal{G}^l(t-s)u_n^{hk}\mathrm{d}s, \varepsilon(v_n^h - w_n^{hk})\rangle_{\mathcal{H}}\\
&-\langle \mathcal{C}^l\theta_n, \varepsilon(w_n^{hk} - w_n)\rangle_{\mathcal{H}} - \langle \mathcal{C}^l\theta_n^{hk}, \varepsilon(v_n^h - w_n^{hk})\rangle_{\mathcal{H}}\\
&+\int_{\Gamma_3} j_\nu^0(w_{n\nu}; w_{n\nu}^{hk} - w_{n\nu}) + j_\nu^0(w_{n\nu}^{hk}; v_{n\nu}^h - w_{n\nu}^{hk})\mathrm{d}a\\
&+\int_{\Gamma_3} j_\tau^0(w_{n\tau}; w_{n\nu}^{hk} - w_{n\nu}) + j_\tau^0(w_{n\tau}^{hk}; v_{n\nu}^h - w_{n\nu}^{hk})\mathrm{d}s.
\end{aligned}$$

We start with the integration factor for all $n = 1, ..., N$, using the results in [3], we have

$$\begin{aligned}
&\langle \int_0^{t_n} \mathcal{G}^l(t_n - s)u_n^{hk}\mathrm{d}s, \varepsilon(v_n^h - w_n)\rangle_{\mathcal{H}}\\
&+\langle \int_0^T \mathcal{G}^l(t-s)u_n\mathrm{d}s - \int_0^{t_n} \mathcal{G}^l(t_n - s)u_n^{hk}\mathrm{d}s, \varepsilon(w_n^{hk} - w_n)\rangle_{\mathcal{H}}\\
&\qquad\qquad \le ck^2 + ck\sum_{n=0}^{N}\|u_n^{hk} - u_n\|_{\mathcal{H}}^2.
\end{aligned} \tag{41}$$

Next, we use the hypotheses $(16) - b$, $(17) - b$, $(19) - d$, $(20) - d$,(41) and [6] to find

$$\begin{aligned}
\alpha_{\mathcal{A}^l}\|w_n^l - w_n^{hk}\|_{\mathbb{V}}^2 \le\ & L_{\mathcal{A}^l}\|w_n^l - w_n^{hk}\|_{\mathbb{V}}\|w_n - v_n^h\|_{\mathbb{V}}\\
&+L_{\mathcal{B}^l}(\|u_n - u_n^{hk}\|_{\mathbb{V}})(\|w_n - w_n^{hk}\|_{\mathbb{V}} + \|w_n^l - v_n^h\|_{\mathbb{V}})\\
&+S_1(u_n, \theta_n) + I_1(w_n^{hk}, w_n, v_n^h) + L_{\mathcal{M}^l}\|\theta_n^l - \theta_n^{hk}\|_{\mathbb{Q}}(\|w_n^l - w_n^{hk}\|_{\mathbb{V}}\\
&+\|w_n^l - v_n^h\|_{\mathbb{V}}) + c_0^2\sqrt{\mu(\Gamma_3)}(\alpha_{j_\nu} + \alpha_{j_\tau})\|w_n^l - w_n^{hk}\|_{\mathbb{V}}^2,
\end{aligned}$$

where S_1 and I_1 are given by

$$\begin{aligned}
S_1(u_n, \theta_n) =\ & \langle \mathcal{A}\varepsilon(w_n), \varepsilon(v_n^h - w_n)\rangle_{\mathcal{H}} + \langle \mathcal{B}(\varepsilon(u_n), \varepsilon(v_n^h - w_n)\rangle_{\mathcal{H}}\\
&-\langle \mathcal{C}\theta_n, \varepsilon(v_n^h - w_n)\rangle_{\mathcal{H}} + \langle F_n, w_n - v_n^h\rangle_{\mathbb{V}}\\
I_1(w_n^{hk}, w_n, v_n^h) =\ & \int_{\Gamma_3} j_\nu^0(w_{n\nu}^{hk}; v_n^h - w_n)\mathrm{d}a + \int_{\Gamma_3} j_\tau^0(w_{n\tau}^{hk}; v_n^h - w_{n\nu})\mathrm{d}a.
\end{aligned}$$

We further assume that $j_\nu(x, .)$ and $j_\tau(x, .)$ are c-locally Lipschtiz on $\mathbb{R}$ and $\mathbb{R}^n$, respectively for (a.e.) $x \in \Gamma_3$, where the Lipschitiz constant $c > 0$ is independent of x. Hence, we have

$$j_\nu^0(w_{n\nu}^{hk}; v_{n\nu}^h - w_{n\nu}) \le c\|w_n - v_n^h\|_{L^2(\Gamma_3)} \quad \text{and} \quad j_\tau^0(w_{n\tau}^{hk}; v_n^h - w_{n\nu}) \le \|w_n - v_n^h\|_{L^2(\Gamma_3)}.$$

Then it should be concluded that

$$I_1(w_n^{hk}, w_n, v_n^h) \le c\|w_n - v_n^h\|_{L^2(\Gamma_3)}.$$

Next, we multiply (7) by an arbitrary element $v \in V$, and then we conclude

$$S_1(u_n,\theta_n) = \int_{\Gamma_3} \sigma\nu.(v_n^h - w_n)\mathrm{d}a \leq c\|\sigma\|\|w_n - v_n^h\|_{L^2(\Gamma_3)} \leq c\|w_n - v_n^h\|_{L^2(\Gamma_3)}. \tag{42}$$

Additionally, use the Cauchy inequality so that for $\epsilon > 0$, we deduce

$$\begin{aligned}&(\alpha_{\mathcal{A}^l} - c_0^2\sqrt{\mu(\Gamma_3)}(\alpha_{j_\nu} + \alpha_{j_\tau}) - 5\epsilon)\|w_n^l - w_n^{hk}\|_{\mathbb{V}}^2 \\ &\quad \leq c(\|w_n^l - v_n^h\|_V^2 + \|u_n^l - u_n^{hk}\|_{\mathbb{V}}^2 + \|\theta_n^l - \theta_n^{hk}\|_{\mathbb{Q}}^2 + \|w_n^l - v_n^h\|_{L^2(\Gamma_3)}).\end{aligned} \tag{43}$$

Moreover, using results in [10], we have

$$\|u_n - u_n^{hk}\|_{\mathbb{V}}^2 \leq c(h^2+k^2) + ck\sum_{i=1}^{n}\|w_i - w_i^{hk}\|_{\mathbb{V}}^2. \tag{44}$$

We combine (43), (44) so that

$$\begin{aligned}&\|w_n - w_n^{hk}\|_{\mathbb{V}}^2 \\ &\quad \leq C\left(\|w_n - v_n^h\|_{\mathbb{V}}^2 + \|\theta_n - \theta_n^{hk}\|_{\mathbb{Q}}^2 + \|w_n - v_n^h\|_{L^2(\Gamma_3)}\right) \\ &\quad +c(h^2+k^2) + ck\sum_{i=1}^{n}\|w_i - w_i^{hk}\|_{\mathbb{V}}^2.\end{aligned} \tag{45}$$

Then, by applying the Gronwall inequality in (45) and combining with (44), we get a positive constant $c > 0$ such that

$$\begin{aligned}&\|w_n - w_n^{hk}\|_{\mathbb{V}}^2 + \|u_n - u_n^{hk}\|_{\mathbb{V}}^2 \leq c(\|w_n - v_n^h\|_{\mathbb{V}}^2 \\ &+\|\theta_n - \theta_n^{hk}\|_{\mathbb{Q}}^2 + \|w_n - v_n^h\|_{L^2(\Gamma_3)}) + c(h^2+k^2) + ck\sum_{i=1}^{n}\|w_i - w_i^{hk}\|_{\mathbb{V}}^2.\end{aligned}$$

For simplification, let us consider

$$\begin{aligned}e_n &= \|w_n^l - w_n^{hk}\|_{\mathbb{V}}^2 + \|u_n^l - u_n^{hk}\|_{\mathbb{V}}^2 \\ g_n &= \|w_n^l - v_n^h\|_{\mathbb{V}}^2 + \|\theta_n^l - \theta_n^{hk}\|_{\mathbb{Q}}^2\|w_n - v_n^h\|_{L^2(\Gamma_3)} + h^2 + k^2.\end{aligned}$$

There exists a positive constant $c > 0$ such that $(e_n \leq cg_n + c\sum_{j=0}^{n} e_j)$ with $c > 0$. Therefore, we use the assumption for $\mathcal{K}^l$ in [6] to get

$$\begin{aligned}&\sum_{l=1}^{2}\alpha_{\mathcal{K}^l}\|\theta_n^l - \theta_n^{hk}\|_{\mathbb{Q}}^2 \\ &\quad \leq \sum_{l=1}^{2}\langle\mathcal{K}^l\nabla\theta_n - \mathcal{K}\nabla\theta_n^{hk}, \nabla(\theta_n - \lambda_n^h)\rangle_{\mathcal{H}^l} + \langle\mathcal{K}^l\nabla\theta_n, \nabla(\lambda_n^h - \theta_n)\rangle_{\mathcal{H}^l} \\ &\quad + \langle\mathcal{K}^l\nabla\theta_n, \nabla(\theta_n - \theta_n^{hk})\rangle_{\mathcal{H}} + \langle\mathcal{K}^l\nabla\theta_n^{hk}, \nabla(\theta_n^{hk} - \lambda_n^h)\rangle_{\mathcal{H}^l}.\end{aligned}$$

Taking $t = t_n$ and $\lambda = \theta_n^{hk}$ in the inequality (3.32) , we use (39) to get

$$\begin{aligned}\sum_{l=1}^{2}\langle\mathcal{K}^l\nabla\theta_n^{hk}, \nabla(\theta_n^{hk} - \lambda_n^h)\rangle_{\mathcal{H}^l} &\leq \sum_{l=1}^{2}\langle\delta\theta_n^{hk}, \lambda_n^h - \theta_n^{hk}\rangle_{\mathcal{H}^l} - \langle\mathcal{M}^l\varepsilon(u_n^{hk}), \lambda_n^h - \theta_n^{hk}\rangle_{\mathcal{H}^l} \\ &+\langle\xi\nabla\varphi_n^{hk}, \lambda_n^h - \theta_n^{hk}\rangle_{\mathcal{H}^l} + \int_{\Gamma_3} j_\theta^0(\theta_n^{hk}; \lambda_n^h - \theta_n^{hk})\mathrm{d}a + \langle h_n, \theta_n^{hk} - \lambda_n^h\rangle_{\mathbb{Q}}.\end{aligned}$$

Now, we deduce the following estimation:

$$\sum_{l=1}^{2} \alpha_{\mathcal{K}^l} \|\theta_n^l - \theta_n^{hk}\|_{\mathbb{Q}}^2 + \langle \delta\theta_n^l - \delta\theta_n^{hk}, \theta_n^l - \theta_n^{hk}\rangle \leq \sum_{l=1}^{2} c(\|\theta_n^l - \lambda_n^h\|_{\mathbb{Q}}^2$$
$$+\|u_n^l - u_n^{hk}\|_{\mathbb{V}}^2) + \langle \delta\theta_n^{hk} - \delta\theta_n^l, \lambda_n^h - \theta_n^l\rangle_{\mathcal{H}^l} + S_2(u_n^l, \theta_n^l) + I_2(\theta_n^{hk}, \theta_n^l, \lambda_n^h), \quad (46)$$

where the quantities S_2 and I_2 are given by the expressions below:

$$S_2(u_n^l, \theta_n^l) = \langle \dot{\theta}^l{}_n, \lambda_n^h - \theta_n^l\rangle_{\mathcal{H}^l} + \langle \mathcal{K}^l \nabla\theta_n^l, \nabla(\lambda_n^h - \theta_n^l)\rangle_{\mathcal{H}^l} - \langle \mathcal{M}^l \varepsilon(u_n^l), \lambda_n^h - \theta_n^l\rangle_{\mathcal{H}^l}$$
$$+\langle h_n, \theta_n^l - \lambda_n^h\rangle_{\mathcal{H}^l}$$

and

$$I_2(\theta_n^{hk}, \theta_n^l, \lambda_n^h) = \int_{\Gamma_3} j_\theta^0(\theta_n^{hk}; \lambda_n^h - \theta_n)\mathrm{d}a.$$

Then, by the same method as for (42), we can deduce that

$$S_2(u_n, \theta_n) \leq c\|\theta_n - \lambda_n^h\|_{L^2(\Gamma_3)}. \quad (47)$$

We have that $j_\theta(x,)$ is locally Lipschitz on $\mathbb{R}$ for (a.e) $x \in \Gamma_3$ for the positive Lipschitz constant $c > 0$ independent of x. Then we have

$$I_2(\theta_n^{hk}, \theta_n, \lambda_n^h) \leq c\|\theta_n - \lambda_n^h\|_{L^2(\Gamma_3)}, \quad (48)$$

we use the inequalities (46),(47) and (48) and the formula

$$2\langle a - b, a\rangle = \|a - b\|^2 + \|a\|^2 - \|b\|^2$$

such that $a = \theta_n - \theta_n^{hk}$ and $b = \theta_{n-1} - \theta_{n-1}^{hk}$, we get

$$\frac{1}{2k}(\|\theta_n - \theta_n^{hk}\|_{\mathbb{Q}}^2 - \|\theta_{n-1} - \theta_{n-1}^{hk}\|_{\mathbb{Q}}^2) \leq \langle \delta\theta_n - \delta\theta_n^{hk}, \theta_n - \theta_n^{hk}\rangle_{\mathcal{H}}. \quad (49)$$

Then, by (49), and replacing n by j in the above relation, summing up from $j = 1$ to n, we deduce the following majoration:

$$2k\sum_{j=0}^{n}\langle \delta\theta_j^{hk} - \delta\theta_j, \lambda_n^h - \theta_j\rangle_{\mathcal{H}} \leq c\|\theta_n - \theta_n^{hk}\|_{\mathbb{Q}}^2 + \|\theta_n - \lambda_n^{hk}\|_{\mathbb{Q}}^2 + \|\theta_0 - \theta_0^h\|$$
$$+c\|\theta_1 - \lambda_1^h\|_{\mathbb{Q}}^2 + \frac{k}{2}\sum_{j=1}^{n-1}\|\theta_j - \theta_j^{hk}\|_{\mathbb{Q}}^2 + \frac{2}{k}\sum_{j=1}^{n-1}\|(\theta_j - \lambda_j) - (\theta_{j+1} - \lambda_{j+1})\|_{L^2(\Omega)}.$$

For simplification, we note $e_n = \|\theta_n^l - \theta_n^{hk}\|_{\mathbb{Q}}^2 + 2k\alpha_{\mathcal{K}^l}\sum_{j=1}^{n}\|\theta_j - \theta_j^{hk}\|_{\mathbb{Q}}^2$ and

$$g_n = k\sum_{j=1}^{n}\{\|\theta_j - \lambda_j\|_{\mathbb{Q}}^2 + \|u_j - u_j^{hk}\|_{\mathbb{V}}^2 + \|\varphi_j - \varphi_j^{hk}\|_{\mathbb{Q}}^2 + \|\theta_j - \lambda_j^h\|_{L^2(\Gamma_3)}\}$$
$$+\frac{1}{k}\sum_{j=1}^{n-1}\|(\theta_j - \lambda_j^h) - (\theta_{j+1} - \lambda_{j+1}^h)\|_{L^2(\Omega)} + \|\theta_0 - \theta_0^h\|_{\mathbb{Q}}^2 + \|\theta_1 - \lambda_1^h\|_{\mathbb{Q}}^2 + \|\theta_n - \lambda_n^h\|_{\mathbb{Q}}^2.$$

Then there exists a positive constant $c > 0$ such that $e_n \leq c g_n + c \sum_{j=1}^{n} e_j$. We use the Gronwall inequality and the estimations (44) to deduce

$$\begin{aligned}
&\|w_n - w_n^{hk}\|_{\mathbb{V}}^2 + \|u_n - u_n^{hk}\|_{\mathbb{V}}^2 + \|\theta_n - \theta_n^{hk}\|_{\mathbb{Q}}^2 \\
&\leq C\left(\|w_n - v_n^h\|_{\mathbb{V}}^2 + \|w_n - v_n^h\|_{L^2(\Gamma_3)}\right) + \sum_{j=1}^{n}\left(\|\theta_j - \lambda_j^h\|_{\mathbb{Q}}^2 + \|\theta_j - \lambda_j^h\|_{L^2(\Gamma_3)}\right) \\
&+ \sum_{j=1}^{n-1} \|(\theta_j - \lambda_j^h) - (\theta_{j+1} - \lambda_{j+1}^h)\|_{L^2(\Omega)}^2 + \sum_{j=1}^{n}\left(\|w_j - w_j^{hk}\|_{\mathbb{V}}^2 + \|u_j - u_j^{hk}\|_{\mathbb{V}}^2 + \|\theta_j - \theta_j^{hk}\|_{\mathbb{Q}}^2\right) \\
&+ \|\theta_0 - \theta_0^h\|_{\mathbb{Q}}^2 + \|\theta_1 - \theta_1^h\|_{\mathbb{Q}}^2 + c(h^2 + k^2).
\end{aligned} \tag{50}$$

Now let us consider the following quantities:

$$\begin{aligned}
e_n &= \|w_n - w_n^{hk}\|_{\mathbb{V}}^2 + \|u_n - u_n^{hk}\|_{\mathbb{V}}^2 + \|\theta_n - \theta_n^{hk}\|_{\mathbb{Q}}^2 \\
g_n &= \|w_n - v_n^h\|_{\mathbb{V}}^2 + \|w_n - v_n^h\|_{L^2(\Gamma_3)} + \sum_{j=1}^{n}(\|\theta_j - \lambda_j^h\|_{\mathbb{Q}}^2 + \|\theta_j - \lambda_j^h\|_{L^2(\Gamma_3)}) \\
&+ \sum_{j=1}^{n-1} \|(\theta_j - \lambda_j^h) - (\theta_{j+1} - \lambda_{j+1}^h)\|_{L^2(\Omega)}^2 + \|\theta_0 - \theta_0^h\|_{\mathbb{Q}}^2 + \|\theta_1 - \theta_1^h\|_{\mathbb{Q}}^2 + h^2 + k^2.
\end{aligned}$$

Then we consider the inequality (50), by applying the Gronwall inequality, we have

$$\begin{aligned}
&\|w_n^2 - w_n^{hk}\|_{\mathbb{V}}^2 + \|u_n^2 - u_n^{hk}\|_{\mathbb{V}}^2 + \|\theta_n - \theta_n^{hk}\|_{\mathbb{Q}}^2 \\
&\leq c(\|w_n^l - v_n^h\|_{\mathbb{V}}^2 + \|w_n - v_n^h\|_{L^2(\Gamma_3)} + \sum_{j=1}^{n}(\|\theta_j - \lambda_j^h\|_{\mathbb{Q}}^2 + \|\theta_j - \lambda_j^h\|_{L^2(\Gamma_3)}) \\
&+ \sum_{j=1}^{n-1} \|(\theta_j - \lambda_j^h) - (\theta_{j+1} - \lambda_{j+1}^h)\|_{L^2(\Omega^l)}^2 + \|\theta_0 - \theta_0^h\|_{\mathbb{Q}}^2 + \|\theta_1 - \theta_1^h\|_{\mathbb{Q}}^2) + c(h^2 + k^2).
\end{aligned} \tag{51}$$

Finally, we use (51) to derive the estimation of Theorem 5.1.

6 Concluding Remarks

This paper has explored a contact problem concerning thermo-viscoelastic materials with memory effects over time. We developed a variational formulation for the model and established the existence and uniqueness of a weak solution. Furthermore, an error analysis was conducted, highlighting the discrepancy between the weak solution and its numerical approximation, which underpins the reliability of the numerical methods employed. The validity of the theoretical results was confirmed through numerical simulation, showcasing the practicality of the proposed approach. Future research will focus on refining the model to accommodate more complex boundary conditions and on investigating further applications in industrial contexts. In conclusion, the presented model provides a robust framework for analyzing contact problems in thermo-viscoelastic materials, offering potential benefits in various engineering domains.

References

[1] O. Baiz, H. Benaissa, Z. Faiz and D. El Moutawakil. Variational-hemivariational inverse problem for electro-elastic unilateral frictional contact problem. *J. Inverse Ill-Posed Probl.* **29** (6) (2021) 917–934.

[2] M. Barbateu, K. Bartosz, W. Han and T. Janiczko. Numerical Analysis Of A Hyperbolic Hemivariational Inequality Arising In Dynamic Contact. *Society for Industrial and Applied Mathematics SIAM* **53** (1) (2015) 527–550.

[3] O. Chau and R. Oujja. Numerical treatment of a class of thermal contact problems. *Mathematics and Computers in Simulation* **118** (2015) 163–176.

[4] A. Djabi. A Frictional Contact Problem with Wear for Two Electro-Viscoelastic Bodies, *Nonlinear Dyn. Syst. Theory* **22** (2) (2023) 167–182.

[5] I. Boukaroura and A. Djabi. Analysis of Problems in Generalized Viscoplasticity under Dynamic Thermal Loading. *Nonlinear Dyn. Syst. Theory* **23** (4) (2023) 367–380.

[6] Z. Faiz and O. Baiz. Analysis and Approximation of Hemivariational Inequality for a Frictional Thermo-electro-visco-elastic Contact Problem with Damage. *Taiwanese J. Math.* **27** (1) (2023) 81–111.

[7] L. Gasinski, A. Ochal and M. Shillor Variational-Hemivariational Approach to a Quasistatic Viscoelastic Problem with Normal Compliance, Friction and Material Damage. *Journal of Analysis and its Applications* **34** (2015) 251–275.

[8] R. Glowinski and J.L. Lions. *Numerical Analysis of variational Inequalities.* North-Holland, Amsterdam, 1981.

[9] W. Han, S. Migorski and M. Sofonea (Eds). *Advences in Variational and Hemivariational Inqualities: Theory Numerical Analysis and Applications.* Springer-Verlag, New York, 2015.

[10] W.Han, M. Sofonea, Numerical analysis of hemivariational inequalities in contact mechanics, *Acta Numerica* (28) (2019) 175–286.

[11] M. Sofonea. Modélisation mathématique en Mécanique du Contact. *Annals of the University of Craiova. Mathematics and Computer Science series* **32** (2005) 67–74.

[12] M. Sofonea and EL.H. Essoufi. A piezoelectric contact problem with slip-dependent coefficient of friction. *Mathematical Modelling and Analysis* **9** (3) (2004) 229–242.

Nonlinear Dynamics and Systems Theory, **25** (2) (2025) 187–205

Analysis of an HIV-1 Infection Model with Delay Including Quiescent Cells and Cell-to-Cell Transmission

Meriem Lamraoui [1*], Bilal Boulfoul [2] and Mahiéddine Kouche [3]

[1] *Laboratory of Numerical Analysis, Optimization and Statistics (LANOS), Badji Mokhtar - Annaba University, 12, P.O.Box, 23000, Annaba, Algeria.*
[2] *Faculty of Technology, University of 20 August 1955, 26, P.O.Box, 21000, Road El Hadaiek-Skikda, Skikda, Algeria.*
[3] *Laboratory of Applied Mathematics (LMA), Badji Mokhtar - Annaba University, 12, P.O.Box, 23000, Annaba, Algeria.*

Received: September 27, 2024; Revised: April 1, 2025

Abstract: In this paper, we propose a model describing the transmission of HIV-1 infection by cell-free virus and cell-to-cell transfer mode under antiretroviral therapy. The model that we propose is derived from that proposed by Kouche et al. [1]. First, we consider the case without delay and we prove that the basic reproduction number of the model is the sum of the basic reproduction number of cell-free infection and that of cell-to-cell infection. We prove that when the basic reproduction number is less than one, the infection is cleared, and when it is greater than one, the endemic steady state is globally asymptotically stable. In the second part of the paper, we introduce an intracellular delay to take into account the incubation period of the infection. We give a complete stability analysis for both free and endemic steady states. Finally, we illustrate our study by some numerical simulations to evaluate the effects of time delay on the virus dynamics. Our analytical and computational results show that the intracellular delay has no effect on the quiescent cells but reduces the viral load.

Keywords: *HIV-1 infection; cell-to-cell transmission; delay; stability analysis; antiretroviral therapy.*

Mathematics Subject Classification (2020): 92B05, 92B99, 34C23, 93D30, 34D23.

* Corresponding author: mailto:meriem.lamraoui@univ-annaba.dz

1 Introduction

In 1984, researchers discovered the primary causative viral agent of AIDS, called the human immunodeficiency virus type 1 (HIV-1). HIV-1 belongs to the family of retroviruses, whose genetic material is RNA. HIV-1 is transmitted by direct inoculation during unsafe sexual contact, transfusion of contaminated blood or blood products, sharing of contaminated needles [2–4].

There are two ways in which viruses move between cells, which are known as cell-free and cell-to-cell infections. In order to eradicate the virus, antiretroviral drug therapy (ART) involves the simultaneous administration of two or more antiviral drugs [5–8].

Recently, some clinical studies conducted *in vivo* showed that infections originating from cell-to-free virus decrease strongly in the presence of certain antiretrovirals, whereas infections involving cell-to-cell spread are markedly less sensitive to the drugs. Different mathematical models have been used to study the dynamics of HIV infection including these two transmission pathways [8].

In a previous paper, Kouche et al. [1] proposed the following model:

$$\begin{cases} \dfrac{dQ(t)}{dt} = \lambda + \rho T(t) - \alpha Q(t) - \mu_Q Q(t), \\ \dfrac{dT(t)}{dt} = \alpha Q(t) - (1-\eta)\gamma T(t) V_I(t) - \rho T(t) - \mu_T T(t), \\ \dfrac{dT^*(t)}{dt} = (1-\eta)\gamma T(t) V_I(t) - \mu_{T^*} T^*(t), \\ \dfrac{dV_I(t)}{dt} = \omega \mu_{T^*} \pi T^*(t) - \mu_V V_I(t), \end{cases} \tag{1}$$

which incorporated a class called quiescent cells Q, which are a class of CD4$^+$ cells of the immune system that cannot be infected by the virus. In this model, it was assumed that the immune system maintains activated the quiescent cells at a rate α and returns to the quiescent state at a rate ρ.

In this paper, our aim is to highlight the combined transmission effect of both cell-free and cell-to-cell virus spreadings through a new model derived from model (1) and including reverse transcriptase inhibitors (RTI) for both transmission pathways. We assume that the transmission spreads from infected cells and free virus to only activated cells through direct contact. Denote by Q the compartment of quiescent cells, T are the healthy activated cells, T^* are the infected cells, V_I is the free infectious virus and V_{NI} is the non infectious virus. Then the model we propose is

$$\begin{cases} \dfrac{dQ(t)}{dt} = \lambda + \rho T(t) - \alpha Q(t) - \mu_Q Q(t), \\ \dfrac{dT(t)}{dt} = \alpha Q(t) - (1-\eta_1)\gamma T(t) V_I(t) - (1-\eta_2)\beta T(t) T^*(t) - \rho T(t) - \mu_T T(t), \\ \dfrac{dT^*(t)}{dt} = (1-\eta_1)\gamma T(t) V_I(t) + (1-\eta_2)\beta T(t) T^*(t) - \mu_{T^*} T^*(t), \\ \dfrac{dV_I(t)}{dt} = \omega \mu_{T^*} \pi T^*(t) - \mu_V V_I(t), \\ \dfrac{dV_{NI}(t)}{dt} = (1-\omega)\mu_{T*} \pi T^*(t) - \mu_V V_{NI}(t), \end{cases} \tag{2}$$

where $t > 0$ is the time. λ is the rate at which new quiescent cells are produced. The death rates of quiescent cells, healthy cells, infected cells and virus are denoted by $\mu_Q, \mu_T, \mu_{T^*}, \mu_V$, respectively. As in model (1), we denote by α the activation rate of Q cells and by ρ the rate of reversion to the quiescent state. β denotes the rate of transmission of the infection by cell-to-cell mode. π is the number of virions produced per one infected cell.

From a mathematical point of view, the use of RTIs will reduce the force of transmission of infection via cell-free and cell-to-cell channels through the parameters η_1 and η_2 which represent the drug effectiveness for both cell-free and cell-to-cell infections, respectively.

In Section 2, we compute the basic reproduction number R_0 of model (2) and we find that R_0 is the sum of the basic reproduction number R_{01} determined by cell-free virus infection and that determined by cell-to-cell infection R_{02}. Further, the local and global stability analysis of both free and endemic steady states is given in terms of R_0. In Section 3, we introduce a delay τ in model (2), which represents the incubation period of the infection. We give the local and global stability analysis of the delay model for both free and endemic steady states. In Section 4, we give some numerical simulations and determine the region of eradication of the infection with respect to the effectiveness of the RTIs drugs. Our simulation results demonstrate that the delay has no effect on the quiescent cells Q but reduces the peak of the viral load and expands the eradication region of the infection. Further, we find that the cell-to-cell infection is less sensitive to RTI drugs than the cell-free one, which allows us to think that cell-to-cell spread is probably an important factor which leads to therapy failure and contributes to the persistence of the viral load. Finally, we end the paper by a conclusion.

2 The ODE Model

2.1 Local stability of equilibria

Since the four first equations in system (2) do not depend on the last equation, the system can be reduced to the following one:

$$\begin{cases} \dfrac{dQ(t)}{dt} = \lambda + \rho T(t) - \alpha Q(t) - \mu_Q Q(t), \\ \dfrac{dT(t)}{dt} = \alpha Q(t) - (1-\eta_1)\gamma T(t)V_I(t) - \beta(1-\eta_2)T(t)T^*(t) - \rho T(t) - \mu_T T(t), \\ \dfrac{dT^*(t)}{dt} = (1-\eta_1)\gamma T(t)V_I(t) + \beta(1-\eta_2)T(t)T^*(t) - \mu_{T^*}T^*(t), \\ \dfrac{dV_I(t)}{dt} = \omega\mu_{T^*}\pi T^*(t) - \mu_V V_I(t). \end{cases} \tag{3}$$

We can see that system (3) has one free steady state $E_0 = (Q_0, T_0, 0, 0)$ given by

$$Q_0 = \frac{\lambda(\rho+\mu_T)}{\alpha\mu_T + \rho\mu_Q + \mu_Q\mu_T}, \quad T_0 = \frac{\alpha\lambda}{\alpha\mu_T + \rho\mu_Q + \mu_Q\mu_T}.$$

First, we compute the basic reproduction number R_0 of model (3) by using the method of the next-generation matrix [9]. Therefore

$$R_0 = R_{01} + R_{02},$$

where $R_{01} = \frac{\omega\pi(1-\eta_1)\gamma T_0}{\mu_V}$ and $R_{02} = \frac{\beta(1-\eta_2)T_0}{\mu_{T^*}}$ are the basic reproduction numbers corresponding to virus-to-cell infection and cell-to-cell transmission, respectively.

Clearly, if $R_0 > 1$, then system (3) has one positive endemic equilibrium $\overline{E} = \left(\overline{Q}, \overline{T}, \overline{T^*}, \overline{V_I}\right)$ with

$$\begin{aligned}
\overline{Q} &= \frac{\lambda\left((1-\eta_1)\,\gamma\omega\pi\mu_{T^*} + \beta(1-\eta_2)\mu_V\right) + \rho\mu_V\mu_{T^*}}{(\alpha+\mu_Q)\left((1-\eta_1)\,\gamma\omega\pi\mu_{T^*} + \beta(1-\eta_2)\mu_V\right)},\\
\overline{T} &= \frac{\mu_V\mu_{T^*}}{\left((1-\eta_1)\,\gamma\omega\pi\mu_{T^*} + \beta(1-\eta_2)\mu_V\right)},\\
\overline{T^*} &= \frac{\alpha\lambda}{\mu_{T^*}\,(\alpha+\mu_Q)}\left(1-\frac{1}{R_0}\right), \quad \overline{V_I} = \frac{\alpha\lambda\omega\pi}{\mu_V\,(\alpha+\mu_Q)}\left(1-\frac{1}{R_0}\right).
\end{aligned}$$

The characteristic equation of system (3) around (Q, T, T^*, V_I) is given by

$$\begin{aligned}
P(\zeta) = \quad & (\zeta+\alpha+\mu_Q)\left[(\zeta+(1-\eta_1)\,\gamma V_I + \beta(1-\eta_2)T^* + \rho + \mu_T)\right.\\
& \times\left\{(\zeta-\beta(1-\eta_2)T+\mu_{T^*})\,(\zeta+\mu_V) - \omega\pi\mu_{T^*}\,(1-\eta_1)\,\gamma T\right\}\\
& +\beta(1-\eta_2)T\,(\zeta+\mu_V)\left((1-\eta_1)\,\gamma V_I + \beta(1-\eta_2)T^*\right)\\
& \left.+\omega\pi\mu_{T^*}\,(1-\eta_1)\,\gamma T\left((1-\eta_1)\,\gamma V_I + \beta(1-\eta_2)T^*\right)\right]\\
& -\alpha\rho\left\{(\zeta-\beta(1-\eta_2)T+\mu_{T^*})\,(\zeta+\mu_V) - \omega\pi\mu_{T^*}\,(1-\eta_1)\,\gamma T\right\}.
\end{aligned} \tag{4}$$

Theorem 2.1

(i) If $R_0 < 1$, then the free equilibrium E_0 is locally asymptotically stable.

(ii) If $R_0 > 1$, then E_0 is unstable.

Proof. The characteristic polynomial $P(\zeta)$ at $E_0 = (Q_0, T_0, 0, 0)$ takes the form

$$\begin{aligned}
P(\zeta) = &\left\{\zeta^2 + (\alpha+\mu_Q+\rho+\mu_T)\,\zeta + \alpha\mu_T + \rho\mu_Q + \mu_Q\mu_T\right\}\\
&\times\left\{\zeta^2 + \mu_{T^*}\left(\frac{\mu_V}{\mu_{T^*}} + 1 - \frac{\beta(1-\eta_2)T_0}{\mu_{T^*}}\right)\zeta + \mu_V\mu_{T^*}\,(1-R_0)\right\}.
\end{aligned} \tag{5}$$

If $R_0 < 1$, we have $\left(1 - \frac{\beta(1-\eta_2)T_0}{\mu_{T^*}}\right) \geq (1-R_0) > 0$. Then all the coefficients of the two polynomials are positive, and by the Routh-Hurwitz theorem, we conclude that all roots of (5) have negative real parts. Hence E_0 is locally asymptotically stable.
If $R_0 > 1$, since

$$P(0) = \mu_V\mu_{T^*}\left((\alpha+\mu_Q)\mu_T + \rho\mu_Q\right)(1-R_0) < 0,$$

further $P(\zeta) \to +\infty$ as $\zeta \to +\infty$, by continuity, we conclude that P has at least one positive real root. Thus E_0 is unstable. We now turn to prove the local stability of the endemic equilibrium $\overline{E}$.

Theorem 2.2 *Assume that*

$$(1-\eta_1)\gamma\omega\pi\mu_{T^*} + \beta(1-\eta_2)\mu_V > \beta\mu_{T^*}.$$

Then if $R_0 > 1$, the endemic equilibrium $\overline{E} = \left(\overline{Q}, \overline{T}, \overline{T^*}, \overline{V_I}\right)$ is locally asymptotically stable.

Proof. The characteristic polynomial $P(\zeta)$ at $\overline{E} = \left(\overline{Q}, \overline{T}, \overline{T}^*, \overline{V_I}\right)$ has the form

$$P(\zeta) = \zeta^4 + a_1\zeta^3 + a_2\zeta^2 + a_3\zeta + a_4,$$

where

$$
\begin{aligned}
a_1 = {} & \left[\alpha+\mu_Q+\rho+\mu_T+\left(\frac{\alpha\lambda\omega\pi\left(1-\eta_1\right)\gamma\mu_{T^*}+\alpha\lambda\beta(1-\eta_2)\mu_V}{\mu_{T^*}\mu_V\left(\alpha+\mu_Q\right)}\right)\times\right.\\
& \left.\left(1-\frac{1}{R_0}\right)\right]+\left[\left(\mu_{T^*}+\mu_V-\beta\frac{\mu_{T^*}\mu_V}{\left(1-\eta_1\right)\gamma\omega\pi\mu_{T^*}+\beta(1-\eta_2)\mu_V}\right)\right],\\
a_2 = {} & \left[\left(\frac{\alpha\lambda\omega\pi\left(1-\eta_1\right)\gamma\mu_{T^*}+\alpha\lambda\beta(1-\eta_2)\mu_V}{\mu_V\mu_{T^*}}\right)\left(1-\frac{1}{R_0}\right)+\mu_T\left(\alpha+\mu_Q\right)+\rho\mu_Q\right]\\
& +\left[\mu_{T^*}+\mu_V-\beta(1-\eta_2)\frac{\mu_{T^*}\mu_V}{\left(1-\eta_1\right)\gamma\omega\pi\mu_{T^*}+\beta(1-\eta_2)\mu_V}\right]\\
& \times\left[\alpha+\mu_Q+\rho+\mu_T+\left(\frac{\alpha\lambda\omega\pi\left(1-\eta_1\right)\gamma\mu_{T^*}+\alpha\lambda\beta(1-\eta_2)\mu_V}{\mu_{T^*}\mu_V\left(\alpha+\mu_Q\right)}\right)\right.\\
& \left.\times\left(1-\frac{1}{R_0}\right)+\frac{\alpha\lambda\beta(1-\eta_2)}{\left(\alpha+\mu_Q\right)}\left(1-\frac{1}{R_0}\right)\right],\\
a_3 = {} & \left[\mu_{T^*}+\mu_V-\beta(1-\eta_2)\frac{\mu_{T^*}\mu_V}{\left(1-\eta_1\right)\gamma\omega\pi\mu_{T^*}+\beta(1-\eta_2)\mu_V}\right]\\
& \times\left[\left(\frac{\alpha\lambda\omega\pi\left(1-\eta_1\right)\gamma\mu_{T^*}+\alpha\lambda\beta(1-\eta_2)\mu_V}{\mu_{T^*}\mu_V}\right)\left(1-\frac{1}{R_0}\right)+\mu_T\left(\alpha+\mu_Q\right)+\rho\mu_Q\right]\\
& +\left[\left(\frac{\alpha\lambda\omega\pi\left(1-\eta_1\right)\gamma\mu_{T^*}+\alpha\lambda\beta(1-\eta_2)\mu_V+\alpha^2\lambda\beta(1-\eta_2)+\alpha\lambda\beta(1-\eta_2)\mu_Q}{\left(\alpha+\mu_Q\right)}\right)\times\right.\\
& \left.\left(1-\frac{1}{R_0}\right)\right],\\
a_4 = {} & \left(\alpha\lambda\omega\pi\left(1-\eta_1\right)\gamma\mu_{T^*}+\alpha\lambda\beta(1-\eta_2)\mu_V\right)\left(1-\frac{1}{R_0}\right).
\end{aligned}
$$

We prove that

$$\Delta_i > 0, \qquad i = 1, 2, 3, 4,$$

where

$$\Delta_1 = a_1, \Delta_2 = a_1a_2 - a_3, \Delta_3 = a_3\Delta_2 - a_1^2a_4, \Delta_4 = a_4\Delta_3.$$

Thus, by the Routh-Hurwicz theorem, $\overline{E}$ is locally asymptotically stable.

2.2 Global dynamics of the model

In this section, we focus our attention on the global stability of both free and endemic steady states of system (3). We first prove the existence of a compact absorbing set for system (3). Define the set

$$G = \left\{(Q, T, T^*, V_I) \in \mathbb{R}_+^4 : Q + T + T^* \leq \frac{\lambda}{\mu} \text{ and } V_I \leq \frac{\lambda\omega\pi\mu_{T^*}}{\mu\mu_V}\right\},$$

where $\mu = \min\left(\mu_Q, \mu_T, \mu_{T^*}\right)$.

Proposition 2.1 *For any positive solution $\left(Q\left(t\right), T\left(t\right), T^*\left(t\right), V_I\left(t\right)\right)$ of system (3), we have*

(i) $\limsup\limits_{t\to+\infty} F\left(t\right) \leq \dfrac{\lambda}{\mu}, \limsup\limits_{t\to+\infty} V_I\left(t\right) \leq \dfrac{\lambda\omega\pi\mu_{T^*}}{\mu\mu_V}$, *where* $F\left(t\right) = Q\left(t\right) + T\left(t\right) + T^*\left(t\right)$.

(ii) $\liminf_{t\to+\infty} Q(t) \geq m_1, \liminf_{t\to+\infty} T(t) \geq m_2,$ *where*

$$m_1 = \frac{\lambda}{\alpha+\mu_Q}, \quad m_2 = \frac{\alpha\lambda}{(\alpha+\mu_Q)\left((1-\eta_1)\gamma\frac{\lambda\omega\pi\mu_{T^*}}{\mu\mu_V} + \frac{\lambda}{\mu} + \rho + \mu_T\right)}.$$

We now turn to prove the global stability of the free steady state E_0.

Theorem 2.3 *If $R_0 < 1$, then the free steady state E_0 is globally asymptotically stable.*

Proof. We first prove that the set

$$B = \left\{(\phi,\psi,\theta,\xi) \in \mathbb{R}_+^4 : \phi \leq Q_0, \psi \leq T_0\right\}$$

is positively invariant for the system (3). Let $(Q(t), T(t), T^*(t), V_I(t))$ be a positive solution of system (3). As we have

$$\begin{aligned}\frac{dQ}{dt} &= \lambda + \rho T - \alpha Q - \mu_Q Q,\\ \frac{dT}{dt} &\leq \alpha Q - \rho T - \mu_T T.\end{aligned}$$

Define the linear cooperative system

$$\begin{aligned}\frac{d\widetilde{Q}}{dt} &= \lambda + \rho\widetilde{T} - \alpha\widetilde{Q} - \mu_Q\widetilde{Q},\\ \frac{d\widetilde{T}}{dt} &= \alpha\widetilde{Q} - \rho\widetilde{T} - \mu_T\widetilde{T}.\end{aligned} \tag{6}$$

By the comparison principle, we have

$$Q(t) \leq \widetilde{Q}(t), \quad T(t) \leq \widetilde{T}(t) \tag{7}$$

for all $t > 0$. Further, since (6) is cooperative, it follows that $\widetilde{Q}(t) \leq Q_0$ and $\widetilde{T}(t) \leq T_0$ for all solution $(\widetilde{Q},\widetilde{T})$ of system (6) such that $\widetilde{Q}(0) \leq Q_0$ and $\widetilde{T}(0) \leq T_0$. By inequality (7), we conclude that

$$Q(t) \leq Q_0, \quad T(t) \leq T_0$$

for all $t > 0$ such that $Q(0) \leq Q_0$ and $T(0) \leq T_0$. Define now the function

$$\varpi(t) = T^* + \frac{(1-\eta_1)\gamma}{\mu_V} T_0 V_I.$$

Since $R_0 < 1$, the derivative of ϖ along the trajectories of (3) gives

$$\begin{aligned}\frac{d\varpi}{dt} &= (1-\eta_1)\gamma T V_I + \beta(1-\eta_2)TT^* - \mu_{T^*}T^*(t) + \frac{\omega\pi(1-\eta_1)\gamma\mu_{T^*}}{\mu_V}T_0T^*\\ &\quad - (1-\eta_1)\gamma T_0 V_I\\ &\leq \beta(1-\eta_2)T_0T^* - \mu_{T^*}T^*(t) + \frac{\omega\pi(1-\eta_1)\gamma\mu_{T^*}}{\mu_V}T_0T^*\\ &= \mu_{T^*}(R_0-1)T^* < 0,\end{aligned} \tag{8}$$

ϖ is then a Lyapunov function on B. Define now the following set:

$$E = \left\{ (\phi, \psi, \theta, \xi) \in B : \frac{d\varpi}{dt} (\phi, \psi, \theta, \xi) = 0 \right\},$$

and denote by M the largest set in E which is invariant with respect to system (3). It is clear that $(Q_0, T_0, 0, 0) \in M$, and thus M is not empty. Let $(\phi, \psi, \theta, \xi) \in M$ and denote by $(Q(t), T(t), T^*(t), V_I(t))$ the corresponding solution. By the invariance of M, $\frac{d\varpi}{dt} = 0$, and by (8), $T^*(t) = 0$ for all $t > 0$. The fourth equation of (3) implies then that $V_I(t) \to 0$ as $t \to +\infty$ and hence $Q(t) \to Q_0$, $T(t) \to T_0$ as $t \to +\infty$. Now, by the invariance of M, $Q(t) = Q_0$, $T(t) = T_0$. Therefore, $M = \{E_0\}$. Finally, since E_0 is locally asymptotically stable, the LaSalle invariance principle [10] implies that E_0 is globally asymptotically stable. To prove the global stability of the endemic steady state $\overline{E}$, we use the method of the Lyapunov function. To this end, we define

$$\begin{aligned}
A &= \alpha Q_0 > 0, \\
B &= \rho \overline{T} \frac{\overline{Q}}{m_1} - \rho m_2 \frac{\overline{Q}}{Q_0} - \alpha m_1 - \mu_T m_2 + \beta(1-\eta_2) M_1 \overline{T} + \mu_T \overline{T} + \frac{\alpha\lambda}{(\alpha + \mu_Q)} + \\
&\quad + \frac{\alpha\lambda\omega\pi (1-\eta_1) \gamma \overline{T}^2}{m_2 \mu_V (\alpha + \mu_Q)}, \\
C &= -\frac{\alpha\lambda}{(\alpha+\mu_Q)} - \frac{\alpha\lambda\omega\pi (1-\eta_1) \gamma \overline{T}^2}{m_2 \mu_V (\alpha + \mu_Q)} < 0.
\end{aligned}$$

Theorem 2.4 *Assume that $R_0 > 1$. Then $\overline{E} = \left(\overline{Q}, \overline{T}, \overline{T^*}, \overline{V_I}\right)$ is globally asymptotically stable if*

$$\frac{-B - \sqrt{B^2 - 4AC}}{2A} \le R_0 \le \frac{-B + \sqrt{B^2 - 4AC}}{2A}.$$

Proof. Define the Lyapunov function as

$$\begin{aligned}
L = &\left(Q - \overline{Q} - \overline{Q} \ln \frac{Q}{\overline{Q}} \right) + \left(T - \overline{T} - \overline{T} \ln \frac{T}{\overline{T}} \right) \\
&+ \left(T^* - \overline{T^*} - \overline{T}^* \ln \frac{T^*}{\overline{T^*}} \right) + \frac{(1-\eta_1)\gamma}{\mu_V} \overline{T} \left(V_I - \overline{V}_I - \overline{V}_I \ln \frac{V_I}{\overline{V}_I} \right).
\end{aligned}$$

It follows from system (3) that

$$\begin{aligned}
\dot{L} &= \dot{Q} \left(1 - \frac{\overline{Q}}{Q} \right) + \dot{T} \left(1 - \frac{\overline{T}}{T} \right) + \dot{T^*} \left(1 - \frac{\overline{T}^*}{T^*} \right) + \frac{(1-\eta_1)\gamma}{\mu_V} \overline{T} \dot{V_I} \left(1 - \frac{\overline{V_I}}{V_I} \right) \\
&= (\lambda + \rho T - \alpha Q - \mu_Q Q) \left(1 - \frac{\overline{Q}}{Q} \right) + (\alpha Q - (1-\eta_1)\gamma T V_I - \beta(1-\eta_2) T T^* \\
&\quad - \rho T - \mu_T T) \left(1 - \frac{\overline{T}}{T} \right) + ((1-\eta_1)\gamma T V_I + \beta(1-\eta_2) T T^* - \mu_{T^*} T^*) \\
&\quad \left(1 - \frac{\overline{T^*}}{T^*} \right) + \frac{(1-\eta_1)\gamma}{\mu_V} \overline{T} (\omega \mu_{T^*} \pi T^* - \mu_V V_I) \left(1 - \frac{\overline{V_I}}{V_I} \right),
\end{aligned} \tag{9}$$

as

$$\lambda = (\alpha + \mu_Q) \overline{Q} - \rho \overline{T},$$

since $\overline{E}$ is a steady state of system (3) and $\mu_{T^*}\overline{T^*} = \dfrac{\mu_V}{\omega\pi}V_I$, and $\overline{T} = \dfrac{\mu_V\mu_{T^*}}{(1-\eta)\gamma\omega\pi\mu_{T^*}+\mu_V\beta}$, we obtain from the precedent equation that

$$
\begin{aligned}
\dot{L} \;=\;& -(\alpha+\mu_Q)\,Q\left(1-\frac{\overline{Q}}{Q}\right)^2+\alpha Q\left(2-\frac{\overline{T}}{T}-\frac{T}{\overline{T}}\right)\\
&+\left(\frac{(1-\eta_1)\,\gamma\omega\pi\mu_{T^*}}{(1-\eta_1)\,\gamma\omega\pi\mu_{T^*}+\mu_V\beta(1-\eta_2)}-1\right)\mu_{T^*}T^*+(1-\eta_1)\,\gamma\overline{TV_I}\\
&\left(3-\frac{TV_I\overline{T^*}}{\overline{TV_I}T^*}-\frac{T^*\overline{V_I}}{\overline{T^*}V_I}-\frac{\overline{T}}{T}\right)+\rho\overline{T}\frac{\overline{Q}}{Q}-\rho T\frac{\overline{Q}}{Q}\\
&-\alpha Q+\alpha Q\frac{T}{\overline{T}}-\mu_T T+\beta(1-\eta_2)\overline{T}T^*+\mu_T\overline{T}-\beta(1-\eta_2)T\overline{T^*}+\mu_{T^*}\overline{T^*}\\
&-2\,(1-\eta_1)\,\gamma\overline{TV_I}+(1-\eta_1)\,\gamma\overline{TV_I}\tfrac{T}{\overline{T}}.
\end{aligned}
\tag{10}
$$

As

$$
2-\frac{\overline{T}}{T}-\frac{T}{\overline{T}}\le 0,\quad 3-\frac{TV_I\overline{T^*}}{\overline{TV_I}T^*}-\frac{T^*\overline{V_I}}{\overline{T^*}V_I}-\frac{\overline{T}}{T}\le 0,
$$

we obtain

$$
\begin{aligned}
\dot{L} \;\le\;& \rho\overline{T}\frac{\overline{Q}}{Q}-\rho T\frac{\overline{Q}}{Q}-\alpha Q+\alpha Q\frac{T}{\overline{T}}-\mu_T T+\beta(1-\eta_2)\overline{T}T^*+\mu_T\overline{T}\\
&-\beta(1-\eta_2)T\overline{T^*}+\mu_{T^*}\overline{T^*}-2\,(1-\eta_1)\,\gamma\overline{TV_I}+(1-\eta_1)\,\gamma\overline{TV_I}\frac{T}{\overline{T}}.
\end{aligned}
\tag{11}
$$

Let $\epsilon>0$ be chosen later. Proposition 2.1 implies that there is $T_\epsilon>0$ such that

$$
\begin{array}{c}
m_1^\epsilon=m_1-\epsilon\le Q\,(t)\le Q_0+\epsilon=Q_0^\epsilon,\\
m_2^\epsilon=m_2-\epsilon\le T\,(t)\le T_0+\epsilon=T_0^\epsilon,\\
T^*\,(t)\le M_1+\epsilon=M_1^\epsilon,\quad t\ge T_\epsilon.
\end{array}
\tag{12}
$$

By (11) and (12), we obtain

$$
\begin{aligned}
\dot{L} \;\le\;& \rho\overline{T}\frac{\overline{Q}}{m_1^\epsilon}-\rho m_2^\epsilon\frac{\overline{Q}}{Q_0^\epsilon}-\alpha m_1^\epsilon+\alpha Q_0^\epsilon\frac{T_0^\epsilon}{\overline{T}}-\mu_T m_2^\epsilon\\
&+\beta(1-\eta_2)M_1^\epsilon\overline{T}+\mu_T\overline{T}+\mu_{T^*}\overline{T^*}+\frac{1}{m_2^\epsilon}\,(1-\eta_1)\,\gamma\overline{T}^2\overline{V_I}.
\end{aligned}
\tag{13}
$$

Since $\dfrac{T_0}{\overline{T}}=R_0$ and $(1-\eta_1)\,\gamma\overline{TV_I}=\dfrac{(1-\eta)\,\alpha\lambda\omega\pi\gamma}{\mu_V\,(\alpha+\mu_Q)}\overline{T}\left(1-\dfrac{1}{R_0}\right)$, we can derive from (13) that

$$
\begin{aligned}
\dot{L} \;\le\;& \rho\overline{T}\frac{\overline{Q}}{m_1^\epsilon}-\rho m_2^\epsilon\frac{\overline{Q}}{Q_0^\epsilon}-\alpha m_1^\epsilon+\alpha Q_0^\epsilon\left(R_0+\frac{\epsilon}{\overline{T}}\right)-\mu_T m_2^\epsilon+(1-\eta_2)\,\beta M_1^\epsilon\overline{T}\\
&+\mu_T\overline{T}+\frac{\alpha\lambda}{(\alpha+\mu_Q)}\left(1-\frac{1}{R_0}\right)+\frac{\alpha\lambda\omega\pi\,(1-\eta_1)\,\gamma\overline{T^2}}{m_2^\epsilon\mu_V\,(\alpha+\mu_Q)}\left(1-\frac{1}{R_0}\right)\\
\le\;& \tfrac{1}{R_0}\left[\alpha Q_0^\epsilon R_0\left(R_0+\frac{\epsilon}{\overline{T}}\right)+\left(\rho\overline{T}\frac{\overline{Q}}{m_1^\epsilon}-\rho m_2^\epsilon\frac{\overline{Q}}{Q_0^\epsilon}-\alpha m_1^\epsilon-\mu_T m_2^\epsilon+(1-\eta_2)\,\beta M_1^\epsilon\overline{T}\right.\right.\\
&\left.\left.+\mu_T\overline{T}+\frac{\alpha\lambda}{(\alpha+\mu_Q)}+\frac{\alpha\lambda\omega\pi\,(1-\eta_1)\,\gamma\overline{T^2}}{m_2^\epsilon\mu_V\,(\alpha+\mu_Q)}\right)R_0-\frac{\alpha\lambda}{(\alpha+\mu_Q)}-\frac{\alpha\lambda\omega\pi\,(1-\eta_1)\,\gamma\overline{T^2}}{m_2^\epsilon\mu_V\,(\alpha+\mu_Q)}\right].
\end{aligned}
$$

By the hypothesis of Theorem 2.4, we have $AR_0^2 + BR_0 + C < 0$. Then we can choose $\epsilon > 0$ small enough so that

$$\dot{L} \leq 0$$

for $t \geq T_\epsilon$. Further, by (10), $\dot{L} = 0$ if and only if $Q = \overline{Q}$, $T = \overline{T}$, $T^* = \overline{T^*}$, $V_I = \overline{V_I}$, the LaSalle invariance principle [10] implies that $\overline{E}$ is globally asymptotically stable.

3 The Delay Model

To take into account the incubation period of the infection, we modify, in this section, the model (3) by introducing a discrete delay τ by assuming that cells become infected τ times after initial infection. To this end, we propose the following system:

$$\begin{cases} \dfrac{dQ(t)}{dt} &= \lambda + \rho T(t) - \alpha Q(t) - \mu_Q Q(t), \\ \dfrac{dT(t)}{dt} &= \alpha Q(t) - (1-\eta_1)\gamma T(t) V_I(t) - \beta(1-\eta_2) T(t) T^*(t) - \rho T(t) - \mu_T T(t), \\ \dfrac{dT^*(t)}{dt} &= e^{-\tau m}(1-\eta_1)\gamma T(t-\tau) V_I(t-\tau) + e^{-\tau m}\beta(1-\eta_2) T(t-\tau) T^*(t-\tau) \\ & \quad -\mu_{T^*} T^*(t), \\ \dfrac{dV_I(t)}{dt} &= \omega \mu_{T^*} \pi T^*(t) - \mu_V V_I(t) \end{cases} \tag{14}$$

with the initial conditions

$$\begin{aligned} &Q(\theta) = \phi_1(\theta), \quad T(\theta) = \phi_2(\theta), \quad T^*(\theta) = \phi_3(\theta), \\ &V_I(\theta) = \phi_4(\theta), \quad \theta \in [-\tau, 0], \end{aligned} \tag{15}$$

where $\phi_i \in C([-\tau, 0], \mathbb{R}_+)$ with $\phi_i(0) > 0$, $i = 1, 2, 3, 4$. It is well known by the theory of functional differential equations [11] that system (14)-(15) has a unique positive solution $(Q(t), T(t), T^*(t), V_I(t))$ defined for all $t > 0$. As in the ODE model, it is easy to see that system (14) has one free steady state $E_0 = (Q_0, T_0, 0, 0)$,

$$Q_0 = \frac{\lambda(\rho + \mu_T)}{\alpha\mu_T + \rho\mu_Q + \mu_Q\mu_T}, \qquad T_0 = \frac{\alpha\lambda}{\alpha\mu_T + \rho\mu_Q + \mu_Q\mu_T}.$$

The basic reproduction number is then given by (see [12])

$$R_0 = \frac{\beta(1-\eta_2)\mu_V e^{-\tau m} + \omega\pi\mu_{T^*}(1-\eta_1)\gamma e^{-m\tau}}{\mu_{T^*}\mu_V} T_0. \tag{16}$$

If $R_0 > 1$, system (14) has the endemic steady state $\overline{E} = \left(\overline{Q}, \overline{T}, \overline{T^*}, \overline{V_I}\right)$ given by

$$\begin{aligned} \overline{Q} &= \frac{\lambda\left(\omega\pi\mu_{T^*}(1-\eta_1)\gamma e^{-\tau m} + \beta(1-\eta_2)\mu_V e^{-\tau m}\right) + \rho\mu_{T^*}\mu_V}{(\alpha + \mu_Q)\left(\omega\pi\mu_{T^*}(1-\eta_1)\gamma e^{-\tau m} + \beta(1-\eta_2)\mu_V e^{-\tau m}\right)}, \\ \overline{T} &= \frac{\mu_{T^*}\mu_V}{\omega\pi\mu_{T^*}(1-\eta_1)\gamma e^{-\tau m} + \beta(1-\eta_2)\mu_V e^{-\tau m}}, \\ \overline{T^*} &= \frac{\alpha\lambda e^{-\tau m}}{\mu_{T^*}(\alpha + \mu_Q)}\left(1 - \frac{1}{R_0}\right), \quad \overline{V_I} = \frac{\alpha\lambda\omega\pi e^{-\tau m}}{\mu_V(\alpha + \mu_Q)}\left(1 - \frac{1}{R_0}\right). \end{aligned} \tag{17}$$

3.1 Local stability of equilibria

3.1.1 Local stability of the free equilibrium

The characteristic equation of system (14) around $E = (Q, T, T^*, V_I)$ is

$$\begin{array}{rcl} P(\zeta) & = & [(\zeta+\alpha+\mu_Q)(\zeta+(1-\eta_1)\gamma V_I+\beta(1-\eta_2)T^*+\rho+\mu_T)-\alpha\rho] \\ & & \times\left[\left(\zeta-\beta(1-\eta_2)Te^{-\tau m}e^{-\zeta\tau}+\mu_{T^*}\right)(\zeta+\mu_V)-\omega\pi\mu_{T^*}(1-\eta_1)\gamma Te^{-\tau m}e^{-\zeta\tau}\right] \\ & & +(\zeta+\alpha+\mu_Q)\left\{\beta(1-\eta_2)T\left((1-\eta_1)\gamma V_I e^{-m\tau}e^{-\zeta\tau}+\beta(1-\eta_2)T^*e^{-\tau m}e^{-\zeta\tau}\right)\right. \\ & & \left.(\zeta+\mu_V)+\omega\pi\mu_{T^*}(1-\eta_1)\gamma T\left((1-\eta_1)\gamma V_I e^{-m\tau}e^{-\zeta\tau}+\beta(1-\eta_2)T^*e^{-\tau m}e^{-\zeta\tau}\right)\right\}. \end{array} \tag{18}$$

Theorem 3.1 *1. If $R_0 < 1$, the free steady state E_0 is locally asymptotically stable for all $\tau \geq 0$.*

2. If $R_0 > 1$, E_0 is unstable for all $\tau \geq 0$.

Proof. At $E_0 = (Q_0, T_0, 0, 0)$, the characteristic equation (18) takes the form

$$\begin{array}{rcl} P(\zeta) & = & \left[\zeta^2+(\alpha+\mu_Q+\rho+\mu_T)\zeta+\alpha\mu_T+\rho\mu_Q+\mu_Q\mu_T\right]\times \\ & & \left[\left(\zeta-\beta(1-\eta_2)T_0e^{-\tau m}e^{-\zeta\tau}+\mu_{T^*}\right)(\zeta+\mu_V)-\omega\pi\mu_{T^*}(1-\eta_1)\gamma T_0e^{-\tau m}e^{-\zeta\tau}\right] \\ & = & 0. \end{array}$$

All the coefficients of the polynomial

$$\zeta^2+(\alpha+\mu_Q+\rho+\mu_T)\zeta+\alpha\mu_T+\rho\mu_Q+\mu_Q\mu_T = 0 \tag{19}$$

are positive, then by the Routh-Hurwitz theorem, we conclude that the equation (19) has two roots with negative real parts. The other roots are determined by the solutions of the quadratic polynomial

$$\zeta^2+\mu_{T^*}\left(\frac{\mu_V}{\mu_{T^*}}+1-\frac{\beta(1-\eta_2)\mu_V T_0 e^{-\tau m}}{\mu_{T^*}\mu_V}e^{-\zeta\tau}\right)\zeta+\mu_{T^*}\mu_V\left(1-R_0e^{-\zeta\tau}\right)=0. \tag{20}$$

Substituting $\tau = 0$ into equation (20), we obtain

$$\zeta^2+\mu_{T^*}\left(\frac{\mu_V}{\mu_{T^*}}+1-\frac{\beta(1-\eta_2)\mu_V T_0}{\mu_{T^*}\mu_V}\right)\zeta+\mu_{T^*}\mu_V(1-R_0)=0. \tag{21}$$

If $R_0 < 1$, all the coefficients of equation (21) are positive. Then equation (21) has two roots with negative real parts.

In the case $\tau > 0$, assume that the equation (20) has two purely imaginary roots $\zeta = ix(\tau)$ $(x > 0)$. Separating real and imaginary parts yields

$$\begin{array}{l} x\beta(1-\eta_2)T_0e^{-\tau m}\sin(x(\tau)\tau)+\mu_{T^*}\mu_V R_0\cos(x(\tau)\tau)=\mu_V\mu_{T^*}-x^2, \\ x\beta(1-\eta_2)T_0e^{-\tau m}\cos(x(\tau)\tau)-\mu_{T^*}\mu_V R_0\sin(x(\tau)\tau)=(\mu_V+\mu_{T^*})x. \end{array}$$

Squaring and adding the two equations give

$$x^4+\mu_{T^*}^2\left(\frac{\mu_V^2}{\mu_{T^*}^2}+1-\left(\frac{\beta(1-\eta_2)\mu_V T_0e^{-\tau m}}{\mu_V\mu_{T^*}}\right)^2\right)x^2+(\mu_V\mu_{T^*})^2\left(1-R_0^2\right)=0. \tag{22}$$

If $R_0 < 1$, then $1 - \left(\frac{\beta(1-\eta_2)\mu_V T_0 e^{-\tau m}}{\mu_V \mu_{T^*}}\right)^2 > \left(1 - R_0^2\right) > 0$, so equation (22) cannot have positive roots and equation (20) cannot have a purely imaginary root. By the general theory of delay differential equations, all roots of (20) have negative real parts provided that $R_0 < 1$ and E_0 is locally asymptotically stable for $\tau > 0$.

If $R_0 > 1$, let $f(\zeta) = \zeta^2 + \left(\mu_V + \mu_{T^*} - \beta(1-\eta_2)T_0 e^{-\tau m} e^{-\zeta\tau}\right)\zeta + \mu_{T^*}\mu_V\left(1 - R_0 e^{-\zeta\tau}\right)$. Since $f(0) = \mu_{T^*}\mu_V(1 - R_0) < 0$ and $f(\zeta) \to +\infty$ as $\zeta \to +\infty$, by continuity, we conclude that $f(\zeta) = 0$ has at least one positive real root. Thus E_0 is unstable.

3.1.2 Local stability of the endemic equilibrium

We now turn to prove the local stability of the endemic steady state $\overline{E}$. At $\overline{E}$, the characteristic equation (18) of system (14) is reduced to the following form:

$$P(\zeta) + Q(\zeta)e^{-\zeta\tau} = 0, \tag{23}$$

where

$$P(\zeta) = \zeta^4 + a_3\zeta^3 + a_2\zeta^2 + a_1\zeta + a_0, \qquad Q(\zeta) = b_3\zeta^3 + b_2\zeta^2 + b_1\zeta + b_0 \tag{24}$$

with

$$\begin{aligned}
a_3 = &\ \alpha + \mu_Q + \rho + \mu_T + \mu_{T^*} + \mu_V + \tfrac{\alpha\lambda(\omega\pi(1-\eta_1)\gamma\mu_{T^*} + \beta(1-\eta_2)\mu_V)e^{-\tau m}}{\mu_{T^*}\mu_V(\alpha+\mu_Q)}\left(1 - \tfrac{1}{R_0}\right),\\
a_2 = &\ \tfrac{\alpha\lambda(\omega\pi(1-\eta_1)\gamma\mu_{T^*} + \beta(1-\eta_2)\mu_V)e^{-\tau m}}{\mu_{T^*}\mu_V}\left(1 - \tfrac{1}{R_0}\right) + (\alpha+\mu_Q)\mu_T + \rho\mu_Q + \mu_{T^*}\mu_V\\
&+ \left(\alpha + \mu_Q + \rho + \mu_T + \tfrac{\alpha\lambda(\omega\pi(1-\eta_1)\gamma\mu_{T^*} + \beta(1-\eta_2)\mu_V)e^{-\tau m}}{\mu_{T^*}\mu_V(\alpha+\mu_Q)}\left(1 - \tfrac{1}{R_0}\right)\right)(\mu_{T^*} + \mu_V),\\
a_1 = &\ \left(\tfrac{\alpha\lambda(\omega\pi(1-\eta_1)\gamma\mu_{T^*} + \beta(1-\eta_2)\mu_V)e^{-\tau m}}{\mu_{T^*}\mu_V}\left(1 - \tfrac{1}{R_0}\right) + (\alpha+\mu_Q)\mu_T + \rho\mu_Q\right)(\mu_{T^*} + \mu_V)\\
&+ (\alpha + \mu_Q + \rho + \mu_T)\mu_{T^*}\mu_V + \tfrac{\alpha\lambda(\omega\pi(1-\eta_1)\gamma\mu_{T^*} + \beta(1-\eta_2)\mu_V)e^{-\tau m}}{(\alpha+\mu_Q)}\left(1 - \tfrac{1}{R_0}\right),\\
a_0 = &\ \alpha\lambda(\omega\pi(1-\eta_1)\gamma\mu_{T^*} + \beta(1-\eta_2)\mu_V)e^{-\tau m}\left(1 - \tfrac{1}{R_0}\right)\\
&+ ((\alpha+\mu_Q)\mu_T + \rho\mu_Q)\mu_{T^*}\mu_V,\\
b_3 = &\ -\tfrac{\beta(1-\eta_2)\mu_{T^*}\mu_V}{\omega\pi(1-\eta_1)\gamma\mu_{T^*} + \beta(1-\eta_2)\mu_V},\\
b_2 = &\ -\mu_{T^*}\mu_V - \tfrac{(\alpha+\mu_Q+\rho+\mu_T)\beta(1-\eta_2)\mu_{T^*}\mu_V}{\omega\pi(1-\eta_1)\gamma\mu_{T^*} + \beta(1-\eta_2)\mu_V},
\end{aligned} \tag{25}$$

$$\begin{aligned}
b_1 = &\ -(\alpha + \mu_Q + \rho + \mu_T)\mu_{T^*}\mu_V - \tfrac{((\alpha+\mu_Q)\mu_T + \rho\mu_Q)\beta(1-\eta_2)\mu_{T^*}\mu_V}{\omega\pi(1-\eta_1)\gamma\mu_{T^*} + \beta(1-\eta_2)\mu_V},\\
b_0 = &\ -((\alpha+\mu_Q)\mu_T + \rho\mu_Q)\mu_{T^*}\mu_V.
\end{aligned} \tag{26}$$

From Theorem 2.2, we know that if $R_0 > 1$ and $\tau = 0$, $\overline{E}$ is locally asymptotically stable. To investigate the stability of equation (23), we will apply the following version of the main theorem of Cooke and Van den Driessche [13].

Proposition 3.1 *Assume that P and Q are analytic functions in the right half-plane $Re(\zeta) > 0$ and satisfy the following conditions:*

1. *$P(\zeta)$ and $Q(\zeta)$ have no common imaginary roots;*
2. *$\overline{P(-iy)} = P(iy)$, $\overline{Q(-iy)} = Q(iy)$ for all $y \in \mathbb{R}$;*

3. $P(0) + Q(0) \neq 0$;
4. $\limsup\limits_{|\zeta| \longrightarrow \infty,\, Re(\zeta) \geq 0} (|Q(\zeta)/P(\zeta)|) < 1$;
5. $F(y) \equiv |P(iy)|^2 - |Q(iy)|^2$ *for the real* y *has at most a finite number of real roots.*

Then the following statements are true:

1. *If the equation* $F(\zeta) = 0$ *has no positive roots, then if (23) is stable at* $\tau = 0$*, it remains stable for all* $\tau \geq 0$*, whereas if it is unstable at* $\tau = 0$*, it remains unstable for all* $\tau \geq 0$.
2. *If the equation* $F(\zeta) = 0$ *has at least one positive root and each root is simple, in this case, as* τ *increases, stability switches may occur. There exists a positive number* τ^* *such that (23) is unstable for all* $\tau > \tau^*$*. As* τ *varies from* 0 *to* τ^**, at most a finite number of stability switches may occur.*

Theorem 3.2 *Under the hypothesis of Theorem 2.2, if* $R_0 > 1$*, the endemic steady state* $\overline{E}$ *is locally asymptotically stable for all* $\tau \geq 0$.

Proof. From Theorem 2.2, we know that if $R_0 > 1$, the infected equilibrium $\overline{E}$ is locally asymptotically stable for $\tau = 0$. To show the stability of the equilibrium $\overline{E}$, we need to analyze the existence of positive roots of the following equation:

$$F(\zeta) = y^8 + A_1 y^6 + A_2 y^4 + A_3 y^2 + A_4, \tag{27}$$

where

$$A_1 = a_3^2 - 2a_2 - b_3^2, \quad A_2 = a_2^2 + 2a_0 - 2a_3 a_1 - b_2^2 + 2b_3 b_1,$$
$$A_3 = a_1^2 - 2a_2 a_0 + 2b_2 b_0 - b_1^2, \quad A_4 = a_0^2 - b_0^2.$$

Clearly, equation (27) has no positive real roots if A_1, A_2, A_3 and A_4 are all positive. The coefficients of $F(\zeta)$ are non-negative. Thus equation (27) has no positive real roots. By Theorem 2.2 and Proposition 3.1, the endemic steady state $\overline{E}$ is locally asymptotically stable for all $\tau \geq 0$.

3.2 Global stability

3.2.1 Global stability of the free equilibrium

In this section, we focus our attention on the global stability of both free and endemic steady states of system (14). Define the set

$$G = \left\{ (Q, T, T^*, V_I) \in \mathbb{R}_+^4 : Q + T + T^* \leq \frac{\lambda e^{-\tau m}}{\mu} \quad \text{and} \quad V_I \leq \frac{\lambda \omega \pi \mu_{T^*} e^{-\tau m}}{\mu \mu_V} \right\},$$

where $\mu = \min(\mu_Q, \mu_T, \mu_{T^*})$. Arguing as in Proposition (2.1), we can prove the following result.

Proposition 3.2 *For any positive solution* $(Q(t), T(t), T^*(t), V_I(t))$ *of system (14), we have the following two assertions:*

1. $\limsup_{t \to +\infty} F(t) \leq M_1, \qquad \limsup_{t \to +\infty} V_I(t) \leq M_2,$

2. $\liminf\limits_{t\to+\infty} Q(t) \geq m_1, \liminf\limits_{t\to+\infty} T(t) \geq m_2,$ *where*

$$\begin{array}{l} F(t) = Q(t) + T(t) + e^{m\tau}T^*(t+\tau), M_1 = \frac{\lambda e^{-m\tau}}{\mu}, \\ M_2 = \frac{\lambda\omega\pi\mu_{T^*}e^{-m\tau}}{\mu\mu_V}, m_1 = \frac{\lambda}{\alpha+\mu_Q}, m_2 = \frac{\alpha m_1}{\beta M_1+(1-\eta)\gamma M_2+\rho+\mu_T}. \end{array} \tag{28}$$

We have the following stability result about E_0.

Theorem 3.3 *If $R_0 < 1$, then the free steady state E_0 of system (14) is globally asymptotically stable for all $\tau \geq 0$.*

Proof. Define the set

$$S = \left\{(\phi_1, \phi_2, \phi_3, \phi_4) \in C\left([-\tau, 0], \mathbb{R}_+^4\right) : \phi_1 \leq Q_0,\ \phi_2 \leq T_0\right\},$$

and let $(Q(t), T(t), T^*(t), V_I(t))$ be a positive solution of system (14). By the comparison principle,

$$Q(t) \leq Q_0, \quad T(t) \leq T_0$$

for all $t \geq 0$ such that $Q(0) \leq Q_0$ and $T(0) \leq T_0$. Thus S is a positively invariant set for system (14). Define the following Lyapunov function:

$$\begin{array}{rcl} U(t) & = & T^*(t) + \frac{(1-\eta_1)\gamma e^{-m\tau}}{\mu_V} T_0 V_I(t) \\ & & +(1-\eta_1)\gamma e^{-m\tau}\int_{t-\tau}^{t} T(s)V_I(s)ds + \beta(1-\eta_2)e^{-m\tau}\int_{t-\tau}^{t} T(s)T^*(s)ds. \end{array}$$

The derivatives of $U(t)$ along the trajectories of (14) give, since $R_0 < 1$,

$$\begin{array}{rcl} \frac{dU}{dt}(t) & = & -\mu_{T^*}T^*(t) + \frac{\omega\pi(1-\eta_1)\gamma\mu_{T^*}e^{-m\tau}}{\mu_V} T_0 T^*(t) - (1-\eta_1)\gamma e^{-m\tau} T_0 V_I(t) \\ & & +(1-\eta_1)\gamma e^{-m\tau}T(t)V_I(t) + \beta(1-\eta_2)e^{-m\tau}T(t)T^*(t) \\ & \leq & \beta(1-\eta_2)e^{-m\tau}T_0T^*(t) + \frac{\omega\pi(1-\eta_1)\gamma\mu_{T^*}e^{-m\tau}}{\mu_V} T_0 T^*(t) - \mu_{T^*}T^*(t) \\ & = & \mu_{T^*}(R_0 - 1)T^*(t) < 0. \end{array} \tag{29}$$

U is then a Lyapunov function. Define now the set

$$E = \left\{(\phi, \psi, \theta, \xi) \in S : \frac{dU}{dt}(\phi, \psi, \theta, \xi) = 0\right\},$$

and denote by M the largest set in E, which is invariant with respect to system (14). It is clear that $(Q_0, T_0, 0, 0) \in M$, M is not empty. Let $(\phi, \psi, \theta, \xi) \in M$ and denote by $(Q(t), T(t), T^*(t), V_I(t))$ the corresponding solution. By the invariance of M, $(Q(t), T(t), T^*(t), V_I(t) \in M$ for all $t > 0$, thus $\frac{dU}{dt} = 0$ and, by (29), $T^*(t) = 0$ for all $t > 0$. The last equation of (14) implies then that $V_I(t) \to 0$ as $t \to +\infty$ and hence $Q(t) \to Q_0$ and $T(t) \to T_0$ as $t \to +\infty$. Now, by the invariance of M, $Q(t) = Q_0$, $T(t) = T_0$ for all $t > 0$. Therefore

$$M = \{E_0 = (Q_0, T_0, 0, 0)\}.$$

Finally, since E_0 is locally asymptotically stable, by the LaSalle invariance principle, E_0 is globally asymptotically stable.

3.2.2 Global stability of the endemic equilibrium

The following theorem assures the global stability of the endemic steady state $\overline{E}$.

Theorem 3.4 *Assume that* $R_0 > 1$ *and let*

$$\begin{aligned} A =& \quad \alpha Q_0 > 0, \\ B =& \quad \rho\overline{T}\frac{\overline{Q}}{m_1^\epsilon} - \rho m_2^\epsilon\frac{\overline{Q}}{Q_0^\epsilon} - \alpha m_1^\epsilon - \mu_T m_2^\epsilon + \beta(1-\eta_2)M_1^\epsilon\overline{T} \\ & +\mu_T\overline{T} + \frac{\alpha\lambda}{\alpha+\mu_Q} + \frac{\alpha\lambda\omega\pi(1-\eta_1)\gamma e^{-\tau m}\overline{T}^2}{m_2^\epsilon\mu_V(\alpha+\mu_Q)} + \frac{\alpha\lambda\beta(1-\eta_2)e^{-\tau m}\overline{T}^2}{m_2^\epsilon\mu_{T^*}(\alpha+\mu_Q)}, \\ C =& \quad -\frac{\alpha\lambda}{\alpha+\mu_Q} - \frac{\alpha\lambda\omega\pi(1-\eta_1)\gamma e^{-\tau m}\overline{T}^2}{m_2^\epsilon\mu_V(\alpha+\mu_Q)} - \frac{\alpha\lambda\beta(1-\eta_2)e^{-\tau m}\overline{T}^2}{m_2^\epsilon\mu_{T^*}(\alpha+\mu_Q)} < 0. \end{aligned}$$

Then if

$$\frac{-B+\sqrt{B^2-4AC}}{2A} \leq R_0 \leq \frac{-B+\sqrt{B^2-4AC}}{2A},$$

the endemic steady state $\overline{E}$ *of system (14) is globally asymptotically stable for all* $\tau \geq 0$.

Proof. Define the Lyapunov function L as follows:

$$\begin{aligned} L(t) =& e^{-m\tau}\left(Q(t)-\overline{Q}-\overline{Q}\ln\frac{Q(t)}{\overline{Q}}\right) + e^{-m\tau}\left(T(t)-\overline{T}-\overline{T}\ln\frac{T(t)}{\overline{T}}\right) \\ & + \left(T^*(t)-\overline{T^*}-\overline{T^*}\ln\frac{T^*(t)}{\overline{T^*}}\right) + \frac{e^{-m\tau}(1-\eta_1)\gamma}{\mu_V}\overline{T}\left(V_I(t)-\overline{V_I}-\overline{V_I}\ln\frac{V_I(t)}{\overline{V_I}}\right) \\ & + (1-\eta_1)\gamma e^{-m\tau}\int_{t-\tau}^{t}\left[T(s)V_I(s)-\overline{TV_I}-\overline{TV_I}\ln\frac{T(s)V_I(s)}{\overline{TV_I}}\right]ds \\ & + \beta(1-\eta_2)e^{-\tau m}\int_{t-\tau}^{t}\left[T(s)T^*(s)-\overline{TT^*}-\overline{TT^*}\ln\frac{T(s)T^*(s)}{\overline{TT^*}}\right]. \end{aligned}$$

Then

$$\begin{aligned} \frac{dL(t)}{dt} =& e^{-m\tau}(\lambda+\rho T-\alpha Q-\mu_Q Q)\left(1-\frac{\overline{Q}}{Q}\right) \\ & + e^{-m\tau}\left(\alpha Q-(1-\eta_1)\gamma TV_I-\beta(1-\eta_2)TT^*-\rho T-\mu_T T\right)\left(1-\frac{\overline{T}}{T}\right) \\ & + \left((1-\eta_1)\gamma e^{-m\tau}T(t-\tau)V_I(t-\tau)+\beta(1-\eta_2)e^{-\tau m}T(t-\tau)T^*(t-\tau)-\mu_{T^*}T^*\right) \\ & \times\left(1-\frac{\overline{T^*}}{T^*}\right) + \frac{e^{-m\tau}(1-\eta_1)\gamma}{\mu_V}\overline{T}\left(\omega\mu_{T^*}\pi T^*-\mu_V V_I\right)\left(1-\frac{\overline{V_I}}{V_I}\right) \\ & +(1-\eta_1)\gamma e^{-m\tau}\left[TV_I-T(t-\tau)V_I(t-\tau)+\overline{TV_I}\ln\frac{T(t-\tau)V_I(t-\tau)}{TV_I}\right] \\ & + \beta(1-\eta_2)e^{-\tau m}\left[TT^*-T(t-\tau)T^*(t-\tau)+\overline{TT^*}\ln\frac{T(t-\tau)T^*(t-\tau)}{TT^*}\right]. \end{aligned}$$

Now $\lambda = (\alpha+\mu_Q)\overline{Q}-\rho\overline{T}$ and $2-\frac{\overline{T}}{T}-\frac{T}{\overline{T}} \leq 0$.

Let $\epsilon > 0$ be chosen later. By Proposition 3.2, there is $T_\epsilon > 0$ such that for all $t > T_\epsilon$ and from the hypotheses of the theorem, $AR_0^2+BR_0+C<0$. We can then choose $\epsilon > 0$

small enough so that

$$\frac{e^{-m\tau}}{R_0}\left[\alpha Q_0^{\epsilon} R_0\left(R_0+\frac{\epsilon}{\overline{T}}\right)+\left(\rho\overline{T}\frac{\overline{Q}}{m_1^{\epsilon}}-\rho m_2^{\epsilon}\frac{\overline{Q}}{Q_0^{\epsilon}}-\alpha m_1^{\epsilon}-\mu_T m_2^{\epsilon}+\beta(1-\eta_2)M_1^{\epsilon}\overline{T}\right.\right.$$
$$\left.+\mu_T\overline{T}+\frac{\alpha\lambda}{\alpha+\mu_Q}+\frac{\alpha\lambda\omega\pi(1-\eta_1)\gamma e^{-\tau m}\overline{T}^2}{m_2^{\epsilon}\mu_V\left(\alpha+\mu_Q\right)}+\frac{\alpha\lambda\beta(1-\eta_2)e^{-\tau m}\overline{T}^2}{m_2^{\epsilon}\mu_{T^*}\left(\alpha+\mu_Q\right)}\right)R_0$$
$$\left.-\frac{\alpha\lambda}{\alpha+\mu_Q}-\frac{\alpha\lambda\omega\pi(1-\eta_1)\gamma e^{-\tau m}\overline{T}^2}{m_2^{\epsilon}\mu_V\left(\alpha+\mu_Q\right)}-\frac{\alpha\lambda\beta(1-\eta_2)e^{-\tau m}\overline{T}^2}{m_2^{\epsilon}\mu_{T^*}\left(\alpha+\mu_Q\right)}\right]\leq 0$$

for $t > T_\epsilon$. Further, $\frac{dL(t)}{dt} = 0$ if and only if $Q = \overline{Q}$, $T = \overline{T}$, $T^* = \overline{T^*}$, $V_I = \overline{V_I}$, then by the LaSalle invariance principle, $\overline{E}$ is globally asymptotically stable.

4 Numerical Simulations

In this section, we perform some numerical simulations to illustrate our stability results and to examine the effect of time delay and the efficacy of RTI treatments on the viral load. The parameters of the model are given in Table 1 [1, 14, 15]. We begin first with

Parameters	Meaning	Values
α	Activation rate of Q cells (day^{-1})	0.042
λ	Rate of Q cells production (ml^{-1})	10^4
μ_{T^*}	Death rate of T^* cells (day^{-1})	0.67
π	Number of virions per T^* cell	104
μ_T	Death rate of T cells (day^{-1})	0.12
$\eta_{1,2}$	Efficiency of treatment	$[0, 1]$
γ	Infection rate of cells per virion (mm^{3}day^{-1})	0.05×10^{-3}
β	Infection rate by cell-to-cell transmission	2×10^{-5} (cell day)$^{-1}$
μ_Q	Death rate of Q cells (day^{-1})	0.00014
μ_V	Clearance of free virion (day^{-1})	30
ρ	Rate of reversion to the quiescent state (day^{-1})	0.017
ω	Proportion of non-infectious virions	0.2
τ	Incubation period of the infection	$0.2 - 2$ days
m	Fractional of cells surviving incubation period	0.05 days

Table 1: Parameters and values of model (19)

the non delay case $\tau = 0$. In Figure 1, we have plotted the solutions of system (3) in the case of absence of the treatment, i.e., $\eta_1 = \eta_2 = 0$, which corresponds to the value of the basic reproduction number $R_0 = 5.39 > 1$. Since $\mu_V > \mu_{T^*}$, the condition of Theorem 2.2 is satisfied and the endemic equilibrium E^* is locally asymptotically stable. Under RTI treatment if we increase both the efficacy of the RTI inhibiting the virus-to-cell and cell-to-cell infections to the values $\eta_1 = 0.8$, $\eta_2 = 0.84$ which correspond to the value of the basic reproduction number $R_0 = 0.97 < 1$, then by Theorem 2.1, the free steady state E_0 is locally asymptotically stable and the infection is cleared (see Figure 2). In Figure 3, we have plotted the region (in red) for which $R_0 < 1$, which corresponds to the eradication of the infection. We can observe that the infection is cleared when the efficacy of the RTI corresponding to the virus-to-cell and cell-to-cell channels is greater than 0.66 and 0.6, respectively.

In the delay case, we consider a different level of therapy intervention with different values of the delay. Since the incubation time of the infection is between 0.5 to 2 days [15], we run our simulations with the following values: $\tau = 0.4,\ 0.8,\ 1.3,\ 1.8$.

Case 1: In the first case, we assume that the effect of drugs efficiency is $\eta_1 = \eta_2 = 0.45$. In Figure 4, we have plotted solutions of system (14) with the following values of the delay: $\tau = 0.2$, $\tau = 0.8$, $\tau = 1.3$, $\tau = 1.8$.

Case 2: In this case, we keep the value of $\eta_1 = 0.45$ fixed and we increase the value of $\eta_2 = 0.8$. The corresponding solutions with different values of the delay are plotted in Figure 5.

Case 3: Here we fix the value of $\eta_2 = 0.45$ and we increase $\eta_1 = 0.8$. The corresponding solutions are plotted in Figure 6.

Case 4: In the last case, we increase the efficiency of RTI treatment for both virus-to-cell and cell-to-cell infections to the values $\eta_1 = \eta_2 = 0.8$. The solutions are plotted in Figure 7.

Numerical simulations show that the increase of the delay time will decrease the peak of viral load and increase the number of activated T-cells. Further, the delay seems to have no effect on the number of quiescent cells. Since the basic reproduction number of the delay model is multiplied by a factor equal to $e^{-m\tau}$ with respect to that of the non delayed model, we conclude that the region of eradication of the infection is more large than that without delay. Figures 5 and 6 show that the increase of efficiency of the RTI treatments for either virus-to-cell or cell-to-cell transmission mode will reduce the viral load and the number of infected cells T^* but is not sufficient to eradicate the infection. In Figure 7, where we have increased the efficiency of treatments for both virus-to-cell and cell-to-cell routes, we observe that the infection is cleared.

In order to quantify infection sensitivity to drugs, we use the transmission index T_x which is defined as the fraction of cells infected in the presence of drugs $T^*_\eta(t)$ divided by the fraction of cells infected in the absence of drugs $T^*(t)$. Thus $T_x = \dfrac{T^*_\eta(t)}{T^*(t)}$.

T_x has two important limiting regimes: $T_x \simeq 0$, which means that few viruses infect each cell, the infection is sensitive to the effect of the drugs, whereas in the case $T_x \simeq 1$, many viruses infect each cell and the infection is insensitive. At the quasi-steady-state assumption (as $t \to +\infty$), we can simplify T_x as $T_x \simeq \dfrac{\overline{T^*_\eta}}{\overline{T^*}}$,

where $\overline{T^*_\eta}$ and $\overline{T^*}$ are, respectively, the steady states of infection cells in the presence and in the absence of drugs. By (17), we have

$$T_x \simeq \frac{\left(1 - \dfrac{1}{R_0(\eta)}\right)}{\left(1 - \dfrac{1}{R_0}\right)}$$

with

$$\begin{aligned} R_0(\eta) &= \frac{(1-\eta_2)\beta\mu_V e^{-\tau m} + \omega\pi\mu_{T^*}\,(1-\eta_1)\,\gamma e^{-m\tau}}{\mu_{T^*}\mu_V} T_0, \\ R_0 &= \frac{\beta(1-\eta_2)\mu_V e^{-\tau m} + \omega\pi\mu_{T^*}\gamma e^{-m\tau}}{\mu_{T^*}\mu_V} T_0. \end{aligned} \tag{30}$$

In Figure 8, we have plotted on the right the transmission index T_x with respect to η_2 for different values of η_1 and on the left, we have plotted T_x with respect to η_1 for different values of η_2. We observe that infections originating from cell-free virus decrease strongly in the presence of drugs, whereas the other plot shows that infections involving cell-to-cell spread are markedly less sensitive to the drugs. The simulations in Figure 8 suggested that cell-to-cell infection permits viral replication even under the anti-retroviral therapy. As pointed out in other clinical studies [14], cell-to-cell spread leads to therapy failure and potentially contributes to viral persistence and hence is a barrier to curing HIV infection.

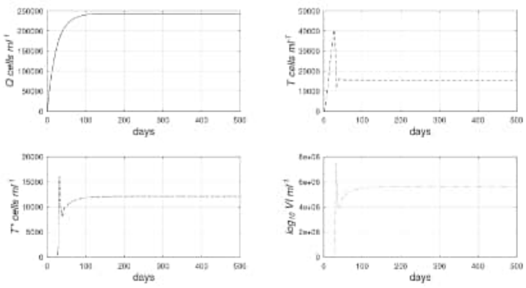

Figure 1: Simulation of solutions of model (3) in the absence of drugs $\eta_1 = \eta_2 = 0$: in this case, $R_0 = 5.36 > 1$, by Theorem 2.2 the endemic steady state E^* is globally stable.

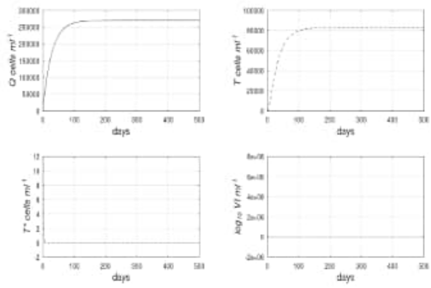

Figure 2: Simulation of solutions of model (3) without delay, where we have taken $\eta_1 = 0.8$ and $\eta_2 = 0.84$: in this case, $R_0 = 0.97 < 1$, by Theorem 2.1, the free steady state E_0 is globally stable and the infection is cleared.

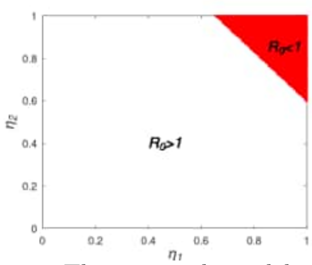

Figure 3: The case without delay: in red is the region of eradication of the infection.

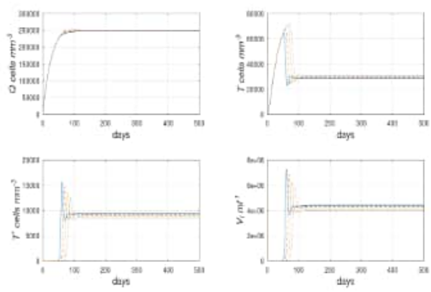

Figure 4: Solutions of system 14 for $\eta_1 = 0.45$, $\eta_2 = 0.45$, $\tau = 0.4$ in solid line (-); $\tau = 0.8$ in dashed line (–); $\tau = 1.3$ in dash-dotted line (-.); $\tau = 1.8$ in dotted line (:).

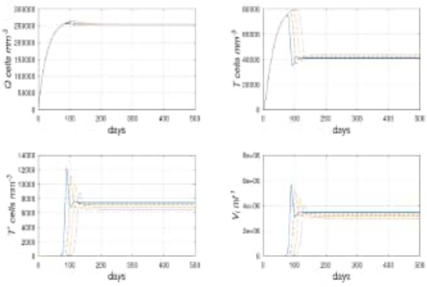

Figure 5: $\eta_1 = 0.45$, $\eta_2 = 0.8$, $\tau = 0.4$ in solid line (-); $\tau = 0.8$ in dashed line (–); $\tau = 1.3$ in dash-dotted line (-.); $\tau = 1.8$ in dotted line (:).

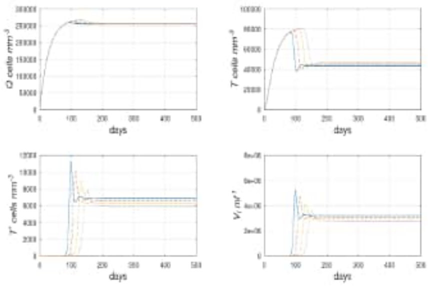

Figure 6: $\eta_1 = 0.8$, $\eta_2 = 0.45$, $\tau = 0.4$ in solid line (-); $\tau = 0.8$ in dashed line (–); $\tau = 1.3$ in dash-dotted line (-.); $\tau = 1.8$ in dotted line (:).

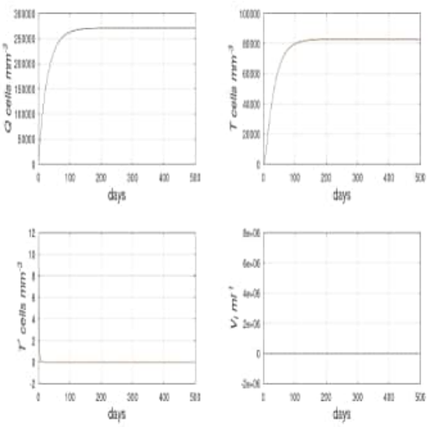

Figure 7: $\eta_1 = 0.8$, $\eta_2 = 0.8$, $\tau = 0.4$ in solid line (-); $\tau = 0.8$ in dashed line (–); $\tau = 1.3$ in dash-dotted line (-.); $\tau = 1.8$ in dotted line (:).

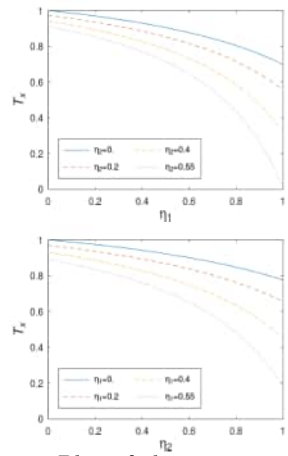

Figure 8: Plot of the transmission index T_x: on the right with respect to η_2 and on the left with respect to η_1, here we have taken $\tau = 2$.

5 Conclusion

This study presents a model incorporating quiescent cells to describe HIV-1 transmission, with an intracellular time delay to account for the role of the non-activated immune system. It demonstrates that the basic reproduction number R_0 is the sum of virus-to-cell and cell-to-cell transmission contributions. The analysis shows that when $R_0 < 1$, the infection is cleared, while for $R_0 > 1$, the endemic steady state is globally asymptotically stable [16].

Numerical simulations indicate that increasing intracellular delay reduces viral load and enhances activated T cells without significantly affecting quiescent cells. Antiretroviral drugs (RTIs) effectively decrease cell-free virus infections but are less effective against cell-to-cell transmission, which can transfer multiple virions simultaneously.

The simulations reveal that improving RTI efficiency to block cell-free infections has only a limited impact on overall HIV infection. Thus, targeting both transmission pathways, virus-to-cell and cell-to-cell, is crucial. The study suggests that cell-to-cell transmission plays a key role in viral spread and should be a primary focus in future vaccination strategies for better effectiveness.

References

[1] M. Kouche, B. Boulfoul and B. Ainseba. Mathematical analysis of an HIV infection model including quiescent cells and periodic antiviral therapy. *International Journal of Biomathematics* **10** (5) (2017) 1750065.

[2] A. Perelson, A. U. Neumann, M. Markowitz, J. Leonard and D. Ho. HIV-1 dynamics in vivo: Virion clearance rate, infectedncell life-span, and viral generation time. *Science* **271** (1996) 1582–1586.

[3] P. W. Nelson and A. Perelson. Mathematical analysis of delay differentiel equation models of hiv-1 infection. *Math. Biosci.* **179** (2006) 73–94.

[4] S. Sayari. A mathematical Study of Wuhan Novel Coronavirus Epidemic Model. *Nonlinear Dynamics and Systems Theory* **22** (1) (2022) 82–96.

[5] R. Culshaw and S. Ruan. A mathematical model of cell-to-cell spread of hiv-1 that includes a time delay. *Math. Biol.* **46** (2003) 425–444.

[6] M. Kouche and B. Ainseba. A mathematical model of Hiv-1 infection including the saturation effect of healthy cell proliferation. *Int. J. Appl. Math. Comput. Sci.* **20** (2010) 601–612.

[7] F. Li and J. Wang. Analysis of an HIV infection model with logistic target-cell growth and cell-to-cell transmission. *Chaos. Solitons and Fractals* **81** (1) (2015) 136–145.

[8] X. Lai and X. Zou. Modeling HIV-1 virus dynamics with both virus-to-cell infection and cell-to-cell transmission. *SIAM. J. Appl. Math.* **74** (2014) 898–917.

[9] P. Driessche and J. Watmough. Reproduction numbers and sub-threshold endemic aquilibria for compartmental models of disease transmission. *Mathematical Biosciences* **180** (2002) 29–48.

[10] J. P. Lasalle. *The stability of Dynamical Systems.* SIAM, Philadelphia, 1976.

[11] J. K. Hale and S. M. Verduyn Lunel. *Introduction to Functional Differential Equations.* Springer, N.Y., 1993.

[12] Y. Kuang. *Delay Differential Equation with Applications in Population Dynamics.* Academic Press, San Diego, 1993.

[13] K. L. Cooke and P. Driessche. On zeros of some transcendental equations. *Funkcialaj Ekvacioj* **29** (1986) 77–90.

[14] S. Iwami, J. S. Takeuchi, S. Nakaoka, F. Mammano, F. Clavel, H. Inaba, T. Kobayashi, N. Misawa, K. Aihara, Y. Koyanagi and K. Sato. Cell-to-cell infection by HIV contributes over half of virus infection. *ELife* **4** (2015) 20121049.

[15] X. Wang, S. Tang, X. Song and L. Rong. Mathematical analysis of an HIV latent infection model including both virus-to-cell infection and cell-to-cell transmission. *J. Biol. Dyn.* **151** (2017) 455–483.

[16] S. Toaha Firman and A. Ribal. Global Stability and Optimal Harvesting of Predator-Prey Model with Holling Response Function of Type II and Harvesting in Free Area of Capture. *Nonlinear Dynamics and Systems Theory* **22** (1) (2022) 105–116.

Nonlinear Dynamics and Systems Theory, **25** (2) (2025) 206–216

Electronic Circuit and Complete Synchronization via Active Backstepping Control for a New Chaotic 3-D Jerk System

A. R. Mamat [1*], M. A. Mohamed [1], S. Vaidyanathan [1,2], A. Sambas [1,3], L. Patria [4] and R. Ramesh [5]

[1] *Faculty of Informatics and Computing, University Sultan Zainal Abidin, Besut Campus 22200, Terengganu, Malaysia.*

[2] *Centre for Control Systems, Vel Tech University, Avadi, Chennai 600062, Tamil Nadu, India.*

[3] *Department of Mechanical Engineering, Universitas Muhammadiyah Tasikmalaya, Tasikmalaya 46196, Indonesia.*

[4] *Department of Information System, Faculty of Science and Technology, Universitas Terbuka, Banten 15437, Indonesia*

[5] *Department of Computer Science and Engineering, KKR and KSR Institute of Technology and Sciences, Vinjanampadu, Vatticherukuru Mandal, Guntur-522017, India.*

Received: July 12, 2024; Revised: April 2, 2025

Abstract: This paper presents the modeling, electronic circuit implementation, and complete synchronization of a new chaotic 3-D jerk system with two quadratic nonlinearities. The proposed jerk system, characterized by the third derivative of its output being a function of lower-order derivatives, exhibits chaotic behavior under specific parameter conditions. The system's dynamics are analyzed, revealing the presence of chaotic attractors through numerical simulations and Lyapunov exponents. An electronic circuit realizing the jerk system is designed using operational amplifiers, resistors, and capacitors, demonstrating chaos through Multisim and MATLAB simulations. Additionally, a backstepping control technique is employed to achieve complete synchronization between the master and slave jerk systems, with potential applications in secure communications and cryptosystems. Theoretical proofs and simulation results validate the effectiveness of the proposed synchronization method.

Keywords: *chaos theory; chaotic systems; dynamical systems; jerk systems; bifurcation; synchronization; backstepping control.*

Mathematics Subject Classification (2020): 34H10, 65P40, 34D06, 34D08, 94C30, 94C60.

* Corresponding author: arm@unisza.edu.my

1 Introduction

Chaos theory has become a fundamental area of study in nonlinear dynamics, with applications spanning across various fields such as physics, engineering, biology, and secure communications [1–3]. A chaotic system is highly sensitive to initial conditions, leading to behavior that appears random and unpredictable despite being deterministic [4, 5]. Among the numerous chaotic systems studied, jerk systems are of particular interest due to their simplicity and ability to exhibit complex dynamical behavior [6]. A jerk system is defined by its output's third derivative (jerk) being a function of lower-order derivatives [8].

The study of chaotic systems has its roots in the pioneering work of Lorenz, who discovered the Lorenz attractor [9], a set of chaotic solutions of the Lorenz system, which has become a classic example of chaos. Since then, numerous chaotic systems have been explored, including the Rossler system, Chua's circuit, and jerk systems [10, 11]. Jerk systems, in particular, are intriguing due to their relatively simple mathematical form and the rich dynamical behavior they exhibit [12].

In a jerk system, the third derivative of a variable with respect to time is expressed as a function of the variable and its first and second derivatives [13]. This form allows for the construction of chaotic systems using basic electronic components such as resistors, capacitors, and operational amplifiers [14]. The electronic realization of chaotic systems not only provides a tangible means of studying chaos but also facilitates practical applications in areas like secure communications, where chaotic signals can be used for encryption.

The introduction of a novel 3-D jerk system with quadratic nonlinearities, as explored in this study, contributes to the ongoing exploration of complex dynamical behaviors such as chaotic attractors and multistability, which are prevalent in both natural and engineered systems. Moreover, the practical implementation of these systems through electronic circuit designs bridges the gap between theoretical models and real-world applications, further enhancing their relevance. The synchronization of such systems, demonstrated here using backstepping control, has significant implications for creating stable, secure systems in various technological domains, thereby underscoring the importance of this research in advancing the understanding and application of chaotic dynamics.

The synchronization of chaotic systems, where two or more chaotic systems are made to exhibit identical behavior over time, has significant implications for practical applications [15]. Techniques such as backstepping control have been developed to achieve synchronization, offering robust methods for controlling chaotic systems.

This paper presents a novel chaotic 3-D jerk system characterized by two quadratic nonlinearities. We explore its dynamic properties through numerical simulations, revealing chaotic behavior under specific parameter settings. The system is then realized electronically, and its chaotic nature is validated through both Multisim and MATLAB simulations. Finally, we employ an active backstepping control technique to achieve complete synchronization between a pair of chaotic jerk systems and demonstrating the method's effectiveness.

The rest of the paper is organized as follows. In Section 2, we present the modeling of the new chaotic 3-D jerk system with two quadratic nonlinearities and analyze its dynamic behavior through numerical simulations. Section 3 describes the electronic circuit implementation of the proposed chaotic system and validates its chaotic behavior using simulations in Multisim and MATLAB. In Section 4, we introduce the backstepping control technique and demonstrate the complete synchronization of master and slave chaotic jerk systems, providing theoretical proofs and simulation results. In Section 5, we conclude the paper by summarizing the contributions of the research and discussing potential applications of the proposed system.

2 Modelling of the New Jerk System

This section presents and examines a new chaotic jerk system with two quadratic nonlinearities. The new jerk system is described as follows:

$$\begin{cases} \dot{x} &= y, \\ \dot{y} &= z, \\ \dot{z} &= -ax + by - z - xy + cy^2. \end{cases} \tag{1}$$

In the jerk system (1), $X = (x, y, z)$ is the 3-D state and a, b, c are positive parameters.

In this paper, we show that the jerk system (1) is chaotic when the parameters are $a = 1$, $b = 0.1$ and $c = 1$.

For numerical simulations in MATLAB, we pick the parameters as $(a, b, c) = (1, 0.1, 1)$ and the initial state as $X(0) = (0.2, 0.2, 0.2)$. Then the Lyapunov exponents (LE) of the jerk system (1) are numerically determined for $T = 1E4$ seconds as

$$l_1 = 0.1252, \; l_2 = 0, \; l_3 = -1.1252. \tag{2}$$

The LE results in Eq.(2) show that the new 3-D jerk system (1) is chaotic and dissipative with the maximal Lyapunov exponent (MLE) found as $l_1 = 0.1252 > 0$. The Kaplan dimension of the new 3-D jerk system can be also determined as

$$D_K = 2 + \frac{1}{|l_3|}(l_1 + l_2) = 2.1113. \tag{3}$$

Figures 1-3 show the phase plots of the jerk system (1) generated in MATLAB using the classical fourth-order Runge-Kutta method for the initial state $(0.2, 0.2, 0.2)$ and the parameter vector $(a, b, c) = (1, 0.1, 1)$.

The equilibrium points of the system described by Equation (1) can be determined by setting in Equation (1) as follows:

$$\begin{cases} 0 &= y, \\ 0 &= z, \\ 0 &= -ax + by - z - xy + cy^2. \end{cases} \tag{4}$$

Thus, the equilibrium points of the system (4) are $E_0 = (0,\ 0,\ 0)$. The Jacobian matrix of the system (1) can be written as

$$J = \begin{pmatrix} 0 & 1 & 0 \\ 0 & 0 & 1 \\ -1 - y & 0.1 - x + 2y & -1 \end{pmatrix}. \tag{5}$$

The Jacobian matrix at the equilibrium point E_0 is expressed as

$$J = \begin{pmatrix} 0 & 1 & 0 \\ 0 & 0 & 1 \\ -1 & 0.1 & -1 \end{pmatrix}. \tag{6}$$

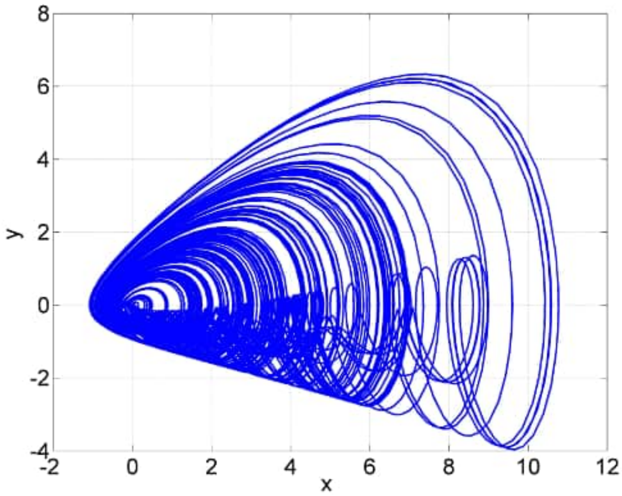

Figure 1: (x, y) plot of the chaotic jerk system (1).

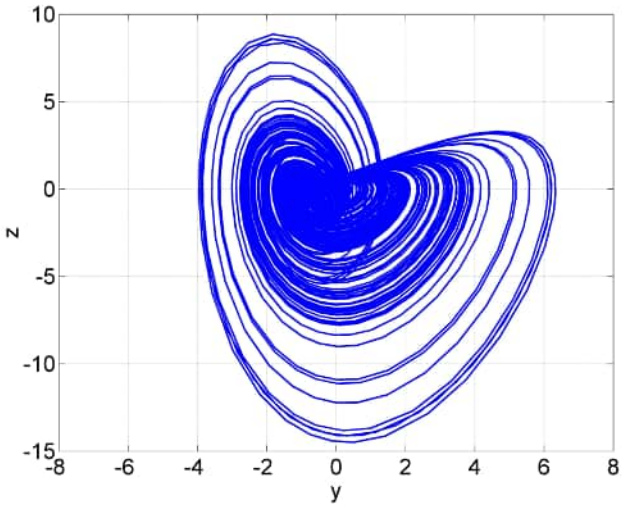

Figure 2: (y, z) plot of the chaotic jerk system (1).

The polynomial characteristic equation of Eq.(6) is given by

$$\lambda^3 + \lambda^2 - 0.1\lambda + 1 = 0. \tag{7}$$

The Jacobian matrix JE_0 has the eigenvalues $-1.5068, 0.2534 \pm 0.7742i$. This shows that the system (1) exhibits the index-2 spiral saddle point, which is unstable.

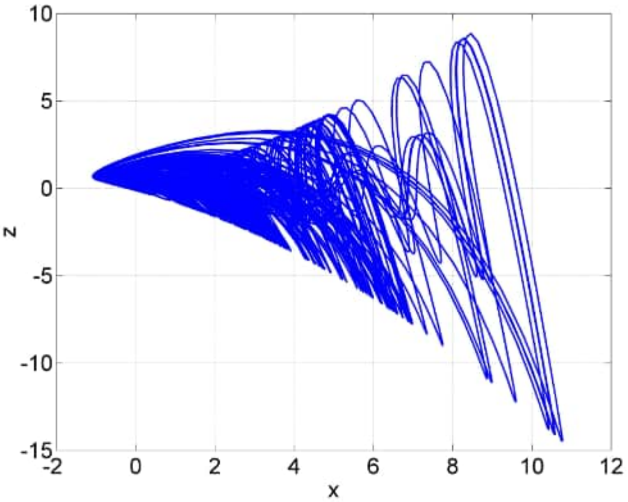

Figure 3: (x, z) plot of the chaotic jerk system (1).

3 Electronic Circuit

The provided circuit diagram represents a jerk system (see Figure 4), which is a type of nonlinear dynamical system known for exhibiting chaotic behavior under certain conditions. A jerk system is characterized by the third derivative of its output (jerk) being a function of lower-order derivatives. The circuit comprises operational amplifiers (op-amps), resistors, and capacitors to realize the jerk function.

In this specific circuit, each section with an op-amp configuration represents different components of the jerk system. The resistors and capacitors determine the time constants and feedback paths, which are crucial for defining the system's dynamic behavior. The input signals (X, Y, and Z) are processed through the network of op-amps to produce a chaotic output. The chaotic nature arises from the nonlinear interactions between the components, causing the system to exhibit sensitive dependence on initial conditions—a hallmark of chaos. The op-amps (TL082CD) are used for their high input impedance and low offset voltage, making them suitable for precise analog computations required in the jerk system.

By using Kirchhoffs circuit laws in Eq.(8), the circuital equations of the designed circuit in Figure 4 are derived as follows:

$$\begin{cases} \dot{x} &= \frac{1}{C_1 R_1} y, \\ \dot{y} &= \frac{1}{C_2 R_2} z, \\ \dot{z} &= -\frac{1}{C_3 R_3} x + \frac{1}{C_3 R_4} y - \frac{1}{C_3 R_5} z - \frac{1}{10 C_3 R_6} xy + \frac{1}{10 C_3 R_7} y^2. \end{cases} \tag{8}$$

Here, x, y, z are the voltages across the capacitors C_1, C_2, and C_3, respectively. We choose the values of the circuital elements as $R_6 = R_7 = 10$ kΩ, $R_4 = 1000$ kΩ, $R_1 = R_2 = R_3 = R_5 = R_8 = R_9 = R_{10} = R_{10} = 100$ kΩ, $C_1 = C_2 = C_3 = 1$ nF. The corresponding phase portraits on the oscilloscope are shown in Fig.5. Multisim simulation has been performed in order to validate the numerical simulation results. A good agreement has been revealed between the results obtained from Multisim software and Matlab software.

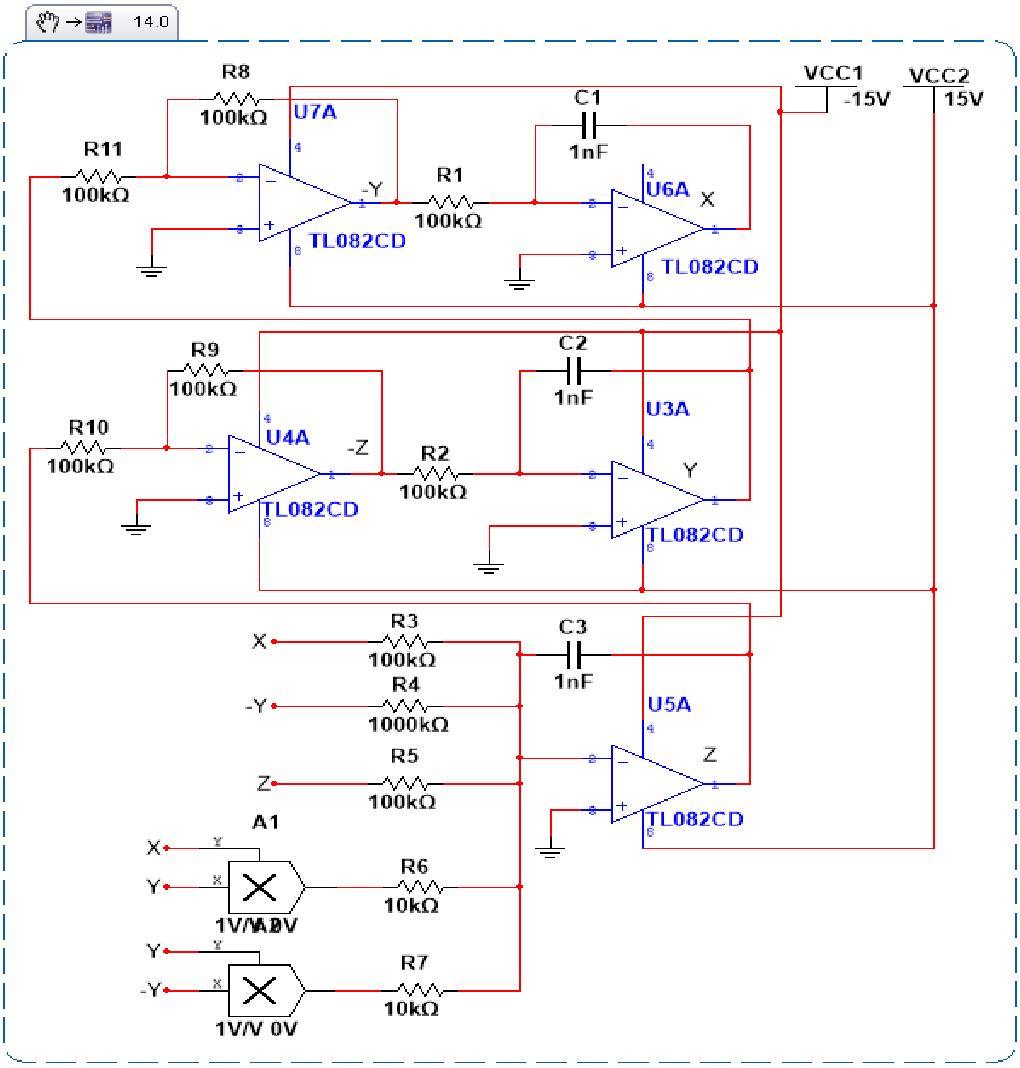

Figure 4: Circuit design of the system (1).

4 Complete Synchronization of the New Chaotic Jerk Systems

In this section, we give a new control application for the chaotic jerk system proposed in Section 2. We consider a pair of the new chaotic jerk systems taken as the *master* and *slave* systems, and we invoke the active backstepping control technique to synchronize the respective states of the master and slave jerk systems. We note that the synchronization of chaotic systems has important applications in engineering, namely in secure communications, cryptosystems, etc.

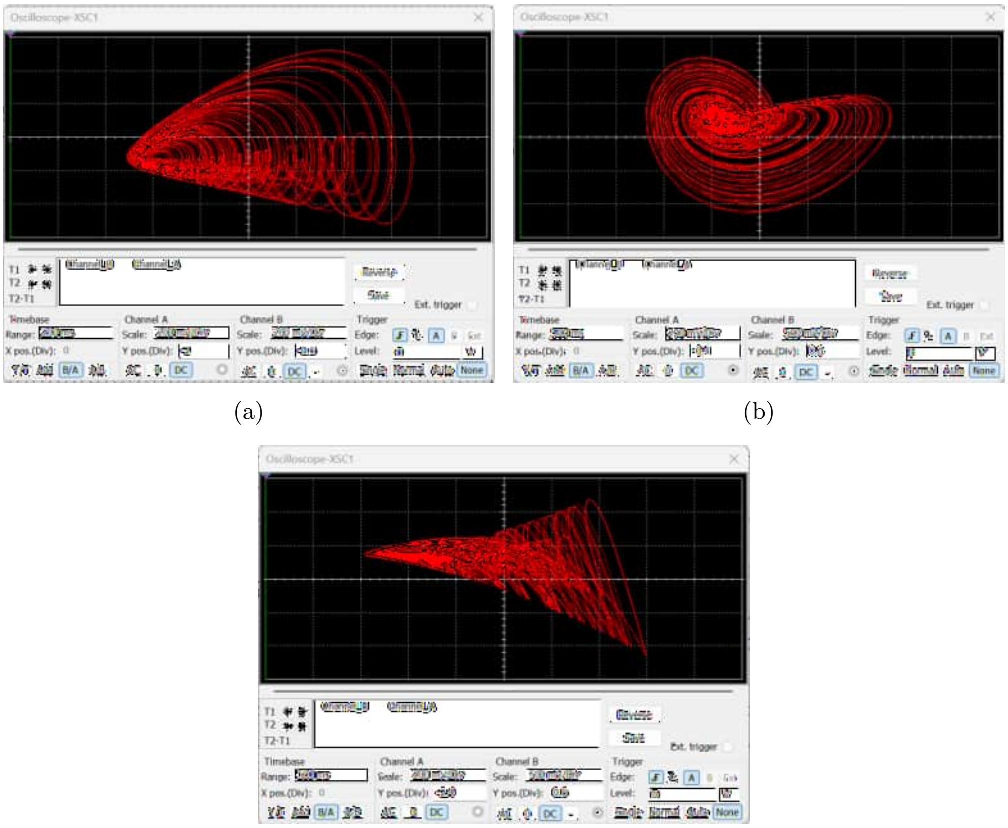

(a) (b)

(c)

Figure 5: 2-D oscilloscope outputs of the new chaotic jerk system: (a) $x-y$ plane, (b) $y-z$ plane, and (c) $x-z$ plane.

As the master system for the synchronization process, we take the new jerk system with the dynamics given by

$$\begin{cases} \dot{x}_1 &= y_1, \\ \dot{y}_1 &= z_1, \\ \dot{z}_1 &= -ax_1 + by_1 - z_1 - x_1y_1 + cy_1^2. \end{cases} \tag{9}$$

As the slave system for the synchronization process, we take the new jerk system with the dynamics given by

$$\begin{cases} \dot{x}_2 &= y_2, \\ \dot{y}_2 &= z_2, \\ \dot{z}_2 &= -ax_2 + by_2 - z_2 - x_2y_2 + cy_2^2 + W(t). \end{cases} \tag{10}$$

In this research work, we use backstepping control to devise a feedback control $W(t)$ to asymptotically synchronize the states of the two jerk systems given by the equations (9) and (10).

We define the synchronization error between the master and slave jerk systems as follows:

$$\begin{cases} e_x &= x_2 - x_1, \\ e_y &= y_2 - y_1, \\ e_z &= z_2 - z_1. \end{cases} \tag{11}$$

The error dynamics can be calculated as

$$\begin{cases} \dot{e}_x &= e_y, \\ \dot{e}_y &= e_z, \\ \dot{e}_z &= -ae_x + be_y - e_z - x_2y_2 + x_1y_1 + c\left(y_2^2 - y_1^2\right) + W(t). \end{cases} \tag{12}$$

Next, we state and prove the main control result for the complete synchronization of the new jerk systems given by the Eqs. (9) and (10).

Theorem 4.1 The backstepping feedback control law defined by

$$W = -(3-a)e_x - (5+b)e_y - 2e_z + x_2y_2 - x_1y_1 - c(y_2^2 - y_1^2) - kq_3 \tag{13}$$

with the feedback gain $k > 0$ and $q_3 = 2e_x + 2e_y + e_z$ achieves complete synchronization between the chaotic jerk systems (9) and (10) for all initial states in $\mathbb{R}^3$.

Proof. We set $q_1 = e_x$.
We define the quadratic Lyapunov function as

$$V_1(q_1) = \frac{1}{2}\, e_x^2. \tag{14}$$

Then we get

$$\dot{V}_1 = q_1\dot{q}_1 = e_xe_y = -q_1^2 + q_1(e_x + e_y). \tag{15}$$

Next, we define $q_2 = e_x + e_y$ so that we can simplify Eq.(15) as follows:

$$\dot{V}_1 = -q_1^2 + q_1q_2. \tag{16}$$

Based on the Eq.(16), we define the quadratic Lyapunov function as

$$V_2(q_1, q_2) = V_1(q_1) + \frac{1}{2}q_2^2 = \frac{1}{2}q_1^2 + \frac{1}{2}q_2^2. \tag{17}$$

A simplification results in

$$\dot{V}_2 = -q_1^2 - q_2^2 + q_2(2e_x + 2e_y + e_z). \tag{18}$$

To simplify the notations in Eq.(19), we set

$$q_3 = 2e_x + 2e_y + ez. \tag{19}$$

Then Eq.(18) reduces to

$$\dot{V}_2 = -q_1^2 - q_2^2 + q_2q_3. \tag{20}$$

As a final step, we take the quadratic Lyapunov function given by

$$V(q_1, q_2, q_3) = V_2(q_1, q_2) + \frac{1}{2}q_3^2. \tag{21}$$

It is easy to see that V is a positive definite function on R^3. It is also very clear that

$$V(q_1, q_2, q_3) = \frac{1}{2}q_1^2 + \frac{1}{2}q_2^2 + \frac{1}{2}q_3^2. \tag{22}$$

Based on the Eq.(22), when we calculate the derivative of V, we get

$$\dot{V} = -q_1^2 - q_2^2 - q_3^2 + q_3 Z, \tag{23}$$

where we define Z as

$$Z = q_2 + q_3 + \dot{q}_3. \tag{24}$$

A simple calculation yields

$$Z = (3 - a)e_x + (5 + b)e_y + 2e_z - x_2 y_2 + x_1 y_1 + c(y_2^2 - y_1^2) + W. \tag{25}$$

Substituting the formula given in Eq.(13) for v into Eq.(25), we get

$$Z = -kq_3. \tag{26}$$

From the Eqs.(23) and (26), we get

$$\dot{V} = -q_1^2 - q_2^2 - q_3^2(1 + k). \tag{27}$$

Since $k > 0$, we see that $\dot{V}$ is a quadratic and negative definite function defined on R^3.

By Lyapunov Stability Theory, we deduce that the error dynamics (12) is globally exponentially stable. This completes the proof.

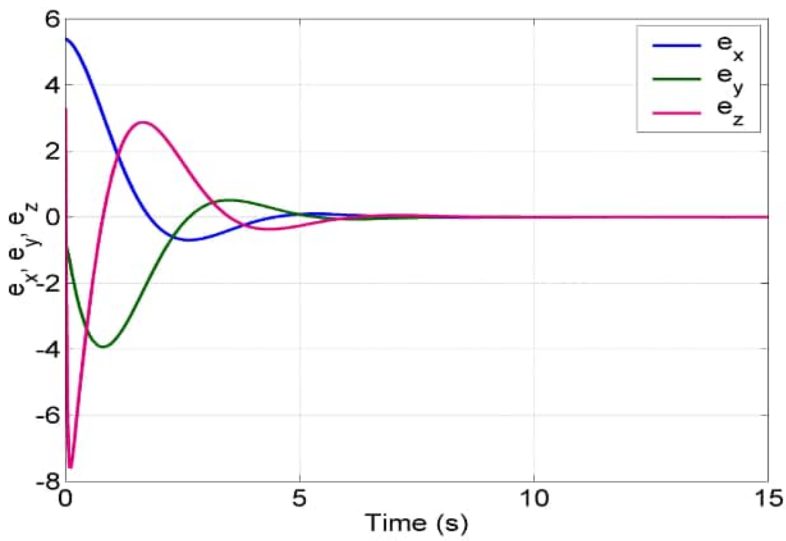

Figure 6: MATLAB plot depicting the exponential convergence of the complete synchronization error between the chaotic jerk systems (9) and (10).

For computer simulations, we consider the chaotic case for the master and slave jerk systems, *viz.* $a = 1$, $b = 0.1$ and $c = 1$. Also, we take $k = 30$.

For simulations, the initial conditions of the master system (9) are taken as $x_1(0) = 1.8,\ y_1(0) = 1.4$ and $z_1(0) = 2.1$.

Also, the initial conditions of the slave system (10) are taken as $x_2(0) = 7.2,\ y_2(0) = 0.5$ and $z_3(0) = 5.4$.

Figure 6 shows the convergence of the synchronization errors ϵ_x, ϵ_y and ϵ_z between the chaotic jerk systems (9) and (10).

5 Conclusion

This study introduces a novel chaotic 3-D jerk system characterized by two quadratic nonlinearities, which sets it apart from previously studied chaotic systems. The specific configuration of the system, including the interplay of its nonlinearities, represents a new contribution to the field of nonlinear dynamics and chaos theory. Additionally, the practical realization of this chaotic system through a custom-designed electronic circuit demonstrates a unique approach to linking theoretical chaos models with physical implementations. The circuit design, validated through Multisim and MATLAB simulations, offers a tangible and reliable method to replicate chaotic behavior in real-world applications.

Acknowledment

This work is funded by the Ministry Education of Malaysia under Grant FRGS/1/2020/STG06/UNISZA/02/2 (RR361).

References

[1] Y. Ghettout, L. Meddour, T. Hamaizia and R. Ouahabi. Dynamic Analysis of a New Hyperchaotic System with Infinite Equilibria and Its Synchronization. *Nonlinear Dynamics and Systems Theory* **24** (2) (2024) 147–158.

[2] A. Sambas, M. Miroslav, S. Vaidyanathan, B. Ovilla-Martínez, E. Tlelo-Cuautle, A. A. Abd El-Latif and T. Bonny. A new hyperjerk system with a half line equilibrium: Multistability, Period doubling reversals, antimonotonocity, electronic circuit, FPGA design and an application to image encryption. *IEEE Access* **12** (2024) 9177–9194.

[3] S. Khajanchi. Chaotic dynamics of a delayed tumor–immune interaction model. *International Journal of Biomathematics* **13** (2) (2020) 2050009.

[4] E. A. Abed, S. K. Mousa and R. K. Jamal. A novel secure communication system using optoelectronic feedback in semiconductor laser. *Journal of Optics* **53** (2) (2024) 913–922.

[5] A. Sambas, A. Mohammadzadeh, S. Vaidyanathan, A. M. Ayob, A. Aziz, M. A. Mohamed and M. A. A. Nawi. Investigation of chaotic behavior and adaptive type-2 fuzzy controller approach for Permanent Magnet Synchronous Generator (PMSG) wind turbine system. *AIMS Mathematics* **8** (3) (2023) 5670–5686.

[6] J. C. Sprott. Simple chaotic systems and circuits. *American Journal of Physics* **68** (8) (2000) 758–763.

[7] J. Ma, P. Zhou, B. Ahmad, G. Ren and C. Wang. Chaos and multi-scroll attractors in RCL-shunted junction coupled jerk circuit connected by memristor. *PloS one* **13** (1) (2018) e0191120.

[8] P. Li, T. Zheng, C. Li, X. Wang and W. Hu. A unique jerk system with hidden chaotic oscillation. *Nonlinear Dynamics* **86** (2016) 197–203.

[9] E. N. Lorenz. Deterministic nonperiodic flow. *Journal of Atmospheric Sciences* **20** (2) (1963) 130–141.

[10] C. Zou and L. Wang. A visual DNA compilation of Rössler system and its application in color image encryption. *Chaos, Solitons & Fractals* **174** (2023) 113886.

[11] N. Kuznetsov, T. Mokaev, V. Ponomarenko, E. Seleznev, N. Stankevich and L. Chua. Hidden attractors in Chua circuit: mathematical theory meets physical experiments. *Nonlinear Dynamics* **111** (6) (2023) 5859–5887.

[12] S. Yan, Y. Cui and X. Sun. A jerk chaotic system with bistable locally active memristor and its analysis of multi-scroll formation mechanism. *The European Physical Journal Plus* **139** (1) (2024) 1–14.

[13] M. Liu, B. Sang, N. Wang and I. Ahmad. Chaotic dynamics by some quadratic jerk systems. *Axioms* **10** (3) (2021) 227.

[14] R. Rameshbabu, K. Kavitha, P. S. Gomathi and K. Kalaichelvi. A New Hidden Attractor Hyperchaotic System and Its Circuit Implementation, Adaptive Synchronization and FPGA Implementation. *Nonlinear Dynamics and Systems Theory* **23** (2) (2022) 214–226.

[15] H. Cheng, H. Li, Q. Dai and J. Yang. Chaos Anti-Synchronization between Fractional-Order Lesser Date Moth Chaotic System and Integer-Order Chaotic System by Nonlinear Control. *Nonlinear Dynamics and Systems Theory* **23** (2) (2023) 207–213.

Nonlinear Dynamics and Systems Theory, **25** (2) (2025) 217–228

Advanced Fixed-Point Results for New Type Contractions via Simulation Functions in b-Metric Spaces with an Application to Nonlinear Integral

Haitham Qawaqneh *

Al-Zaytoonah University of Jordan, Amman 11733, Jordan

Received: February 5, 2024; Revised: March 17, 2025

Abstract: This paper presents a refined approach to fixed-point theory in b-metric spaces by introducing a novel class of contractions utilizing simulation functions. The proposed framework generalizes and strengthens existing results, providing deeper insights into the underlying structure of b-metric spaces. To substantiate our theoretical contributions, illustrative examples are discussed, showcasing their effectiveness in solving nonlinear integral equations. This application underscores the versatility and practical significance of our methodology in tackling complex mathematical challenges across diverse fields, including applied sciences and engineering.

Keywords: *b-metric space; simulation function; fixed point; integral equation.*

Mathematics Subject Classification (2020): 93C10, 93C30, 93C43, 46T20.

1 Introduction

Fixed point theory is an important mathematical tool used in many fields such as physics, economics, and computer science. Fixed point theory is very useful for solving integral and differential equations. This makes it very important for application in mathematics and science. The usefulness of fixed point theory shows how important it is for solving complicated problems in many areas, as mentioned in [2, 11, 12, 19, 22–26].

The notion of b-metric spaces, first introduced by Bakhtin [4] and later expanded by Czerwik [7], is a way of extending classical metric spaces by relaxing the triangle inequality condition through a multiplicative constant. Unlike standard metric spaces,

* Corresponding author: mailto:h.alqawaqneh@zuj.edu.jo

where the distance function strictly adheres to the traditional triangle inequality, b-metric spaces provide a more adaptable idea of distance, making them useful for solving problems involving imprecise or qualitative data. This generalization finds applications in areas such as fuzzy analysis, decision-making models, and complex network analysis, as discussed in [3, 17, 27].

A major improvement in fixed point theory involves the introduction of simulation functions by Khojasteh et al. [16]. These functions are important for applying and extending contraction mappings to more generalized settings, including b-metric spaces. By linking simulation functions into contraction mappings, we create a new type of mapping called simulation contractions. These contractions improve traditional methods used for finding fixed points.

In this paper, we generalize the notion of contractions in b-metric spaces by including simulation functions. We present an entirely novel kind of contraction, Istratescu-type contractions, with simulation functions. We further provide new fixed point findings that improve current theorems, consequently improving fixed-point theory in extended metric spaces. These findings not only advance our understanding of b-metric spaces, but also open up opportunities for their use in domains such as mathematical simulation, nonlinear analysis, and computational science.

2 Preliminaries

We begin with some important fundamental concepts.

Definition 2.1 [4], [7] Let Γ be a nonempty set and let $\tau \geq 1$ be a real number. A function $d_\beta : \Gamma \times \Gamma \to [0, \infty)$ is called b-metric on Γ if it satisfies the following conditions for all $a, b, c \in \Gamma$:

(1) $d_\beta(a, b) = 0$ if and only if $a = b$,

(2) $d_\beta(a, b) = d_\beta(b, a)$,

(3) $d_\beta(a, c) \leq \tau[d_\beta(a, b) + d_\beta(b, c)]$.

The structure (Γ, d_β, τ) is referred to as a b-metric space.

A b-metric space extends metric spaces by including a parameter $\tau > 1$ that improves the triangle inequality.

Example 2.1 Consider the set $\Gamma = [0, 1]$ equipped with the function $d_\beta : \Gamma \times \Gamma \to [0, \infty)$ defined by

$$d_\beta(a, b) = |a - b|^\tau$$

for all $a, b \in \Gamma$, where $\tau = 3$.

It is simple to demonstrate that $(\Gamma, d_\beta, 3)$ satisfies the criteria of a b-metric space but is not a standard metric space.

Definition 2.2 [4] Let (Γ, d_β, τ) be a b-metric space. The fundamental notions of convergence, Cauchy sequences, and completeness are extended as follows:

(i) Convergence: A sequence $\{a_n\} \subseteq \Gamma$ is said to converge to a point $a \in \Gamma$ if

$$\lim_{n \to \infty} d_\beta(a_n, a) = 0.$$

(ii) Cauchy Sequence: A sequence $\{a_n\}$ in Γ is called a Cauchy sequence if, for every $\epsilon > 0$, there exists an index $n(\epsilon) \in \mathbb{N}$ such that

$$d_\beta(a_n, a_m) < \epsilon \quad \text{for all } m, n \geq n(\epsilon).$$

(iii) Completeness: The b-metric space (Γ, d_β, τ) is said to be complete if every Cauchy sequence $\{a_n\}$ in Γ converges to some point $a \in \Gamma$.

Lemma 2.1 *[8] Let (Γ, d_β, τ) be a b-metric space with $\tau \geq 1$, and suppose that the sequences $\{a_n\}$ and $\{b_n\}$ in Γ b-converge to $a, b \in \Gamma$, respectively. Then the following inequalities hold:*

$$\frac{1}{s} d_\beta(a,b) \quad \leq \lim_{n\to\infty} \inf d_\beta(a_n, b_n) \leq \lim_{n\to\infty} \sup d_\beta(a_n, b_n) \leq s^2 d_\beta(a,b).$$

In particular, if $a = b$, then we have

$$\lim_{n\to\infty} d_\beta(a_n, b_n) = 0.$$

Furthermore, for every $c \in \Gamma$, we obtain

$$\frac{1}{s} d_\beta(a,c) \leq \lim_{n\to\infty} \inf d_\beta(a_n, c) \leq \lim_{n\to\infty} \sup d_\beta(a_n, c) \leq s^2 d_\beta(a,c).$$

Definition 2.3 [16] A function $\Omega : [0,\infty) \times [0,\infty) \to \mathbb{R}$ is called a simulation function (SF) if it satisfies the following conditions:

1. $\Omega(0,0) = 0$;
2. $\Omega(u,v) < v - u$ for all $u, v > 0$;
3. If $\{u_n\}$ and $\{v_n\}$ are sequences in $(0,\infty)$ converging to some $\gamma \in (0,\infty)$, then

$$\lim_{n\to\infty} \sup \Omega(u_n, v_n) < 0.$$

Example 2.2 [16] Let $\phi_i : [0,\infty) \to [0,\infty)$ be continuous functions for $i = 1,2,3$ satisfying $\phi_i(u) = 0$ if and only if $u = 0$. Define the functions $\Omega_i : [0,\infty) \times [0,\infty) \to \mathbb{R}$ as follows:

1. For every $u, v \in [0,\infty)$, set $\Omega_1(u,v) = \phi_1(v) - \phi_2(u)$, where $\phi_1(u) < u \leq \phi_2(u)$ for each $u > 0$.
2. Define $\Omega_2(u,v) = v - \frac{f(u,v)}{g(u,v)}$ for all $u, v \in [0,\infty)$, where $f, g : [0,\infty)^2 \to (0,\infty)$ are continuous functions satisfying $f(u,v) > g(u,v)$ for all $u, v > 0$.
3. Let $\Omega_3(u,v) = v - \phi_3(v) - u$ for all $u, v \in [0,\infty)$.

Lemma 2.2 *[27]. Let (Γ, d_β, τ) be a b-metric space. A sequence $\{a_n\} \subseteq \Gamma$ is called Cauchy if there exists a constant $c \in [0,1)$ such that for every $n \in \mathbb{N}$, the following inequality holds:*

$$d_\beta(a_n, a_{n+1}) \leq c \cdot d_\beta(a_n, a_{n-1}).$$

3 Main Result

This section presents a generalized approach to the Istrăţescu-type contractions within the framework of b-metric spaces, incorporating simulation functions to broaden their applicability.

Definition 3.1 Let Γ be a nonempty set, and consider a function $d_\beta : \Gamma \times \Gamma \to \mathbb{R}$ that satisfies the conditions of a b-metric space with parameters $\tau \geq 1$ and $c \in [0,1]$. Define an auxiliary function $\alpha : \Gamma \times \Gamma \to [0,+\infty)$, and let $T : \Gamma \to \Gamma$ be an α-admissible Istrăţescu ω-contraction if the following relation holds for all $a, b \in \Gamma$:

$$\omega(\alpha(a,b)d_\beta(T^2a, T^2b), c \cdot M(a,b)) \geq 0, \tag{1}$$

where
$$M(a,b) = d_\beta(Ta,Tb) + |d_\beta(Ta,T^2a) - d_\beta(Tb,T^2b)|.$$

Theorem 3.1 *Let (Γ, d_β, τ) be a b-metric space with coefficient τ, and let $T : \Gamma \to \Gamma$ be a mapping. Suppose the following conditions hold:*

1. *There exists a simulation function ω.*
2. *The mapping T is α-orbital admissible, and there exists $a_0 \in \Gamma$ such that $\alpha(a_0, Ta_0) \geq 1$.*
3. *The mapping T is continuous; or*
4. *The mapping T^2 is continuous and $\alpha(Ta,a) \geq 1$ for all $a \in \Gamma$.*

Then T has a unique fixed point.

Proof. Consider the sequence $\{a_n\}$ in Γ defined by $a_{n+1} = Ta_n$ and $a_{n+2} = T^2a_n$ for all $n \in \mathbb{N} \cup \{0\}$.

If $a_n = a_{n+1}$ for some $n \in \mathbb{N} \cup \{0\}$, then T has a fixed point, completing the proof. Otherwise, assume $a_n \neq a_{n+1}$ for all $n \in \mathbb{N} \cup \{0\}$, which implies $d_\beta(a_n, a_{n+1}) \neq 0$. Using the given contraction condition, we obtain

$$\omega\big(\alpha(a_n, a_{n+1})d_\beta(T^2a_n, T^2a_{n+1}), c \cdot M(a_n, a_{n+1})\big) \geq 0, \tag{2}$$

where

$$M(a_n, a_{n+1}) = d_\beta(Ta_n, Ta_{n+1}) + \big|d_\beta(Ta_n, T^2a_n) - d_\beta(Ta_{n+1}, T^2a_{n+1})\big|.$$

Expanding (2), we derive

$$\omega\big(d_\beta(a_{n+2}, a_{n+3}), c \cdot (d_\beta(a_{n+1}, a_{n+2}) + |d_\beta(a_{n+1}, a_{n+2}) - d_\beta(a_{n+2}, a_{n+3})|)\big) \geq 0. \tag{3}$$

Using the properties of ω and simplifying, we obtain

$$d_\beta(a_{n+2}, a_{n+3}) < c \cdot (d_\beta(a_{n+1}, a_{n+2}) + |d_\beta(a_{n+1}, a_{n+2}) - d_\beta(a_{n+2}, a_{n+3})|). \tag{4}$$

From this, we analyze two cases
Case 1: If $d_\beta(a_{n+1}, a_{n+2}) \leq d_\beta(a_{n+2}, a_{n+3})$, then

$$d_\beta(a_{n+2}, a_{n+3}) < c \cdot d_\beta(a_{n+2}, a_{n+3}), \tag{5}$$

which is a contradiction since $c < 1$.

Case 2: If $d_\beta(a_{n+1}, a_{n+2}) > d_\beta(a_{n+2}, a_{n+3})$, then

$$d_\beta(a_{n+2}, a_{n+3}) < \frac{2c}{1-c} d_\beta(a_{n+1}, a_{n+2}). \tag{6}$$

By induction, we get

$$d_\beta(a_n, a_{n+1}) < \left(\frac{2c}{1-c}\right)^{n-1} d_\beta(Ta_0, T^2 a_0). \tag{7}$$

Since $\frac{2c}{1-c} < 1$, it follows that

$$\lim_{n\to\infty} d_\beta(a_n, a_{n+1}) = 0. \tag{8}$$

Thus, $\{a_n\}$ is a Cauchy sequence in the complete b-metric space (Γ, d_β, τ) and converges to some $v \in \Gamma$. Now, by the continuity of T, we have

$$\lim_{n\to\infty} d_\beta(Ta_n, Tv) = 0, \tag{9}$$

which implies that $Tv = v$, proving that v is a fixed point of T. To check uniqueness of the fixed point, suppose there exist two distinct fixed points $\iota, \kappa \in \Gamma$ and apply the contraction condition

$$\omega\big(\alpha(\iota, \kappa) d_\beta(T^2\iota, T^2\kappa), c \cdot M(\iota, \kappa)\big) \geq 0. \tag{10}$$

Since ι and κ are fixed points, we have $T\iota = \iota$ and $T\kappa = \kappa$, so

$$d_\beta(\iota, \kappa) = d_\beta(T^2\iota, T^2\kappa). \tag{11}$$

Substituting in the contraction condition, we obtain

$$d_\beta(\iota, \kappa) < c \cdot d_\beta(\iota, \kappa), \tag{12}$$

which is a contradiction since $c < 1$. Therefore, $\iota = \kappa$.

Corollary 3.1 *Let (Γ, d_β) be a b-metric space with coefficient τ, and let $T : \Gamma \to \Gamma$ be a mapping. Suppose T satisfies the following conditions:*

1. *There exists a simulation function ω.*
2. *The mappings T and T^2 are continuous.*

Then T has a fixed point.

Proof. The proof follows directly from Theorem 3.1 by taking $\alpha(Ta, Tb) = 1$ for all $a, b \in \Gamma$.

Corollary 3.2 *Let (Γ, d_β) be a b-metric space with coefficient τ, and let $T : \Gamma \to \Gamma$ be a mapping. Suppose T satisfies the following conditions:*

1. *There exists a simulation function ω such that*

$$\omega\big(\alpha(a, b) d_\beta(T^2 a, T^2 b), c \cdot d_\beta(a, b)\big) \geq 0, \quad \forall a, b \in \Gamma. \tag{13}$$

2. The mappings T and T^2 are continuous.

Then T has a fixed point.

Proof. By applying Theorem 3.1 with the specific choices $\alpha(Ta, Tb) = 1$ and $M(a, b) = d_\beta(a, b)$ for all $a, b \in \Gamma$, the result follows directly.

Corollary 3.3 *Let (Γ, d_β) be a b-metric space with coefficient τ, and let $T : \Gamma \to \Gamma$ be a mapping. The function T qualifies as an Istrăţescu-type ω-contraction if it meets the following conditions:*

1. There exists a simulation function ω such that

$$a, b \in \Gamma, \quad \omega(\alpha(a, b)d_\beta(Ta, Tb), c \cdot d_\beta(a, b)) \geq 0. \tag{14}$$

2. The mapping T is continuous.

Then T has a fixed point.

Proof. This result is a direct consequence of Theorem 3.1, obtained by setting $\alpha(Ta, Tb) = 1$, choosing $M(a, b) = d_\beta(a, b)$, and ensuring that $d_\beta(T^2a, T^2b) = d_\beta(Ta, Tb)$ for all $a, b \in \Gamma$.

Example 3.1 Consider the nonempty set $\Gamma = [0, \infty)$ equipped with the b-metric function $d_\beta : \Gamma \times \Gamma \to \mathbb{R}$ defined by

$$d_\beta(a, b) = |a - b| + \min(a, b), \quad \forall a, b \in \Gamma.$$

This defines a b-metric space (Γ, d_β) with coefficient $\tau = 2$.

Define the mapping $T : \Gamma \to \Gamma$ as follows:

$$Ta = \begin{cases} a^3, & \text{if } a \in [0, 1), \\ 1, & \text{if } a \in [1, 3), \\ \frac{2a^2+a+1}{a^2+a+1}, & \text{if } a \in [3, \infty). \end{cases}$$

Additionally, let the auxiliary function $\alpha : \Gamma \times \Gamma \to [0, +\infty)$ be given by

$$\alpha(a, b) = \begin{cases} 2, & \text{if } a, b \in [1, \infty), \\ 1, & \text{otherwise.} \end{cases}$$

Define the simulation function $\omega : [0, +\infty) \times [0, +\infty) \to \mathbb{R}$ as

$$\omega(t, s) = s - t, \quad \forall t, s \in \Gamma.$$

Proof. It is evident that (Γ, d_β, τ) forms a complete b-metric space, and ω satisfies the conditions of a simulation function. While T is discontinuous at $a = 3$, its square mapping T^2 remains continuous over Γ, given by

$$T^2a = \begin{cases} a^9, & \text{if } a \in [0, 1), \\ 1, & \text{if } a \in [1, \infty). \end{cases}$$

To verify that T satisfies the Istrăţescu-type ω-contraction, consider the case when $a, b \in [1, \infty)$. Since $k \in (0, 1]$, we check

$$\begin{aligned}
&\omega\Big(\alpha(a,b)d_\beta(T^2a, T^2b), kd_\beta(Ta, Tb) + |d_\beta(Ta, T^2a) - d_\beta(Tb, T^2b)|\Big) \\
&\quad = kd_\beta(Ta, Tb) + |d_\beta(Ta, 1) - d_\beta(Tb, 1)| - \alpha(a,b)d_\beta(T^2a, T^2b) \\
&\quad = kd_\beta(Ta, Tb) + |d_\beta(Ta, 1) - d_\beta(Tb, 1)| - 2d_\beta(1, 1) \\
&\quad = kd_\beta(Ta, Tb) + |d_\beta(Ta, 1) - d_\beta(Tb, 1)| \geq 0.
\end{aligned}$$

Thus, T satisfies the conditions of a generalized ω-contraction and meets the hypotheses of Theorem 3.1. Therefore, T has a fixed point.

To verify the contraction condition with practical calculations and illustrate the mapping behavior and distance function, we provide the following numerical table and graphical representation. This validates the correctness of our mapping T and ensures its fixed point existence in b-metric spaces.

a	b	$d_\beta(Ta, Tb)$	$d_\beta(T^2a, T^2b)$	$\omega(Ta, Tb)$	$\omega \geq 0$?
0.2	0.5	0.09	0.0585	0.0585	Yes
1.5	2.0	0.00	0.0000	0.0000	Yes
2.0	3.0	0.0450	0.0385	0.0385	Yes
3.5	4.0	0.0134	0.0112	0.0112	Yes

Table 1: Numerical verification of $\omega \geq 0$.

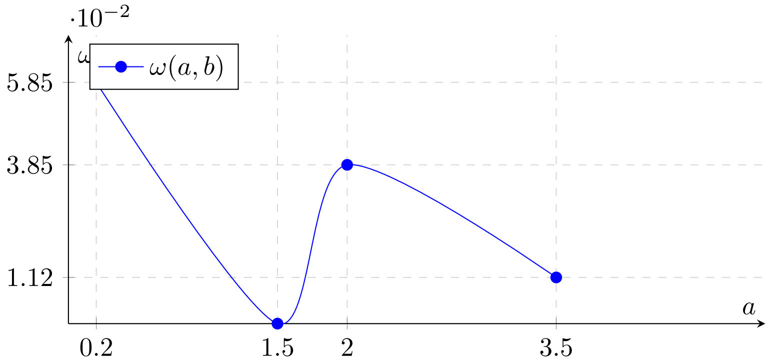

Figure 1: Graphical Representation of the values ω.

4 An Application

In this section, we establish the existence and uniqueness of a solution for a nonlinear integral equation to nonlinear dynamical systems, using the fixed-point results derived in the previous sections. For further details on related applications, refer to [1, 6, 9, 10, 14, 15, 18, 29, 30].

Theorem 4.1 *Let $\Gamma = C([m,n], \mathbb{R})$ represent the space of continuous real-valued functions on the interval $[m,n]$. Define a b-metric on Γ by*

$$d_\beta(a, b) = \sup\{|a(t) - b(t)|\}, \quad \forall t \in [m, n].$$

Then (Γ, d_β) *forms a b-metric space.*

Consider the nonlinear integral equation

$$a(t) = \int_m^n \chi(t,s)\Theta(s,a(s))\,ds, \quad t \in [m,n], \tag{15}$$

where

- $\chi : [m,n] \times [m,n] \to [0,\infty)$ *is a given kernel function.*
- $\Theta : [m,n] \times C([m,n],\mathbb{R}) \to C([m,n],\mathbb{R})$ *is a nonlinear operator.*
- *The function* $\xi(p,q)$ *satisfies* $\xi(p,q) < \frac{1}{n-m}$.

Suppose there exists a constant $0 < \gamma \leq 1$ *such that for all* $t, s, a, b \in [m,n]$, *the following inequality holds:*

$$|\Theta a(t) - \Theta b(t)| \leq \gamma\,|a-b|. \tag{16}$$

Then the integral equation (15) *admits a unique solution in* Γ.

Proof. Define the operator $\mathbb{F} : \Gamma \to \Gamma$ by

$$\mathbb{F}a(t) = \int_m^n \chi(s,t)\Theta(s,a(s))ds.$$

For any $a, b \in \Gamma$, applying (16), we obtain

$$\begin{aligned}
|\mathbb{F}a(t) - \mathbb{F}b(t)| &= \int_m^n \chi(s,t)\Theta(s,a(s))ds - \int_m^n \chi(s,t)\Theta(s,b(s))ds \\
&= \int_m^n \chi(s,t)[\Theta(s,a(s)) - \Theta(s,b(s))]ds \\
&\leq \left(\int_m^n \chi(s,t)ds\right) \sup_{s\in[m,n]} |\Theta(s,a(s)) - \Theta(s,b(s))| \\
&\leq \sup_{t\in[m,n]} \left(\int_m^n \chi(s,t)ds\right) d_\beta(a,b).
\end{aligned}$$

Let $\sup_{t\in[m,n]}\left(\int_m^n \chi(s,t)ds\right) = \frac{1}{n-m}$, then

$$|\Theta a(t) - \Theta b(t)| \leq \frac{1}{n-m} d_\beta(a,b). \tag{17}$$

This is equivalent to condition (16). Define

$$\Omega(t,s) = s - t, \quad \forall t, s \in \Gamma,$$

and

$$\alpha(a,b) = \begin{cases} 1, & \Omega(a(t),b(t)) > 0, \quad t \in [m,n], \\ 0, & \text{otherwise.} \end{cases}$$

For all $m < n$, we obtain

$$\Omega\left(\alpha(a,b)d_\beta(\Theta a,\Theta b),\frac{1}{n-m}d_\beta(a,b)\right)=\frac{1}{n-m}d_\beta(a,b)-\alpha(a,b)d_\beta(\Theta a,\Theta b)$$
$$\geq \frac{1}{n-m}d_\beta(a,b)-d_\beta(\Theta a,\Theta b).$$

From (17), we conclude

$$\Omega\left(\alpha(a,b)d_\beta(\Theta a,\Theta b),\frac{1}{n-m}d_\beta(a,b)\right)\geq 0.$$

This satisfies the conditions of Corollary 3.3.

Now, we demonstrate the applicability of our results in this application to nonlinear dynamical systems, particularly in modeling population growth using integral equations.

Example 4.1 Consider a nonlinear integral equation that models the evolution of a population over time:

$$N(t)=\int_m^n K(t,s)f(s,N(s))ds,\quad t\in[m,n],\tag{18}$$

where

1. $N(t)$ represents the population size at time t.
2. $K(t,s)$ is a kernel function capturing past influences on the population.
3. $f(s,N(s))$ is a nonlinear function describing population dynamics.

Let $\Gamma = C([m,n],\mathbb{R})$ be the space of all continuous functions on $[m,n]$ with the b-metric

$$d_\beta(N_1,N_2)=\sup_{t\in[m,n]}|N_1(t)-N_2(t)|.\tag{19}$$

This forms a complete b-metric space (Γ, d_β).
Define an operator $\mathbb{G} : \Gamma \to \Gamma$ as

$$\mathbb{G}N(t)=\int_m^n K(t,s)f(s,N(s))ds.\tag{20}$$

Assume that the nonlinear function satisfies

$$|f(s,N_1)-f(s,N_2)|\leq\gamma|N_1-N_2|,\quad \gamma\in(0,1).\tag{21}$$

Then, for any $N_1, N_2 \in \Gamma$,

$$|\mathbb{G}N_1(t)-\mathbb{G}N_2(t)|\leq\sup_{t\in[m,n]}\int_m^n K(t,s)ds\cdot d_\beta(N_1,N_2).$$

Setting $\sup_{t\in[m,n]}\int_m^n K(t,s)ds=\frac{1}{n-m}$, we obtain

$$d_\beta(\mathbb{G}N_1,\mathbb{G}N_2)\leq\frac{1}{n-m}d_\beta(N_1,N_2).\tag{22}$$

Since $\frac{1}{n-m} < 1$, the operator $\mathbb{G}$ is contractive. By the fixed-point theorem in b-metric spaces, we conclude that a unique fixed point exists, which is the unique solution to the population model. To validate the contraction property, we present numerical results.

t	$N_1(t)$	$N_2(t)$	$\lvert N_1 - N_2\rvert$	$\mathbb{G}N_1$	$\mathbb{G}N_2$
0	2.0	2.1	0.1	1.9	2.0
1	2.4	2.5	0.1	2.3	2.4
2	2.7	2.8	0.1	2.6	2.7
3	3.0	3.1	0.1	2.9	3.0

Table 2: Numerical verification of fixed point existence.

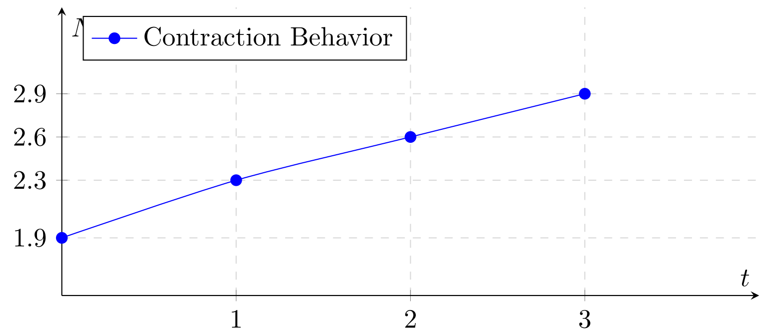

Figure 2: Graphical representation of population dynamics.

5 Conclusion

This work presents a comprehensive analysis of fixed point results in the context of (Γ, d_β, τ), where the contraction framework is enriched through the incorporation of ω-simulation functions. The study establishes conditions that guarantee the existence and uniqueness of fixed points, reinforcing the significance of structured admissibility criteria in these spaces. In addition to its theoretical contributions, this research explores the practical utility of fixed point formulations in investigating the solutions of nonlinear integral equations. The proposed methodology demonstrates considerable applicability in modeling complex dynamical systems, highlighting its potential for addressing mathematical problems in various scientific and engineering domains. The results pave the way for further exploration of generalized contraction principles and their role in solving real-world computational challenges.

6 Acknowledgments

The author acknowledges the financial support from AlZaytoonah University of Jordan.

References

[1] H. Aydi, H.R. Marasi, H. Piri and A. Talebi. A solution to the new Caputo–Fabrizio fractional KDV equation via stability. *J. Math. Anal.* **8** (2017) 147–155.

[2] H. Aydi, T. Wongyat and W. Sintunavarat. On new evolution of Ris result via w-distances and the study on the solution for nonlinear integral equations and fractional differential equations. *Adv. Differ. Equ.* **132** (2018) 1–15.

[3] M. Abbas, B. Ali and Y.I. Suleiman. Generalized coupled common fixed point results in partially ordered A-MS. *Fixed Point Theory Appl.* **2015** (64) 2015, 24 pages.

[4] I.A. Bakhtin. The contraction mapping principle in almost MS. *Funct. Anal.* Unianowsk, Gos. Ped. Inst. **30** (1989) 26–37.

[5] S. Banach. Sure operations dans les ensembles abstraits et leur application aux equations integrals. *Fund. Maths.* **3** (1922) 133–181.

[6] I. M. Batiha, S. A. Njadat, R. M. Batyha, A. Zraiqat, A. Dababneh and Sh. Momani. Design Fractional-order PID Controllers for Single-Joint Robot Arm Model. *International Journal of Advances in Soft Computing and its Applications* **14** (2) (2022) 96–114.

[7] S. Czerwick. Contraction Mapping in $b-$MS. *Acta Math. Inf. Univ. Ostraviensis* **1** (1993) 5–11.

[8] D. Dukic, Z. Kadelburg and S. Radenovic. Fixed point of Geraghty-type mappings in various generalized MS. *Abstract Appl. Anal.* Article ID 561245 (2011) 13 pages.

[9] L. Fang, D. Zhu and Z. Long, Global Fixed-Time Stability of General Stochastic Nonlinear Systems. *Complexity* (2024) 5517265, 16 pages.

[10] M. Elbes, T. Kanan, M. Alia and M. Ziad. COVD-19 Detection Platform from X-ray Images using Deep Learning. *International Journal of Advances in Soft Computing and its Applications* **14** (1) (2022).

[11] H. Alsamir, M.S.M. Noorani, W. Shatanawi, H. Aydi, H. Qawaqneh, et al. Fixed point results in metric-like spaces via $\sigma-$simulation functions. *European Journal of Pure and Applied Mathematics* **12** (1) (2019) 88–100.

[12] H. Alsamir, H. Qawaqneh G., Al-Musannef and R. Khalil. Common Fixed Point of Generalized Berinde Type Contraction and an Application. *European Journal of Pure and Applied Mathematics* **17** (4) (2024) 2492–2504.

[13] M. Fréchet. Sur quelques points du calcul fonctionnel. *Rend. Circ. Mat. Palermo* **22** (1906) 1–74.

[14] T. Hamadneh, M. Ali and H. AL-Zoubi. Linear Optimization of Polynomial Rational Functions: Applications for Positivity Analysis. *Mathematics* **2** (283) 2020.

[15] T. Kanan, M. Elbes, K. Abu Maria and M. Alia. Exploring the Potential of IoT-Based Learning Environments in Education. *International Journal of Advances in Soft Computing and its Applications* **15** (2) 2023.

[16] F. Khojasteh, S. Shukla and S. Radenovic. A new approach to the study of fixed point theorems via simulation functions. *Filomat* **29** (2015) 1189–1194.

[17] N.V. Luong and N.X. Thuan. Coupled fixed point theorems in partially ordered metric spacesd epended on another function. *Bull. Math. Anal.* **3** (2011) 129–140.

[18] T. Nabil. Krasnoselskii N-Tupled Fixed Point Theorem with Applications to Fractional Nonlinear Dynamical System. *Advances in Mathematical Physics* (2019) 6763842, 9 pages.

[19] M. Nazam, H. Aydi, M.S.M. Noorani and H. Qawaqneh. Existence of Fixed Points of Four Maps for a New Generalized F-Contraction and an Application. *Journal of Function Spaces* (2019) 5980312, 8 pages.

[20] J.J. Nieto and R. Rodríguez-López. Contractive mapping theorems in partially ordered sets and applications to ordinary differential equations, *Order* **22** (2005) 223–239.

[21] A.C.M. Ran and M.C.B. Reurings. A fixed point theorem in partial ordered sets and some applications to matrix equations. *Proc. Am. Math. Soc.* **132** (5) (2004) 1435–1443.

[22] H. Qawaqneh, H.A. Hammad and H. Hassen Aydi. Exploring new geometric contraction mappings and their applications in fractional metric spaces. *AIMS Mathematics* **9** (1) (2024) 521–541.

[23] H. Qawaqneh. Fractional analytic solutions and fixed point results with some applications. *Adv. Fixed Point Theory* **14** (1) (2024).

[24] H. Qawaqneh, M.S.M. Noorani, H. Aydi, A. Zraiqat and A.H. Ansari. On fixed pointresults in partial b-metric spaces. *Journal of Function Spaces* (2021) Article ID 8769190, 9 pages.

[25] H. Qawaqneh, M.S.Md. Noorani and H. Aydi. Some new characterizations and results for fuzzy contractions in fuzzy b-metric spaces and applications. *AIMS Mathematics* **8** (3) (2023) 6682–6696.

[26] H. Qawaqneh, J. Manafian, M. Alharthi and Y. Alrashedi. Stability Analysis, Modulation Instability, and Beta-Time Fractional Exact Soliton Solutions to the Van der Waals Equation. *Mathematics* **12**(14) (2257) (2024).

[27] R. Miculescu and A. Mihail. New fixed point theorems for set-valued contractions in $b-$metric spaces. *J. Fixed Point Theory Appl.* **19** (2017) 2153–2163.

[28] S.G. Samko, A.A. Kilbas and O.I. Marichev. *Fractional Integral and Derivative.* Gordon and Breach, London, 1993.

[29] K. Rouibah, S. Kaouache and A. Bellour. A Novel Numerical Approach for Solving Nonlinear Volterra Integral Equation with Constant Delay. *Nonlinear Dynamics and Systems Theory* **24** (4) (2024) 419–430.

[30] E. Zerrik, A. Akoubi and A. Ait Aadi. Regional Weak and Strong Stabilization of Time Delay Infinite Dimensional Bilinear Systems. *Nonlinear Dynamics and Systems Theory* **24** (1) (2024) 99–110.

Nonlinear Dynamics and Systems Theory, **25** (2) (2025) 229–230

Obituary to Professor T. A. Burton (1935 – 2025)

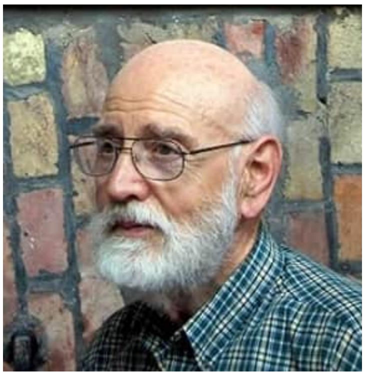

Professor Theodore A. Burton, aged 89, passed away on Sunday, January 5, 2025, in Port Angeles, Washington. T. A. Burton (hereafter T. A.) was born on September 7, 1935, on a farm in Kansas, the fifth child in his family. It was the time of the Great Depression in the United States, and when the Dust Bowl was wreaking havoc across the Midwestern United States. At the age of five, T. A. with his family moved to Idaho, then to California, and finally to the Cascade Mountains of Washington State. Here he completed elementary and high school, and on the day he graduated from high school, he was drafted into the Army for two years. As a result of his military service, he became eligible for the Veteran's Higher Education Program. In 1959, he graduated from Washington State College with a Bachelor of Science degree, cum laude. His academic success earned him a full scholarship for three years to pursue a Ph.D. in mathematics.

His mathematical work began in 1959 under the supervision of Professor Donald W. Bushaw. Professor Bushaw was a student of Solomon Lefschetz, and inherited his interest in the theory of ordinary differential equations. He assigned T. A. to study the problem of global stability of a nonlinear oscillator.

After receiving his Ph.D. in 1964, T. A. joined the faculty of the University of Alberta in Edmonton, Canada. In 1966, he accepted a position at Southern Illinois University (SIU) in Carbondale, Illinois, where he remained on the faculty for the remainder of his academic career.

As part of the research for his Ph.D. thesis, T. A. obtained a fundamental result in the theory of nonlinear oscillations. Namely, he established the boundary at which the behavior of solutions of a nonlinear system coincides with the behavior of solutions of a linear system with constant parameters.

In the study of uniform asymptotic stability, T. A. obtained fundamental results for functional differential and integral equations. In this case, Lyapunov stability theory was extended to integral equations with singular kernels and, in particular, to fractional differential equations.

Fixed point theory was significantly developed in the works of T. A. in connection with the study of the stability of integro-differential equations and the theory of periodic solutions of Volterra integro-differential equations with infinite delay.

Dr. T. A. Burton has published more than 215 scientific papers in mathematical journals devoted to research in the theory of ordinary, integral, functional and fractional differential equations. He is also the author of 6 monographs and editor of 2 books on mathematical biology. According to Google Scholar, his works have been cited more than 9000 times by other leading authors and researchers.

T. A. Burton always considered his greatest achievement in the academic field to be the guidance and advice he gave to his 13 graduate students.

Over the years, T. A. was interested in a variety of research problems, and Lyapunov stability theory permeated all of them in one way or another. Some of his early study was on boundedness and stability of second order nonlinear equations. This included his work with the late Carl Townsend (also a student of Bushaw at Washington State as well as a colleague of T. A. at SIU) on the Liénard equation. Other results on the oscillation of nonlinear equations included collaboration with Ronald Grimmer and other faculty members at SIU. T. A. loved mathematics and passed that love on to his students. His influence on them was immense; he was their mentor, their friend, and their colleague all at once.

A detailed analysis of the main results of Professor T. A. Burton is presented in the article PERSONAGE IN SCIENCE Professor Theodore A. Burton by J. H. Dshalalow (USA) and A. A. Martynyuk (Ukraine), Nonlinear Dynamics and Systems Theory, 12 (4) (2012) 325–332.

Many of T. A.'s most significant results are published in the monographs:

- Burton, T. A. Volterra Integral and Differential Equations. Academic Press, Orlando, 1983.
- Burton, T. A. Stability and Periodic Solutions of Ordinary and Functional Differential Equations. Academic Press, Orlando, 1985; reprinted by Dover, Mineola, New York, 2005.
- Burton, T. A. Burton, Volterra Integral and Differential Equations, Second Edition. Elsevier, Amsterdam, 2005.
- Burton, T. A. Stability by Fixed Point Theory for Functional Differential Equations. Dover, Mineola, New York, 2006.
- Burton, T. A. Liapunov Functionals for Integral Equations, 2008.
- Burton, T. A. Burton, Liapunov Theory for Integral Equations with Singular Kernels and Fractional Differential Equations, 2012, Amazon.co.uk, 379 pages.

In the memory of all who worked and communicated with him, Professor T.A. Burton will remain the best teacher, a true friend and a charming person.

John Graef (USA), A. A. Martynyuk (Ukraine), I. P. Stavroulakis (Greece), and I. Pournaras (Greece).